Multifunctional Silk Nerve Guides for Axon Outgrowth

A dissertation submitted by

Marie C. Tupaj

In partial fulfillment of the requirements for the degree of

Doctor of Philosophy
in
Biomedical Engineering

TUFTS UNIVERSITY
Medford, Ma, USA

February 2012

Advisor:

Professor David L. Kaplan
Dept. of Biomedical Engineering, Tufts University

Abstract

Peripheral nerve regeneration is a critical issue as 2.8% of trauma patients present with this type of injury, estimating a total of 200,000 nerve repair procedures yearly in the United States. While the peripheral nervous system exhibits slow regeneration, at a rate of 0.5 mm – 9 mm/day following trauma, this regenerative ability is only possible under certain conditions. Clinical repairs have changed slightly in the last 30 years and standard methods of treatment include suturing damaged nerve ends, allografting, and autografting, with the autograft the gold standard of these approaches. Unfortunately, the use of autografts requires a second surgery and there is a shortage of nerves available for grafting. Allografts are a second option however allografts have lower success rates and are accompanied by the need of immunosuppressant drugs. Recently there has been a focus on developing nerve guides as an "off the shelf" approach. Although some natural and synthetic guidance channels have been approved by the FDA, these nerve guides are unfunctionalized and repair only short gaps, less than 3 cm in length.

The goal of this project was to identify strategies for functionalizing peripheral nerve conduits for the outgrowth of neuron axons *in vitro*. To accomplish this, two strategies (bioelectrical and biophysical) were indentified for increasing axon outgrowth and promoting axon guidance. Bioelectrical strategies exploited electrical stimulation for increasing neurite outgrowth. Biophysical strategies tested a range of surface topographies for axon guidance. Novel methods were developed for integrating electrical and biophysical strategies into silk films in 2D. Finally, a functionalized nerve conduit system was developed that integrated all strategies for the purpose of attaching, elongating, and guiding nervous tissue *in vitro*. Future directions of this work include silk conduit translation into a rat sciatic nerve model *in vivo* for the purpose of repairing long (> 3 cm) peripheral nerve gaps.

Acknowledgements

First and foremost, I would like to thank Professor David Kaplan for providing me this opportunity to study in the biomedical engineering program and for his mentorship over many years. This learning and research experience will be unforgotten and treasured. I cannot thank you enough for guiding this project. You were the first professor I met at Tufts, not only in graduate school, but as a freshman years ago. Little did I know at that time what an influential person you would be in my life. I am grateful for the encouragement to explore my ideas and the time to solve new problems creatively.

Next, I would like to thank my committee members, Professor Mark Cronin-Golomb, Professor Fiorenzo Omenetto, Professor Michael Levin, Professor Cristian Staii, and Professor Kacey Marra for their ideas, feedback, and guidance as this project has evolved and developed.

I would like to thank Professor Irene Georgakoudi and several past and current members of the Optical Diagnostics for Diseased and Engineered Tissues (ODDET) Lab, including William Rice, Cherry Greiner, Shamaraz Firdous, and Joanna Xylas. Irene spent many hours reviewing data and guiding the first paper while Bill and Shamaraz were critical in microscope training at the start of my research projects in biomedical engineering. Cherry and Joanna have answered questions, given advice, and offered support during my time here.

I would also like to acknowledge several of the post-doctoral associates in the Kaplan Lab including Sarah Sundelacruz, Waseem Khan Raja, Min Tang-Schomer, and James White. Sarah led the way on the first membrane potential projects, while Waseem, Min, and James were especially helpful with research discussions and project ideas over the last months.

I would like to remember and acknowledge my long time office mates Michaela Reagan, Reynald Lescarbeau, and Lin Sun for being enjoyable, easy going colleagues to share work space, eating space, and conversation space with day after day.

I am grateful to staff members Milva Ricci and Carmen Preda for consistently ordering lab supplies and coordinating lab space during experiments.

I would like to acknowledge my husband, Andrew Tupaj, and family members, Marie and Martin Tupaj, Mary Hronik, Carolyn Hronik, Emily Hronik, and Anthony Petrovich. Thank you for your encouragement, questions, and interest in this research.

Finally, I would like to acknowledge the rest of the Kaplan Lab members most of whom I have worked with at some point over the last few years. I thoroughly enjoyed working and learning in a lab with an extremely talented, passionate and diverse group of scientists from all over the world. I hope to see you again, making a difference, in the field. Be well.

Table of Contents

List of Tables and Figures

Chapter 1: INTRODUCTION: NEURAL TISSUE ENGINEERING

1.1 Introduction

Injury to peripheral nerves is fairly common and usually results in a skeletal muscle atrophy and poor functional recovery (Gu et al., 2010a). It is known that for nerve repair to occur, axons need guidance from the proximal stump towards the target organ and connection to the distal stump prior to atrophy. Unfortunately, axon outgrowth is a slow process. While short gap (< 3 cm) peripheral nerve injuries have shown regenerative success, restoration of more severe nerve injuries is difficult, and long-gap (> 3 cm) nerve injuries have not seen complete recovery despite clinical intervention. While several strategies, including the addition of neurotrophic factors, stem cell and glial cell transplantation, gene therapy, and the development of nerve guidance channels, have been tested *in vitro* and *in vivo* for enhancing peripheral nerve regeneration, each strategy has its drawbacks. In fact, there has not been one strategy identified for complete functional recovery. In the first chapter, an overview of the clinical impact, peripheral nervous system structure and functionality, and the clinical treatments for repairing peripheral nerve injuries are discussed. Next, the current research in the field is summarized along with the regenerative potential and drawbacks of each strategy. Finally, our project, a functionalized nerve guide that combines the regenerative potential of bioelectrical and biophysical strategies, which will be explained over the next several chapters, is outlined and how this project can be used to improve overall axon outgrowth during the nerve repair process is described.

1.2 Clinical Significance

1.2.1 Peripheral Nerve Injuries

Peripheral nerve injury (PNI) is a critical issue as 2.8% of trauma patients present with this type of injury (Potucek et al., 2009) estimating a total of 200,000 nerve repair procedures yearly in the United States

(Willerth et al., 2007). By 2012, an estimated 1.5 billion people will suffer from peripheral nerve injury in the U.S., Europe, and Japan due to complications from diabetic neuropathy, human immunodeficiency virus (HIV)**,** and chemotherapy (Report, 2003). During a time of war, 14-18% of injuries affect the peripheral nervous system altering both sensation and muscle function (Potucek et al., 2009).

Following PNI, acute sensory problems include the loss of sensation and pain. Over the long term, chronic problems that may develop include peripheral neuropathy, desensitization of the injured area, hyperalgesia, better known as an exaggerated sense of pain for the given stimuli, or allodynia, which is described as pain caused from innocuous stimuli (Oh, 2006). Annual compensation from doctors visits and missed work due to pain caused by PNI total $50 billion per year (Bonica et al., 2001; Cum, 2000). Following PNI, motor problems include muscle weakness and spasms with more severe conditions leading to paralysis.

1.2.2 Limb Amputation

Approximately 1.9 million people are living with limb loss in the United States as a result of trauma, cancer, vascular problems, or congenital defects (Dillingham, 2002)(**Figure 1.1**). Projected lifetime cost for patients and their families undergoing amputation in the United States in 2002 was approximately $509,275 (MacKenzie et al., 2007). Disabilities and a change to a sedentary lifestyle due to limb loss can increase risk of other diseases. In a recent report that examined the care of amputees following combat, 27% of upper limb amputees were not employed or reemployed following their amputation, and 67% of upper limb amputees had to change jobs following amputations (Hubbard Winkler, 2009) making limb regeneration not only an increased risk for additional health problems, but also a permanent decrease in earning potential.

In lizards that have the ability to regenerate new tails following amputation, it has been demonstrated that successful regeneration is correlated with an adequate quantity of nervous tissue at the injury site

(thornton, 1970a; Whimister, 1978a). This regenerative ability is noted as it may be translatable to human limb regeneration in the future. Furthermore, it emphasizes another application for nervous tissue regeneration.

Figure 1.1: Limb Amputation Statistics by Cause, Unites States, 1988 to 1996 (Dillingham, 2002)

1.3 Neurobiology Background

1.3.1 Peripheral Nervous System Architecture

Although nerve cells can be classified into many different categories, a neuron consists of the same basic morphologically defined parts, including a cell body, dendrites, axon, and presynaptic terminals (Kandel et al., 2000). The cell body, known as the soma, is the cells' metabolic center and ranges from 5 - 50 µm or more in diameter (Alberts et al., 2002; Kandel et al., 2000). The dendrites are defined as the many

short processes that extend from the cell body and the axon is the long tubular process extending from the cell body. Axons are approximately 1-3 µm in diameter and can extend up to 1 meter or longer in length from the spinal cord to the distal extremities (Kandel et al., 2000). Newly formed processes, before they are able to be distinguished between an axon and dendrite, are commonly termed neurites.

Neuron axons may be myelinated or unmyelinated. Myelin is produced by glial cells (Kandel et al., 2000). Glial cells, which are defined as Schwann Cells in the peripheral nervous system, are wrapped, starting at a point termed the inner mesaxon and ending at a point termed the outer mesaxon, around the axon in concentric circles (Kandel et al., 2000). One myelin sheath typically runs 600 µm in length around the axon (Potter et al., 2011) and is separated from the next myelin sheath by a 30 µm gap, termed the Node of Ranvier. Myelin is composed of 70% lipid and 30% protein, with a high concentration of cholesterol and phospholipid, similar to that of a plasma membrane (Kandel et al., 2000).

Individual axons and myelin are surrounded by a collagen covering termed the endoneuriun (**Figure 1.2**). Anatomically, one axon and myelin sheath enclosed by the endoneurium is a nerve fiber. Several nerve fibers that are bundled together and enclosed by the perineurium compose one fassicle. Several fassicles that are bundled together by a connective tissue is defined as the epineurium (Campbell, 2008). Blood vessels lie longitudinally within the epineurium and send branches across the perineurium to create a capillary network in the endonerium (Campbell, 2008; Mackinnon et al., 1988).

Nerve cells located in the peripheral nervous system (PNS) are characterized as either sensory neurons or motor neurons (Kandel et al., 2000). Sensory nerve cells make up the afferent signaling pathway, propagating information from the peripheral nerve endings towards the spinal cord and terminating in the brain, specifically the brain stem and thalamus (Hunt, 2005). Motor nerves make up the efferent signaling pathways bringing information from the brain towards the muscles and glands (Kandel et al.,

2000). Cell bodies of sensory neurons are located in the dorsal root (Oh, 2006), while cell bodies of the peripheral motor nerves are located in the ventral horn (Kandel et al., 2000; Mason et al., 2011).

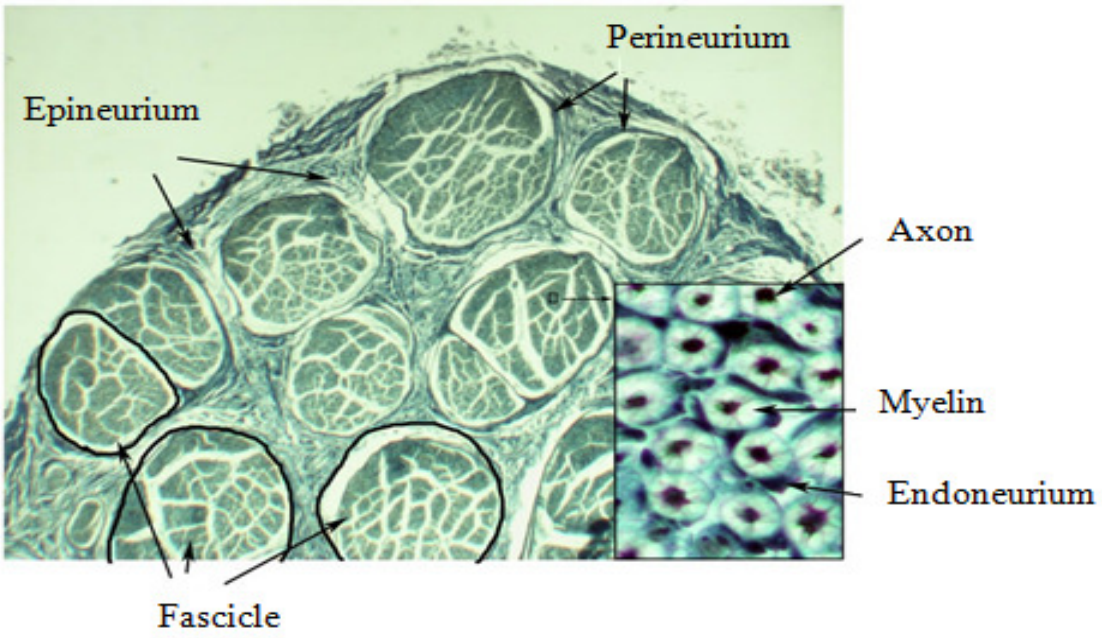

Figure 1.2: Histological cross-section of the human sciatic nerve. Adapted from (Lozano et al., 2003). The rat sciatic nerve contains approximately 27,000 nerve fibers including heavily myelinated motor axons and myelinated and unmyelinated sensory axons (Wallman et al., 2001). The largest nerve fibers range from 12-20 µm in diameter (Wallman et al., 2001).

1.3.2 Neuron Characterization

For distinguishing neurons, by method of morphological characterization, from other types of nervous tissue, neurons have processes that are, on average, at least three times longer than the width of the cell body (**Figure 1.3A,B**). This is in contrast to glial cells, the supporting structure of the nervous system, that exhibit shorter processes and larger cell bodies.

The most accurate method for classifying cells in culture as neurons is through the presence of neural proteins. Common protein markers for identifying neurons include β3-tubulin and neurofilament

(Arien-Zakay et al., 2007; Oe et al., 2006). β3-tubulin, also known as tuj-1, is expressed in microtubules and encodes for a structural protein found in neuron axons and cytoskeleton (Kandel et al., 2000). Neurofilament is type IV intermediate, 10 nm in diameter, also found in the neural axoskeleton that may play a role in transport to axons and dendrites (Kandel et al., 2000). Images of immunostains that show the presence of β3-tubulin and neurofilament is in **Figure 1.3C** and in **Figure1.3D** respectively.

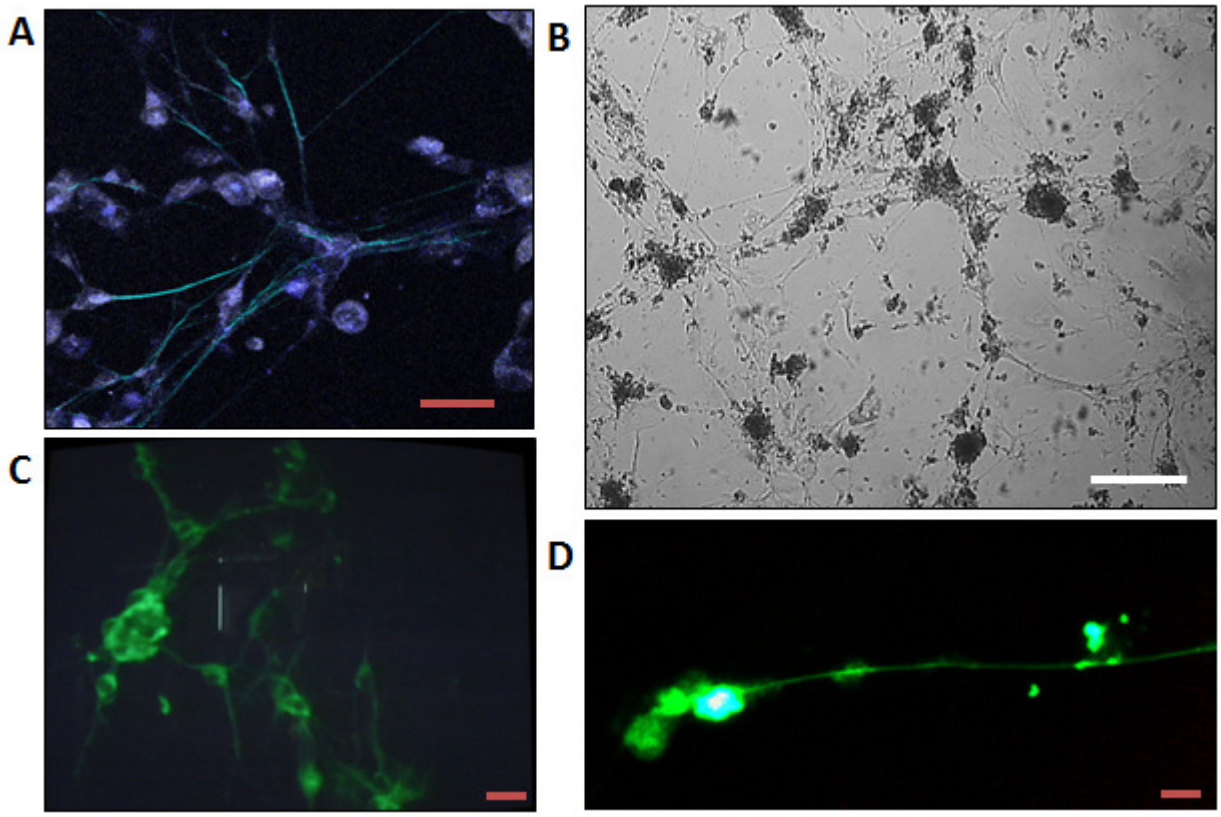

Figure 1.3: Morphological and biochemical methods for neuron identification. (a) Image of live neurons in culture. The cell body is in purple, the axon is blue. (b) Image of neurons in culture. Cell bodies of p19 neurons tend to aggregate in culture and form interconnected functional axonal networks. Immunostains reveal the presence of proteins (c) β3-tubulin and (d) neurofilament. These proteins are located in the soma and axons, of the neurons in culture. Pink scale bar is 50 µm. White scale bar is 150 µm (Images by Marie Tupaj, unpublished data, 2008).

1.3.3 Peripheral Nervous System Functionality

Membrane potential is established, in all cells, as the difference in total ionic charge of anions and cations between the intercellular and extracellular fluid of the plasma membrane (Kandel et al., 2000). Resting membrane potential, described as the condition when net ionic flow across the membrane is zero (Alberts et al., 2002), can be quantified across the membrane in any cell type using the Goldman Equation,

$$E_m = \frac{RT}{F} \ln\left(\frac{P_k[K^+]out + P_{Na}[Na^+]out + P_{Cl}[Cl^-]in}{P_k[K^+]in + P_{Na}[Na^+]in + P_{Cl}[Cl^-]out}\right)$$

where E_m = Resting membrane potential; R = universal gas constant equal to 8.314 $J \cdot K^{-1} \cdot mol^{-1}$; T = absolute temperature in Kelvin; F = Faraday Constant equal to 96,485 $coulombs \cdot mol^{-1}$; and P_i = Permeability of ion i (Kandel et al., 2000). In this equation, resting membrane potential is dependent on the contributions of K^+, Na^+, and Cl^- ion concentrations and the permeability of each ion across the cell membrane. Resting membrane potential is typically between - 60 mV and - 70 mV in neurons (Kandel et al., 2000), though this is variable depending on neuron source.

Although neurons have a resting potential between -60 to -70 mV, their membrane potential is able to quickly and significantly shift from changes in local ion concentration (Kandel et al., 2000). Because of this ability, neurons are known as excitable cells. For sensing and quickly responding to large shifts in membrane potential, voltage gated ion channels (VGICs) are located in the neuron's cell membrane. VGICs are typically composed of a pore made up of four protein subunits with negatively charged ends each containing 6 transmembrane domains, a selectivity filter, a voltage sensor, and activation and inactivation gates (hunt et al., 2001; Julius et al., 2001). Voltage sensors in VGICs contain highly positively charged domains. Voltage sensors repel and open the VGIC gate when sensing changes in local

ion concentration from an extracellular stimulus. This response starts the process known as an action potential.

Action potentials occur when the voltage sensor senses that local ion concentration reaches threshold potential of approximately -50 mV. At this time, positively charged voltage sensors move, open the voltage gated Na^+ channels, and there is an influx of sodium ions, down its concentration gradient driving membrane depolarization. From this, more Na^+ channels begin to open and the influx of sodium ions continues until almost an equilibrium potential of approximately +50 mV, at which point the sodium channel becomes inactivated. To bring the cell membrane back to its original resting potential, an outward flux of potassium ions flow through potassium channels, driving hyperpolarization (Hunt, 2005; McCleskey et al., 1999) (**Figure 1.4A**).

The event of an action potential is known as an "all or nothing" response, meaning that all changes in ion concentration below the threshold potential will not generate an action potential and all stimuli that reach above the threshold potential will generate an action potential (Kandel et al., 2000).

1.3.4 Membrane Potential Control for Growth and Regeneration

Experimental data has demonstrated that varying cell membrane voltage potential can initiate cell proliferation and differentiation (Blackiston et al., 2009; Cone Jr, 1970; Sundelacruz et al., 2009). Furthermore, different membrane potential levels can yield varying mitotic effects thus providing a means for controlling the mitotic cycle (Cone Jr, 1970). Altering transmembrane potential can be accomplished through altering extracellular ion concentrations via the addition of pharmacological agents and ionophores (Adams et al., 2006a, b; Cone Jr, 1970). For example, mature neurons have demonstrated the ability to reenter the mitotic cycle following changes in membrane potential utilizing ionophores such as ouabain, gramidicin, and veratridine (Cone et al., 1976).

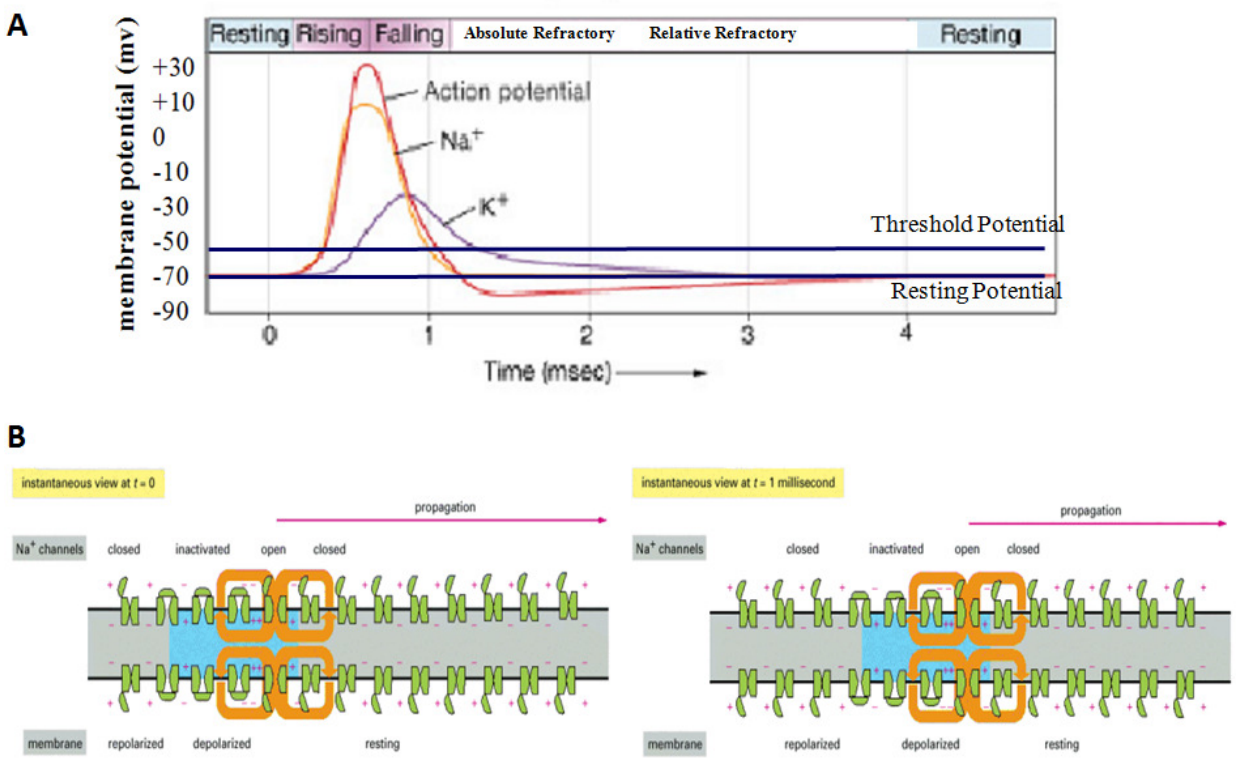

Figure 1.4: Neuron Functionality (a) The contributions of inward sodium ion flow and outward potassium ion flow to action potential generation. Approximate values for resting potential and threshold potential are indicated by the blue lines. The events of an action potential can be broken down into resting, rising, falling, absolute refractory and relative refractory periods. The duration of an action potential in humans is approximately 1 ms. (b) Action potential propagation down a neuron axon. Action potentials can deliver time sensitive information across long distances. The area of depolarization is shown in blue. The current direction is given by the arrow in purple. Image on the left is the position of VGICs at time, t = 0. Image of the right is the position of VGICs at t = 1 millisecond. Different types of VGICs are selective, based on size and charge, for ions such as Na^{+}, Ca^{2+}, K^{+}, and Cl^{-}. VGICs switch between active open, active closed and inactivated states. The active open state allows for an influx of ions following changes in extracellular ion concentration. The active closed state is during the resting phase. VGIC inactivation is the period when the ion channel cannot be activated. This ensures that the

signal propagates in the forward direction. Nerve conduction velocities depend on fiber diameter and myelination (Alberts et al., 2002; Costanzo, 2002; Cum, 2000; Hunt, 2005; Julius et al., 2001).

1.3.5 Neural Cell Sources for *In Vitro* Experiments

Several neuronal cell sources have been used for peripheral nerve experiments *in vitro*. Cell sources for peripheral nerve studies have included stem cell lines, primary cells, bone marrow mesenchymal stem cells, induced pluripotent stem cells (Denham et al., 2011), and human embryonic stem cells (Ma et al., 2008). Some common stem cell lines include the p19 stem cell line (Banker et al., 1998; Holy et al., 2011; McBurnery, 1993; Ulrich et al., 2006; Zhao et al., 2011), the SH-SY5Y stem cell line (Kullenberg et al., 2008; Pahlman et al., 1990), and the PC12 cell line (Banker et al., 1998; Yao et al., 2010b; Yao et al., 2009)(**Table 1**). Primary cells for peripheral nervous system studies are most commonly dorsal root ganglia (Cheng et al., 2011; Griffin et al., 2011; Jin et al., 2011).

p19 stem cells are derived from pluripotent embryonal teratocarcinoma in a C3H/He mouse, having stable euploid male karotypes (McBurnery, 1993). In culture, p19 stem cells are observed to grow in colonies, p19 stem cells have the morphology of a 'napolean's hat' and p19 stem cells double approximately every 24 hours (p19 proliferation rates taken by Marie Tupaj, unpublished data, 2008). p19 stem cells are able to differentiate down several lineages into fibroblasts, endothelial cells, neurons, neuroglia, skeletal, and cardiac cells (Banker et al., 1998; Ulrich et al., 2006). Like most cells undergoing neural differentiation, p19 stem cells differentiate into neurons following exposure of at least 0.5 µM retinoic acid (jones-villeneuve et al., 1982). Retinoic acid is non-toxic to p19 cells and binds to cellular proteins that interacts with RA-response elements (Ulrich et al., 2006) Retinoic acid differentiates stem cells into neurons by initiating transcription of target neuronal genes including sonic hedgehog, paired box 6 (pax-6), achaete-scute complex homolog 1 (mash-1), and wingless-type mouse mammary tumor virus integration site family, member 1 (wnt-1)(Ulrich et al., 2006).

Once differentiated, p19 neurons exhibit morphological characteristics of cortical neurons; p19 neurons exhibit a well defined cell body and axons that typically do not branch. p19 neurons have been shown to establish functional synapses 1-2 weeks following the addition of retinoic acid (Finley et al., 1996), proving their ability to differentiate fully down the neural lineage. P19 cells are amenable to transfection. p19 cells may differentiate into several neuron or neuroglial and the quantify of neural differentiated p19 stem cells may depend on the initial cell seeding density (Kitani et al., 1997).

The SH-SY5Y stem cell line originates from a human child neuroblastoma (Li et al., 2007a). SH-SY5Y stem cells double approximately every two days. SH-SY5Y stem cells are simpler to work with in culture and more readily differentiate into one cell type as compared to the p19 cell line. With the addition of at least 1 µM retinoic acid, SH-SY5Y stem cells differentiate into neurons over approximately 2 weeks. For a shorter differentiation period, some studies add a neurotrophic factor, such as NGF or BDNF, to the neural differentiation media (Agholme et al., 2010). Morphologically, SH-SY5Y neurons have a less well defined cell body than the p19 cells line and exhibit neurite branching. SH-SY5Y neurons express synaptic proteins such as synaptic vesicle protein, Sv2, and synaptic structures with their neighboring neurons, however SH-SY5Y functionality has not been well established in the literature (Agholme et al., 2010).

Neuroscience lacks appropriate models to study the nervous system *in vitro*. Currently, dorsal root ganglia are the most common *in vitro* model for peripheral neural tissue engineering. Dorsal root ganglia are the sensory peripheral nerve cell bodies that lie in sacks outside the spinal column. DRGs can be dissected between the lumbar 4 (L4) - lumbar 5 (L5) section of the spinal column (Tegeder et al., 2006). Care needs to be taken during dissections for avoiding contamination and dissecting ganglia only, without the addition of fibroblasts.

PC12 cells are another common cell line utilized for neural tissue engineering experiments *in vitro*. PC12 cells are a cancer cell line from the rat adrenal medulla utilized for neural differentiation (Fedoroff et al.). PC12 cells are a model cell line for studying sprouting and neurotrophin signaling in primary neurons (Klesse et al., 1999). PC12 cells enter into mitotic arrest and differentiate over 7-10 days following exposure to 100 ng/mL nerve growth factor and culture media containing 1% horse serum. PC12 cells are also amenable to transfection.

Table 1.1 Some Common Neural Cell Sources (p19 and SH-SY5Y images by Marie Tupaj; Dorsal Root Ganglia dissection and image by Xiaodong Yang, Unpublished Data, 2008)

Cell Type/Source	**Cell Culture & Cell Morphology**		**Characteristics**
p19 Stem Cells/ Mouse Embryonic Carcinoma	Undifferentiated Stem Cells 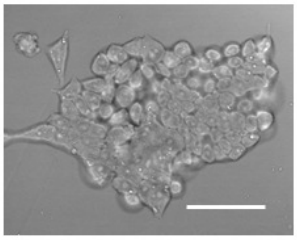	Differentiated Neurons 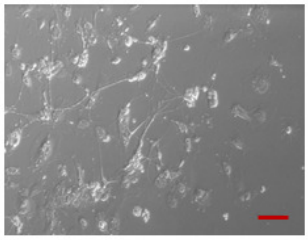	- Well-defined cell body - Cortical neuron morphology - Murine source - Amenable to transfection - Differentiates into several cell types in culture
SH-SY5Y Stem Cells/ Human Neuroblastoma	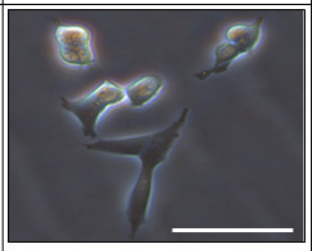	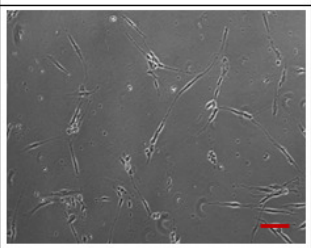	- peripheral nervous system model - differentiation period w/o growth factor (10 days) - neuron cell body less defined - human source - one cell type in culture
Dorsal Root Ganglia (DRG)/Mouse		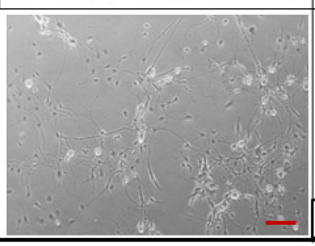	- Ideal model of peripheral nervous system - Aquire multiple cell types in culture (i.e. fibroblasts) - Lengthy dissection process
			Scale = 50 um Scale =50 um

1.3.6 Peripheral Nerve Injury and Regeneration

While there are over hundreds of nerve injury classifications, which are dependent on factors such as symptoms, damage, and prognosis, injury to the peripheral nerves may be generally classified into three main categories: neurapraxia, axonotmesis, and neurotmesis (Campbell, 2008). For injuries that are classified as a first degree injury, neurapraxia, the entire nerve structure remains intact and complete functional recovery occurs (Campbell, 2008). In contrast, for nerve injuries that are categorized as the most severe, neurotmesis, the nerve and surrounding connective tissue is destroyed (Campbell, 2008); Regeneration does not occur spontaneously without clinical intervention (Campbell, 2008). Second degree nerve injuries, axonotomies regenerate spontaneously and slowly under certain conditions at a rate of 0.5 mm – 9 mm/day (Burnett et al., 2004). In this case, the distal stump is separated from its cell body (**Figure 1.5A**) and initially undergoes Wallerian Degeneration (Alberts et al., 2002). Within 48 hours following injury, macrophages are recruited to the degenerating distal nerve fiber and phagocytosis of cellular debris, disconnected fibers, and pre-existing myelin begins (Mackinnon et al., 1988; Yamada et al., 2010) (**Figure 1.5B**). Within 72 hours, Schwann cells proliferate and begin to line the injured nerve gap and extracellular matrix. Myelinated and unmyelinated fibers proximal to the nerve injury and proximal to the last Node of Ranvier begin to sprout

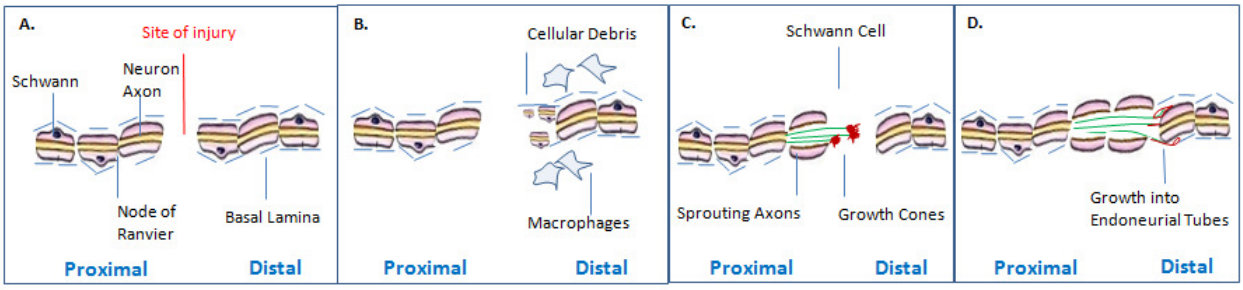

Figure 1.5: Peripheral Nerve Regeneration following injury (a) Axotomy (b) Wallerian Degeneration (c) Axon Sprouting (d) Axon Guidance into the distal stump (Image by Marie Tupaj, Unpublished, 2010).

new axons (**Figure 1.5C**)(Mackinnon et al., 1988). Newly developed growth cones, which are located at the end of each sprouting axon, are directed between the outer Schwann cell surface and the Schwann cell basil lamina into what is known as endoneurial tubes (**Figure 1.5D**)(Mackinnon et al., 1988). Laminin molecules in the basal lamina of Schwann Cells guide the growth cones of regenerating fibers into these areas. Axonal sprouts will grow slowly towards the distal end of the injured axon, which is dependent on the surrounding microenvironment (Cao et al., 2011). Initially more fibers will regenerate than needed, then degenerate over time if not matched with the distal end of the nerve. Factors that determine regenerative success include removal of axon and Schwann cell debris, a supportive basal lamina, and growth factor secretion (Shim et al., 2010).

1.4 Clinical Interventions and Clinical Devices

While axotomies having less than a 10 mm gap are able to spontaneously sprout new processes from the proximal stump and direct outgrowth into endoneurial tubes of the distal stump, peripheral nerve injuries greater than 10 mm are typically not repaired without intervention. Furthermore, timely medical attention, typically within 48 hours prior to the development of scar tissue, is necessary for preventing permanent damage. The best outcome to date is slow (up to 1 year) functional recovery.

The best methods for repairing peripheral nerves include autografts or primary repair using tension-free sutures (Hill et al., 2011). Unfortunately primary repair using tension-free suturing works only for short gaps where the nerve is not stretched more than approximately than 10-15% (Belkas et al., 2004). When the gap is too long for reattaching without stretching, a “bridge material” is needed. A bridge material for nerve repair is used to support and guide the proximal stump towards the distal stump.

The autograft has been the ‘gold standard’ of bridge materials. Autografts take a less important nerve, such as the medial, sural and lateral antebrachial cutaneous nerves (Grawanis et al., 2005), from

another area of the patient and use this nerve to bridge the gap between the proximal and distal stumps of the injured nerve. Unfortunately autografts have drawbacks. For example, autografts require a second surgery and the quality of the graft may not be good. The nerve diameter between the donor and recipient nerve may not be the same or the patient may not have enough nerves for sacrifice (Pettersson et al., 2011). In addition, autografts may cause increased scar tissue or painful neuromas at the recipient site (Pettersson et al., 2011). Finally, functional outcomes using autografts are still suboptimal (Scholz et al., 2010).

Clinically approved FDA devices for guiding the proximal stump to the distal stump, known as nerve guides, include the Neurotube® composed of a poly(glycolic) acid (PGA) mesh (Weber et al., 2000); Neurolac® composed of poly(DL-lactide-co-caprolactone); SaluTunnel™ made of polyvinyl alcohol (PVA); and Neuroflex™, Neurogen® ,and NeuroMatrix™ all composed of a type I collagen matrix (Kehoe et al., 2011) (**Table 1.2**). However, to date, the FDA has not approved a natural degradable guide for healing long (> 3 cm) peripheral nerve gaps.

Table 1.2: FDA Approved Nerve Guides

	Nerve Guide Product	**Material**	**Guide Length**
1.	Neurotube®	A poly(glycolic) acid (PGA) mesh	2-4 cm
2.	Neurolac®	Poly(DL-lactide-co-captrolactone)	3 cm
3.	Neuroflex™	Type I Collagen	2.5 cm
4.	SaluTunnel™	Polyvinyl Alcohol (PVA)	6.35 cm
5.	Neurogen®	Type I Collagen	2-3 cm
6.	NeuroMatrix™	Type I Collagen	2.5 cm

1.5 Current Neural Tissue Engineering Strategies for Peripheral Nerve Repair

Requirements for complete functional peripheral nerve repair include preventing distal stump atrophy, axon reconnection of the proximal and distal stumps, and the remyelination of newly repaired axons. Even if conditions are favorable for spontaneous repair, incomplete functional recovery may occur. For example, distal stump atrophy of sensory axons will result in a loss of total sensation in the affected area. Incomplete motor axon outgrowth, due to vascular supply limitations, may lead to lower detected compound muscle action potentials (CMAPs). Incomplete axon reinnervation into the target tissue will result in a loss of motor control. Incomplete remyelination in heavily myelinated motor nerve chains will result in slower action potentials and longer muscle reaction times.

Strategies currently researched for successful nerve repair include (1) the addition of growth factors, (2) stem cell and glial cell transplantation, (3) gene therapy, and (4) the design of natural and synthetic guidance channels (Lari et al., 2001; Murakami et al., 2003; Pan et al., 2007; Pan et al., 2006; Pollock, 1995). The following sections discuss the outcomes and drawback of these current strategies.

1.5.1 Growth Factors

It is well known that neurotrophic factors are released endogenously by peripheral nervous tissue following injury. To date, scores of studies in the literature have reported the use of growth factors, such as nerve growth factor (NGF), glial cell-derived neurotrophic factor (GDNF), brain derived neurotrophic factor (BDNF), neurotrophin-3 (NT-3), and neurotrophic factor -4/5 (NT -4/5) (Lykissas et al., 2007), for repairing peripheral nerve injuries. Some of the most recent growth factor studies have been summarized in **Table 1.3**.

Currently, NGF is the most well characterized and the most well studied growth factor for treating peripheral nerve injuries (Aloe, 2011). After injury, there is a less than adequate amount of endogenous

NGF produced and released by Schwann cells for complete recovery (Dhar et al., 2007). To date, there have been many studies that evaluate nerve recovery following exogenous delivery of NGF to the site of injury. Studies that have been reported include examining the effects of NGF on supporting cell survival, axon guidance, cell migration, proliferation, and differentiation (Thomas et al., 2010). For example, one study that was published in 2010 incorporated NGF into nanofibrous conduits then implanted them into a rat sciatic nerve defect. An increased number of mature nerve fibers were found at week 10 of healing (Wang et al., 2010a). In addition to improvements in structural nerve regeneration, NGF has increased functional recovery compared to control groups without growth factors (Wang et al., 2010a). A second study reported increased nerve conduction velocities in addition to increased axon density and increased axon diameter compared to nerve conduits that did not contain NGF (Xu et al., 2011). Finally, the addition of growth factors may improve growth or migration of supporting tissue such as Schwann cells, which in turn may facilitate axon regeneration (Madduri et al., 2010a).

Unfortunately, not all studies have reported enhanced regeneration from NGF (Kemp et al., 2011). One study, found that regenerative effects from NGF were dose and duration dependent (Kemp et al., 2011). In addition, some reports have stated that nerve growth factors such as NGF promote the regeneration of nociceptive axons, but have little effect on other adult sensory nerves, such as mechanoreceptors, thermoreceptors, and proproceptors, and motor axons.

For the purpose of repairing multiple axon subpopulations, some laboratories have tried incorporating multiple growth factors (**Table 1.3**) (Madduri et al., 2010a). For example, one study incorporated both 40 ng NGF and 40 ng GDNF into a collagen conduit for the repair of 10 mm rat sciatic nerve defect (Madduri et al., 2010a). Results revealed significant increases in Schwann cell migration into the conduits' proximal end within the first two weeks of regeneration (Madduri et al., 2010a). Increases in overall axon number, axon density, and number of myelinated axons were found from groups

containing both NGF and GDNF (Madduri et al., 2010a). The absence of cross- reactivity between growth factors was verified. Functional testing was not completed (Madduri et al., 2010a).

Not all studies that target the repair of peripheral nerves use the typical neurotrophic factors. Some studies employ growth factors that were not originally identified for the differentiation and regeneration of nervous tissue. These growth factors include bone morphogenetic protein 2 (BMP -2), insulin like growth factor 1 (IGF-1), and fibroblast growth factor (FGF) (**Table 1.3**). In one study, 40 µl of 200 ng/ml BMP-2 was injected locally twice a day for 7 days into rats with injured facial nerves (Wu et al., 2010). Axon number, axon diameter, and axon cross-section were significantly greater in the BMP-2 treated group than in controls at 4 weeks post-injury (Wu et al., 2010). In a second study, rat sciatic nerve defects were treated using 15 µg IGF-1 (Emel et al., 2011). 30 days post injury, the sciatic functional index showed functional improvement over the saline group (Emel et al., 2011). The G-ratio was also significantly higher compared to controls (Emel et al., 2011). The mechanism behind growth factors which were not originally identified for regenerating nervous tissue, such as BMP, IGF, and FGF, has not been widely investigated to date.

Although nerve growth factors have been successfully incorporated into biomaterial delivery systems, demonstrated the ability to protect neurons from injury induced death, and promote regeneration (Kandel et al., 2000), there are still drawbacks to these treatments. For example, the half life of these proteins is typically short (De Boer et al., 2011; De Boer et al., 2010) and growth factors in solution form are not expected to be effective (Esaki et al., 2011). Release kinetics varies dependent on the growth factor, biomaterial, and delivery method. Doses have yet to be optimized. Other strategies for peripheral nerve repair, which eliminate the concerns regarding growth factor instability or drug delivery kinetics, include stem cell therapy.

Table 1.3: A Summary of Growth Factors Utilized for Peripheral Nerve Repair

Growth Factor(s)	***Delivery Methods***	***Repair Site***	***Outcomes***	***References***
NGF	Nanofibers & Conduits	Rat Sciatic Nerve	↑ Mature Nerve Fibers, ↑ Functional Recovery ↑ Nerve conduction velocities, prevention of connective tissue ingrowth	(Wang et al., 2010a; Xu et al., 2011)
GDNF	Microspheres	Rat Sciatic Nerve	↑ Gastrocnemius twitch force ↑ Improved Tissue Integration Nerve Fibers across entire area of regeneration	(Kokai et al., 2011)
GDNF or BDNF	Transfection into Neural Stem Cells (NSC)	Rat Sciatic Nerve	↑ Myelination from GDNF NSC & BDNF NSC ↑Size of Regenerated Tissue from GDNF NSC & BDNF NSC ↑Blood Vessels from GDNF NSC ↑ Functional Gait from GDNF NSC & BDNF NSC	(Fu et al., 2011)
NGF & GDNF	Collagen tube impregnation	Rat Sciatic Nerve	↑ Early (2-week) regeneration	(Madduri et al., 2010a)
BMP-2	Injection	Rabbit Facial Nerve	Denser axons Thicker axons ↑ Tau Protein	(Wu et al., 2010)
IGF-1	Injection	Rat Sciatic Nerve	↑ Functional Recovery Faster sensory recovery ↑ G-ratios	(Emel et al., 2011)

1.5.2 Stem Cell Therapy

Stem cells are recognized as the predominant contributor in tissue engineering due to their ability to proliferate, exhibit self maintenance, differentiate into many cell types, and retain multilineage potential. Here we briefly discuss the main stem cell sources for peripheral nerve repair, including neural stem cells (NSCs), mesenchymal stem cells (MSCs), and adipose derived stem cells (ADSCs) (**Table 1.4**).

Neural stem cells were first isolated in 1992 from embryonic (Reynolds et al., 1992a) and adult central nervous system tissue (Reynolds et al., 1992b). Following isolation, NSCs were identified to be self-

renewing and to have multipotent qualities. For the importance in peripheral nerve regeneration, neural stem cells have been able to differentiate into neurons *in vivo* and form synapses with the target skeletal muscles, resulting in decreased atrophy. One study reported that implanted fetal neural stem cells into rat defects were able to form synapses with the regenerating tibial nerves (Gu et al., 2010a; Gu et al., 2010b). At 3 and 5 months post injury, compound muscle action potentials (CMAPs) were detected in the NSC transplanted group. CMAPs could not be detected at any time in the controls. Histologically, it was determined through the expression of β3-tubulin that implanted NSCS could differentiate into neurons(Gu et al., 2010a). NSCs could form synapse proteins, such as synaptophysin and neuromuscular junctions (Gu et al., 2010a).

Stem cells not only provide sustenance surrounding the regenerating nerves, but they are good for differentiating into nervous tissue needed at the site of injury. For example, Schwann cells are important in peripheral nerve regeneration for the purpose of neurotrophic factor secretion at the site of injury, axon guidance towards the distal stump, and myelin secretion around the regenerated nerves. Unfortunately, it is difficult to harvest enough pure Schwann cells in a time efficient manner for transplantation (Di Summa et al., 2011). To solve this cell shortage, some studies have differentiated stem cells into Schwann cells then transplanted the differentiated Schwann cells into the injury site. For example, one study differentiated mesenchymal stem cells into Schwann cells then transplanted them into an injured rat sciatic nerve (Ladak et al., 2011). The differentiated Schwann cells exhibited motor axon outgrowth comparable to primary Schwann cells and greater compared to the control group without Schwann cells (Ladak et al., 2011). Fifty percent of the differentiated mesenchymal stem cells were comparable with the native Schwann cells, as they stained positive for Schwann cell markers including S100, glial fibrillary acidic protein (GFAP), and nerve growth factor receptor (NGFR).

Adipose tissue is another good source for stem cells because they are easy to obtain, safe to harvest with minimally invasive surgical techniques, available in abundant quantities, and have favorable culture and expansion properties (Erba et al., 2010). Adipose derived stem cells (ADSCs) are extracted from adipose tissue and have the ability to differentiate down several lineages including the neural lineage into astrocytes, ogliodendrocytes, and neurons (Tobita et al., 2011). ADSCs have been able to accelerate the growth of blood vessels and nerve sprouts, which may be due to their ability to secrete myelin components, growth factors such as vascular endothelial growth factor (VEGF), basic fibroblast growth factor (bFGF) and hepatocyte growth factor (HGF), and neurotrophic growth factors such as BDNF, NGF, and GDNF (Lopatina et al., 2011; Santiago et al., 2009). In one study, ADSC seeded conduits were able to increase axon outgrowth in a 1 cm rat sciatic nerve gap significantly better than growth factor seeded conduits (Erba et al., 2010). In addition, greater Schwann cell invasion into the distal stump was noted 14 days following transplantation (Erba et al., 2010).

Functional improvements have been observed using ADSCs as well. For example, transplanted ADSCs into the mouse peroneal nerve accelerate functional recovery over a two week period compared to negative controls (Lopatina et al., 2011). Specifically, a 3.7 fold higher action potential amplitude was detected compared to the control, suggesting that more fibers were involved in conduction (Lopatina et al., 2011). A 1.7 fold reduction of latency period was identified 7 days after injury, indicating better myelination and increased fiber thickness (Lopatina et al., 2011).

Unfortunately, stem cells do not offer complete nerve repair which may be due to several factors. For example, it is well known that differentiated stem cells may not be an exact model of the native nervous tissue (Potter et al., 2011). Harvested stem cells from the host tissue are difficult to purify and may

contain a heterogenous population. Finally, stem cell sources may vary from culture to culture. Future studies using implanted stem cells need to assess long term survival, up until regeneration is complete.

Table 1.4: A Summary of Stem Cell Therapies for Peripheral Nerve Repair

Stem Cell Therapy	***Stem Cell Implantation Site***	***Outcome***	***Reference***
Neural Stem Cells (NSC)	Rat Tibial Nerve	Synapse formation with implanted neural stem cells	(Gu et al., 2010a; Gu et al., 2010b)
Mesenchymal Stem Cells (MSC) Skin-Derived Mesenchymal Stem Cells	Rat Sciatic Nerve Dog Sciatic Nerve Porcine peripheral nerves	-Promote motor axon outgrowth -nerve regeneration and functional recovery ↑ Nerve bundles ↑ Schwann cell protein	(Ding et al., 2010; Ladak et al., 2011; Pereira Lopes FR et al., 2010) (Park et al., 2011)
Adipose Derived Stem Cells (ADSC)	Rat Sciatic Nerve	-axonal outgrowth -Schwann Cell Proliferation into the distal stump -Distal Nerve End Protection	(Erba et al., 2010; Lopatina et al., 2011; Santiago et al., 2009)

1.5.3 Gene Therapy Strategies

Due to the short half life of some neurotrophic factors and the inability of delivery systems to release drugs within the required "therapeutic window," there is a need to identify efficient and innovative ways for delivering drug to treat nervous tissue damage. Drug delivery via gene therapy is a unique method that allows for a continuous supply of neurotrophic factor release at the injury site. Gene therapy works by using DNA as the drug and aims to express the therapeutic gene at the site injury (Li et al., 2008b). Since gene therapy is able to target nervous tissue specifically, this method can release growth factors according to the physiological role of neurotrophins *in vivo* within the key area of damage. In the past, gene therapy has been investigated for use in the central nervous system as a novel method for delivering drugs across the blood brain barrier. However, this therapy has also been reported for delivering growth factors for repairing the peripheral nervous system. Genes that have

been delivered to peripheral nerve injuries include those that encode for growth factors, such as NGF, HGF, and BMP-7. The main transfection methods for gene delivery to the peripheral nervous system include the herpes simplex virus and the adenovirus (**Table 1.5**) however additional viruses such as the lentivirus and adeno associated virus have been utilized in addition to methods such as electroporation (Mason et al., 2011). Benefits and drawbacks of the herpes simplex viral vectors and the adenovirus for delivering neurotrophic genes and their ability to regenerate peripheral nerve injuries are described in the following paragraphs.

The herpes simplex virus (HSV) is a vector that has shown aptitude for infecting the nervous system and can maintain long term dormancy in neurons (Esaki et al., 2011; Mason et al., 2011). Results using HSV have been positive for promoting peripheral nerve regeneration. For example, one study micropipetted 10^6 plaque forming units (pfu) of HSV- hepatocyte growth factor (HGF) onto a compressed murine facial nerve. Between days 7 – 12, mice exposed to the HSV-HGF vector exhibited faster recovery from paralysis due to nerve compression than the control group (Esaki et al., 2011). By day 14, the HGF and control groups completely recovered from paralysis (Esaki et al., 2011). Functional changes were also detected. For example, the amplitude of the compound muscle action potential of the buccinator muscle was greater on day 7 and day 14 in mice treated with HGF than the control group (Esaki et al., 2011).

Another study utilized HSV to transfect NGF into human embryonic kidney (HEK-293) cells. HEK-293 cells are good because they have little to no immune response due to their embryonic nature and are stable, allowing for easier transfection. NGF transfected HEK-293 cells were then transplanted into the rat sciatic nerve following injury. Increases in small diameter nerve fibers and an increased functional index were reported (Scholz et al., 2010).

The adenovirus is another common vector the second vector, historically identified for transfection of growth factor genes for nerve regeneration. In one study, HGF was injected along with acellular nerve guides following a rat sciatic nerve injury (Li et al., 2008b). Results revealed increased neovascularization at week 16 compared to accellular nerve guides alone (Li et al., 2008b).

Genes encoding growth factors have also been transfected into supporting nervous tissue, such as Schwann cells and fibroblasts, which are then transplanted at the site of injury (Mason et al., 2011). Gene therapy has also been examined for knocking down inhibitory molecules, such as neuroglycan 2 (NG2), that promote glial scar tissue formation (Donnelly et al., 2010). However, this has been reported in literature for central nervous system repair, such as in the spinal cord.

Table 1.5: A Summary of Gene Therapies for Peripheral Nerve Repair

Gene	Transfection Method	Delivery Method	Injury Site	Outcome	Reference
NGF	Herpes Simplex Virus	HEK-293 Cells	Sciatic Nerve	↑ small diameter (< 6 μm) nerve fibers ↑ functional index	(Scholz et al., 2010)
HGF	Herpes Simplex Virus	Injected into injury site	Murine facial nerve	Faster recovery from nerve compression ↑ muscle compound action potential	(Esaki et al., 2011)
HGF	Adenovirus	Injected into Primary Muscle Cells	Rat Sciatic Nerve	↑Neovascularization ↑ Axon Outgrowth	(Li et al., 2008b)
BMP -7	Adenovirus shuttle vector	Injected into injury site	Rat Sciatic Nerve	↓ Macrophage Activation ↓ Nerve Demyelination ↓ Axonal Degeneration ↑ Schwann Cell Proliferation	(Tsai et al., 2010)

Drawbacks with gene therapy include the difficulty of turning genes on at the start of repair and then off when repair is complete. In addition, neurons are difficult cell type to transfect. For viruses, like the HSV

it is difficult to be efficient without being neurotoxic. Finally, FDA approval for clinical use may be difficult due to biosafety concerns. For example, the introduction of vector impurities may cause an inflammatory response and the possibilities of introducing gene mutations may pose an increased cancer risk (Mason et al., 2011). Materials that are already FDA approved may be an easier and faster method for clinical translation.

1.5.4 Nerve Graft Strategies

For replacing the autograft, tissue engineered nerve grafts (TENGs) made out of synthetic, natural, and biological materials are currently being researched. Synthetic materials have included poly(lactic acid) (PLA), poly(lactic-co- glycolic acid) (PLGA), poly(ε-caprolactone) (PCL), polyamidoamines (PAA), poly(ethylene glycol) (PEG), and silicone (**Table 1.6**); natural materials have included chitosan, collagen, gelatin, fibronectin, hyaluronan, keratin, and silk (**Table 1.7**); biological materials have included artery, vein, muscle, tendon, or skin (**Table 1.8**).

Synthetic materials that are used for tissue engineered nerve grafts typically posses mechanical integrity but can vary in degradability from biodegradable to not degradable (**Table 1.6**). Synthetic tubes that are not degradable may cause foreign body response, scar formation, and infection and may require a second surgery to remove. In addition, if synthetic materials are not fully absorbable, they pose risk for chronic inflammation and nerve compression (Kakinoki et al., 1995; Lundborg et al., 1982; Madison et al., 1988; Madison et al., 1987; Navarro et al., 1996; Robinson et al., 1991). Silicone is one of the early synthetic materials that were used as a bridge material. Since silicon is not able to degrade or expand; it is considered a biologically inert material, and may be needed to be removed following repair. One study implanted silicone tubes into the human ulnar and median nerves for repairing short gap (up to 1 cm) peripheral nerves (Braga-Silva, 1999; Lundborg et al., 2004). Five years following treatment, there

was not any difference between the silicone tubing and microsurgical repair(Lundborg et al., 2004). However, results began to vary with the longer nerve gaps (Braga-Silva, 1999; Lundborg et al., 2004).

Table 1.6: A Summary of Synthetic Materials Utilized for Tissue Engineered Nerve Grafts (TENGs)

Nerve Graft Biomaterial	**Material Properties**	**Regenerative Outcome**	**Reference**
Ceramic particles (genipin-cross-linked gelatin)	Biodegradable No large inflammation	Nerve fiber morphology similar to normal nerves ↑ sciatic functional index	(Yang YC et al., 2011; Yang YC et al., 2010)
Polyamidoamines (PAA) (hydrogels)	Biocompatible Biodegradable Tunable elasticity Low interfacial tension	↑ regeneration (fiber density, axon size, & myelin thickness)	(Magnaghi et al., 2011)
poly(ε-caprolactone) (PCL)	Mechanically Strong Selectively Permeable Hydrophilic	↑myelination ↑ nerve fibers	(Liu et al., 2011; Oh et al., 2008)
Poly(ethylene glycol) (PEG)	Biocompatible Soluble/gels exhibit favorable hydration Tunable mechanical properties	↓ leakage of lactate dehydrogenase ↓ formation of reactive oxygen species ↑ exploratory behavior ↓ beta-amyloid precursor protein (APP) accumulation	(Cho et al., 2010; Koob et al., 2006; Koob et al., 2008)
Poly(lactic-co-glycolic acid) (PLGA)	Rigid Inflammatory	Sustain nerve regeneration ↑ axon diameter Thicker myelin sheath	(Chang et al., 2007b; Chang CJ et al., 2005; De Boer et al., 2011; Oh SH et al., 2008)
polyvinyl chloride (PVC)	Mechanically Strong	↑ myelination	(Penna V et al., 2011)
Silicone	Biologically Inert Not Degradable	Growth factor accumulation in graft Poor growth and myelinatoin	(Braga-Silva, 1999; Lundborg et al., 2004)

Some groups have developed synthetic degradable grafts. In one study, a polyamidoamine hydrogel graft was used to repair the rat sciatic nerve (Magnaghi et al., 2011). Increases in fiber density, axon

size, and myelin thickness were observed compared to the sham (Magnaghi et al., 2011). However, resorption of these conduits may result in inflammatory reactions and fibrosis around the area of implant.

It has been stated that natural materials offer better regeneration quality than synthetic material (Li, 2008). However, natural materials tend to have weak mechanical properties (**Table 1.7**). Several of the natural materials such as alginate, collagen, fibrin, fibronectin and keratin have been utilized in the form of a gel.

Table 1.7: A Summary of Natural Materials Utilized for Tissue Engineered Nerve Grafts (TENGs)

Nerve Graft Biomaterial	**Material Properties**	**Regenerative Outcome**	**Reference**
Alginate Matrix	Gentle Gelling Biologically Inert	Schwann cell viability ↑ growth profile (with fibronectin)	(Mosahebi et al., 2003; Sufan et al., 2001)
Chitosan	Poor degradability Mechanically weak Inflammatory reaction	↑ myelination ↑ % in CMAPs	(Li X et al., 2010; Simões MJ et al., 2010)
Collagen	Biocompatible Degradable Mechanically weak	Partial nerve function	(Cao et al., 2011; Ding et al., 2011; Phillips JB et al., 2005)
Fibrin	Controllable gelation Soft Angiogenic	Axon growth Tissue Integration	(Kalbermatten et al., 2009; Scott et al., 2011)
Fibronectin	Mechanically weak	Schwann cell, fibroblast growth	(Ahmed et al., 2003)
Gelatin	Mechanically weak Plasticity Adhesiveness Cheap	Unmyelinated axon outgrowth Schwann cell increase	(Chen et al., 2005; Liu, 2008)
Hyaluronan	Non-immunogenic Degraded by hydrolysis Angiogenic byproducts	Attachment, proliferation, micro vascular integration	(Zavan et al., 2008)
Keratin	Biocompatible Mechanically weak	↑ axon density ↑ axon diameter ↑ conduction delay ↑ amplitude recovery	(Apel PJ et al., 2008; Hill et al., 2011)
poly 3-hydroxybutyrate (PHB)	Biodegradable	↑ Schwann cells	(Mohanna et al., 2003)
Silk	Biocompatible	↑ proximal sprouts	(Ghaznavi et al., 2011;

	Mechanically stable Varying degradation rates	↑ distal connections ↑ nervous tissue density	Lin et al., 2011; Yang et al., 2011)

Several biological materials including artery, vein, muscle, tendon, and skin have been utilized for creating grafts to repair nerve defects. While biological materials do not offer structural integrity or functionality (Di Summa et al., 2010), biological materials have been suggested for use as tissue engineered nerve grafts as they are a good option for preventing immunogenicity. One study compared vein and dermal grafts for repairing a 10 mm nerve gap. Density and average nerve fiber area was greater in the venous group compared to the dermal group (Fatemi MJ et al., 2010). In the dermal group, fibrous tissue was present through the graft and few axons were present. To avoid lumenal collapse, some studies have tried decellularized artery grafts instead of venous grafts (Sun et al., 2011).

Allografts are another option from biological material used for bridging nerve gaps. Unfortunately, the availability of donor nerves for allografts is limited. The implantation of allografts will require the use of immunosuppresent drugs by the patient (Di Summa et al., 2010).

Table 1.8: A Summary of Some Biological Materials Utilized for Tissue Engineered Nerve Grafts (TENGs)

Nerve Graft Biomaterial	**Material Properties**	**Regenerative Outcome**	**Reference**
Artery	Biocompatible Mechanically weak	↑ myelination	(Sun et al., 2011)
Vein	Biocompatible Mechanically weak	↑ density ↑ area of nerve fiber (compared to dermal conduit)	(Fatemi MJ et al., 2010; Marcoccio et al., 2010)

Many papers have reported using biomaterial composites for nerve guides in order to exploit more of the required material properties. Some examples include the fabrication of collagen and laminin crosslinked scaffolds (Cao et al., 2011), collagen/poly(e-caprolactone) electrospun fibrous nerve

conduits (Yu et al., 2011), chitosan and PLA composite nerve conduits (Xie et al., 2008). For the purpose of a mechanically strong outer layer and a soft inside layer some reports have demonstrated grafts using a synthetic outer shell filled with a natural soft biomaterial for the inner layer. However, fillers need to allow for cell and chemical migration into the tube and gels may limit oxygen and nutrient diffusion (Goto et al., 2010).

Tissue engineered nerve grafts have been designed into several shapes including tubes, sieves, rectangular scaffolds, and cuffs. The tubular shape of the nerve graft is good for preventing the invasion of fibroblasts, preventing the invasion of inflammatory particles, helping to align Schwann cells, and ultimately cultivating a microenvironment for repair (Fatemi MJ et al., 2010). For conduits to be effective for regeneration, the conduits' material needs to be biocompatible with nervous tissue, have a degradation rate that is commensurate with the time of regeneration, have little to no immune response, be mechanically stable, and allow for molecular diffusion. The simplest graft to translate into the clinic for long gap peripheral nerve repair is to use an already FDA approved material. To satisfy all of the above requirements, it is clear that there is a need to utilize a versatile biomaterial that can be functionalized to satisfy multiple needs.

1.6 Silk Fibroin for Neural Tissue Engineering

1.6.1 Silk Structure and Function

Silk is a well known natural material originating from sources including spider, silkworms, honeybees, scorpions, mites, and flies (Altman et al., 2002). Depending on the source, silk differs widely in structure and properties (Altman et al., 2002). Silk that originated from the *Bombyx mori* silkworm is composed of a heavy chain fibroin approximately 391 kDa and a light chain fibroin 27 kDa, held together by a disulfide bond with glue-like proteins termed sericins that bind fibers formed from the fibroins (Sofia et al., 2001;

Zhou et al., 2000). B. mori silk is composed of a core repeating primary glycine-alanine-serine sequence ending with approximately 100 amino acid N terminal and C terminal domain (Omenetto et al., 2010). B. mori silk is mostly hydrophobic with short hydrophilic charged sequences (Omenetto et al., 2010).

Silk is widely utilized in biomedical applications due to its high mechanical strength, toughness, and processibility**.** Silk is enzymatically degradable, dependent upon beta sheet content, and more biocompatible than other commonly used FDA approved synthetic materials, such as Poly(lactic-co-glycolic acid) (Altman et al., 2003; Panilaitis et al., 2003). Silk can be processed into scaffolds, films, gels and fibers. Silk has been studied extensively in a variety of *in vitro* and *in vivo* settings (Etienne et al., 2009; Kim et al., 2010a; Wang et al., 2008). Modifiable material parameters include degradation time, surface topography, porosity size and number, and mechanical strength.

1.6.2 Silk Fibroin for Nerve Repair

As a biomaterial, silk has been shown to have good biocompatibility with peripheral nervous tissue (Yang et al., 2007a). Since silk is fully degradable, it leaves less of an effect on nerve compression and chronic inflammation. In addition, silk fibroin films have been used in applications for conformal bio-integrated electronics for detecting electrical activity in the cortex (Kim DH et al., 2010).

1.6.3 Silk for Peripheral Nerve Guides

Currently, the autograft continues as the 'gold standard' for healing peripheral nerve injuries. Unfortunately, functional outcomes using autografts are still suboptimal (Scholz et al., 2010) and typically do not work or are not available for repairing long gaps. While some studies have shown that tissue engineered nerve grafts (TENGs) may work equally as well as the autograft, there has yet to be a graft that has proven superior to the autologous nerve graft. Here we summarize the current approaches utilizing conduits and limitations to these approaches (**Table 1.9**).

Table 1.9: Current Approaches and Current Limitations of Peripheral Nerve Guides

Current Nerve Guide Approaches	Limitation
1. Synthetic materials (Non-degradable, constrictive) (Chang et al., 2007a; Kakinoki et al., 1995; Lietz et al., 2006; Oh et al., 2008; Xie et al., 2008) 2. Fast Degradation, Lack of Mechanical Integrity (Ahmed et al., 2003; Whitlock et al., 2009; Yao et al., 2010a)	Conduit Biomaterials
1. Non-Functionalized Conduits (Yang et al., 2007b) 2. Limited Functionality (Allmeling et al., 2006; Madduri et al., 2010c; Uebersax et al., 2007)	Short Gap Regeneration (Limited Axon Outgrowth, Guidance)

It would be ideal to have a replacement nerve guide that works at least as well as the autograft. The engineered guide would avoid the use of another nerve or require a second surgery. This guide would be biodegradable, and biocompatible (Kehoe et al., 2011), available "off the shelf," and utilized to treat nerve injuries even after a one-month delay (Kehoe et al., 2011; Shi et al., 2010).

To foster an environment for peripheral nerve repair, nerve designs must mimic the native peripheral nerve architecture and must be flexible, porous, promote the release of nerve growth factors (endogenous or exogenous), allow for extracellular matrix deposition and Schwann cell migration, provide cues for guiding sprouting axons from the proximal to distal stump, increase the rate of axon outgrowth to prevent distal stump atrophy, and allow for remyelination of newly repaired axons (Kehoe et al., 2011). Nervous tissue, including Schwann cells, will need to adhere, proliferate, and migrate through the conduit. The graft will allow for cell and matrix alignment in addition to neovascularization.

1.7 Functionalized Silk Nerve Guides for Axon Outgrowth

While silk is a promising material for nerve regeneration, we need a design that functionalizes conduits promoting neuron attachment, elongation and guidance. The goal of this project was to identify

strategies then functionalize silk nerve conduits for the attachment, elongation and guidance of neuron axon *in vitro*. We hypothesized that electronic biomaterial systems based on silk proteins will provide novel 'living like' systems for attaching, elongating, and guiding peripheral nerves. To accomplish this, a combination of novel biophysical, biochemical, and bioelectrical strategies were integrated into a silk nerve conduit system. Strategies that were explored included biochemical, growth factors and attachment proteins, biophysical, surface topographies, and bioelectrical, electrical stimulation. Best strategies were then combined on flexible silk substrates. Finally, tools were integrated into a silk nerve conduit then tested for effectiveness *in vitro.* The overall design is shown in **Figure 1.6**. Each of these strategies and their effect on axon outgrowth are described in the following chapters.

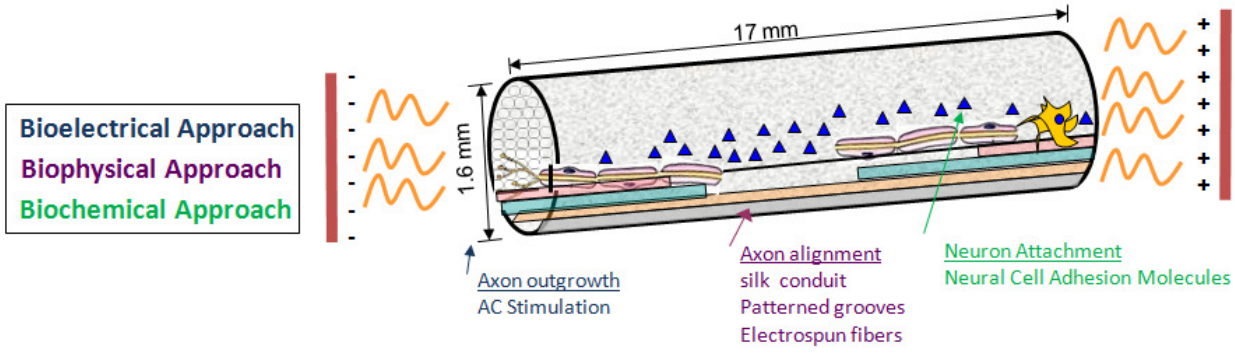

Figure 1.6: A Design of a Multi-functional Silk Nerve Guide. Conduit dimensions are based on the repair of a critically sized defect of a rat sciatic nerve (Image by Marie Tupaj, Unpublished, 2008).

Chapter 2: BIOELECTRICAL STRATEGIES

2.1. Introduction

Restoration of functional peripheral nerves is a complex process. Following injury, the first challenge is to accelerate axon outgrowth prior to distal stump atrophy. While several strategies have been attempted, there is not one method for complete functional restoration.

Neurons are well known as excitable cells and can be characterized by an array of electrical properties including resting membrane potential, action potential frequency, action potential duration, resistance, and capacitance. These electrical properties are present in neural tissues, vary by tissue health, tissue age and are present in developing, normal, and wounded tissues and organisms (**Figure 2.1**).

Although the presence of electrical signals was first identified over 300 years ago, the application of electrical stimuli has not been fully exploited for restoring tissue function. Electric fields have several advantages over alternative approaches, including the absence of toxic chemicals, the absence of immunogenic responses in the host tissue, and cost friendly applications when compared with growth factors and many chemicals. In addition, electric field techniques require little cell handling and processing. Many devices used for electrical stimulation employ simple equipment designed with a basic theoretical understanding of electromagnetism. Furthermore, devices that incorporate electrodes into tissues work well for repeatedly treating the same specific area depending on size in culture or *in vivo*. Finally, electrodes can be used for acquiring data, specifically monitoring action potentials at the area of treatment.

Past studies have demonstrated that electrical stimulation alters several properties of engineered tissues including cell differentiation, proliferation, morphology, adhesion, migration, and function (**Table 2.1**). For example, while uniform DC field stimulation typically directs cell orientation, alters cell

morphology, and directs cell migration, AC fields enhance cell differentiation and increase tissue function following field application (Hronik-Tupaj et al., 2011a) (**Table 2.1**).

While the effects of electrical stimulation has been examined on several cell types, on several tissue types, and on neuron regeneration *in vivo*, there have been few studies that have examined the effects of electric fields on neuron outgrowth *in vitro* (Graves et al., 2011; Koppes et al., 2011). The objective of this study was to apply a range of moderate electric field strengths and assess effects on axon differentiation and axon outgrowth on SH-SY5Y stem cells undergoing neural differentiation.

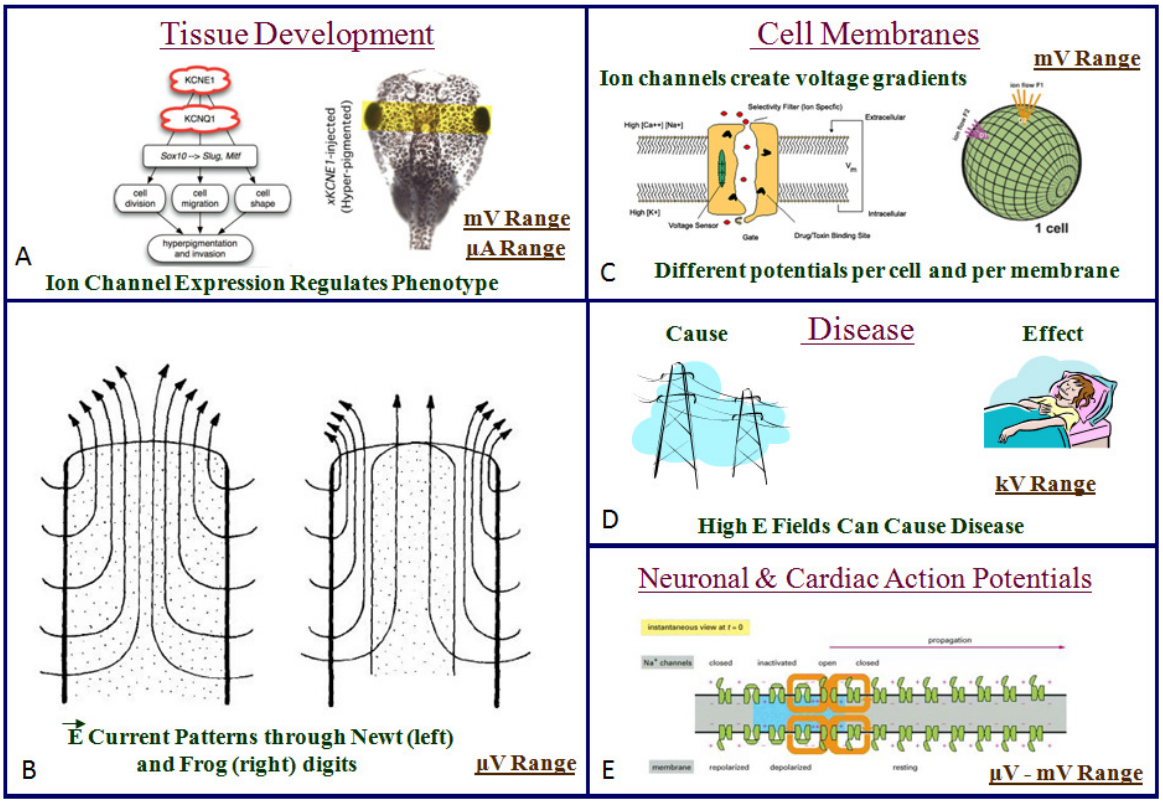

Figure 2.1 - Electric fields are innate in organisms (a) During cell development, ion channel expression regulates phenotype. In this image, overexpression of potassium voltage-gated channel subfamily E member 1 (KCNE1) induces hyperpigmentation in frog embryos (Morokuma et al., 2008). Current flow is in the µA range. Voltage potential is in the mV range. (b) Electric currents radiate outward, in the µA

range, perpendicular to wounds and amputations in newts and frog digits (Borgens et al., 1979; Hotary et al., 1994). (c) Differences in ion concentration across cell membranes create voltage gradients. Voltages in the mV range are measured across the intercellular and extracellular space in cells. Different potentials are measured per cell and per membrane. Electric field strength across a cell's membrane is on the order of 1 million V m^{-1} as the distance across the cell membrane is in the nm range. (d) Exposure to high strength electromagnetic fields in the kV range may cause disease or earlier disease onset, while changes in a tissues' permittivity or conductivity may be a biomarker of disease (Joines et al., 1994). (e) Voltage potentials are detected in the mV range in the intercellular space and in the µV range in the extracellular space of cardiac and neuronal tissues. Ionic current propagation, detected in the mV range, is the method of physical signal transduction in excitable tissues (Hronik-Tupaj et al., 2011a).

Table 2.1: Tissue Responses to DC and AC Fields (Hronik-Tupaj et al., 2011a)

Tissue Response to Applied DC Fields	**Cells & Tissue Type**	**References**
Morphology (orientation)	Cardiac, Human Adipose Derived Stem Cells, Rat Mesenchymal Stem Cells, Human Skin Cells	(Dube et al., 2005; Sun et al., 2006; Tandon et al., 2009a; Tandon et al., 2009b)
Migration	Corneal Epithelial Cells, Adipose Derived Stromal Cells, Vascular Endothelial Cells, Keratinocytes, Fibroblasts (Mouse Embryo & Human)	(Chang et al., 1996; Hammerick et al., 200; Onuma et al., 1985; Sheridan et al., 1996; Zhao et al., 1996; Zhao et al., 2004; Zhao et al., 1997)
Differentiation	Human Dermal Fibroblasts, Human Mesenchymal Stem Cells, Bovine Chondrocytes	(Akanji et al., 2008; Jennings et al., 2008; Sun et al., 2007)
Tissue Response to Applied AC Fields	**Cells & Tissue Type**	**References**
Functionality	Neuron (Rat), Muscle (Skeletal & Cardiac)	(Borschel et al., 2004; George et al., 2008; Ito et al., 1983; Kondo et al., 2008; Shimizu et al., 2002)
Differentiation	Human Mesenchymal Stem Cells, Bovine Cartilage, SAOS-2 Cells (Human Sarcoma Osteogenic), Mouse Osteoblasts (MC3T3-E1)	(Brighton et al., 2006; Diniz et al., 2002; Fassina et al., 2006; Hronik-Tupaj et al., 2011b; Radisic et al., 2004)
Proliferation	Primary Rat Osteoblasts, Human Bone Marrow Stem Cells, Human	(Aaron et al., 2004b; Fassina et al., 2007; Ijiri et al., 1996; Sun et

	Osteoblasts (SAOS-2), Primary Bone (Rabbit)	al., 2009a; Tsai et al., 2007)
Morphology	Human Chondrocytes, Jurkat Cells, SAOS-2	(Jahns et al., 2007; Sebastian et al., 2007a; Sebastian et al., 2007b)
Adhesion	Fibroblasts (Rat Tendon & Human), Rat Bone Marrow Osteoprogenitors, Rat Bone Marrow MSCs	(Blumenthal et al., 1997; Sun et al., 2006)

2.2 Materials & Methods

2.2.1 Alternating Current (AC) Device Design

24K gold sheets (Rio Grande, Albuquerque, NM), having thickness of 0.25 mm, were cut into dimensions of 2 mm x 10 mm then secured, using conductive silver paste (TedPella, Redding, CA), to 99.95% biocompatible, non-corrosive platinum wire (Surepure Chemetals, Florham Park, NJ), 0.005 inches in diameter. The conductive silver paste was allowed to dry overnight. The following day, gold electrodes and platinum wire were secured inside a 60 mm diameter Petri-dish with non-toxic silicone aquarium glue (PETCO, San Diego, CA). Silicone glue was allowed to dry for at least 2 days.

2.2.2 SH-SY5Y Stem Cell Culture

SH-SY5Y stem cells (ATCC, Manassas, VA), originating from a human neuroblastoma cell line, were thawed, then expanded in culture at a density of 5,000 cells/cm^2 using a 50:50 composition of DMEM/F12 (Invitrogen Corp., Grand Island, NY), 10.0% fetal bovine serum (Invitrogen Corp.), and 1.0% penicillin-streptomycin (Invitrogen Corp.). Stem cells were incubated at 37°C in 5% CO_2. Media was changed two times per week and passaged at 80% confluency. All experiments used stem cell passage numbers between P1-P6.

2.2.3 Toxicity Assessment of Chamber Materials

SH-SY5Y stem cells were plated at a density of 5,000 cells/cm^2 in 60 mm petri dishes containing either approximately 5 µL of silver paste, approximately 50 µL of silver paste, approximately 5 µL of silicone glue, or approximately 50 µL of silicone glue. As a control, SH-SY5Y stem cells were seeded at a density of 5,000 cells/cm^2 in 60 mm petri dishes without silver paste or silicone glue. On day 3 and day 5, phase contrast images were taken of SH-SY5Y stem cells in each group. Images were taken in 3 areas per sample in the same field of view. Cell attachment, morphology, and proliferation were compared to the control group.

2.2.4. SH-SY5Y Cell Culture Media Conductivity Measurements

SH-SY5Y cell culture media containing a 50:50 composition of DMEM/F12 (Invitrogen Corp., Grand Island, NY), 10.0% fetal bovine serum (Invitrogen Corp.), and 1.0% penicillin-streptomycin (Invitrogen Corp.) was poured into a 10 cm petri dish. Electrodes were placed 5 mm apart and voltage was applied at 50 mV, 75 mV, 100 mV, 125 mV, 250 mV 300 mV, 400 mV and 500 mV at 20 Hz, 100 Hz, 1000 Hz, and 10,000 Hz frequencies. Current was measured through the chamber, graphed as current vs. voltage (I-V) and resistance was calculated as the slope of the graph. Resistivity was calculated as the resistance multiplied by cross-sectional area divided by length, and media conductivity was calculated as the inverse of resistivity and reported in S/m. The value of media conductivity was added to our COMSOL Multiphysics® electric field model (as described below). We assumed that the media conductivity did not vary between electrical stimulation treatments or between media changes.

2.2.5. Electric Field Modeling

Electric field strength modeling across the chamber was completed using the electrostatics module for stationary objects in COMSOL Multiphysics® (Burlington, MA), version 4.2, software. COMSOL

Multiphysics® approximates partial differential equations by finite element analysis methods. Electric field strength was calculated through equations:

$\nabla \cdot \boldsymbol{D} = \rho$; $\boldsymbol{D} = \varepsilon_0 \varepsilon_r \mathbf{E}$; $\boldsymbol{E} = -\nabla \boldsymbol{V}$; where **D** = electric field flux (V m); ρ = relative permittivity; ε_0 = electric constant = $8.85418782 \times 10^{-12}$ $F \cdot m^{-1}$; ε_r = dielectric constant; **E** = electric field strength (V/m), **V** = applied max voltage (A Ω). Briefly, the AC chambers were constructed using the COMSOL geometry feature. Chamber materials were either selected from the COMSOL Multiphysics® material library or created for the study. Materials utilized in the model included gold and cell culture media. The material properties were defined as follows: gold ($\sigma = 4.5 * 10^7$ S/m; ρ = 9.0) and SH-SY5Y neuron culture media (σ = 14.4 S/m; ρ = 78), where σ = materials' conductivity and ρ is the materials' relative permittivity (Eisuke Ishikawaa et al., 1997; Hyung-Kew L et al., 2005; Sun et al., 2009a). Conductivity of neuron culture media was measured. The waveform applied to the model was a 0.120 V 1 kHz, sine wave. The geometry was meshed as a coarse free tetrahedral then solved for voltage (mV), electric field strength (mV/m) and direction.

2.2.6 SH-SY5Y Stem Cell Seeding, Neural Differentiation & Field Application

For sterilization, AC chambers were soaked in 70% ethanol for 1 hour, washed 4 times with PBS, then exposed to ultraviolet light overnight in a laminar flow hood. The following day, SH-SY5Y stem cells were seeded at a density of 5,000 cells/cm^2 into AC chambers then connected to 22 gauge solid wire and placed in parallel with two additional chambers, allowing for multiple simultaneous sample stimulation. The chambers sat in one of six wells per tray, which were made from Teflon® (McMaster-Carr, Santa Fe Springs, CA). For neuron differentiation, 1 µM retinoic acid (RA) (Kim et al., 2008) and 50 ng/mL of nerve growth factor (NGF) (Oe et al., 2006; Price et al., 2006) was added to the media. Differentiating SH-SY5Y stem cells were exposed to either 120 mV 20 Hz, 120 mV 1000 Hz, or 500 mV 1000 Hz for 45 minutes over 9 days. All treatments occurred at 37°C. Prior to each treatment, the voltage across each chamber

was measured to verify correct field strength. As a control, SH-SY5Y stem cells were seeded into 60 mm cell culture dishes. 1 µM RA and 50 ng/mL NGF were added to the media.

2.2.7 Live-Dead Stain

On day 9 following stimulation, media was aspirated from the AC chamber, and a phosphate buffered saline solution containing 2 µM calcein AM and 4 µM EthD-1 (Invitrogen Corp., Grand Island, NY) was added directly to the neurons. Neurons were incubated at 37°C for 30 minutes. For detecting live cells, neurons were imaged with a fluorescence microscope using 494 nm and 517 nm filters. For detecting dead cells in the same field of view, a second image was taken using 528 nm and 617 nm filters. Images of the live and dead cells were overlayed using ImageJ (National Institutes of Health, Bethesda, MD, USA). Differentiated unstimulated SH-SY5Y neurons were used as a positive live control. As a dead negative control, SH-SY5Y neurons were soaked in ethanol for 10 minutes, then stained using the calcein and EthD-1 working solution.

2.2.8 Real time-Polymerase Chain Reaction (RT-PCR)

On day 3, day 6, and day 9, media was removed from the AC chambers and neural differentiating SH-SY5Y stem cells were trypsinized, resuspended in cell culture media, then centrifuged at 1250 rpm for 5 minutes. Following centrifugation, the supernatant was removed, cells were lysed in 1 mL of trizol (Invitrogen Corp, Grand Island, NY) then stored at -80°C. mRNA was collected using the Qiagen RNEasy Extraction kit (Qiagen, Valencia, CA). mRNA was converted to cDNA using the PTC-100 Programmable Thermocontroller (MJ Research, Inc., Waltham, MA). cDNA was amplified with the TaqMan Universal PCR Master Mix (Applied Biosystems, Foster City, CA) and the ABI Prism 7000 Sequence Detection System (Applied Biosystems). RT-PCR determined gene expression levels of mid marker nestin (Applied Biosystems, Carlsbad, CA Assay ID #: Hs000120_s1) and late marker β3-tubulin (Applied Biosystems, Carlsbad, CA Assay ID #: Hs00801390_s1). TaqMan® gene expression assays were purchased through

Applied Biosystems (Carlsbad, CA). Relative gene expression was normalized to the housekeeping gene GAPDH (Assay ID #: Hs99999905_m1) and calculated using the formula $2^{(\text{Ct value of GAPDH} - \text{Ct value of gene of interest})}$ as previously used in our lab (Mauney et al., 2007) and recommended by the manufacturer (Perkin Elmer User Bulletin #2, Applied Biosystems, Foster City, CA). The threshold cycle (Ct) was selected in the linear range of fluorescence for all genes. Sample size is n = 6.

2.2.9 Immunostaining

AC Chambers containing SH-SY5Y differentiating neurons were fixed at room temperature for 30 minutes in 4% paraformaldehyde then permeabilized for 5 minutes in 0.3% triton X-100 and PBS. Following permeabilization, samples were incubated at 37°C for 2 hours with a primary rabbit anti-mouse β3-tubulin antibody (Sigma-Aldrich, St. Louis, MO) in 10% fetal bovine serum and PBS. Following incubation with the primary antibody, samples were washed 3 times in PBS then incubated at room temperature for 30 minutes with a secondary antibody, a fluorescein isothiocyanate (FITC) – conjugated goat anti-rabbit IgG (Sigma-Aldrich, St. Louis, MO). Following incubation of the secondary antibody, samples were washed three times in PBS and imaged in distilled water using a Leica DMIL fluorescence microscope (Leica, Wetzlar, Germany) with 470 nm $\pm$ 20 nm and 525 $\pm$ 25 nm filters. Staining was completed on day 3, day 6, and day 9. Six images were taken per group per time point. As a negative control, undifferentiated SH-SY5Y stem cells were seeded at 5,000 cells/cm^2 in 60 mm petri dishes, allowed to attach overnight, and stained.

2.2.10 Quantification of Axon Length

Axon outgrowth was quantified from programs written in MATLAB and graphed on day 3, day 6, and day 9. The number of cells quantified was n = 30 per group, per time point.

2.2.11 Quantification of Axon Branching

Axon branching was quantified on day 3, day 6, and day 9 as the number of branches stemming from the main axon. Sample size was n = 30, per group, per time point.

2.2.12 Statistical Analysis

RT-PCR measurements were reported as the mean $\pm$ 1 standard deviation. Axon length and axon branching was reported as the mean $\pm$ 1 standard error, $\sigma = \sigma/\sqrt{n}$. Standard error was used when reporting axon length and axon branching to take into account the large sample size. Statistical significance was reported in all cases using an unpaired two-tailed t-tests with a 95% confidence interval ($p < 0.05$).

2.3 Results and Discussion

2.3.1 Alternating Current (AC) Device Design

The AC chamber is imaged in **Figure 2.2B**. Chambers were scaled up for ease of stimulating multiple samples at once (**Figure 2.2C**). As electrodes are in direct contact with the media (**Figure 2.2B**), the mechanism of this device is the transfer of electric current to ionic current across the electrode-electrolyte interface(Hronik-Tupaj et al., 2011a). For the purpose of modeling an infinite electric field in 2D, the length of the gold electrodes was at least twice the distance between electrodes (**Figure 2.2A**). For an even field distribution between the electrodes, a straight electrode edge was fabricated. In the literature, it has been reported that several groups have constructed their own simple AC stimulation chambers, depending on the type of parameters, and requirements that are needed (Borschel et al., 2004; Fassina et al., 2007; Serena et al., 2008; Tandon et al., 2009a).

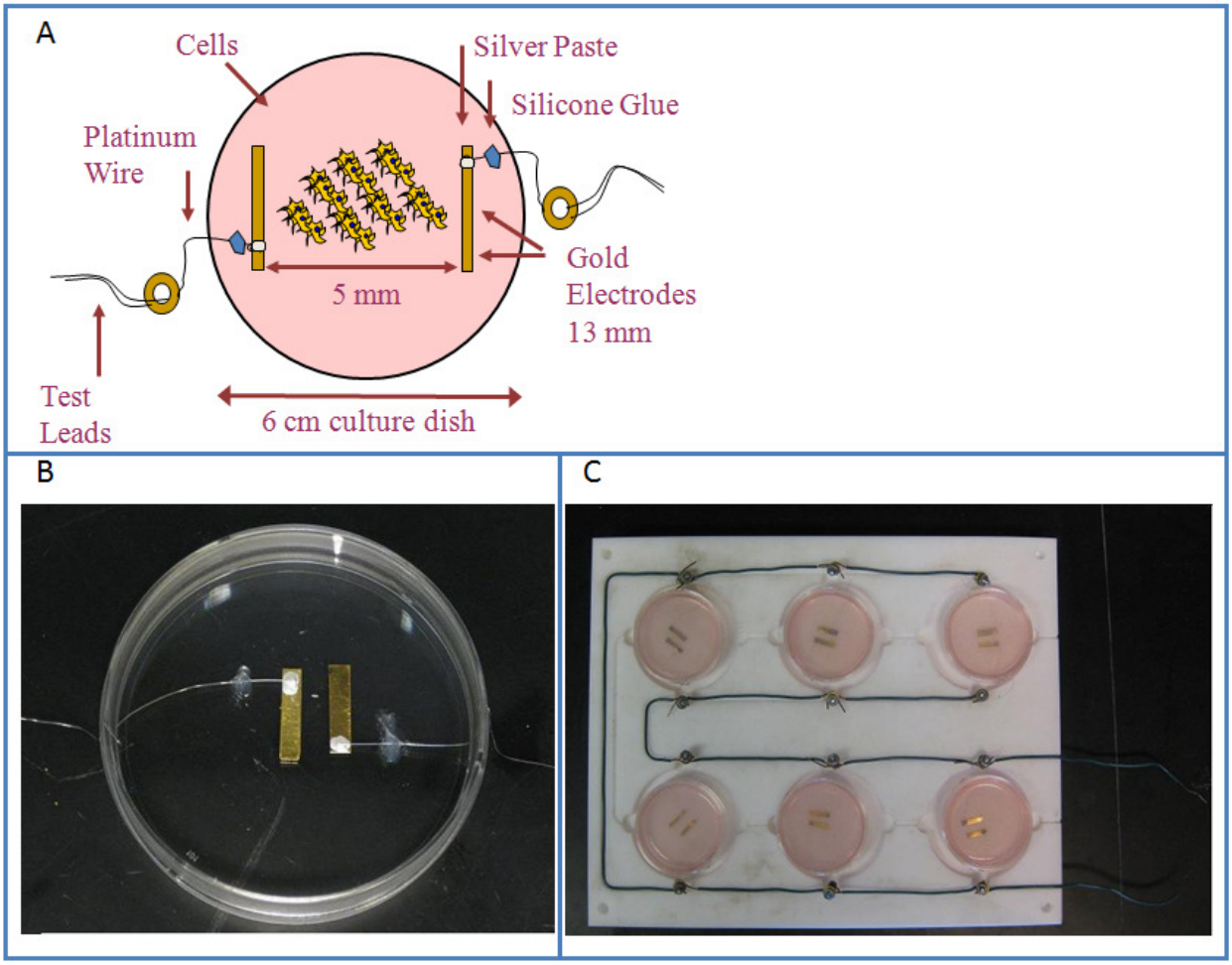

Figure 2.2: An AC Chamber for neural stimulation (a) Design of a Simple AC Stimulation Chamber (Dimensions labeled - Not drawn to scale). (b) Fabrication of a Simple AC Stimulation Chamber (c) Fabrication of Multi-well AC chambers (Hronik-Tupaj et al., 2011a).

2.3.2 SH-SY5Y Neural Stem Cell Culture & Differentiation

The SH-SY5Y stem cell line was utilized for the bioelectrical studies as it is a model system that is particularly sensitive for responding to environmental stimuli (Brunetti et al., 2010). Moreover, SH-SY5Y cells were used as axonal outgrowth and axon branching occurs gradually over a period of approximately 7-10 days (**Figure 2.3**), allowing for the ability to monitor axon outgrowth during electrical stimulation (Lopes et al., 2010).

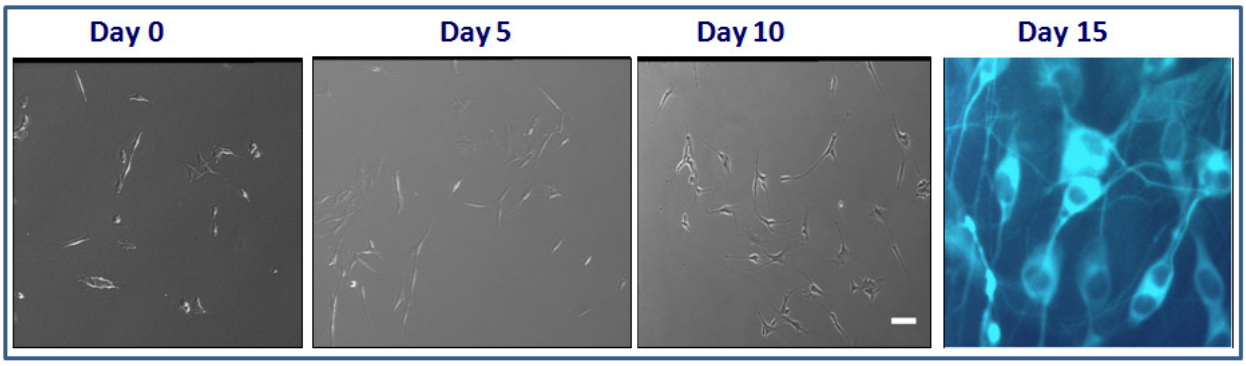

Figure 2.3: SH-SY5Y Stem Cell culture and SH-SY5Y Neural Cell Differentiation. The day 15 image shows an immunostain of neural marker β3-tubulin to confirm the presence of nervous tissue. Scale bar is 100 µm (Images by Marie Tupaj, Data Unpublished, 2010).

2.3.3 Material Toxicity on SH-SY5Y Stem Cells

SH-SY5Y stem cells are attached and proliferating between day 2 (**Figure 2.4A**) and day 5 (**Figure 2.4B**) in cell culture dishes containing either approximately 5 µL of silver paste, 50 µL of silver paste, 5 µL of silicone glue, or 50 µL of silicone glue. By observation, on day 5, there are less SH-SY5Y cells in the dishes containing the 5 µL of silver paste and the 50 µL of silver paste than in the control group (**Figure 2.4A-C**). From examining the live-dead stain results, SH-SY5Y cells in all groups express viability over 5 days in culture (**Figure 2.4C**). From these results, it can be suggested that the amount of silver paste and silicone glue utilized may be an important to consider for avoiding cell toxicity. Many past studies have reported the use of silicone glue, and silver in biomedical devices, such as dressings and creams, scaffolds, and electrode tips (Chuangsuwanich et al., 2011; Kawada et al., 2002; Selimovic et al., 2011; Xing et al., 2011).

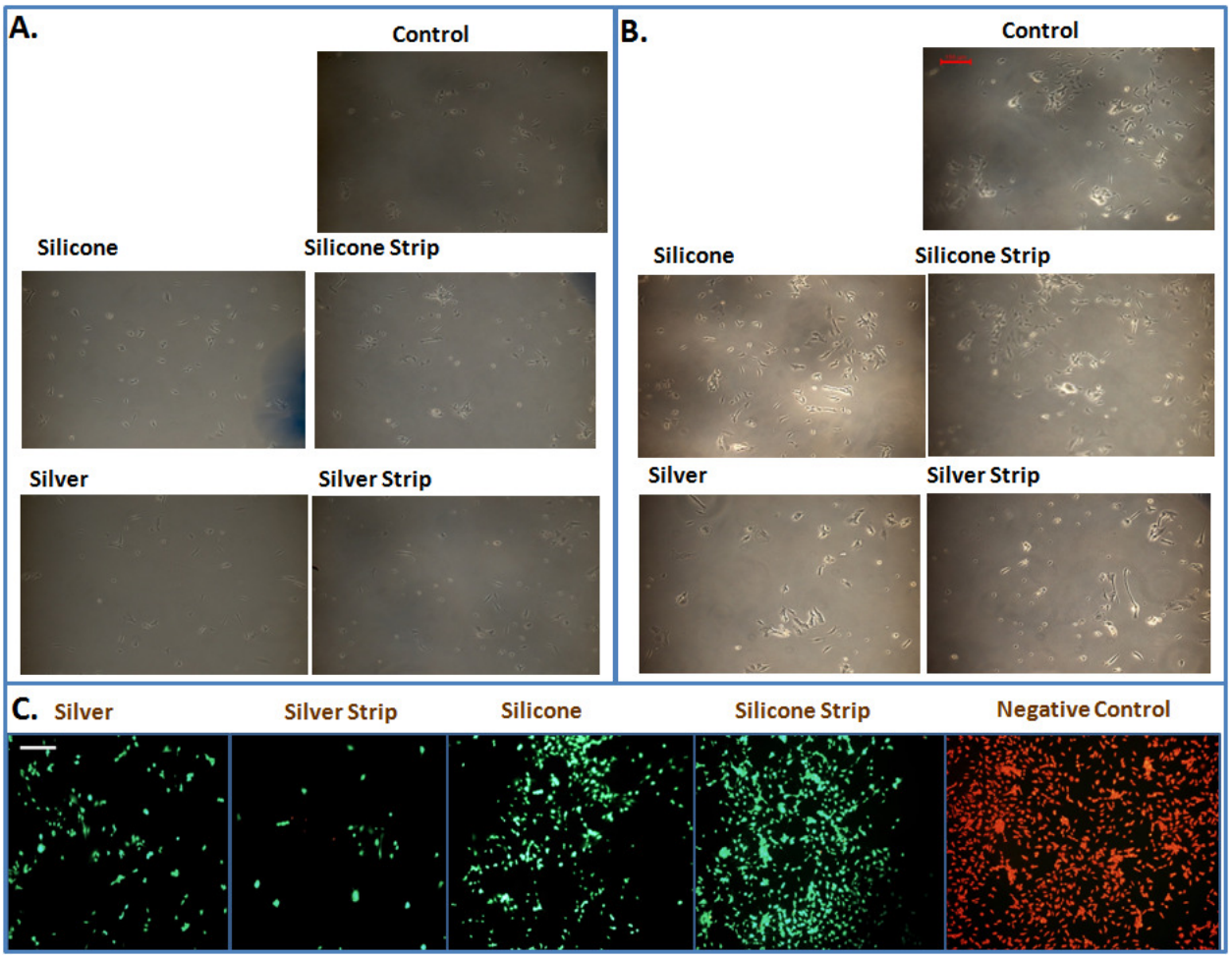

Figure 2.4: Toxicity Study Results. Images of SH-SY5Y stem cell attachment and proliferation on (a) day 2 & (b) day 5 in culture. Red scale bar is 150 µm. (c) Images of SH-SY5Y stem cell viability on day 5 in culture. White scale bar is 150 µm.

2.3.4 Conductivity Measurements

SH-SY5Y media conductivity was 7.52 S/m, 11.7 S/m, 14.4 S/m and 91.7 S/m at 20 Hz, 100 Hz, 1 kHz, and 10 kHz, respectively (**Figure 2.5**). SH-SY5Y media conductivity measurements were proportional to increasing frequency. Increases in conductivity according to increases in frequency are due to the capacitive effect at the electrode-electrolyte interface.

Conductivity is a measure of all the anion and cations in solution. Changes in media conductivity may also indicate a change hydrogen cation concentration, thus a change in pH level. pH changes will be discussed more in Chapter 6.

A.

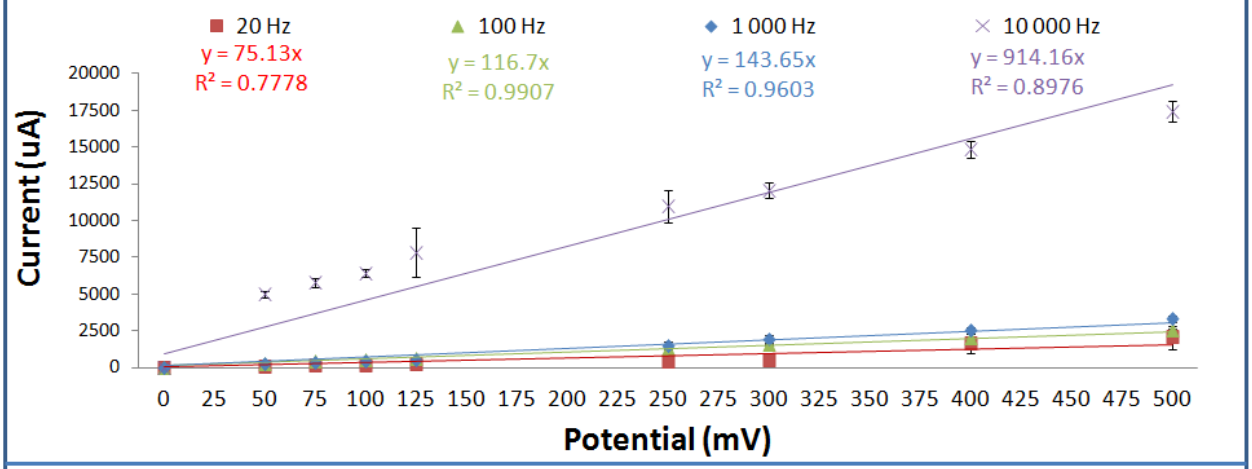

B.

Sample	20 Hz (50% duty cycle)	100 Hz (50% duty cycle)	1000 Hz (50% duty cycle)	10 000 Hz (50% duty cycle)
Resistance (Ω)	$13.3 * 10^{-6}$	$8.57 * 10^{-6}$	$6.96 * 10^{-6}$	$1.09 * 10^{-6}$
Cross-Sectional Area (m^2)	$50 * 10^{-6}$	$50 * 10^{-6}$	$50 * 10^{-6}$	$50 * 10^{-6}$
Length (m)	$5 * 10^{-3}$	$5 * 10^{-3}$	$5 * 10^{-3}$	$5 * 10^{-3}$
Resistivity (Ohm·m)	0.133	0.0857	0.0696	0.0109
Conductivity (S/m)	7.52	11.7	14.4	91.7

Figure 2.5: SH-SY5Y Media Conductivity Measurements (a) Current vs. Voltage (I-V) graph of neural media (b) Media conductivity calculations at 20 Hz, 100 Hz, 1 kHz, and 10 kHz.

2.3.5 Electric Field Modeling of AC Chamber

Modeling allows us to efficiently and accurately calculate and view several electrical parameters, including field strength and field direction, across the entire chamber. Below is a model of the applied voltage and the electric field strength across the entire chamber (**Figure 2.6A,B**). The maximum electric

field strength is 24 mV/mm between the electrodes when applying a 120 mV 20 Hz signal and a 120 mV, 1 kHz signal. The maximum electric field strength between the electrodes is 100 mV/mm when applying a 500 mV 1 kHz signal. Electric field strength between the gold electrodes is constant at the same chamber depth as noted by the arrow size. The applied parameters (field strength, frequency, time) were chosen according to similar field strengths as reported in the literature (Haastert-Talini et al., 2011; Hronik-Tupaj et al., 2011b; Koppes et al., 2011). As there have been few reported studies on neural electric field stimulation *in vitro*, parameters used for neural stimulation *in vivo,* and parameters used for electrical stimulation on other cells were considered for our studies. *In vivo*, hippocampal neurons have exhibited electric fields ranging from 0.5 mV/mm to 20 mV/mm depending on physiological condition (Ariza et al., 2010).

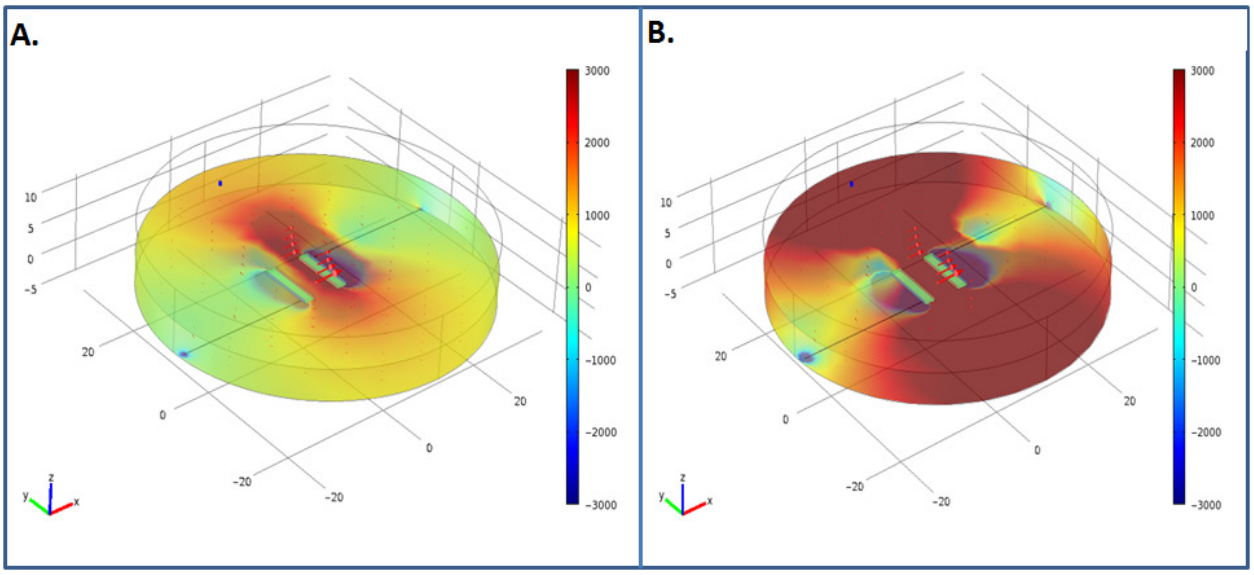

Figure 2.6 Electric Field Strength Models of AC Chamber (a) 120 mV 1 kHz (b) 500 mV 1 kHz. Color bar shows field strength (mV/cm). Red arrow shows electric field direction.

2.3.6 Gene Expression

Gene expression levels of nestin and β3-tubulin were quantified using RT-PCR on day 3, day 6 and day 9 following exposure to 120 mV 20 Hz, 120 mV 1 kHz, and 500 mV 1 kHz for 45 minutes each day (**Figure 2.7**). Nestin markers were upregulated ($p < 0.05$) on day 6 following exposure to 120 mV 1000 Hz (**Figure 2.7B**). β3-tubulin markers were upregulated ($p < 0.05$) on day 6 when exposed to 120 mV 1 kHz and 500 mV 1 kHz (**Figure 2.7E, 2.7F**). Gene expression levels of nestin and β3-tubulin were upregulated in most stimulation groups on day 3, day 6, and day 9 during differentiation. Nestin is a mid neural differentiation marker, an intermediate filament that identifies neuroepithelial cells (Reynolds et al., 1992b).

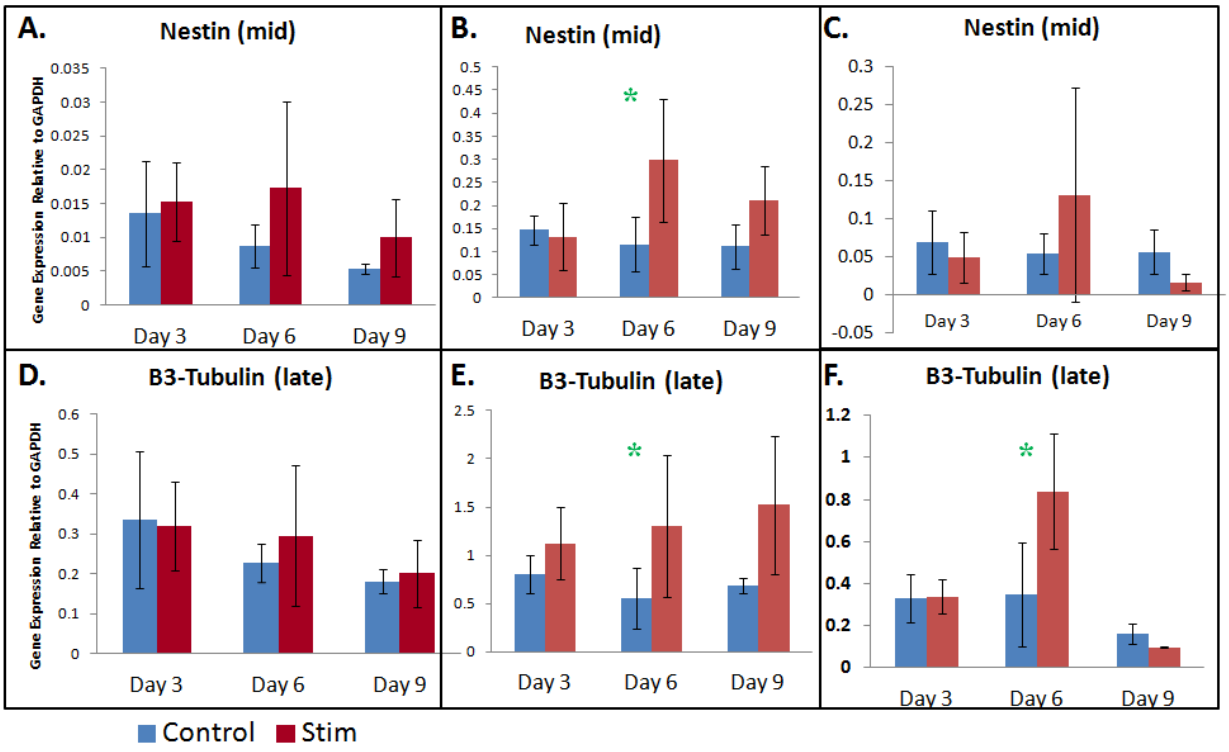

Figure 2.7: Neural Differentiation During Electrical Stimulation. Nestin gene expression levels following exposure to (a) 120 mV 20 Hz, (b) 120 mV 1 kHz, and (c) 500 mV 1 kHz on day 3, day 6, and day 9 during

neural differentiation. B3-tubulin gene expression levels following exposure to (d) 120 mV 20 Hz, (e) 120 mV 1 kHz, and (f) 500 mV 1 kHz on day 3, day 6, and day 9 during neural differentiation.

2.3.7 β3-Tubulin Protein Expression

While gene expression levels was examined in neural differentiating SH-SY5Y stem cells treated with moderate electrical stimulation, protein expression was also examined to observe whether levels of gene expression were translated to protein expression. **Figure 2.8** shows images of SH-SY5Y stem cells undergoing neural differentiation on day 3, day 6, and day 9. SH-SY5Y stem cells were immunostained for β3 tubulin. On day 9, undifferentiated SH-SY5Y stem cells were immunostained and imaged as a negative control (image not shown). From the images, it is observed that β3-tubulin expression increases between days 3 and day 6 in all groups. Axon length is also longer at the later time points. In addition, there are more cells expressing β3- tubulin on day 9 than on day 3.

Some neural *in vitro* studies have found increased axon outgrowth with electric field strengths ranging from 10 mV/mm to 100 mV/mm (Koppes et al., 2011). Other studies have shown differences in the applied electric field and regenerative potential at varying frequencies and duty cycles (Graves et al., 2011). Some studies have examined the effects of electric fields on cell proliferation, and noted varying effects (Ariza et al., 2010). In future experiments, assays examining cell proliferation following electric field stimulation would be interesting.

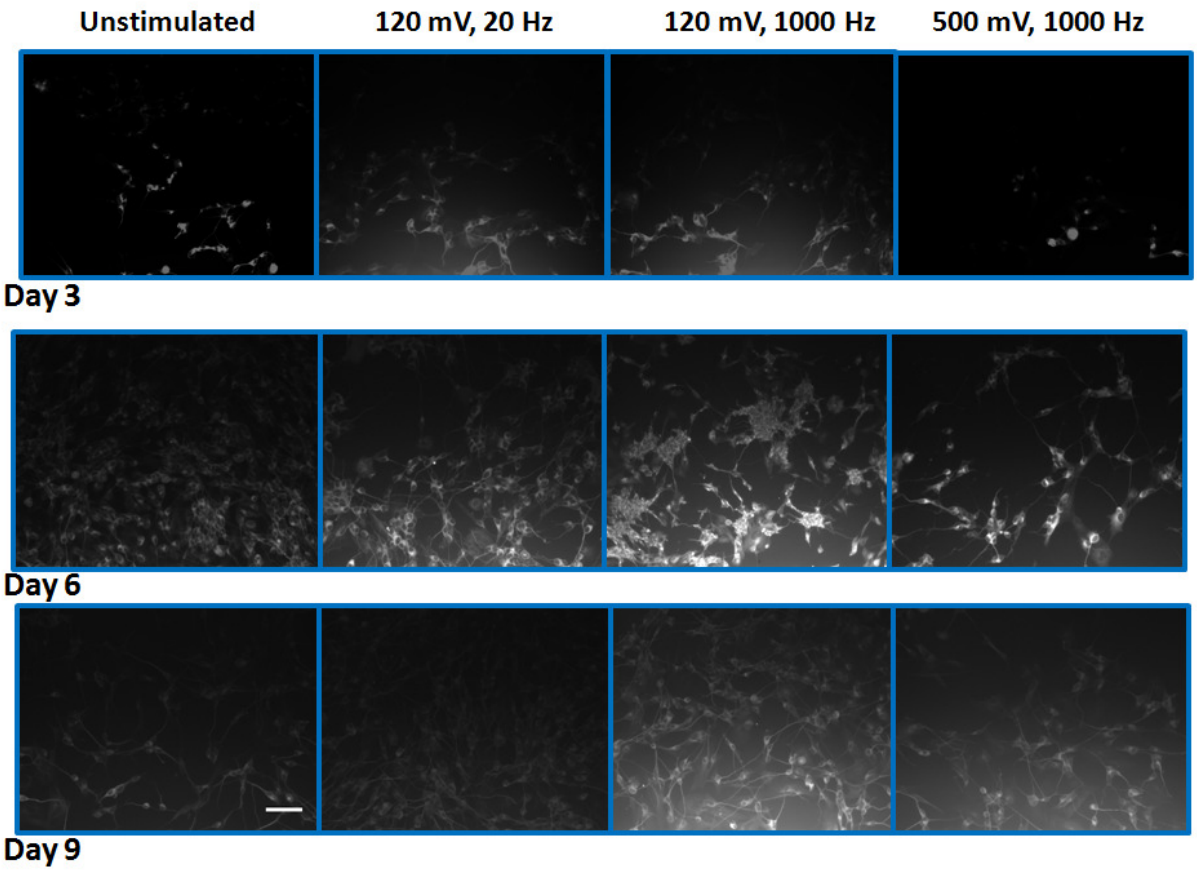

Figure 2.8: β3-Tubulin Expression on SH-SY5Y stem cells undergoing neural differentiation. Scale bar is 50 µm.

2.3.8 Quantification of Axon Outgrowth

From the fluorescent immunostain images, axon length was quantified on day 3, day 6, and day 9 (**Figure 2.9A**). Following 3 days of electrical stimulation, there were not any statistical differences ($p < 0.05$) in axon length between stimulated groups and the control group. On the 9th day of stimulation, axon length was greater ($p < 0.05$) following exposure to 120 mV 1 kHz compared to the control group. Possible mechanisms of electric fields stimulation on neural differentiation and axon outgrowth are described in Chapter 6.

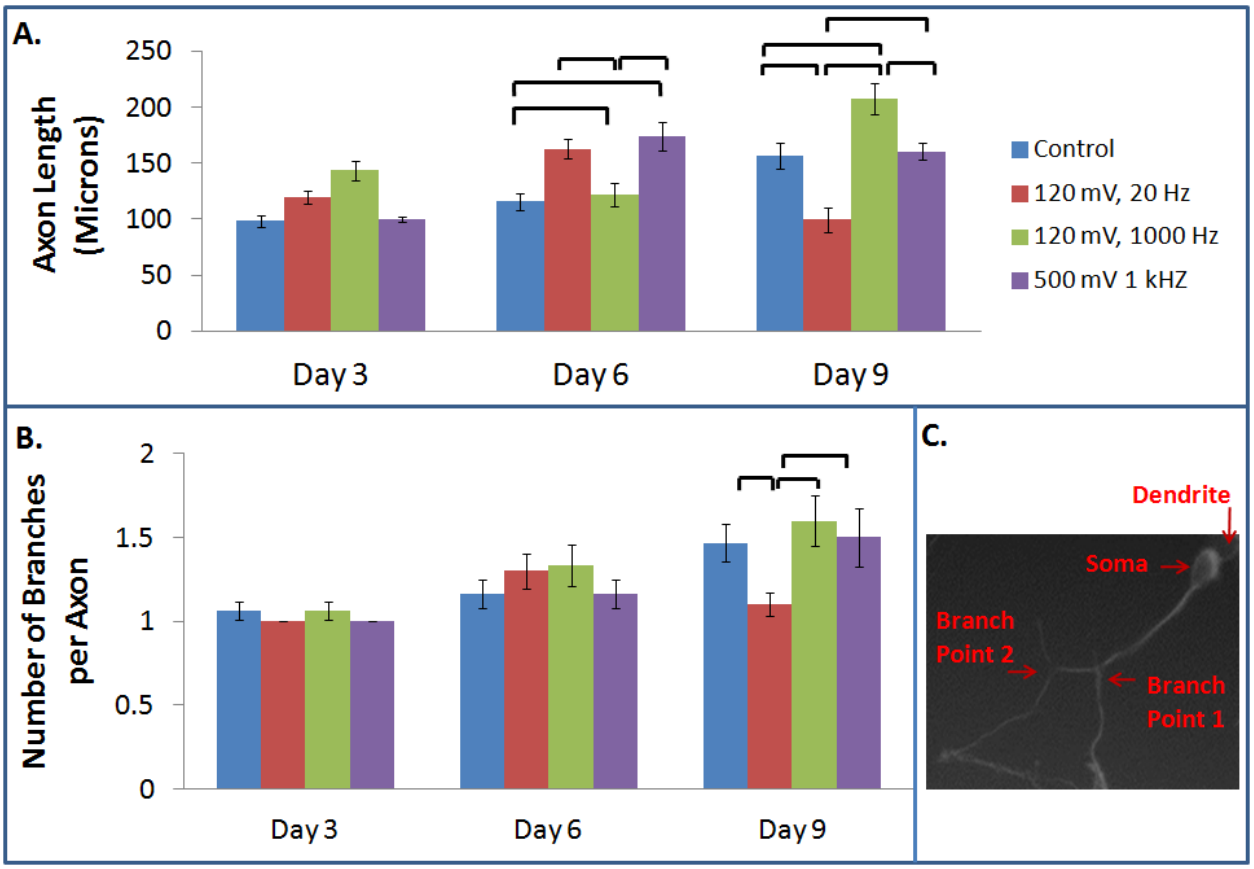

Figure 2.9: Axon Length and Branching (a) Axon length over 9 days in SH-SY5Y stem cells undergoing neural differentiation. Statistical differences are marked by a bracket ($p < 0.05$). (b) Axon branching over 9 days in SH-SY5Y stem cells undergoing neural differentiation. Statistical differences are marked by a bracket ($p < 0.05$). (c) Image of SH-SY5Y neuron with branches. Dendrite, soma and branch points are marked.

2.3.9 Quantification of Axon Branching

Axon branching occurs as a result of growth cone splitting. Over 9 days the average number of branches per axon increased in all groups (**Figure 2.9B**). On day 9, the number of axon branches was greater ($p < 0.05$) in 500 mV, 1 kHz, than in 120 mV, 20 Hz. Over 9 days, there were not any statistically significant differences between the control group and the stimulated groups in the number of axon branches. One paper that reported the effects of electric fields on neurite branching (McCaig, 1990) stated that electric

field polarization was an important factor in neural branching and that neural branching occurred towards the cathode.

2.3.10 Cell Viability

For assessing cell viability, a live-dead stain was completed on day 9 following electrical stimulation treatment (**Figure 2.10**). It was observed that SH-SY5Y neurons were viable in chambers and viable under all parameters.

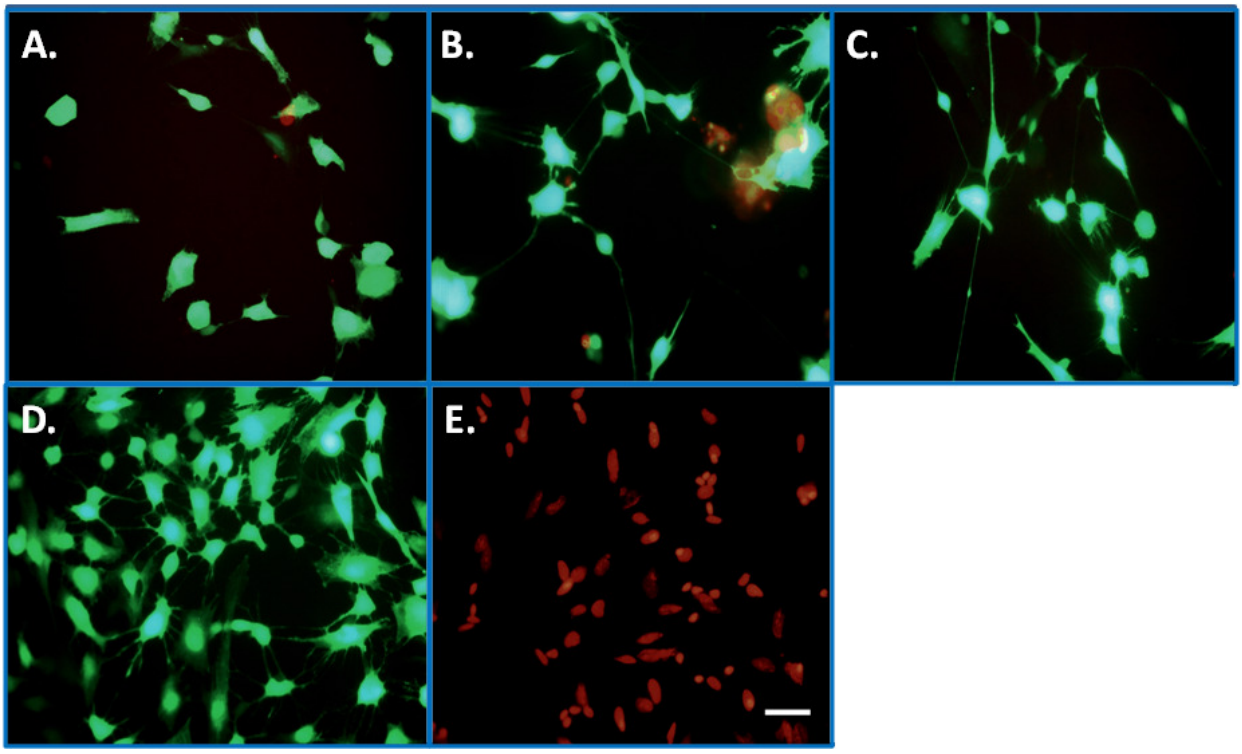

Figure 2.10: Cell Viability Following Exposure to 9 Days of Electrical Stimulation. (a) 120 mV 20 Hz (b) 120 mV 1 kHz (c) 500 mV 1 kHz (d) Unstimulated live control (e) Dead control. Live cells are stained in green. Dead cells are stained in red. Scale bar is 50 µm.

2.4 Conclusions

In conclusion, the silver and silicone toxicity studies did not reveal observable differences in SH-SY5Y stem cell numbers 2 days following plating. 5 days following stem cell plating, there were fewer SH-SY5Y stem cells observed in dishes containing the 50 μL silver. However, there were not any observable changes in cell morphology over this time. From these images, it was demonstrated that the silver and silicone materials were biocompatible in 5 uL and 50 uL quantities over a period of 5 days. As a result, these materials were also incorporated into some of our additional devices, as described in later Chapters.

Identifying optimal stimulation conditions is ciritical for ensuring cell viability and maximizing axon outgrowth. For these studies, it was determined that SH-SY5Y differentiating neurons were viable in the AC electric chambers and in the presence of electric field strengths of 24 mV/mm and 100 mV/mm for 45 minutes daily. It was shown that neural gene expression, specifically, mid marker nestin and late marker β3-tubulin, are upregulated by electrical stimulation. β3-tubulin markers were increased on day 6 ($p < 0.05$) at 24 mV/mm 1 kHz and at 100 mV/mm 500 mV 1 kHz compared to unstimulated groups. β3-tubulin protein expression was increased in all groups over all 9 days. Overall, axon length was greatest under the conditions of 24 mV/mm 1 kHz. Finally, we concluded that bioelectric stimulation is one option for enhancing neural differentiation and axon outgrowth. These studies provided information on optimal field strengths for use in future studies.

Chapter 3: BIOPHYSICAL STRATEGIES

3.1 Introduction

By 2012 an estimated 1.5 billion people will suffer from peripheral nerve injury in the U.S., Europe, and Japan due to complications from diabetic neuropathy, HIV, and chemotherapy (Report, 2003). For complete nerve regeneration, sprouting axons of the proximal stump need to align with and grow into the endoneurial tubes of the distal stump. When clinical intervention is required, biomaterials may be implanted at the site of injury for the purpose of axon regeneration and guidance.

It is well known that physical properties of a material, such as substrate topography, rigidity, charge, and wettability are valuable tools for influencing tissue regeneration (Brunetti et al., 2010). For directing cell alignment, strategies such as surface patterning and surface topographies have been investigated. Surface patterning has been utilized to align several cell types including fibroblasts, corneal epithelial cells, skeletal myoblasts, skeletal myocytes, stem cells, tenocytes, and neurons (Fujita et al., 2009; Gil et al., 2010; Kapoor et al., 2010; Lawrence et al., 2009; Wang et al., 2010b). Surface topographies have also been utilized for aligning extracellular matrix proteins, such as collagen (Kapoor et al., 2010). Surface topography size has been reported to range from the nanometer to micrometer scale (**Table 3.1**).

For directing and aligning nerve cells, topographies, such as grooves, holes, aligned fibers, and roughness have been tested (Hoffman-Kim et al., 2010). For example, in one study, lines (i.e., ridges, grooves) 2 µm and 200 nm thick, and holes 2 µm and 200 nm thick demonstrated increased axon formation and axon extension in hippocampal neurons compared to neurons on smooth surfaces (Fozdar et al., 2010a, b). Results showed that neurons preferred 200 nm thick features over 2 µm features for alignment (Fozdar et al., 2010a, b); In addition, neurons preferred circular features over lines (Fozdar et al., 2010a, b). Surface features, such as lines, have been more helpful for axon polarization than chemical cues, such as ligands (Gomez et al., 2007a).

The addition of roughness to smooth surfaces is another option utilized for directing neuron growth. One study reported that the amount of focal adhesion complexes of SH-SY5Y neurons varies following exposure to varying nanometer roughness (Brunetti et al., 2010). Focal adhesion complexes are 5 – 200 nm in size and are responsible for neuron attachment to substrates.

Microchannels have also played a part in directing neuron growth. Specifically, spiral ganglion neurons were plated on hexyl methacrylate (HMA) and 1,6-hexanediol dimethacrylate (HDDMA) channels having grooves of 50 µm width and channel depths of 0.6 - 1.0 µm (Clarke et al., 2011). By day 2, spiral ganglion grew within the grooves of the channel (Clarke et al., 2011). Interestingly, neurons from explants turned in the direction of the groove (Clarke et al., 2011). The degree of turn was dependent on the angle of the pattern from the explants (Clarke et al., 2011). Another avenue for increasing alignment, poly-L-lactic acid (PLLA) electrospun fibers, nanometer and micrometer in diameter, have demonstrated the ability to align sensory and motor neurons 24 hours after plating (Leach et al., 2011).

The field has begun to incorporate electrospun fibers and patterns into guidance channels (Li et al., 2007b; Madduri et al., 2010c; Sun et al., 2010; Yucel et al., 2010a). In particular, fibers and patterns have been able to align nerve cells in nerve guidance channels (Sun et al., 2010; Yucel et al., 2010a). Specifically, it was found that patterns of small ridges (5 µm width) and larger grooves (20 µm width) favored alignment (Sun et al., 2010). However, to date, few *in vitro* or *in vivo* studies have been completed with surface modified nerve guidance channels.

In the following set of experiments, our goal was to incorporate a range of surface topographies into *B. mori* silk fibroin, then study the effects on p19 neuron outgrowth and alignment. The surface topographies examined included patterned silk fibroin films and electrospun silk fibroin fibers. Silk fibroin films had pattern dimensions of 40 µm width grooves, 3.5 µm width grooves having 50 nm - 350

nm depths, or 3.5 µm width grooves having 400 nm - 500 nm depths. Electrospun silk fibers were spun as aligned low density fibers, aligned high density fibers, unaligned low density fibers, and unaligned high density fibers.

Table 3.1: Surface Topographies Utilized for Neuron Alignment

Shape	**Size**	**Surface or Biomaterial**	**References**
Lines, holes	2 µm, 300 nm	Quartz	(Fozdar et al., 2010b) (Fozdar et al., 2010a)
Roughness	35-100 nm	Gold	(Brunetti et al., 2010)
Microchannels	1-2 µm wide; 400-800 nm deep 50 µm wide; 0.6 – 1.0 µm deep	Methacrylate Polydimethylsiloxane (PDMS)	(Clarke et al., 2011; Gomez et al., 2007b)
Electrospun Fibers	Micron, nanometer	Poly(epsilon-caprolactone); Poly lactide	(Hong et al., 2010; Leach et al., 2011)
Channels (with fibers, patterns, pores incorporated)	1.5 mm diameter	Poly (e-caprolactone) Polyester	(Hong et al., 2010; Sun et al., 2010; Yucel et al., 2010a)

3.2 Materials and Methods

3.2.1 Silk Fibroin Purification

Silk fibroin solution was purified from Japanese *Bombyx mori* cocoons as described previously (Kang et al., 2009; Kim et al., 2005). Briefly, cocoons were cut, boiled for 30 minutes in Na_2CO_3 for sericin removal, washed in deionized water, and dried overnight. The following day, silk fibroin fibers were dissolved in lithium bromide at 60°C for 4-6 hours. Dissolved silk fibroin was injected into 3,500 MW dialysis cassettes (Thermo Fisher Scientific Waltham, MA). Dialysis was performed in deionized water for two days. Following dialysis, silk solution was removed from cassettes and centrifuged twice at 9,000 rpm at 4°C for 20 minutes. Following centrifugation, 1 mL of fibroin solution was dried in a 60°C oven.

The dried solution was weighed for measuring silk fibroin concentration. This process resulted in a final concentration of purified silk fibroin solution 6-8% weight by volume (w/v).

3.2.2 Electrospun Silk Fibers

Six – eight percent silk fibroin solution was mixed in an 80/20 (v/v) ratio with a 5% polyethylene oxide (PEO) solution, then poured into a 20 mL syringe. The 20 mL syringe was placed in a Sage Syringe Pump (Thermo Fisher Scientific Waltham, MA) that flowed the silk solution at 5-10 µL/min through a 16 gauge stainless steel capillary tube. To spin silk fibers, the 80/20 silk/PEO solution was subjected to a 9 $\pm$ 2 kV voltage. Silk fibers were electrospun at room temperature, 20-22°C, at approximately 20% humidity. To minimize fiber beading, the silk/PEO solution was stored at 4°C until directly before spinning.

For creating low density aligned fibers and high density aligned fibers, silk fibers were spun on to a rotating wheel for 1 minute or 5 minutes, respectively. Unaligned low density fibers and unaligned high density fibers were created by depositing electrospun silk fibers directly onto glass coverslips that were connected to the ground plate (**Figure 3.1**). Unaligned low density fibers were spun for 1 minute, while unaligned high density fibers were spun for 1 hour. Following electrospinning, fibers were methanol treated then dried overnight to induce beta-sheet formation.

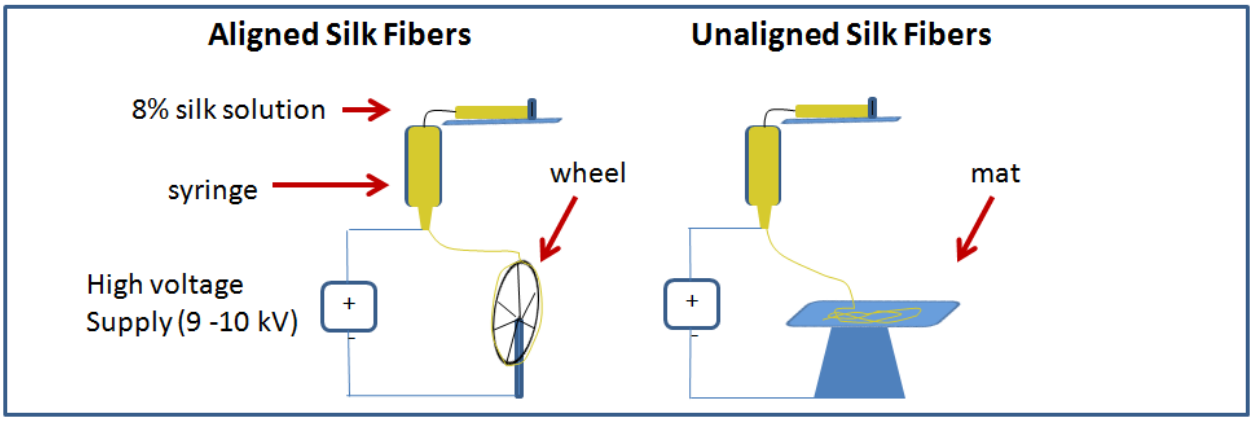

Figure 3.1: Fabrication of electrospun silk fibers (left) Setup for electrospinning aligned low density and aligned high density fibers (right) Setup for electrospinning unaligned low density and unaligned high density fibers. (Images by Marie Tupaj, Unpublished, 2010)

3.2.3 Fabrication of Patterned Silk Films

Surface patterns were created through laser etching 40 µm width patterns, 'Pattern H' and 'Pattern I' into a glass. 'Pattern H' had a 3.5 µm width and 342 nm ± 18.0 nm depth. 'Pattern I' had a 3.5 µm width and 500 nm depth. Dimensions were chosen based on what has been tried previously in our lab for successful alignment on human corneal fibroblasts (Gil et al., 2010).

For mold fabrication of the grooved glass surfaces, a polydimethylsiloxane (PDMS) mixture was prepared by mixing a base and a curing agent (Ellsworth Adhesives, Germantown, WI) in a 9:1 ratio (w/w) and poured over the grooved glass slides. The PDMS mold was dried at 60°C for 2-3 hours before being peeled from the grooved glass slide. For patterned silk film fabrication, a 6 - 8% silk solution was poured over the grooved PDMS mold and allowed to dry slowly for 1 - 2 days. Once dried, silk film patterns were peeled off the mold then treated with methanol to induce β-sheet formation (**Figure 3.2**).

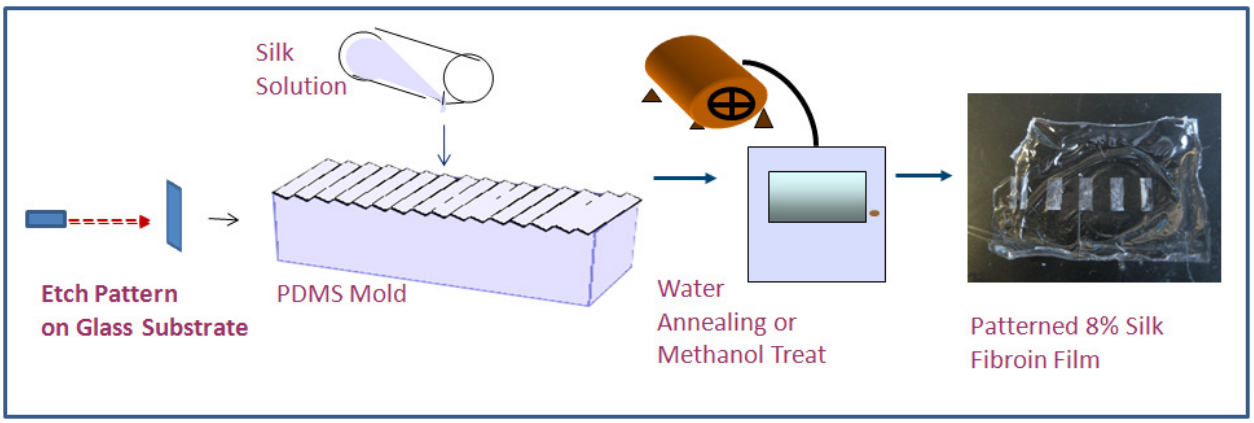

Figure 3.2: Patterned Silk Film Processing Methods (Image by Marie Tupaj, Unpublished, 2010)

3.2.4 p19 Stem Cell Culture

p19 stem cells (ATCC, Manassas, VA), originating from a mouse embryonic carcinoma cell line, were expanded in culture at a density of 5,000 cells/cm^2 using minimum essential media (Invitrogen Corp., Grand Island, NY) consisting of 7.5% calf serum (Thermo Fisher Scientific, Waltham, MA), 2.5% fetal bovine serum (Invitrogen Corp.), and 0.1% penicillin-streptomycin (Invitrogen Corp.). Cells were incubated at 37°C in 5% CO_2. Media was changed two times per week. p19 stem cells were passaged at 60-70% confluency and all experiments used stem cell passage numbers between P1-P3.

3.2.5 p19 Neuron Differentiation

p19 stem cells were plated at 5,000 cells/cm^2 into non-adherent dishes (Sigma-Aldrich, St. Louis, MO) using expansion medium containing 0.5 µM retinoic acid (Sigma-Aldrich, St. Louis, MO). On day three, floating p19 aggregates undergoing differentiation were collected and separated into a single cell suspension using 0.25% trypsin-EDTA and a polished glass Pasteur Pipette tip. Cells were replated into non-adherent dishes containing expansion media and 0.5 µM retinoic acid. On day 5, differentiated aggregates were collected, separated into single cells and stained with a 1,1'-dioctadecyl-3,3,3',3'-tetramethylindocarbocyanine perchlorate (DiI) (Invitrogen, Grand Island, NY) stain.

Briefly, DiI was diluted in culture media containing the differentiated neurons to a final concentration of 10 µM then incubated at 37°C for 30 minutes. Following incubation, diI stained p19 neurons were centrifuged at 1000 rpm for 5 minutes. The DiI containing cell culture media was aspirated and fresh neuron culture media was replaced. DiI works by diffusing through the cell membrane lipid bilayer and is non-toxic to cells over a period of 4 weeks in culture (Kuffler, 1990). DiI staining prior to cell seeding allows for the detection of cellular fluorescence without background fluorescence from the silk films or silk fibers.

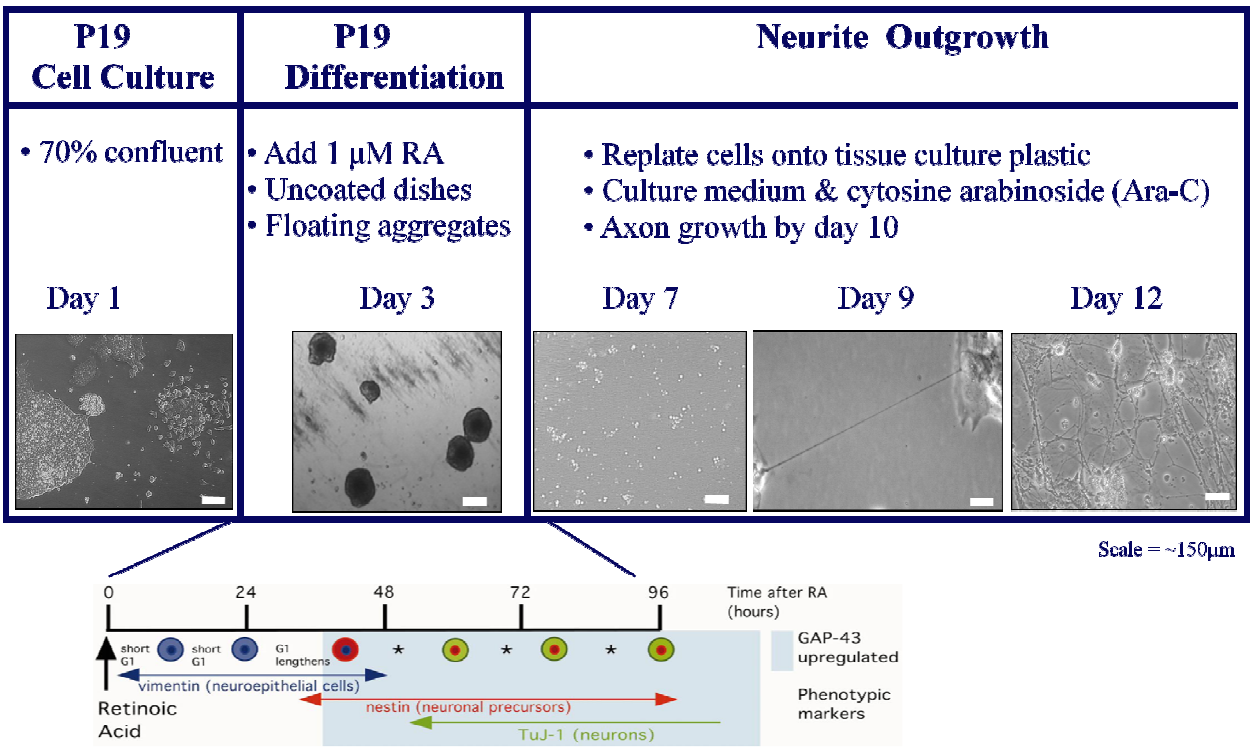

Figure 3.3: p19 Stem Cell Culture and p19 Neural Differentiation (top) 12 day overview of p19 stem cell culture, p19 neuron differentiation, p19 neurite outgrowth, and p19 network formation. Scale bar is 150 µm (p19 cell culture, p19 differentiation, and neurite outgrowth images by Marie Tupaj, unpublished data, 2008). (bottom) The 96 hour p19 neural differentiation process may be tracked by the percentage of vimentin, nestin, and tuj-1 expression in the cells. Vimentin is an early stage neural differentiation marker expressed in neuroepithelial cells. Nestin is a mid stage differentiation marker present in neural precursors. Tuj-1, otherwise known as β3-tubulin, is a late stage neuron differentiation marker. Tuj-1 is expressed in microtubules and is a common marker for identifying nervous tissue. Differentiation timeline by (Mani et al., 2001).

3.2.6 Surface Preparation and Neuron Seeding onto Patterned Silk Films and Electrospun Silk Fibers

To ensure sterilization, patterned silk films and electrospun silk fibers were soaked in 70% ethanol for 1 hour, washed 4 times with phosphate buffered saline (PBS), and then exposed overnight to ultraviolet

(UV) light in a laminar flow hood. To promote neuron attachment, sterilized silk films and sterilized electrospun silk fibers were placed in 6-well plates, then soaked for 1 hour in a 1 mM laminin (Sigma-Aldrich, St. Louis, MO) concentrated solution. After 1 hour, the laminin solution was aspirated and neuron culture media was added to the chamber. Laminin has been reported to increase neuron attachment to surfaces (Darmon, 1982; Smallheiser et al., 1984).

Following surface preparation, the DiI stained p19 neurons were plated at a density of 250,000 neurons/cm^2 on all silk films and electrospun silk fibers groups. p19 neurons were seeded on silk films that included 40 µm width patterned silk films, 'Pattern H' silk films, and 'Pattern I' silk films (n = 3). p19 neurons were seeded on electrospun silk fibers that included aligned low density fibers, aligned high density fibers, unaligned low density fibers, and unaligned high density fibers (n = 3). To remove any non-differentiated cells, 5 µg/ml cytosine arabinoside was added to the media the following day (Mani et al., 2000; Shen et al., 2004) (**Figure 3.3**).

3.2.7 Confocal Imaging

On day 3 following seeding, confocal images of dil stained p19 neurons seeded on 40 µm grooved films, 'Pattern H' silk films, 'Pattern I' silk films, aligned low density electrospun silk fibers, aligned high density electrospun silk fibers, unaligned low density electrospun silk fibers, and unaligned high density electrospun silk fibers were acquired using a two-photon ready Leica DM IRE2 confocal microscope (Leica, Wetzlar, Germany). Images were taken at 540 nm excitation and 565 nm emission using a 20x objective, numerical aperture 0.7. Images were taken of 3 samples per group, 3 images per sample.

For the neurons plated on the electrospun fiber groups, transmission images were acquired using a two-photon ready Leica DM IRE2 confocal microscope (Leica, Wetzlar, Germany) in the same field of view as the nerve cells. Confocal images and transmission images were overlayed to produce one image of the neurons and fibers.

3.2.8 Optical Microscopy

On day 3 following seeding, phase contrast images were taken of neurons seeded on 40 μm grooved silk films, 'Pattern H' silk films, and 'Pattern I' silk films silk films using an Axiovert S100 inverted microscope (Zeiss, Germany).

3.2.9 Axon Outgrowth Data Analysis and Statistics

Measurements of axon outgrowth, not including the soma, were completed through programs previously written in MATLAB (MathWorks, Natick, MA). Axon length was reported as the mean $\pm$ 1 standard error about the mean. At least 5 cells per image were quantified. Statistical significance was reported using unpaired two-tailed t-tests. For reporting a large number of comparisons between time points, the Bonferroni Correction factor was applied to correct for multiple comparisons of artifacts. For determining statistical significance using the Bonferroni Correction factor, alpha was set as $\alpha = 0.05/ 21 = 0.002$.

3.2.10 Axon Alignment Data Analysis and Statistics

Axon alignment was calculated as the angle, in degrees, between the groove or fiber and the axon. An angle of 0 degrees meant that the axon was parallel with the grooved film or fiber. An angle of 90 degrees meant that the axon was perpendicular to the grooved film or fiber. Angle of axon alignment was reported as the mean $\pm$ 1 standard error about the mean. Statistical significance was reported using unpaired two-tailed t-tests. For reporting a large number of comparisons between time points, the Bonferroni Correction factor was applied to correct for multiple comparisons of artifacts. For determining statistical significance using the Bonferroni Correction factor, alpha was set as $\alpha = 0.05/ 21 = 0.002$. To provide information on alignment over the neuron population, the angle of axon alignment from the grooved surface was graphed every 10 degrees as the percent of total neurons on silk film.

3.3 Results and Discussion

3.3.1 Fabrication of Electrospun Silk Fibers and Patterned Silk Films

Phase contrast microscopy images were taken of electrospun silk fibers (**Figure 3.4**) and silk films (**Figure 3.5**). Unaligned and aligned electrospun silk fibers are approximately 1 - 2 µm in diameter. Fiber density in the unaligned low density group is 7 fibers / (50 µm). Fiber density in the unaligned high density group is 16 fibers / (50 µm). Fiber density in the aligned low density group is 6 fibers / (50 µm). Fiber density in the aligned high density group is 24 fibers / (50 µm).

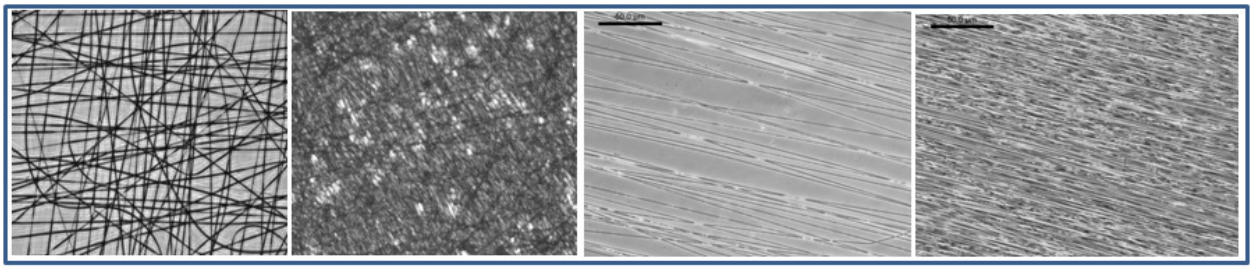

Figure 3.4: Electrospun silk fibers: (left – right) unaligned low density fibers, unaligned high density fibers, aligned low density fibers, and aligned high density fibers. Scale bar is 50 µm.

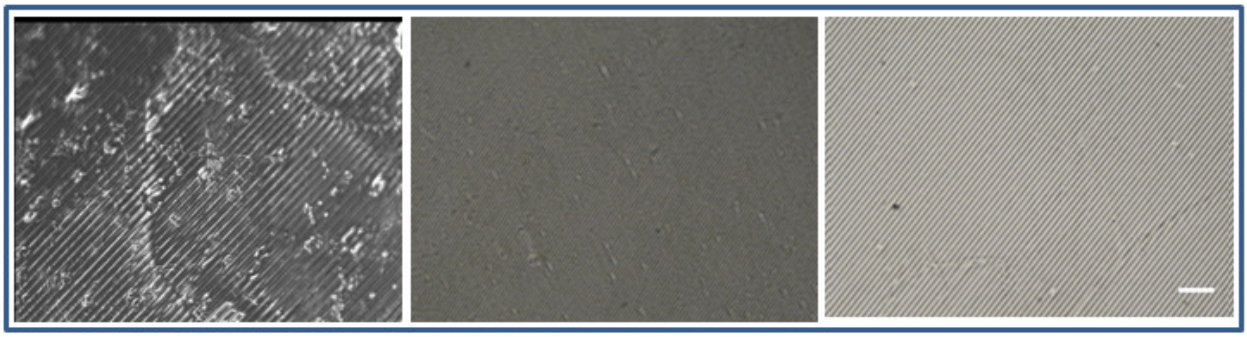

Figure 3.5: Patterned Silk Films: (left – right) 40 µm width grooves, 3584 nm width grooves having 342 nm depth, and 3.5 µm width grooves having 400-500 nm depth. Scale bar is 100 µm.

3.3.2 Images of p19 Neurons on Electrospun Silk Fibers

Confocal images were taken of dil stained p19 neurons on electrospun silk fibers (**Figure 3.6**). From the images, it was observed that neurons on aligned fibers had significantly longer axons than those on unaligned fibers. Furthermore, neurons seeded on low density aligned fibers appeared to have more elongated morphology than neurons on low density unaligned fibers. In the unaligned fiber group, some p19 neurons appear as if they may be attempting to follow along the fibers' curved ridges. Finally, there was little axon outgrowth observed on the high density unaligned fibers.

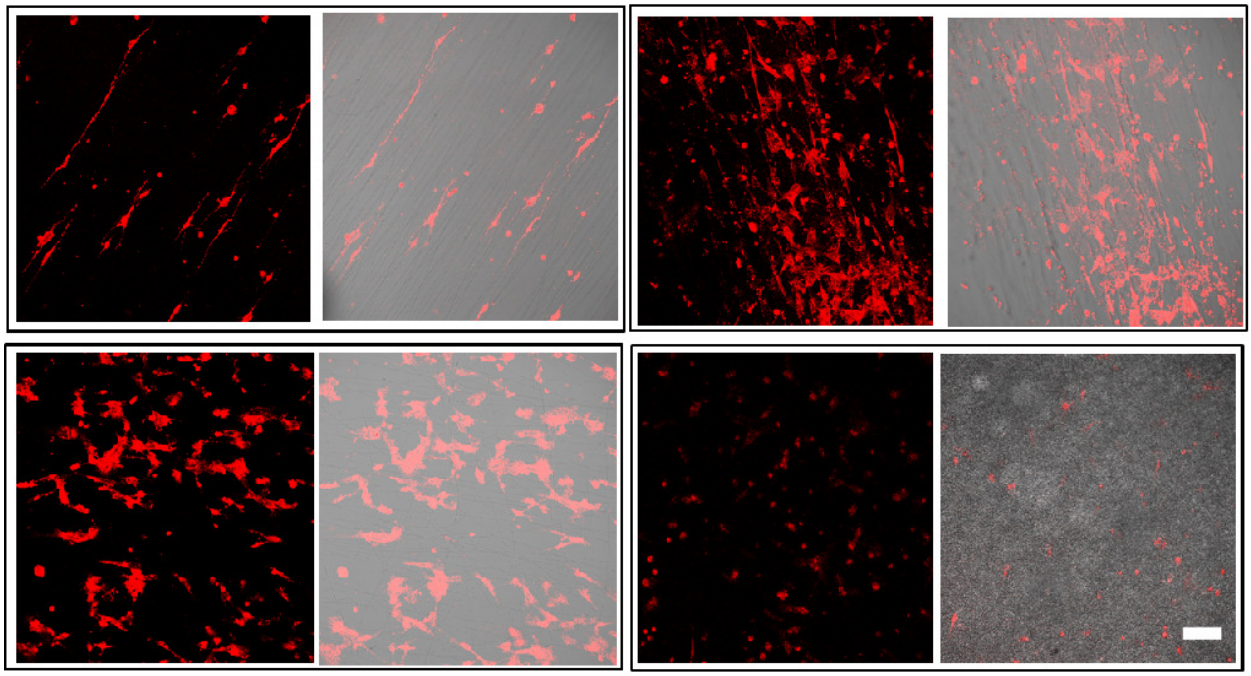

Figure 3.6: DiI stained p19 neurons on electrospun silk fibers 3 days after seeding: (top left) Aligned low density electrospun fibers, (top right) Aligned high density electrospun fibers, (bottom left) unaligned low density electrospun fibers, (bottom right) unaligned high density electrospun fibers. The left panel in each group is a confocal image of DiI stained p19 neurons only. The right panel in each group is an overlay image of DiI stained p19 neurons and a transmission image of the electrospun fibers. Scale bar is 100 µm.

3.3.3 Images of p19 Neurons on Silk Films

Confocal and phase contrast microscopy images were taken of the dil stained p19 neurons on silk films (**Figure 3.7**). Neuron cell bodies are approximately 10 µm in diameter and are observed to rest on top of the grooves, not between the grooves. p19 axon alignment on patterned films is in the direction of the grooves.

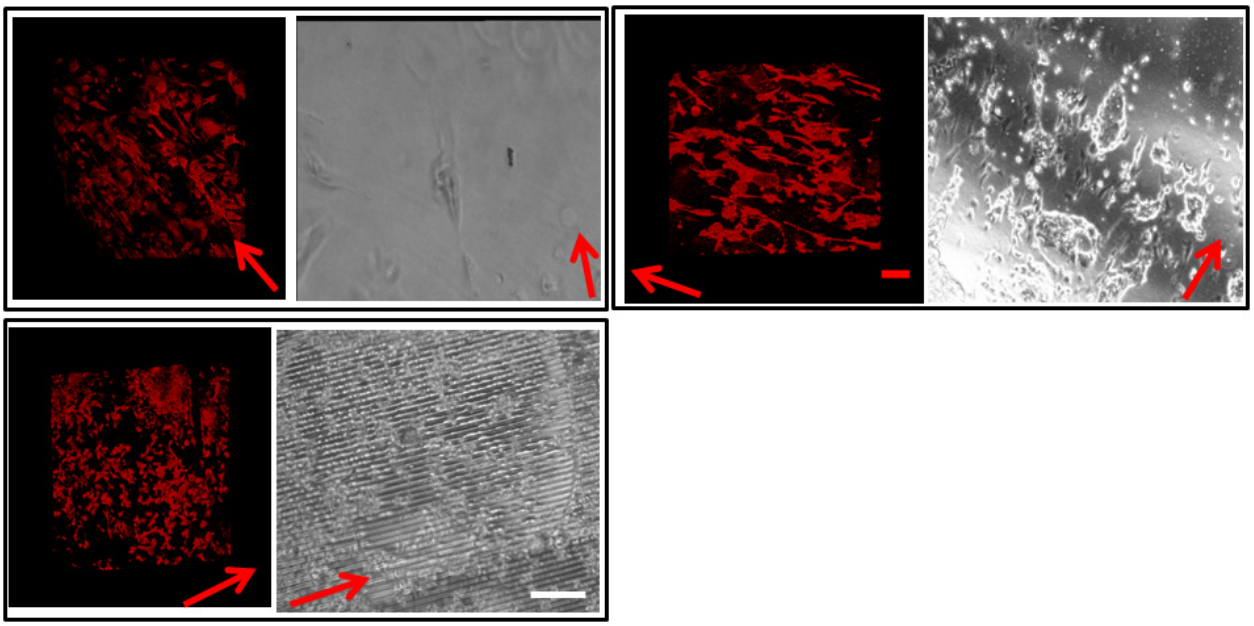

Figure 3.7: p19 neurons on 6-8% silk fibroin films 3 days after seeding. (top left) Neurons seeded on 'pattern H' silk films. (top right) Neurons seeded on 'Pattern I' silk films. (bottom left) Neurons seeded on 40 µm width grooved films (left panel) Confocal images of DiI stained neurons on silk films. (right panel) Optical microscopy images of neurons on silk films. Red scale bar is 100 µm and corresponds to all confocal images. White scale bar is 100 µm for all optical microscopy images. Red arrow shows the direction of the groove.

3.3.4 Axon Outgrowth on Patterned Silk Films and Electrospun Silk Fibers

On day 3 following seeding, average axon length were greater on electrospun silk microfibers compared to patterned silk films (**Figure 3.8**). Aligned low density electrospun silk fibers supported the greatest amount of axon outgrowth with average axon length of 45 µm. 'Pattern I' silk films supported the largest amount of neurite outgrowth of all silk film groups with an average axon length of 33 µm. There were not any statistical differences ($p < 0.002$) between neurons seeded on aligned low density fibers and the neurons on the 'Pattern I' films. There were statistical differences ($p < 0.002$) in axon length between the neurons seeded on aligned low density fibers and the neurons on the '40 um width' and 'Pattern H' films. It has been reported that the high surface area to volume ratio and topography of electrospun fibers mimics the extracellular matrix, which may promote axon outgrowth (He et al., 2010).

Within the silk film groups, the width of the groove had less of an effect on axon outgrowth

The spacing between the elecgtrospun fibers, defined as fiber density, also had an effect on axon outgrowth. Specifically, unaligned low density fibers, which had a fiber density of 7 fibers per 50 µm, supported more outgrowth ($p < 0.002$) than the unaligned high density fibers, which had a fiber density of 24 fibers per 50 µm (**Figure 3.8**). Aligned low density fibers also supported more outgrowth ($p < 0.002$) than aligned high density fibers (**Figure 3.8**).

Finally, the orientation of electrospun fibers had an effect on axon outgrowth. Aligned low density electrospun fibers supported significantly more outgrowth than unaligned high density fibers ($p < 0.002$) (**Figure 3.8**). Currently our aligned fibers are spun in one direction on a rotating wheel allowing for fiber crossing. Fiber crossing may impede axon growth. Creating highly aligned fibers may increase axon outgrowth even further (Lee et al., 2010a; Wang et al., 2009).

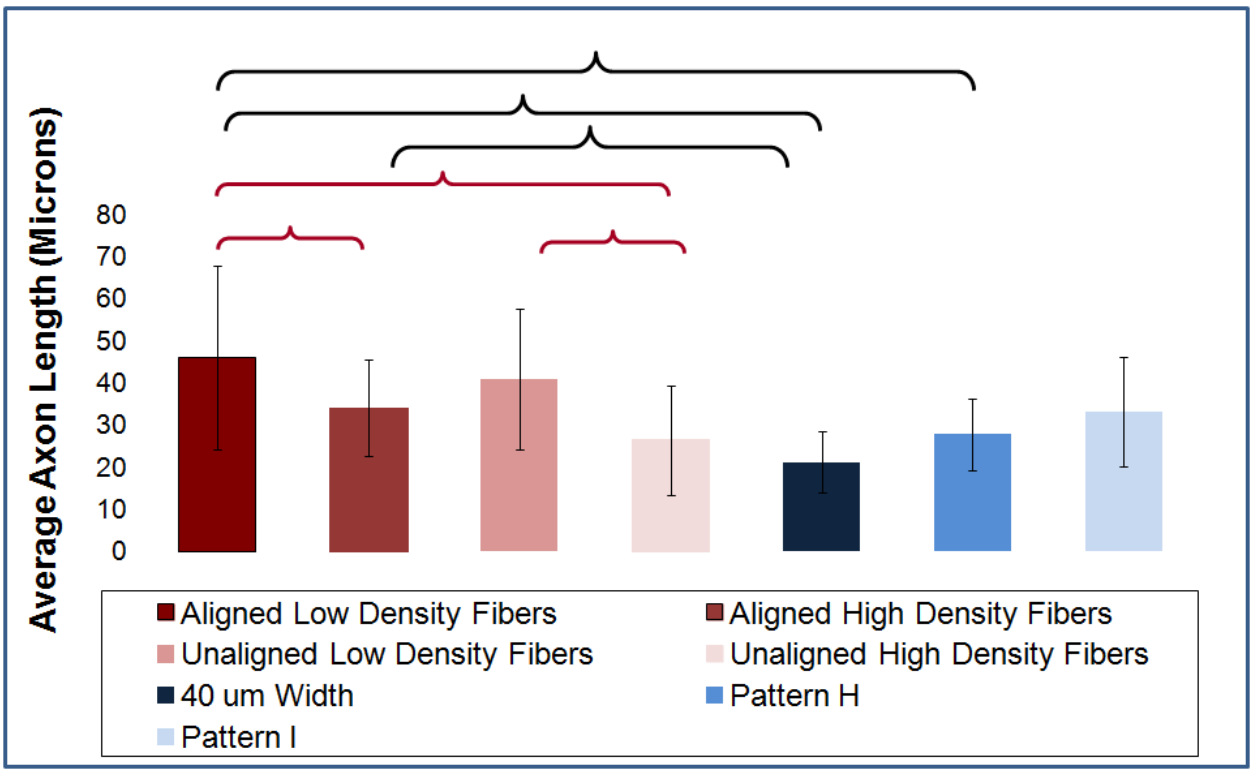

Figure 3.8: Average axon length on electrospun silk fibers and patterned silk films. The red bracket is statistical differences ($p < 0.002$) between fiber groups. The blue bracket is statistical differences between film groups ($p < 0.002$). The black brackets are statistical differences ($p < 0.002$) between both groups.

3.3.5 Axon Alignment on Patterned Silk Films and Electrospun Silk Fibers

Patterned silk fibroin films with grooves 3.5 µm wide and approximately 500 nm depth allowed for 57.7% axon alignment 0 - 10 degrees from the direction of the groove and 76.9% axon alignment 0 – 20 degrees from the direction of the groove (**Figure 3.9B**). p19 neuron axons plated on aligned low density electrospun fibers exhibited 53% alignment 0 – 10 degrees from the fiber and 90% alignment 0 - 20 degrees from the direction of the fiber (**Figure 3.9B**).

P19 neurons on low density electrospun fibers and 3.5 um width films were easy to quantify. It was more difficult to characterize alignment when axons were not grown since the neuron morphology exhibited more overall circularity.

P19 neurons aligned in parallel with the electrospun fiber or grooved silk film. However, width may have an effect on axon direction compared to the groove direction (Xie et al., 2009). It was reported that neurons aligned in parallel with grooves 2 um - 40 um and perpendicular to grooves that were 40um – 80 um (Xie et al., 2009).

While neurons exhibited alignment on electrospun fibers and patterned films, functionality may be of a concern. Neuron synapses and cell-cell communication, specifically action potentials, may be evaluated further through functional imaging or immunohistochemistry techniques.

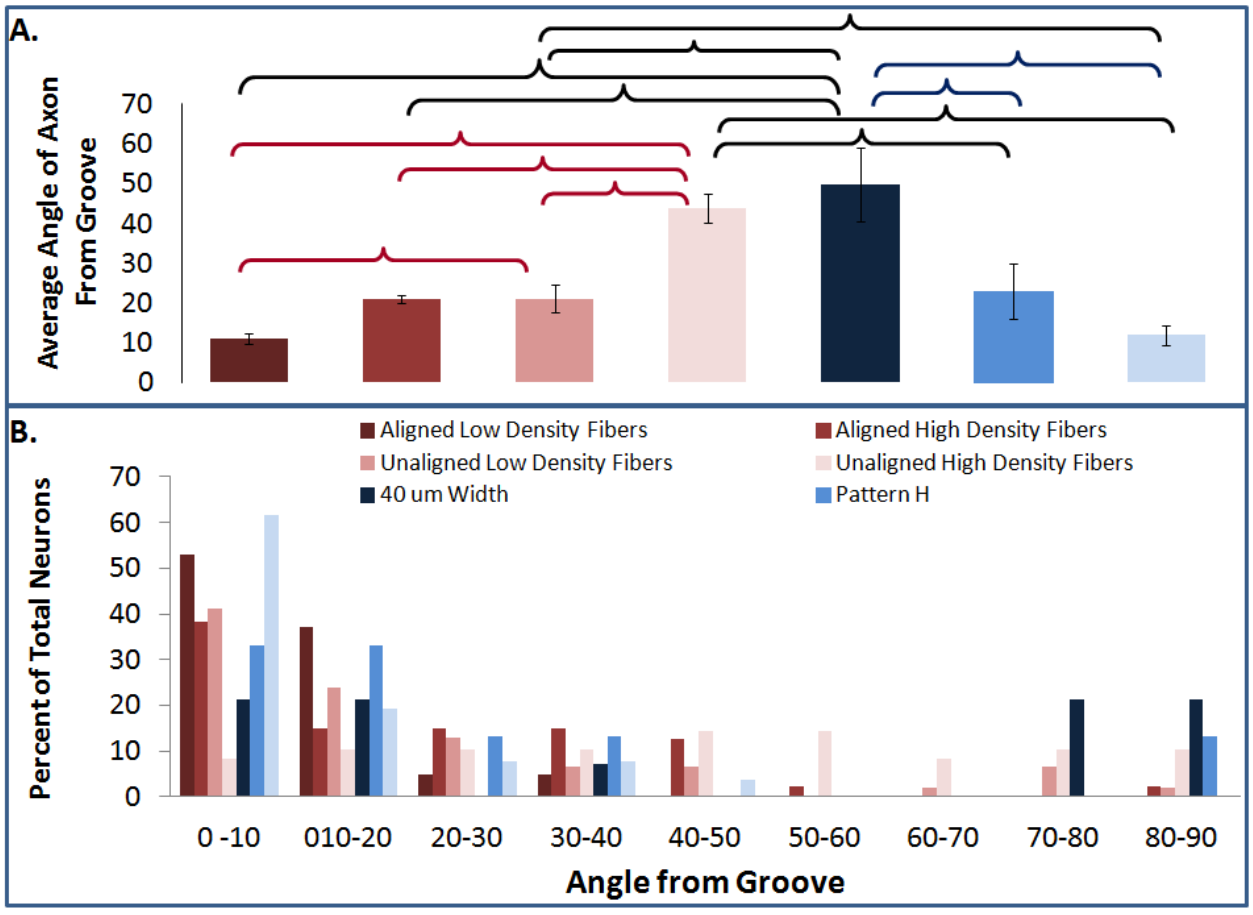

Figure 3.9: Axon alignment on electrospun silk fibers and patterned silk films 3 days after seeding. (a) Average axon alignment on day 3 following seeding. The red bracket is statistical differences ($p < 0.002$) between fiber groups. The blue bracket ($p < 0.002$) is statistical differences between film groups. The black brackets are statistical differences ($p < 0.002$) between both groups. (b) Axon alignment of p19 neurons seeded on electrospun fibers and patterned films is binned within every 10° from the groove on day 3 following seeding.

3.4 Conclusions & Future Directions

In conclusion, patterned silk films and electrospun silk fibers were useful tools for promoting axon outgrowth and axon alignment along the direction of the groove or fiber. On day 3 following seeding, average axon length were greater on electrospun silk fibers compared to patterned silk films. Specifically, aligned low density electrospun silk fibers supported the greatest amount of axon outgrowth with an average axon length of 45 μm. There were not any statistical differences ($p < 0.05$) between aligned low density fibers and 'Pattern I' silk films.

In regards to alignment, there were also not any statistical differences ($p < 0.05$) between aligned low density fibers and 'Pattern I' silk films. Patterned silk fibroin films with grooves 3.5 μm wide and approximately 500 nm depth allowed for 57.7% axon alignment 0 - 10 degrees from the direction of the groove and 76.9% axon alignment 0 – 20 degrees from the direction of the groove. p19 neuron axons plated on aligned low density electrospun fibers exhibited 53% alignment 0 – 10 degrees from the fiber and 90% alignment 0 - 20 degrees from the direction of the fiber.

Future directions include assessing outgrowth and alignment from altering fiber diameter. The addition of drugs and protein coatings may enhance axon outgrowth along fibers and silk films. The design of multi-layer films and fibers or the combination of films and fibers may be the next step for enhancing alignment or functionality.

Chapter 4: TOOLBOX INCORPORATION IN 2D: DESIGN, CHARACTERIZATION, AND NEURON RESPONSE ON PATTERNED SILK ELECTRONIC FILMS

4.1 Introduction

Peripheral nerve regeneration is a critical issue as 2.8% of trauma patients present with this type of injury (Uebersax et al., 2007). By 2012, an estimated 1.5 billion people will suffer from peripheral nerve injury in the U.S., Europe, and Japan due to complications from diabetic neuropathy, HIV, and chemotherapy (Report, 2003). During a time of war, 14-18% of injuries affect the peripheral nervous system altering both sensation and muscle function (Potucek et al., 2009). Clinical options for such injuries have changed only slightly in the last 30 years, with standard methods of treatment including suturing damaged nerve ends, grafting sensory nerves, and nerve transfers, with autografts as the gold standard (Belkas et al., 2004). Despite current treatments, only 10% of the patients regain complete functional recovery (Witzel et al., 2005).

Recent strategies investigated for repairing nerves include: (1) the addition of nerve growth factors, (2) stem cell and glial cell transplantation, (3) gene therapy, (4) functional electrical stimulation, and (5) natural and synthetic guidance channels (Lari et al., 2001; Murakami et al., 2003; Pan et al., 2007; Pan et al., 2006; Pollock, 1995). In addition, surface topographies, ranging from the nanometer to micrometer scale, such as grooves, aligned fibers, roughness, and pores, have been identified to help direct and align nerve cells (Brunetti et al., 2010; Clarke et al., 2011; Fozdar et al., 2010a, b; Gomez et al., 2007b; Hoffman-Kim et al., 2010; Hong et al., 2010; Leach et al., 2011). It is also known that electric fields have an impact on cell adhesion, proliferation, and differentiation (Akanji et al., 2008; Blumenthal et al., 1997; Brighton et al., 2006; Diniz et al., 2002; Fassina et al., 2006; Hronik-Tupaj et al., 2011b; Ijiri et al., 1996; Sun et al., 2009b; Sun et al., 2007; Sun et al., 2006) and have been utilized to increase axon outgrowth, accelerate axon repair, and increase muscle reinnveration (Gordon et al., 2010; Gordon et al., 2009a; Gordon et al., 2009b). Furthermore, a combination of strategies, such as multiple growth factors,

electrical stimulation with gene transfer, and implanted stem cells as an adjuvant therapy with growth factors, have been utilized for the improved recovery of injured nerves (Alrashdam et al., 2011; Kemp et al., 2008; Madduri et al., 2010b).

Silk from the *Bombyx mori* silkworm is composed of a heavy chain fibroin approximately 391 kDa, and a light chain fibroin 27 kDa, held together by a disulfide bond, with glue-like proteins termed sericins that bind fibers formed from the fibroins (Sofia et al., 2001; Zhou et al., 2000). Silk can be processed into many material formats such as porous scaffolds, films, gels, fibers and hollow tubes (Altman et al., 2003; Panilaitis et al., 2003; Sundar et al., 2010). For use in biomedical applications, silk has demonstrated biocompatibility with peripheral nervous tissue repair (Benfenati et al., 2010; Ghaznavi et al., 2011; Lin et al., 2011; Pritchard et al., 2010; Szybala et al., 2009; Wilz et al., 208; Yang et al., 2007a) and is fully degradable to amino acids, thus avoiding complications such as nerve compression and chronic inflammation. Silk can be formed into materials with good mechanical strength and flexibility for regenerative medicine needs, including conformal bio-integrated electronics to fit curvilinear tissues in the central nervous system (Kim et al., 2010b).

In the present study, our objective was to combine electrodes and surface topographies on flexible silk substrates to assess the combined effects of patterning and electrical stimulation on axon alignment and axon outgrowth. Here we demonstrate methods for depositing electronic components onto silk films with morphologically patterned surfaces. Morphologically patterned films with electronic interfaces were compared to controls, including flat electronic silk films, patterned silk films and flat silk films, to assess impact on neural cell outgrowth and alignment.

4.2 Materials & Methods

4.2.1 Fabrication of Flat & Patterned Silk Electronic Films (E-Films)

Silk Fibroin Purification - Silk fibroin solution was extracted from Japanese *B. mori* cocoons as described previously (Kang et al., 2009; Kim et al., 2005). Briefly, cocoons from the silkworm were cut, boiled for 30 minutes in Na_2CO_3 for sericin removal, washed, and dried overnight. The following day, silk fibers were dissolved in 9.3M lithium bromide at 60°C for 4-6 hours. Dissolved silk solution was injected into 3,500 molecular weight dialysis cassettes (Thermo Fisher Scientific, Waltham, MA). Dialysis in deionized water was performed over 36 hours resulting in a final solution of 6 - 8% silk fibroin.

Patterned Silk Films - A polydimethylsiloxane (PDMS) mold was prepared by mixing a base and a curing agent (Ellsworth Adhesives, Germantown, WI) in a 9:1 ratio (w/w) then pouring this mixture over grooved glass slides. PDMS was dried at 60°C for 2-3 hours before being peeled from the grooved glass slide. Dimensions of 3.5 μm width grooves with 500 nm depth were chosen based on our previous studies for successful alignment of fibroblasts (Gil et al., 2010). For patterned silk film fabrication, 6 - 8% silk fibroin solution was poured onto the grooved PDMS mold and allowed to dry slowly for 1-2 days. Once dried, patterned silk films were peeled off the PDMS mold.

Flat Silk Films - Flat silk films were made by pouring 6-8% silk fibroin solution onto a smooth PDMS surface then allowed to dry 1-2 days. Once dried, the silk films were peeled off the surface.

Electrode Deposition on Silk Films - An electrode mask (Boston Lasers, Haverhill, MA) was generated by laser etching a pattern into a 2.7 cm x 4.3 cm x 0.2 cm black delrin slide. The mask was secured on top of a silk film. Electrodes were deposited via sputter coating on top of the mask and silk film using a Cressington 208HR Sputter Coater (Watford, England). Following electrode deposition, the electronic-

silk films were treated with methanol and dried overnight to induce β-sheet formation. Electrode materials deposited on the silk films included gold, titanium, and platinum/palladium.

4.2.2 E-Film Characterization

Silk E-Film Thickness – The thickness of the flat and patterned silk e-films was examined using confocal reflectance microscopy (Larson et al., 2011). Briefly, the reflectance signal off of the top surface of the silk film and the reflectance signal off of the bottom surface of the silk film were recorded using a depth scan. Film thickness was calculated as the distance between the reflectance of the top a bottom film surfaces. Excitation was at 488 nm, emission was at 488 $\pm$ 2 nm.

Electrode Conductivity & One-to-One Electrode Correlation - To verify that the electrodes deposited on the silk films were conductive down the length of the electrode and that there was not any crosstalk with neighboring electrodes, a 1V test signal was applied at one end of each electrode. For each test signal applied, voltage measurements were taken across 5 areas per electrode and 5 electrodes per film.

Effects of Electrode Thickness - Electrodes were deposited at thicknesses of 24.9 nm, 74.8 nm, and 99.6 nm as measured by the Cressington Thickness Controller (Watford, England). Conductivity measurements were taken across electrodes of 24.9 nm, 74.8 nm, and 99.6 nm thickness. The voltage drop across the electrodes were measured then graphed as a percent of the original potential. Sample size was n = 20. Measurements were taken at 1V, 1 V 20 Hz, and 1 V 1 kHz.

Conductivity in a Hydrated Environment – For the purpose of assessing electrode adhesion to the silk film surface, conductive electronic films having a thickness of at least 74.8 nm were placed in phosphate buffered saline (PBS) at room temperature. At 1 day, 2 days, 7 days, and 14 days the films were removed from the PBS and allowed to dry overnight. The next day conductivity measurements were taken. Following measurements, the films were placed back into PBS until the next time point. Measurements

were taken at 1V, 1 V 20 Hz, and 1 V 1 kHz at all time points. Conductivity measurements on the electrodes were also taken prior to hydration for the purpose of a baseline measurement. Sample size was n = 20.

4.2.3 Design of a Patterned Silk E-Film Material Interface & Chamber

For the purpose of holding the silk films down in a hydrated environment, silk films were secured between a square PDMS well and a 24 mm x 30 mm x 0.15 mm cover glass slide through plasma sterilization. For the purpose of interfacing electronic silk films with an external stimulator, a 99.95% gold wire (Surepure Chemetals, Florham Park, NJ), 0.01 cm in diameter, was cut 8 cm long and attached to the electronic silk film using a conductive silver paste (Ted Pella, Redding, CA). The silver paste was allowed to dry overnight. The following day the electronic silk film with the external gold wire interface was placed into a 60 mm cell culture dish. The external gold wire and silver adhesive interface was embedded in silicon aquarium glue (PETCO, San Diego, CA). The entire silk film interface was allowed to dry at room temperature for at least two days.

As an alternative interface, based on the application of silk proteins as adhesives, e-gel (Yucel et al., 2010b) was used in place of silver paste for electrode attachment to e-films. The e-gel was formed by exposing a 20-30% concentrated silk solution to a 5 V electric field for 10 - 15 minutes. Following gelation, the e-gel was collected in a syringe and applied as glue to attach the gold wire to the electrode films. The e-gel material interface was allowed to dry overnight. Conductivity measurements were taken across the e-gel and silver paste material interface, with and without the chambers. Sample size was n = 20.

4.2.4 Silk Film Surface Preparation

E-film chambers were soaked in 70% ethanol for 1 hour, washed 4 times with PBS, then exposed to ultraviolet light overnight in a laminar flow hood. Following sterilization, the silk films were soaked for 1 hour in 1 mM laminin (Sigma-Aldrich, St. Louis, MO). After 1 hour, the laminin solution was aspirated and neuron culture media was added to the chamber. Laminin has been reported to increase neuron attachment to surfaces (Darmon, 1982; Smallheiser et al., 1984).

4.2.5 p19 Stem Cell Culture

p19 stem cells (ATCC, Manassas, VA), originating for a mouse embryonic carcinoma cell line, were expanded in culture at a density of 5,000 cells/cm^2 using minimum essential media (Invitrogen Corp., Grand Island, NY) consisting of 7.5% calf serum (Thermo Fisher Scientific, Waltham, MA), 2.5% fetal bovine serum (Invitrogen Corp.), and 0.1% penicillin-streptomycin (Invitrogen Corp.). Stem cells were incubated at 37°C in 5% CO_2. Media was changed two times per week. All experiments used stem cell passage numbers between P1-P3.

4.2.6 p19 Neuron Differentiation

p19 stem cells were plated at 5,000 cells/cm^2 into non-adherent dishes (Sigma-Aldrich, St. Louis, MO) using expansion medium containing 0.5 µM retinoic acid (Sigma-Aldrich, St. Louis, MO). On day three, floating p19 aggregates undergoing differentiation were collected and separated into a single cell suspension using 0.25% trypsin-EDTA and a polished glass Pasteur Pipette tip. Single cells were replated into non-adherent dishes containing expansion media and 0.5 µM retinoic acid. On day 5, differentiated aggregates were collected, separated into single cells, and plated onto silk films at a density of 100,000 neurons/cm^2. To remove any non neural differentiated cells, 5 µg/ml cytosine arabinoside was added the following day (Mani et al., 2000; Shen et al., 2004). Media was changed two times per week.

Retinoic acid differentiates p19 stem cells into neurons by initiating transcription of target neuronal genes including sonic hedgehog, paired box 6 (pax-6), achaete-scute complex homolog 1 (mash-1), and wingless-type mouse mammary tumor virus integration site family, member 1 (wnt-1)(Ulrich et al., 2006).

4.2.7 Cell Viability on Electronic Patterned Silk Film

For assessing cell viability on e-films, alamarBlue® (Invitrogen Corp, Grand Island, NY) was used to examine cell proliferation following plating. The alamarBlue® assay was completed as described previously (Hronik-Tupaj et al., 2011b). Briefly, a 9:1 (v/v) dilution of alamarBlue® to neuronal culture medium was added to the samples and allowed to incubate for 2.5 hours. Following incubation, 100 uL of the media in each sample was pipetted into a 96 well plate. Fluorescence measurements, reported in arbitrary units (A.U.), were taken of the media at 560 nm excitation, 590 nm emission. To obtain cell numbers, a standard curve, that measured fluorescence from the reduction of alamarBlue® in wells containing a known number of cells, was used. Sample size per group per time point was n = 3. Three replicates per sample were measured. Results were graphed as the mean $\pm$ one standard deviation. As a control, results were compared to neurons seeded on silk films without electrodes.

4.2.8 Electric Field Modeling

Electric field strength modeling across silk e-films was completed using the electrostatics module for stationary objects in COMSOL Multiphysics® (Burlington, MA), version 4.2, software. COMSOL Multiphysics® approximates partial differential equations by finite element analysis methods. Electric field strength was calculated through equations:

$\nabla \cdot \boldsymbol{D} = \rho$; $\boldsymbol{D} = \varepsilon_0 \varepsilon_r \mathbf{E}$; $\boldsymbol{E} = -\nabla \boldsymbol{V}$; where **D** = electric field flux (V m); ρ = relative permittivity; ε_0 = electric constant = $8.85418782 \times 10^{-12}$ F·m^{-1}; ε_r = dielectric constant; **E** = electric field strength (V/m), **V** =

applied max voltage (A Ω). Briefly, the electronic silk films, interface, and chambers were constructed using the geometry feature. E-Film and chamber material properties were either selected from the COMSOL Multiphysics® material library or created for the study using existing material properties in the literature. Materials utilized included, gold, silk, PDMS, glass, p19 neuron culture media, and polystyrene. The material properties were defined as follows: gold ($\sigma = 4.5 * 10^7$ S/m; $\rho = 9.0$), silk ($\sigma = 16$ S/m; $\rho = 3.0$), glass ($\sigma = 1 * 10^{-14}$ S/m; $\rho = 4.2$), PDMS ($\sigma = 2.59 * 10^{-14}$ S/m; $\rho = 2.7$), and p19 neuron culture media ($\sigma = 0.431$ S/m; $\rho = 78$), where σ = materials' conductivity and ρ is the materials' relative permittivity (Eisuke Ishikawaa et al., 1997; Hyung-Kew L et al., 2005; Sun et al., 2009a). p19 neuron culture media conductivity was determined from measured values. The waveform applied to the model was a 0.120 V, 1 kHz, sine wave. The geometry was meshed as a coarse free tetrahedral then solved for voltage (V), and electric field strength (V/m), and current density (A/m^2).

4.2.9 Electric Field Setup

The 99.95% pure gold wire from the chambers were connected to 22 gauge solid wire and placed in parallel with two additional chambers. The chambers sat in one of six wells per tray, which were made from noryl. Noryl has a high melting point, approximately 154°C, for sterilization purposes. Prior to stimulation, current-voltage measurements were taken across patterned electronic silk films in neuronal culture media. Resistivity was calculated as approximately 1.55 MΩ. Conductivity of neuron culture media across patterned electronic films was calculated as 4.30 mS/cm. The signal applied to each silk film was 120 mV, 1 kHz using a TENMA universal waveform generator (TENMA Test Equipment, Springboro, OH). Voltage applied across each silk film was verified prior to stimulation. Electric field application was performed in the incubator for 45 minutes daily and the experiments ran over 7 days. Experimental groups consisted of patterned electronic silk films, flat electronic silk films, patterned silk films without stimulation, and flat silk films without stimulation.

4.2.10 Fluorescence Microscopy

An 8 mM calcein acetoxymethyl ester (calcein AM) stock solution (Invitrogen Corp., Grand Island, NY) was mixed with phosphate buffered saline to obtain a 2 µM calcein AM solution. Following solution preparation, cell culture media was aspirated from the patterned electronic silk films, flat electronic silk films, patterned silk films, and flat silk film groups then the 2 µM calcein AM solution was added directly to the cells. Cells were incubated at 37°C for 30 - 45 minutes. Following incubation, the calcein solution was removed from the samples and fresh PBS was added directly to the cells. Cells were imaged with a Leica DMIL fluorescence microscope (Leica, Wetzlar, Germany) with 470 nm $\pm$ 20 nm and 525 $\pm$ 25 nm filters.

Fluorescent images were taken of neurons seeded on patterned electronic silk films, flat electronic silk films, patterned silk films and flat silk films on day 1, day 3, day 5, and day 7. Day 1 was the day following neuron seeding. Images were taken in two samples per group, three images per dish for a total of 6 images. Axon alignment and axon outgrowth were quantified using programs written in MATLAB (MathWorks, Natick, MA). Axon alignment was calculated as the angle, from 0 - 90 degrees, between the grooved silk surface and axon. An angle of 0 degrees meant that the axon was parallel with the silk film pattern. An angle of 90 degrees meant that the axon was perpendicular to the pattern. Axon alignment was reported as the average angle from the grove on day 1, day 3, day 5 and day 7. Axon alignment was also reported as the percent of total neuron axons lying at every 10 degrees (i.e., 0-10°, 10-20°, 20-30°, 30-40°, 40-50°, 50-60°, 60-70°, 70-80°, 80-90°) from the grove (Gil et al., 2010). The relationship of alignment between axons and the direction of neurons seeded on the patterned films was not examined or quantified. Axon outgrowth was quantified and graphed as average length of axon, including the cell body. The number of cells quantified was n = 36 for each group, per time point.

4.2.11 Real Time-Polymerase Chain Reaction (RT-PCR)

For assessing gene expression, silk films were removed from the chamber and washed with PBS. mRNA was extracted using trizol (Invitrogen Corp, Grand Island, NY) then stored at -80°C. cDNA was amplified with the TaqMan Universal PCR Master Mix (Applied Biosystems, Foster City, CA) and the Stratagene Mx300 (Agilent Technologies, Santa Clara, CA) RT-PCR machine. RT-PCR determined gene expression levels of β3-tubulin (Applied Biosystems, Carlsbad, CA Assay ID #: Mm00727586_s1). β3-tubulin, also known as tuj-1, encodes for a structural protein found in neuron axons and cytoskeleton. β3-tubulin is expressed in microtubules and is a common marker for identifying nervous tissue (Arien-Zakay et al., 2007; Kandel et al., 2000; Oe et al., 2006). Relative gene expression was normalized to the housekeeping gene GAPDH (Assay ID #: Mm99999915_g1) and calculated using the formula $2^{(\text{Ct value of GAPDH} - \text{Ct value of gene})}$ as previously described (Mauney et al., 2007). The concentration threshold (Ct) value was set in the linear range of fluorescence for all genes. Gene expression levels were calculated as the mean $\pm$ one standard deviation. Samples were taken on day 1, day 3, day 5, and day 7.

4.2.12 Immunostaining

Neurons seeded on patterned electronic silk films, flat electronic silk films, patterned silk films and flat silk films were fixed at room temperature for 30 minutes in 4% paraformaldehyde then permeabilized for 5 minutes in 0.3% triton X-100 and PBS. Following permeabilization, samples were incubated at 37°C for 2 hours with a primary rabbit anti-mouse β3-tubulin antibody (Sigma-Aldrich, St. Louis, MO) in 10% fetal bovine serum and PBS. Following incubation with the primary antibody, samples were washed 3 times in PBS then incubated at room temperature for 30 minutes with a secondary antibody, an Alexa Fluor® 568 goat anti-rabbit IgG (Invitrogen Corp, Grand Island, NY). Following incubation of the secondary antibody, samples were washed three times in PBS and imaged in distilled water using a Leica DMIL fluorescence microscope (Leica, Wetzlar, Germany) with 560 nm + 20 nm and 645 + 40 nm filters.

Staining was completed on day 1, day 3, day 5, and day 7. Three images were taken per group. p19 stem cells seeded on flat silk films were stained and imaged as a negative control.

4.2.13 Statistical Analysis

All quantitative measurements were graphed and reported as the mean $\pm$ 1 standard error, $\sigma = \sigma/\sqrt{n}$, unless otherwise noted. Statistical significance was calculated using unpaired two-tailed t-tests with a 95% confidence interval ($p < 0.05$) unless otherwise noted.

4.3 Results

4.3.1 Electronic Patterned Silk Film Fabrication and Properties

E-films were successfully fabricated with varying surface topographies, electrode dimensions, pattern/electrode orientation, and electrode material. Silk film surface topographies included 40 µm width grooves, 3.5 µm width grooves having a 350 nm depth, and 3.5 µm width grooves having a 500 nm depth (**Figure 4.1A**). Electrodes deposited on silk films measured 0.5 mm x 4.0 mm, 1.0 mm x 4.0 mm, and 2 mm^2 electrode pads with an 8 mm x 50 µm electrode array (**Figure 4.1B**). Electrodes were oriented perpendicular, parallel, and at a 45° from the silk film patterns (**Figure 4.1C**). Electrode materials deposited by the sputtering target included platinum/palladium, titanium, and gold (**Figure 4.1D**). E-films were approximately 90 µm thick (thickness measurements not shown).

Silk films were conductive down the length of each electrode when a 1 V signal was applied. No crosstalk was observed in neighboring electrodes (**Figure 4.2A – 4.2E**). Twenty-five areas, specifically 5 areas per electrode and 5 electrodes per silk film, were chosen across the electronic silk films for taking conductivity measurements (**Figure 4.2F**). Electrodes 24.9 nm thick on flexible silk films exhibited little to no conductivity. Electrodes 74.8 nm thick were 88.8 ± 2.54%, 86.2 ± 3.97%, and 91.7 ± 0.01% conductive at 1 V, 1 V 20 Hz, and 1 V 1 kHz (**Figure 4.3B**). Electrodes having a thickness of 99.6 nm were

90.2 ± 1.1%, 91.3 ± 0.03%, and 91.6 ± 0.02% conductive at 1 V, 1 V 20 Hz, and 1 V 1 kHz (**Figure 4.3B**). Conductivity of electrodes 74.8 nm thick and 99.6 nm thick was statistically higher ($p < 0.05$) than the conductivity of electrodes having a 24.9 nm thickness. Images of electrodes deposited on patterned silk films having 24.9 nm, 74.8 nm, and 99.6 nm thickness are shown in **Figure 4.3A**. Differences in electrode thickness are noted by the electrode color differences in the figures.

Prior to hydration, electrodes deposited on silk films were 91.1 ± 5.16%, 99.6 ± 4.10%, and 99.9 ±0.0% conductive at 1 V, 1 V 20 Hz, and 1 V 1 kHz. One day following hydration the electrodes were 69.7 ±11.9%, 79.9 ±8.71%, and 84.9 ± 8.19% conductive at 1 V, 1 V 20 Hz, and 1 V 1 kHz, respectively. At 2 days, electrodes were 75.5 ± 9.7%, 81.3 ± 9.41%, and 84.9 ± 8.20% conductive at 1 V, 1 V 20 Hz, and 1 V 1 kHz, respectively. At 7 days, electrodes were 60.1 ± 0.01%, 89.8 ± 6.87%, and 90.3 ± 6.57% conductive at 1 V, 1 V 20 Hz, and 1 V 1 kHz, respectively. At 14 days, electrodes were 40.0 ± 0.01%, 56.9 ± 10.3%, and 68.6 ± 9.40% conductive at 1 V, 1 V 20 Hz, and 1 V 1 kHz, respectively. Statistical differences ($p < 0.05$) between the conductivity of hydrated electrodes and the conductivity of electrodes prior to hydration were at 2 weeks for all groups (**Figure 4.4A**). An average of 90% conductive can be explained as 90 out of every 100 hydrated electrodes were functional.

Both the e-gel and the silver paste were options in attaching external electronics to the silk e-films. The e-gel interface (**Figure 4.3D**) was 78.2 ± 8.26%, 80.8 ± 8.5%, and 81.1±8.38% conductive at 1 V, 1 V 20 Hz, and 1 V 1 kHz, respectively. The e-gel interface with chamber was 57.7± 11.3%, 67.0 ± 10.5% and 71.7 ± 7.36% conductive at 1 V, 1 V 20 Hz, 1V 1 kHz, respectively. The silver interface (**Figure 4.3D**) was 74.8 ± 9.92%, 84.9 ± 8.20%, and 89.9 ±6.88% conductive at 1 V, 1 V 20 Hz, and 1 V 1 kHz, respectively. The silver interface with chamber was 84.8 ± 8.18%, 89.9 ± 6.89% and 74.8 ± 9.92% conductive at 1 V, 1 V 20 Hz, and 1 V 1 kHz, respectively. Conductivity between the electronic silk film interface and the

electronic silk film interface with PDMS chamber groups did not show significant differences ($p < 0.05$) (**Figure 4.3D**).

4.3.2 Responses on Electronic Patterned Silk Films

p19 cells attached and proliferated on 1 mM laminin coated gold e-films, 1 mM laminin coated platinum and palladium e-films, 1 mM laminin coated titanium e-films, and 1 mM laminin coated non-electrode silk films on day 1, day 3, day 5, and day 7 (images of cells not shown). All groups increased in cell number between day 1, day 3, day 5, and day 7 (**Figure 4.4B**).

An image of the electronic silk film and chamber that was modeled is shown in **Figure 4.5A**. The applied stimulation strength, electric field strength, and electric field direction across silk films in media are shown in **Figure 4.5B, 4.5C**. Current density and direction is shown in **Figure 4.5B**. Electric field strength across the silk film was 20 mV/mm. Ionic current density in the center of the chamber was approximately 2μA/mm^2.

Fluorescent images of the p19 neurons growing on flat silk films without stimulation, flat electronic silk films, patterned silk films without stimulation, and patterned electronic silk films are presented on days 1, 3, 5, and 7 (**Figure 4.6**). Directions of film patterns are noted by red arrows. Since neurons were stained with calcein acetoxymethyl ester (calcein AM), a polyanionic dye that is retained in live cells, all of the neurons that were imaged were living.

Differences in average axon alignment were found between the patterned silk films and the flat silk films at all time points ($p < 0.05$) (**Figure 4.7A**). Differences between axon alignment on the patterned films without electrodes and the patterned electronic films were found on days 3, 5, and 7 ($p < 0.05$) (**Figure 4.7A**). Quantification of axon alignment on the flat silk films, the flat electronic silk films, the patterned silk films, and the patterned electronic silk films are reported within every 10 degrees (i.e., 0-10°, 10-20°,

20-30°, 30-40°, 40-50°, 50-60°, 60-70°, 70-80°, 80-90°) from the groove on day 1 (**Figure 4.7B**), day 3 (**Figure 4.7C**), day 5 (**Figure 4.7D**) and day 7 (**Figure 4.7E**). The percentage of neurons on patterned films that are aligned within 0 – 20 degrees of the groove increased from 75.8% to 99.9% on days 1 to 7. The percentage of neurons on patterned electronic films that are aligned 0 - 20 degrees from the groove were 81.4% aligned on day 1 and 67.7% on day 7. The neurons on the flat groups were 35.3%, 26.5%, 28.5% and 16.6% aligned on days 1, 3, 5, and 7, respectively. The neurons on the flat electronic groups were 20.7%, 40%, 34.4%, and 23.4% aligned on days 1, 3, 5, and 7.

The assessment of cell transcripts revealed statistical differences in β3-tubulin gene expression on day 1 and day 3 ($p < 0.05$) between the stimulated flat silk films and the stimulated patterned silk films and the stimulated patterned silk films and the non-stimulated flat silk films. Furthermore, there were differences on day 3 ($p < 0.05$) between the electronic patterned group with stimulation and the patterned group without stimulation. Finally, the assessment of cell transcripts revealed statistical differences in β3-tubulin gene expression on day 5 and day 7 ($p < 0.05$) between the flat electronic group and the patterned group without stimulation (**Figure 4.8A**).

Axon outgrowth in the flat, patterned, flat electronic, patterned electronic groups increased from day 1 to day 3 following seeding on silk films (**Figure 4.8B**). On day 5, there were statistical differences ($p < 0.05$) in axon length between the patterned films, with and without stimulation, and the flat silk film groups. On day 7, there was a difference ($p < 0.05$) in axon length in the patterned electronic group compared to the patterned, flat, and flat electronic groups. Neurons revealed protein expression of β3-tubulin in all groups on day 1, day 3, day 5, and day 7 (**Figure 4.9**). Immunostaining was compared to a negative control of non-differentiated p19 stem cells (image not shown).

4.4 Discussion

We investigated several techniques for electrode deposition on flexible yet biocompatible patterned silk film surfaces including resistance evaporation, e-beam evaporation, and soft lithography. The sputtering techniques allow for efficient deposition of functional electrodes onto flexible surfaces that contain topographical surface patterns. These methods can be accomplished at room temperature under conditions that do not alter the protein structure of the biomaterial. Sputtering allows for deposition of several metal conducting materials including gold, titanium, platinum/palladium, gold/palladium, and nickel, in air, without the use of chemical solvents.

Different materials were utilized to form functional electronic material interfaces including e-gel, silver paste, and silicon glue. While e-gel is not conductive it is a strong adhesive and is biocompatible (Yucel et al., 2010b). Silver paste is a conductor, though not adequate as a strong adhesive. Furthermore, silver containing paste can be toxic to cells (Ziegler et al., 2006). Silicon glue may also be used as a non-conductive, biocompatible, strong adhesive (Peignot et al., 2004). Combinations of these materials are an option for optimizing conductivity and attachment.

The metal electrodes bond to the 90 μm thick, flexible 6-8% silk fibroin film over two weeks in a hydrated environment. Decreases in conductivity were observed as the silk films degraded in a hydrated environment over two weeks (**Figure 4.4A**). Silk degradation time in water is dependent upon several factors such as beta-sheet content and film thickness (Lawrence et al., 2010; Lu et al., 2010). As the films degraded the electrodes dispersed, resulting in a degradable device. Parameters may be tailored for the amount of treatment time needed in an in vivo environment.

The patterned electronic films were comparable in alignment to the patterned films the day after plating (day 1), however, axon alignment, 0 -10 degrees from the groove, in the patterned electronic films decreased on day 3 from 48.1% to 35.6% while the patterned films without electrical stimulation

increased from 44.8% to 54.3%. Here, the role of the electric field is unknown. While direct currents have been demonstrated to align cells perpendicular to the electric fields (Dube et al., 2005; Hronik-Tupaj et al., 2011a; Sun et al., 2006; Tandon et al., 2009b), there have not been extensive studies examining the effects of alternating current fields on cell alignment. In some images, we observed that the neurons aligned better on the grooved silk film when they were located in closer proximity to the electrode. Electrode placement, electrode spacing, and electrode thickness on topographical surfaces may have an effect on axon alignment or outgrowth, which will be a topic for future investigation.

Nerve cells require multiple cues (i.e., biophysical, biochemical, bioelectrical) for regeneration (Lee et al., 2011). While surface topography and biochemical cues such as growth factors are widely used to control nerve growth, there are only a handful of papers that examine the effects of electrical stimulation on nerve cells *in vitro*. Electrical stimulation may be a promising option for nerve regeneration due to the conductive properties of nervous tissue. In the present work we applied both biophysical and bioelectrical approaches to assess neuron responses. While, nerve axon outgrowth was greater ($p < 0.05$) on day 5 in the patterned films than on the flat films (**Figure 4.8B**), there were more neurite branching present on the flat films than on patterned films. Overall, quantification of axon outgrowth of optical microscopy images followed quantification of gene expression. Finally, outgrowth of nerve axons was greatest within the first three days following plating (**Figure 4.8B**). Over time, detachment of neurons from the silk surface occurred, decreasing average axon length and total nerve tissue. As a result, there is a need to research additional surface coatings for long term nerve cell attachment.

AC electric current transfers to ionic current via the electrode-electrolyte interface. Mechanistically, it has been reported that electrical stimulation increases remyelination, guides extracellular matrix deposition, activates endogenous brain derived neurotrophic factor (BDNF) release in hippocampal neurons, and increase endogenous nerve growth factor (NGF) release in cultured Schwann cells (Huang

et al., 2010; Wan et al., 2010a; Wan et al., 2010b). It is known that the release of NGF activates tyrosine kinase receptor A (Trk-A) and p75NTR, a low affinity binding receptor. The TrkA receptor activates intracellular phosphorylation of tyrosine residues known to signal the phosphoinositide 3-kinases/Akt (PI-3K/Akt) pathways and the mitogen activated protein kinase (MAPK) pathway (Kaplan et al., 2000; Kiryushko et al., 2004). The PI3-kinase/Akt pathway plays a role in neuron survival following injury (Kaplan et al., 2000). The MAPK pathways are known as central mediators in axon sprouting and neural differentiation (Airaksinen et al., 2002; Kaplan et al., 2000; Waetzig et al., 2005).

4.5 Conclusions

In conclusion, neural effects from electronic topographical surfaces have not been well studied. The present paper provides methods for electrode incorporation onto films and options for creating conducting topographical surfaces and electronic-silk film interfaces. Effects of these systems on neuron axons in the presence of electric fields were demonstrated. Future directions include examining the effects of electrode placement within the silk films and the effects of different electrode-pattern orientations. Examining silk-electronics in different forms such as tubes, scaffolds, and gels may also prove useful for medically-related devices. Finally, different surface topographies may be examined including multi-directional surfaces patterns and nano and micrometer electrospun silk fibers to obtain additional control of outcomes. Probing the mechanistic basis for the responses will also be critical to future optimization of the techniques described here in vitro and in vivo.

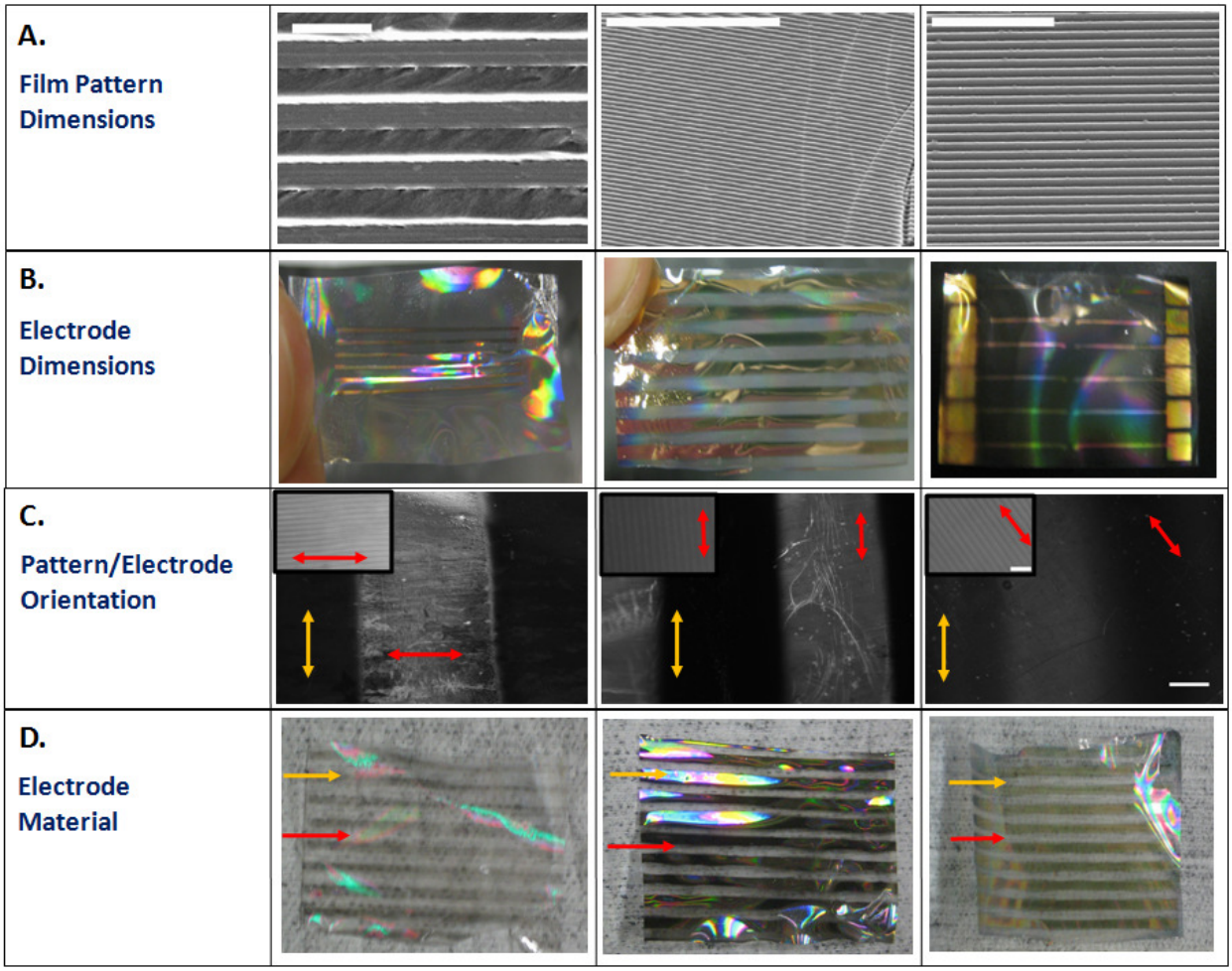

Figure 4.1: Electronic Patterned Silk Film Designs

(a) Patterned Silk Film Dimensions: (left) 40 µm width grooves, (middle) 3.5 µm width grooves having 350 nm depth, and (right) 3.5 µm width grooves having 500 nm depth. Scale bar is 40 µm. (b) Electrode dimensions included (left) 0.5 mm x 4 mm, (middle) 1.0 mm x 4 mm, and (right) 2 mm^2 electrode pads with an 8 mm x 50 µm electrode array (c) Electrodes are oriented (left) perpendicular, (middle) parallel, or (right) at 45° from the grooved surface patterns. Scale bar is 500 µm. Red arrows are showing the direction of the patterns on the silk film. Yellow arrows are pointing to the direction of the electrodes. Scale bar of silk film patterns in upper left hand corner is 20 µm. (d) Electrode deposition utilizing (left)

platinum/palladium, (middle) titanium, and (right) gold. Red arrows are pointing to the silk film. Yellow arrows are pointing to the electrodes.

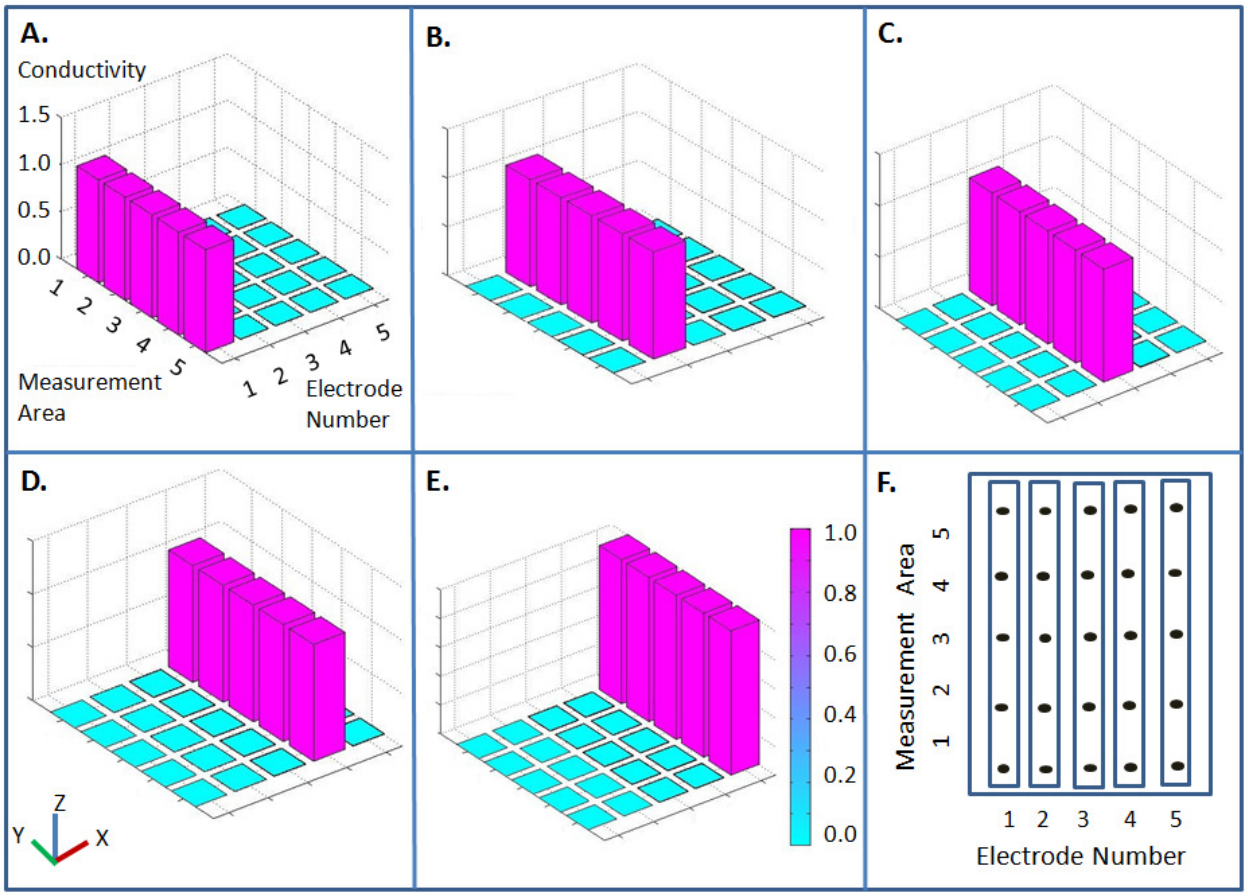

Figure 4.2: Electrode Conductivity Across Silk Films

Conductivity measurements on silk e-films in response to (a) Stimulation of electrode #1 (b) Stimulation of electrode #2 (c) Stimulation of electrode #3 (d) Stimulation of electrode #4 (e) Stimulation of electrode #5. (f) Conductivity of measurement locations on electronic silk films.

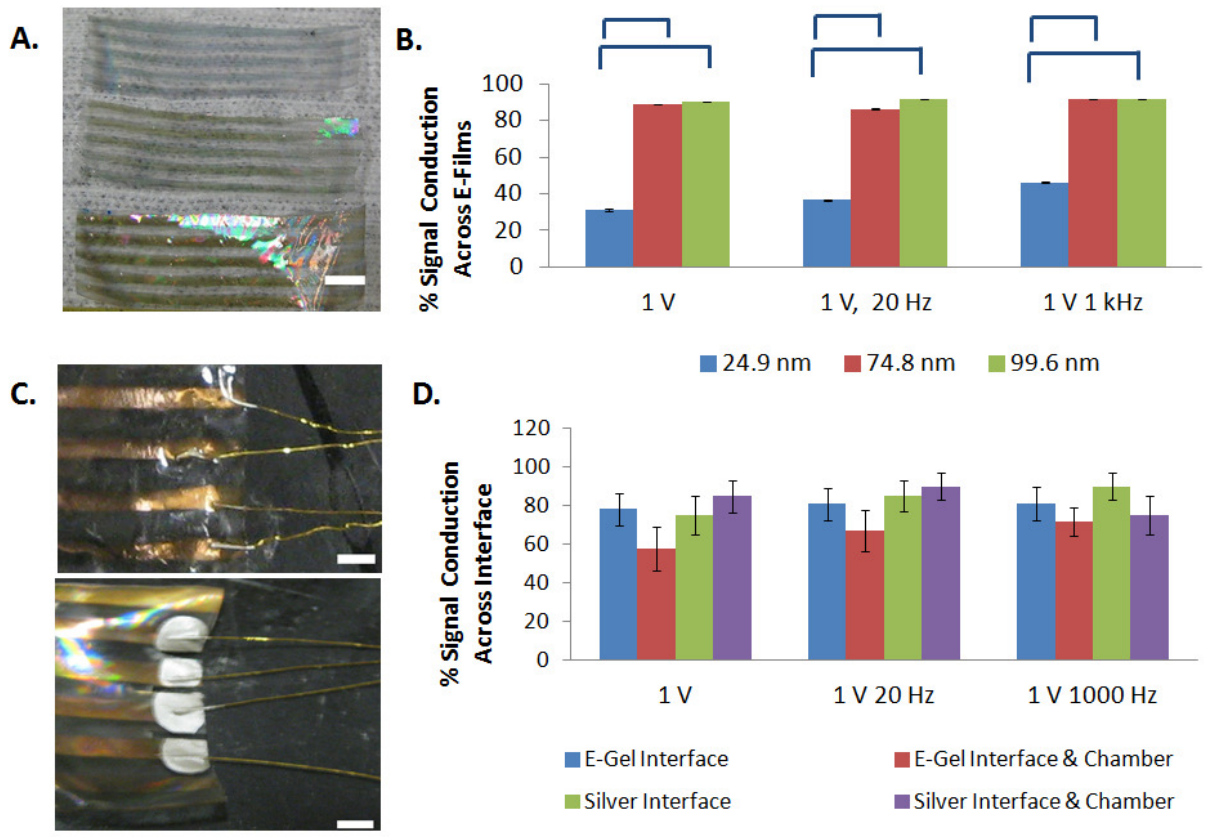

Figure 4.3: Conductivity Across Electronic Silk Films

(a) Images of electrode thickness on silk films at 24.9 nm (top film), 74.8 nm (middle film), and 99.6 nm (bottom film). Scale bar is 10 mm. (b) Conductivity measurements across electronic films at 24.9 nm, 74.8 nm, and 99.6 nm thickness. Statistical significance between groups is marked by a bracket ($p < 0.05$). (c) (top) e-gel interface across silk films and (bottom) silver interface across silk films. Scale in both images is 2 mm. (d) Conductivity Across Interface and Chamber. Statistical significance between groups is marked by an asterisk (* $p < 0.05$).

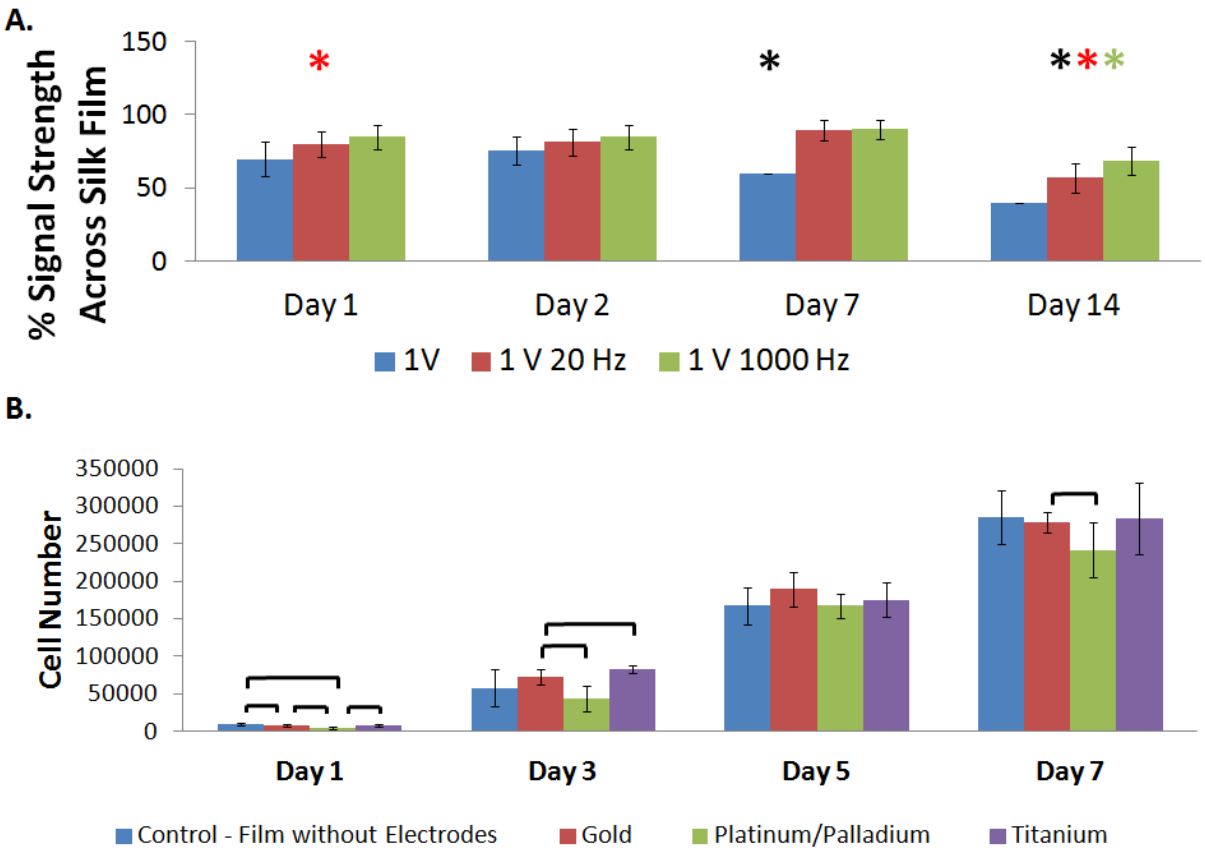

Figure 4.4: Time Studies of E-Film Functionality

(a) Measurements of electrode conductivity at 1 V, 1 V 20 Hz, and 1 V 1 kHz in a hydrated environment over two weeks. Statistical significance is marked by an asterisk (* $p < 0.05$) and denotes a statistical difference in electrode conductivity compared to conductivity prior to hydration. (b) Cellular proliferation on day 1, day 3, day 5, and day 7. Groups included p19 cells seeded on silk films without electrodes, platinum palladium electronic silk films, gold electronic silk films, and titanium electronic silk films. Statistical differences in cell number are marked by a bracket ($p < 0.05$).

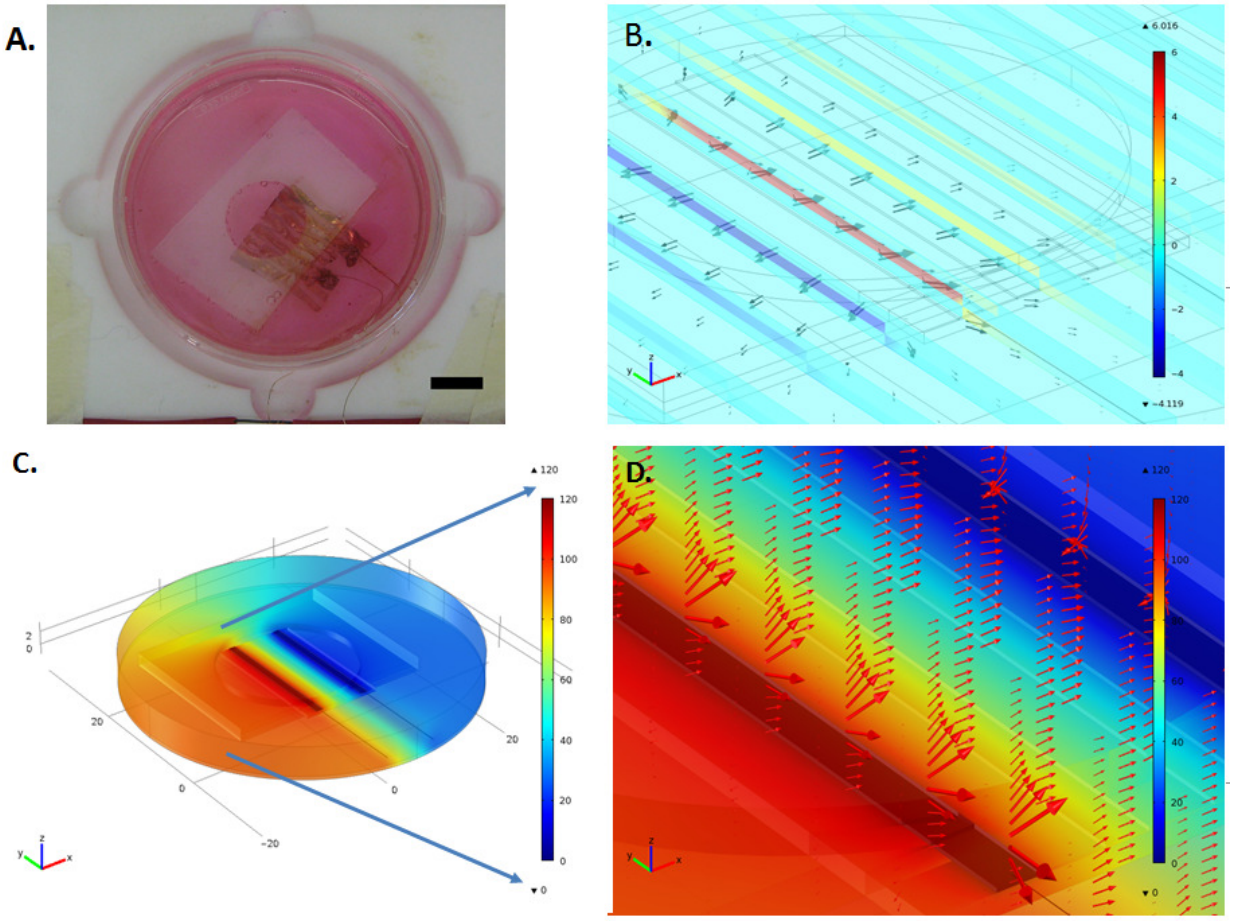

Figure 4.5: Electronic Silk Film Modeling

(a) Image of the modeled electronic silk film and chamber. Scale bar = 1 cm. (b) Current density across chamber. (c) Maximum voltage potential applied to chamber. (d) Electric field strength and electric field direction is illustrated by the red arrows.

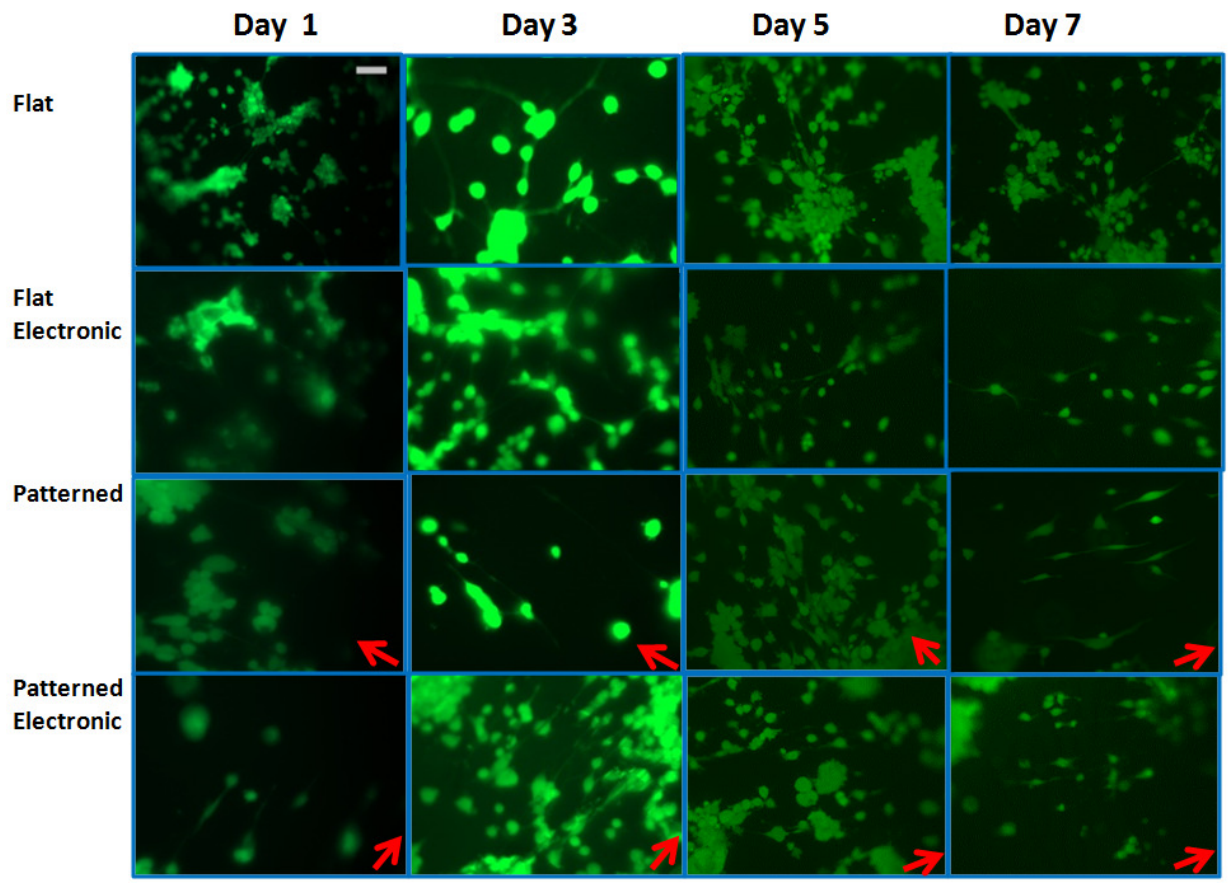

Figure 4.6: Fluorescent Microscopy Images

Fluorescent microscopy images of p19 neurons on flat silk films, flat electronic silk films, patterned silk films, and patterned electronic silk films on day 1, day 3, day 5, and day 7. Pattern direction is noted by the red arrows. Scale bar is 75 μm.

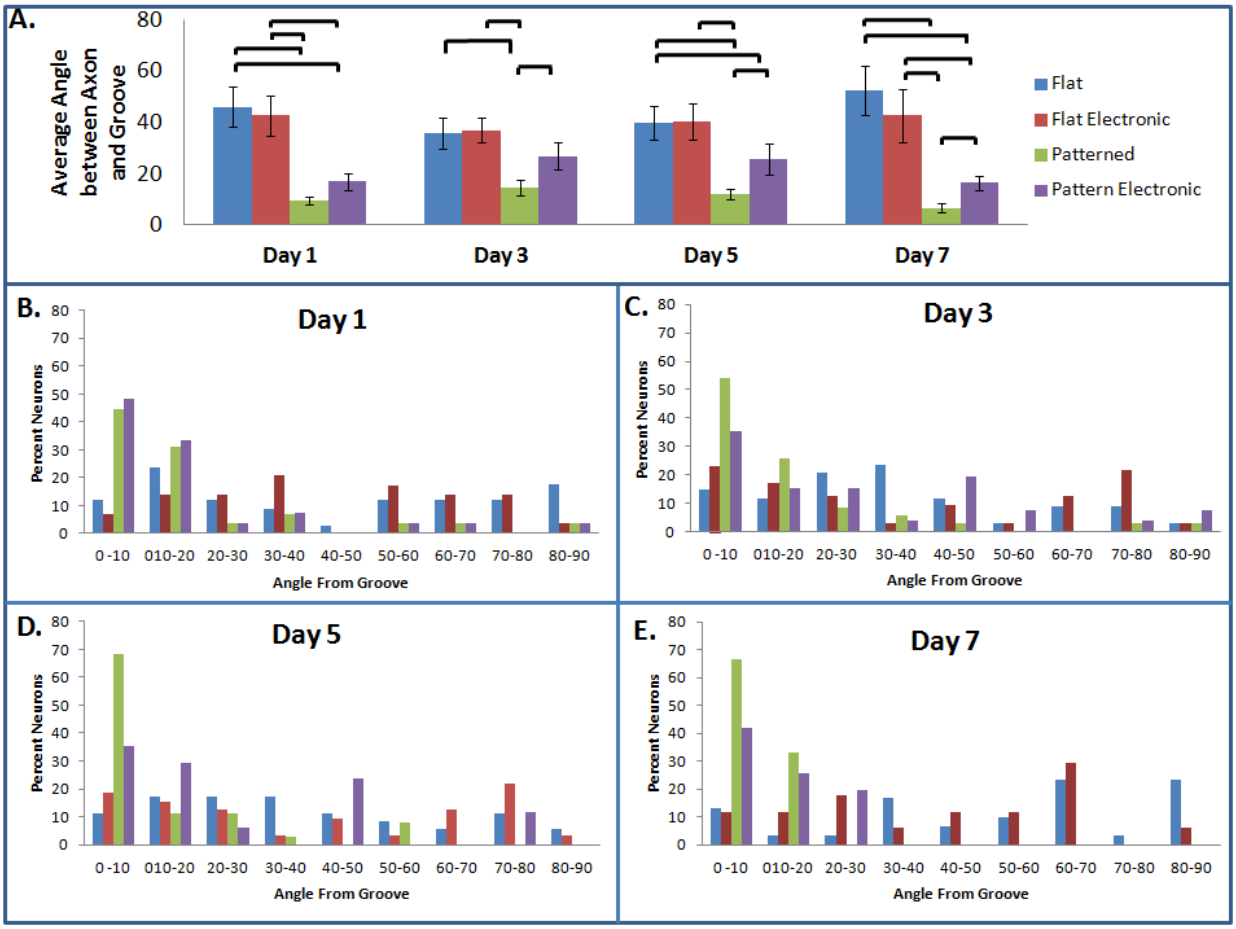

Figure 4.7: Quantification of Axon Alignment

(a) Average axon alignment on day 1, day 3, day 5, and day 7. Statistical significance between groups is marked by a bracket ($p < 0.05$). Quantification of axon alignment on (b) day 1, (c) day 3, (d) day 5, and (e) day 7. Axon alignment on flat silk films, flat electronic silk films, patterned silk films, and patterned electronic silk films is binned within every 10° to provide information on alignment over the neuron population.

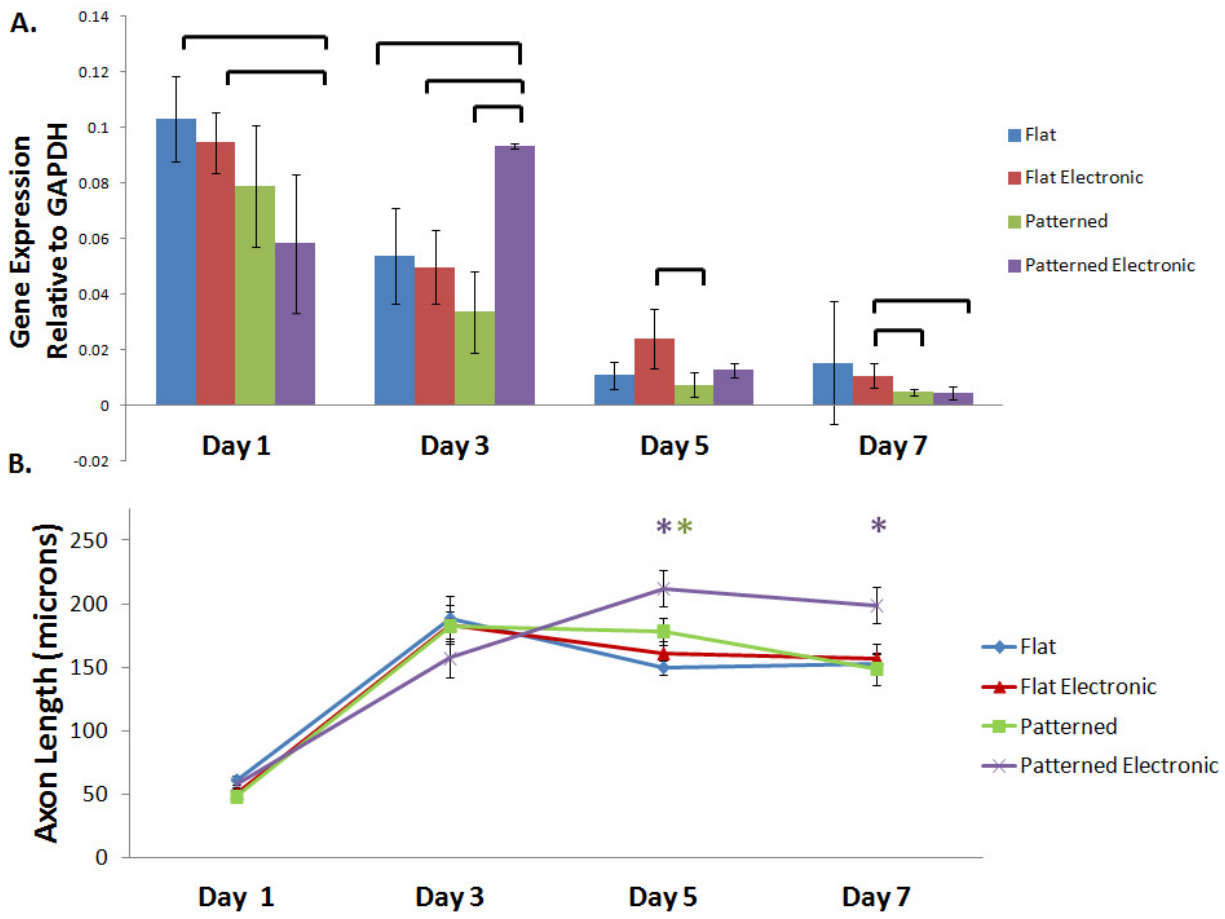

Figure 4.8: Quantification of Axon Outgrowth

(a) β3-tubulin mRNA expression relative to GAPDH vs. time. (b) Average axon outgrowth on day 1, day 3, day 5, and day 7. Statistical significance between groups is marked by an asterisk (* $p < 0.05$).

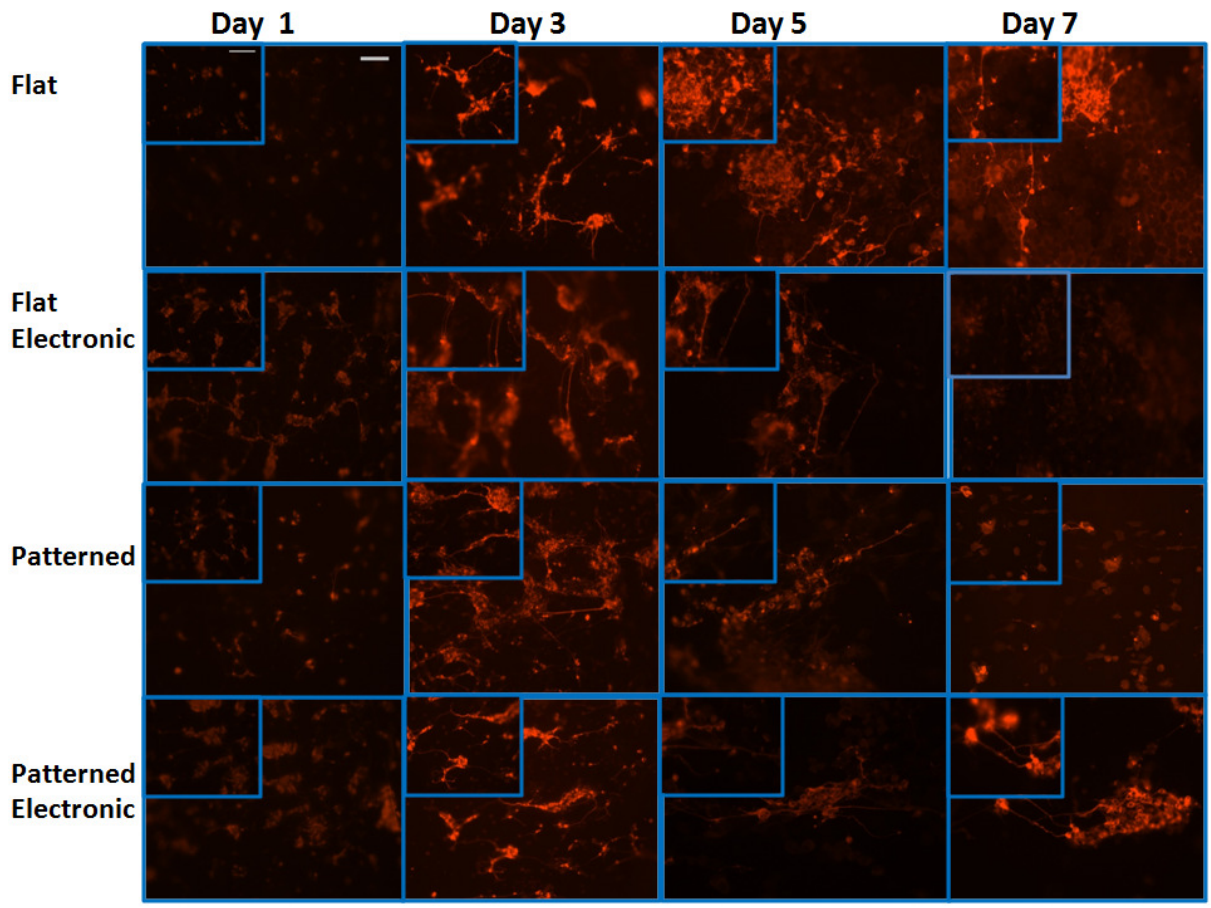

Figure 4.9: β3-Tubulin Protein Expression

Immunofluorescence staining of β3-tubulin expression on day 1, day 3, day 5 and day 7. Scale bar is 75 µm.

Chapter 5: TOOLBOX INCORPORATION IN 3D: SILK FIBROIN TUBES FOR AXON OUTGROWTH

5.1 Introduction

While strategies for peripheral nerve repair were reported as early as 1836, still today there is not one method for successful long gap peripheral nerve repair. Although the autograft continues as the gold standard for the coaptation of severed nerve ends, there is limited availability of peripheral nerves for transplant, especially for long-gap nerve injuries. For enhancing the repair of nervous tissue, several approaches such as the addition of nerve growth factors, stem cell and glial cell transplantation, gene therapy, functional electrical stimulation, surface topographies, and natural and synthetic guidance channels have been investigated (Lari et al., 2001; Murakami et al., 2003; Pan et al., 2007; Pan et al., 2006; Pollock, 1995; Runge et al., 2010). Many of these approaches have been incorporated into nerve guides. Currently few studies have incorporated electrodes into nerve guides or developed nerve guides using conductive polymers (Benmerah et al., 2009; Haastert-Talini et al., 2011; Lee et al., 2010b; Runge et al., 2010). Even fewer studies have examined the cellular response. The few studies that have examined electric field stimulation on neurons have reported promising results in the early stages. For example, one article discussed that short-term low frequency electrical stimulation at the proximal stump may enhance long gap peripheral nerve injury (Haastert-Talini et al., 2011).

To date, there has not been any work reported on electrode incorporation into patterned degradable silk conduits for peripheral nerve regeneration and axon outgrowth. Our objectives included design, fabrication and characterization of a patterned electronic silk nerve guides, design and implementation of a neural stimulation system, and the identification of the effects of electrical stimulation, either gradient stimulation, stimulation parallel to the length of the guide, or stimulation perpendicular to the length of the guide.

5.2 Materials and Methods

5.2.1. Fabrication of Electronic Patterned Silk Films (E-films)

Silk Fibroin Purification - Silk fibroin solution was purified from Japanese *Bombyx mori* cocoons as described previously (Kang et al., 2009; Kim et al., 2005). Briefly, cocoons were cut, boiled for 30 minutes in Na_2CO_3 for sericin removal, washed in deionized water, and dried overnight. The following day, silk fibroin fibers were dissolved in lithium bromide at 60°C for 4-6 hours. Dissolved silk fibroin was injected into 3,500 MW dialysis cassettes (Thermo Fisher Scientific Waltham, MA). Dialysis was performed in deionized water for two days. Following dialysis, silk solution was removed from cassettes and centrifuged twice at 9,000 rpm at 4°C for 20 minutes. Following centrifugation, 1 mL of fibroin solution was dried in a 60°C oven. The dried solution was weighed for measuring silk fibroin concentration. This process resulted in a final concentration of purified silk fibroin solution 6-8% weight by volume (w/v).

Patterned Silk Films - A polydimethylsiloxane (PDMS) mold was prepared by mixing a base and a curing agent (Ellsworth Adhesives, Germantown, WI) in a 9:1 ratio (w/w) then pouring this mixture over grooved glass slides. PDMS was dried at 60°C for 2-3 hours before being peeled from the grooved glass slide. For patterned silk film fabrication, 6 - 8% silk fibroin solution was poured onto the grooved PDMS mold and allowed to dry slowly for 1-2 days. Once dried, patterned silk films were peeled off the PDMS mold.

Electrode Deposition onto Patterned Films - An electrode mask (Boston Lasers, Haverhill, MA) was generated by laser etching a pattern into a 2.7 cm x 4.3 cm x 0.2 cm black delrin slide. The mask was secured on top of a silk film. Gold electrodes were deposited via sputter coating on top of the mask and silk film using a Cressington 208HR Sputter Coater (Watford, England). Following electrode deposition, the electronic-silk films were treated with methanol and dried overnight to induce β-sheet formation.

5.2.2 Fabrication of Electronic Patterned Silk Nerve Guides (E-Guides)

Electronic silk nerve guides were constructed in two-layers. For the inside layer, a patterned electronic silk film (e-film) was rolled around a stainless steel post then methanol treated to induce β-sheet formation. Following an initial methanol treatment, a 6-8% silk solution was applied to secure the seam of the silk film around the stainless steel post then methanol treated for the purpose of holding a tubular shape prior to the addition of an outer silk layer. For creating an outer layer, alternating dips into a 20-30% concentrated silk solution and methanol was repeated 3 times. An outer layer was created for the purpose of enhancing mechanical integrity of the guide. For the purpose of creating porosity and decreasing nerve guide brittleness, 7% PEO was mixed in with the 25% silk solution. Guides were left to dry overnight. The following day, the guides were soaked for one day in a surfactant for post removal then soaked for two days in water for PEO removal. Controllable guide parameters included electrode design, nerve guide diameter, and porosity. Electrode designs included electrode deposition parallel and perpendicular to the silk film patterning, electrode gradients and electrode placement on one end of the nerve guide. Inner nerve guide diameters included widths of 0.5 mm, 1.5 mm, 3.0 mm, and 5.0 mm guides. A range of guides were fabricated using silk to PEO ratios of 100% Silk 0% PEO, 98% Silk 2% PEO, 90% silk 10% PEO, 80% Silk 20% PEO, and 75% Silk 25% PEO.

For the purpose of connecting electronic silk nerve guides to an external stimulator, a 99.95% gold wire (Surepure Chemetals, Florham Park, NJ), 0.01 cm in diameter, was cut 8 cm long and attached to the electronic silk nerve guides using a conductive silver paste (Ted Pella, Redding, CA). The silver paste was allowed to dry overnight. The following day the electronic nerve guide with the external gold wire interface was placed into a 60 mm cell culture dish and secured using non-toxic silicone glue (PETCO, San Diego, CA).

5.2.3 Design of an External Neural Stimulator

A PCI-6221 data acquisition board (National Instruments, Austin, TX), having two 16-bit 250 kS/S output ports, was inserted into a PCI slot of an Dell OptiPlex 960 (Round Rock, TX) then connected to a 68 pin I/O connector block (National Instruments, Austin, TX). For increasing the number of available output channels, a 22 gauge solid wire was connected from each output channel of the 68 pin I/O connector block to a solderless breadboard (You Do It Electronics, Needham, MA). Four 22 gauge solid wires were connected from the breadboard on one end and to steel alligator clips (You Do It Electronics, Needham, MA) on the other end. Alligator clips were used to clip the external gold wires from the nerve guides to the stimulation system. For avoiding external electromagnetic interference, a 2' x 2' x 1.5' Faraday Cage was built around the connector block, breadboard, and culture dish.

Following hardware installation, NI-Daq driver software and LabVIEW 2009 was installed on the computer. Two tasks were created in the driver software to map the physical output channels on the data acquisition board to virtual channels that interfaced with LabVIEW. Next a LabVIEW program was written to generate user specific waveforms for neural stimulation. Adjustable stimulation parameters included frequency (< 1 MHz), offset, pulse shape (sine, square, triangle), and amplitude (< 10V). The LabVIEW program was designed to execute the desired waveform to the two output channels either separately, simultaneously, or sequentially.

5.2.4 Scanning Electron Microscopy (SEM)

Silk tubes having varying pattern dimensions and orientations were cut open and sputter coated with approximately 40 nm of gold using a SC502 sputter coater (Bio-Rad, Hercules, CA). Silk tubes containing varying silk/PEO ratios were also sputter coated at the same thickness. All silk tubes were imaged using a JSM-840 Scanning Electron Microscope (JEOL USA, Peabody, MA).

5.2.5 Electronic Patterned Silk Nerve Guide Conductivity Measurements

Inside the Nerve Guide – In Chapter 4, we demonstrated that electrodes, having at least 74.8 nm thickness, deposited on silk films were conductive across the length of the film and were conductive following submersion in a hydrated environment over 2 weeks. To test whether the electronic films were conductive inside a wrapped conduit, quick and simple conductivity tests were performed. Specifically, one lead of an ohmmeter was placed on one of the electrodes inside the tube and the other lead was placed on the same electrode located on the outside of the tube. Electrodes were determined as conductive or not conductive if the ohmmeter could send a current down the electrode and measure a resistance. Sample size was n = 30 electrodes.

Across Connector Pads - Conductivity measurements were taken across the 99.95% gold wire, which was attached to the nerve guide connector pads via the silver paste, and inside electronic patterned silk nerve guide. Sample size was n = 30 electrodes.

In a Hydrated Environment – For the purpose of assessing electrode adhesion to the silk film surface, conductive nerve guides were placed in phosphate buffered saline (PBS) at room temperature. At one week, the nerve guides were removed from the PBS and allowed to dry overnight. The next day conductivity measurements were taken using an ohmmeter. Sample size was n = 30 electrodes.

5.2.6 Electronic Patterned Silk Nerve Guide Mechanical Testing

E-guides were fabricated then hydrated in PBS at room temperature for 3 days prior to testing. For performing tensile tests, a 3366 Series Dual Column Tabletop Universal Test System (Instron, Norwood, MA) with a load cell of 100 N was used. For the purpose of calculating the nerve guide cross-sectional area and converting the applied force into stress per square area, the inner nerve guide diameter and thickness of the nerve guide wall was measured using calipers. Tensile tests were completed at a rate of

pull of 1 mm per minute then graphed as a stress-strain curve. As a measure of nerve guide elasticity, the Young's Modulus was quantified from the slope in the linear region of the stress-strain curve. Ultimate tensile strength was graphed as the highest stress value achieved during the test. Sample size was n = 3 guides.

5.2.7 SH-SY5Y Stem Cell Culture

SH-SY5Y stem cells (ATCC, Manassas, VA), originating from a human neuroblastoma cell line, were thawed, then expanded in culture at a density of 5,000 cells/cm^2 using a 50:50 composition of DMEM/F12 (Invitrogen Corp., Grand Island, NY), 10.0% fetal bovine serum (Invitrogen Corp.), and 1.0% penicillin-streptomycin (Invitrogen Corp.). Stem cells were incubated at 37°C in 5% CO_2. Media was changed two times per week and passaged at 80% confluency. All experiments used stem cell passage numbers between P1-P6.

5.2.8 Silk Nerve Guide Seeding Density Study

1,1'-dioctadecyl-3,3,3',3'-tetramethylindocarbocyanine perchlorate (DiI) was diluted in cell culture media containing neural stem cells to a final concentration of 10 μM then incubated at 37°C for 30 minutes. Following incubation, dil stained stem cells were centrifuged at 1000 rpm for 5 minutes. The DiI containing cell culture media was aspirated and fresh neuron culture media was replaced. DiI stained stem cells were seeded into sterile silk nerve guides at densities of either 1 million cells/cm^2, 2 million cells/cm^2 or 4 million cells/cm^2. Following three days of culture, silk nerve guides were cut in half and imaged in PBS using confocal microscopy. Confocal images were acquired using a two-photon ready Leica DM IRE2 confocal microscope (Leica, Wetzlar, Germany). Cell images were taken at 540 nm excitation and 565 nm emission using a 20x objective, numerical aperture 0.7. Transmission images of the silk tube was taken using a 20X objective, numerical aperture 0.7, in the same field of view as the

confocal images of the stained cells. Confocal and transmission images were overlayed to view stem cells attached to silk nerve guides.

5.2.9 Electronic Nerve Guide Preparation and SH-SY5Y Stem Cell Seeding

Prior to cell seeding, electronic nerve guides were sterilized in 70% ethanol for 1 hour, washed 4 times with PBS, then exposed to ultraviolet light overnight in a laminar flow hood. For neural cell attachment, the silk guides were soaked for 1 hour in 0.1 mg/mL poly -d lysine (Sigma-Aldrich, St. Louis, MO). After 1 hour, the poly -d lysine solution was aspirated and SH-SY5Y stem cells were injected at a density of 1 million cells/cm^2 to the inside of the guides. Next, cells were allowed to attach to the inside of the nerve guides for 45 minutes. Additional neuronal cell culture media was then added to the chamber.

5.2.10 Nerve Guide Experimental Setup

The following morning, neural differentiation components, 1 µM retinoic acid (RA) (Kim et al., 2008) and 50 ng/mL of nerve growth factor (NGF) (Oe et al., 2006; Price et al., 2006), were added to the neural culture media. Groups included a control group, a gradient stimulation group, a group with parallel electrodes, and a group with perpendicular electrodes. The waveform signal applied to the parallel and perpendicular electrode groups was 120 mV 1 kHz. The voltage applied to the nerve guide system was verified prior to stimulation. The electric field application was performed for 45 minutes daily and the experiments ran over 7 days. Neural differentiation media was changed twice weekly.

5.2.11 Live-Dead Stain

On day 3 and day 7 following cell seeding, media was aspirated from the nerve guides, and a phosphate buffered saline solution containing 2 µM calcein AM and 4 µM EthD-1 (Invitrogen Corp., Grand Island, NY) was added directly to the neurons. Neurons were incubated at 37°C for 30 minutes. For detecting

live cells, neurons were imaged with a Leica DMIL fluorescence microscope (Leica, Wetzlar, Germany) with 470 nm ± 20 nm and 525 ± 25 nm filters. For detecting dead cells in the same field of view, a second image was taken using 560 nm ± 20 nm and 645 ± 40 nm filters. Images was n = 3.

5.2.12 Statistical analysis

Conductivity measurements were graphed and reported as the mean ± 1 standard error, $\sigma = \sigma/\sqrt{n}$. Mechanical measurements was reported as the mean ± 1 standard deviation with a sample size of n = 3 guides. Statistical significance was reported using two-tailed t-tests with a 95% confidence interval ($p < 0.05$).

5.3 Results

5.3.1 Silk Nerve Guide Designs

Nerve guides fabricated incorporated a range of electrode designs, patterned film dimensions, film compositions, tube porosities, and varying tube diameter. Electrodes and patterns were successfully incorporated into the inner layer of nerve guides (**Figure 5.1A, 5.1B**). Pores were successfully incorporated into the outside layer of the nerve guide (**Figure 5.1C**). Pore size varied in tubes with varying silk and PEO ratios.

5.3.2 Nerve Guide Conductivity

Electronic nerve guides were 73.3 ± 10.1%, 66.6 ± 10.7%, and 60 ± 12.5% conductive within the silk tube, across the electrode pads, and 1 week following hydration, respectively (**Figure 5.2A**). There were not any statistical differences ($p < 0.05$) in conductivity between all three conditions. An image of the silk tube and interface is shown in **Figure 5.2B**.

5.3.3 Nerve Guide Mechanical Measurements

Stress-strain graphs, Young's Modulus, and ultimate tensile strength are shown in **Figure 5.3**. Statistical differences (red asterisk, $p < 0.05$) in the Young's Modulus values are shown between the 75/25, 80/20 and the 90/10 tubes compared with the 98/2 Silk/PEO tubes. Statistical differences (blue asterisk, $p < 0.05$) in Young's Modulus values are shown between the 75/25 and the 80/20 tubes compared with the 100/0 silk/PEO tubes. There were not any statistical differences ($p < 0 .05$) in the Young's Modulus between the 75/25, 80/20 groups or the 90/10 Silk/PEO groups. There are not any statistical differences ($p < 0.05$) in Young's Modulus between the silk tube groups having a 98/2 and 100/0 silk to PEO ratio.

Statistical differences ($p < 0.05$) in ultimate tensile strength are shown between the 75/25, 80/20 and 90/10 Silk/PEO groups and the 98/2 and 100/0 Silk/PEO groups. There are not any differences ($p < 0.05$) in ultimate tensile strength between the silk tubes having a 98/2 and 100/0 silk to PEO ratio.

5.3.4 Design of an External Neural Stimulator

The design of our neural stimulation system is shown in **Figure 5.4A**. For stimulation, neurons are placed inside the Faraday Cage and treatment parameters are inputted from the control panel on the desktop computer (**Figure 5.4B, C**).

5.3.5 Neural Cell Imaging Inside Silk Guides

Confocal images of DiI stained stem cells over a range of seeding densities (**Figure 5.5)**. Cells are attached to silk tubes three days following cell seeding (**Figure 5.5**). Nerve guides were successfully incorporated with neural differentiating SH-SY5Y stem cells at densities of 1 million cells/cm^2 and cells were viable day 3 and day 7 after seeding (**Figure 5.6-7**).

5.4 Discussion

5.4.1 Silk Nerve Guide Designs

Nerve Guide Porosity – It is known that nerve guides that contain pores and allow for permeability of the surrounding environment increase peripheral nerve regeneration over guides that are not porous (Belkas et al., 2004). In our multifunctional patterned electronic silk nerve guides, we incorporated pores into the outside silk layer. In future work, porous electrode designs could be incorporated into the inner electronic silk film layer for the purpose of increased nutrient diffusion, increased electrode surface area, and decreased electrode impedance.

Nerve Guide Wall Thickness - Nerve guide wall thickness of less than approximately 0.81 mm has also been shown to play a role in nerve regeneration (Belkas et al., 2004). Our silk guides had a wall thickness of approximately 0.5 mm. This wall thickness can be tailored depending on the number of silk coatings added to our tubes.

Nerve Guide Elasticity - The Young's Modulus for the electronic patterned silk nerve guides ranges from 0.058 MPa to 0.243 MPa following three days of hydration in PBS. The Young's Modulus in the longitudinal direction for peripheral nerves has been reported as approximately 8.5 - 40 MPa (Bueno et al., 2008). From our measurements, our nerve guides are more elastic than the native peripheral nerve in the longitudinal direction.

The lower the material's elastic modulus, the lower the stiffness of the material. Stiffness has played a role in neuron attachment and growth on surfaces (Balgude et al., 2001; Scott et al., 2010). For example, decreases in biomaterial stiffness such as in agarose gel and collagen allows for increases in neurite extension of PC12 and DRG neurons (Balgude et al., 2001; Scott et al., 2010). Stiffness is another

requirement needed for consideration when developing future guides, especially when studying them *in vitro*. A lower stiffness allows for increased neuron attachment during *in vitro* experiments.

Nerve Guide Strength - Ultimate tensile strength of the guides ranges from 0.439 MPa to 3.15 MPa following three days of hydration. Ultimate tensile strength in our nerve guides vary depending on porosity. Maximum stress on peripheral nerves has been reported as 11.7 MPa (Bueno et al., 2008). If a higher strength guide is needed in the future, reinforced nerve silk guides may be developed with our 'toolbox'. One option for reinforced nerve guides is through the incorporation of electrospun silk fibers. Methods for electrospun silk fiber incorporation into single channel silk nerve guides was successfully developed in our lab (Methods by Marie Tupaj, Not shown, 2010). These methods could be incorporated into the electronic guides. They may also be helpful for alignment. Other options for reinforced guides may be the use of a higher concentration, greater than 20-30%, of silk solution in the outside layer.

Silk Nerve Guide Degradation – Our silk nerve guides need to allow for conductivity, mechanical integrity and stability over the course of healing. Currently, our short term hydration studies showed no change in nerve guide conductivity over 1 week. Over the long term, spatially controlled growth factor incorporated silk nerve guides have been implanted in rat sciatic nerve defects for up to 6 weeks (Lin et al., 2011). In past studies, silk tubes have shown little degradation, as determined through mass lost, over 10 days in PBS (Lovett et al., 2007). Tube porosity did not affect degradation (Lovett et al., 2007). It has been reported that silk degradation time processed in films is dependent on β-sheet content (Lawrence et al., 2010). β-sheet content may be induced in silk through methanol treatment or water annealing and it has been found that a three-fold increase in β-sheet content is seen in films treated with methanol over water annealing (Lawrence et al., 2010). Altering the amount of β-sheets is one way to tailor degradation of film incorporated multifunctional nerve guide for healing long gaps.

Finally, while little change has been observed in the mechanical integrity of silk tubes in PBS over 10 days (Lovett et al., 2007), over the long term, mechanical properties will change as the tubes degrade.

5.4.2 E-Guide Effects on Axon Growth

SH-SY5Y differentiating neurons in our studies were viable over 7 days without the need for a bioreactor system (perfusion or spinner). Nerve guides used in our studies were 3 mm in diameter to allow for nutrient and oxygen diffusion through the guides.

Differentiating nerve cells were exposed to electric fields parallel to patterning, perpendicular to patterning, and in a gradient way in the nerve guide. Gradient electrical stimulation may be used for increasing release of endogenous neurotrophic factors towards the distal stump for guiding neuron axon growth in that direction. Neurotrophic factor release in a gradient way may avoid the "candy store effect" of neuron growth halted in one area due to increased concentration of neurotrophic factors.

5.5 Conclusions & Future Directions

In conclusion, we developed methods and fabricated electronic patterned silk nerve guides with varying electrode designs, patterning, porosities, and diameters. It was demonstrated that e-guides were conductive inside the tube and following 1 week in a hydrated environment. Silk nerve guide designs exhibited varying strength and varying elasticity that was dependent on porosity. Specifically, guides having higher porosity were characterized by a lower elastic modulus and a lower ultimate temsile strength. Guides having a lower porosity were characterized by a higher elastic modulus and a higher ultimate tensile strength.

Seeding densities inside the silk guides were optimized at 1 million cells/cm^2. Neural differentiating SH-SY5Y stem cells were attached and viable inside the electronic patterned silk nerve guides over 1 week. Increased axon outgrowth was observed between day three and day seven following perpendicular and

gradient stimulation. Finally, a system for stimulating nerve cells in culture and in silk guides was developed.

In vitro studies in this project utilized the common SH-SY5Y cell line (**Table 1.1**). Future nerve guide studies will include the use of primary peripheral cells, dorsal root ganglia. Studies examining responses of severed neuron axon growth inside silk guides would also provide interesting information.

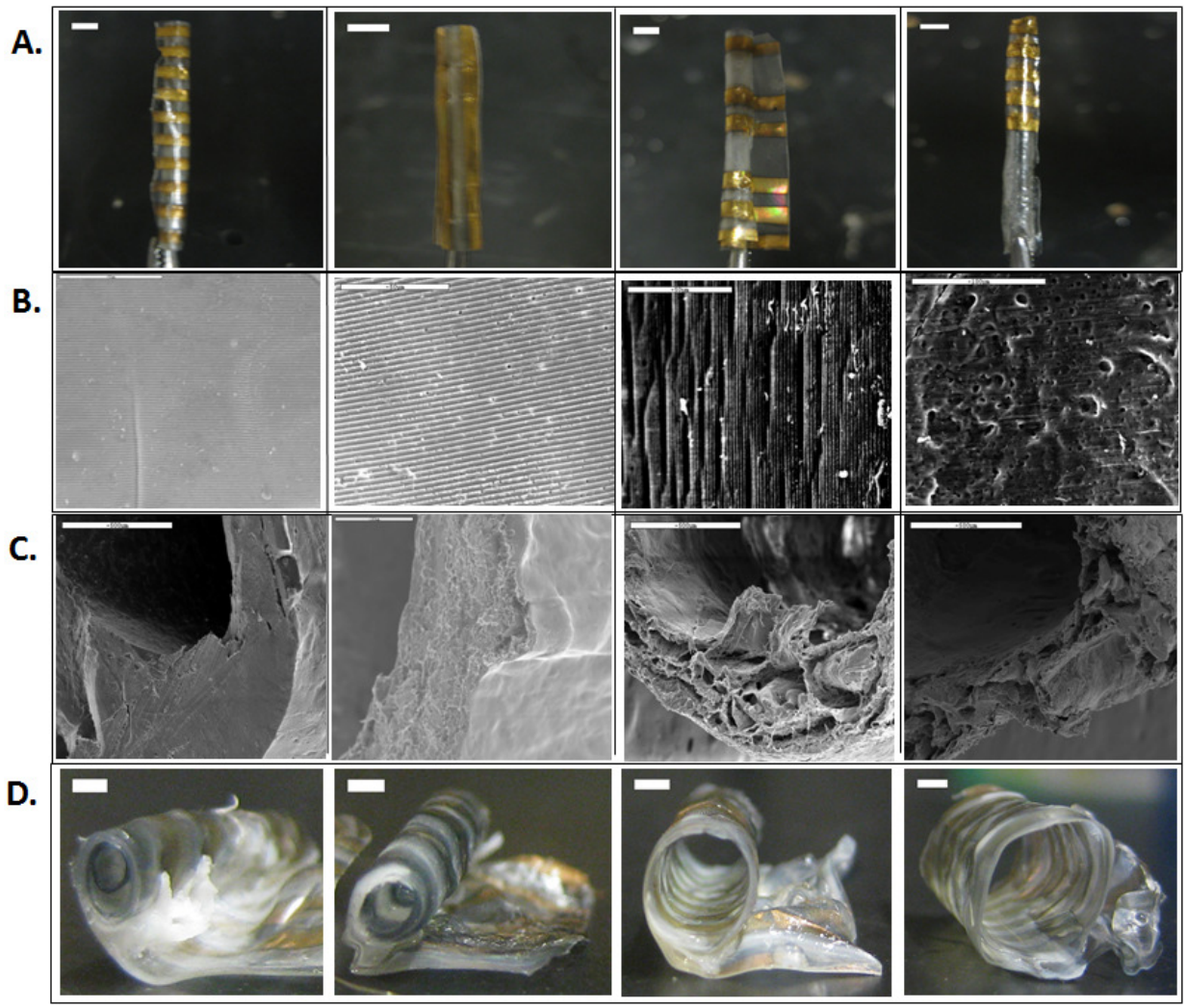

Figure 5.1 Electronic Patterned Silk Nerve Guide Designs (a) Electrode Designs in silk nerve guides (left to right) electrode incorporation perpendicular to length of nerve guide conduit, electrode incorporation parallel to length of nerve guide conduit, electrode incorporation for gradient stimulation, and electrode incorporation at one end of the guide for proximal or distal stimulation. For a clear image of the electrodes, the inside layer of nerve guide is shown only. Scale bar is 1 mm. (b) Pattern incorporation into silk nerve guides (left to right) 'Pattern H" incorporation having dimensions of 3584 nm width with approximately 108 nm depth, 'Pattern I' incorporation having dimensions of 3.5 um width with approximately 500 nm depth, 'Pattern I' oriented perpendicular inside the silk tube, and 'Pattern I' incorporation into a porous silk film with a 90/10 Silk to PEO ratio. Scale bar is 50 um. In the last image

the scale bar is 100 um. (c) Nerve Guide Composition (left to right) 100% silk and 0% PEO, 90% silk and 2% PEO, 80% silk and 20% PEO, 75% silk and 25% PEO. The larger pores are seen in silk nerve guides that have a greater percentage of PEO. Scale bars are 500 um, except middle left image, scale bar is 100 um. Outside layer only is imaged. (d) Nerve Guide Diameter (left to right) 1.0 mm, 1.5 mm, 3.0 mm, and 5.0 mm. To view film pattern, inside layer only is imaged. Scale bars are 1.5 mm.

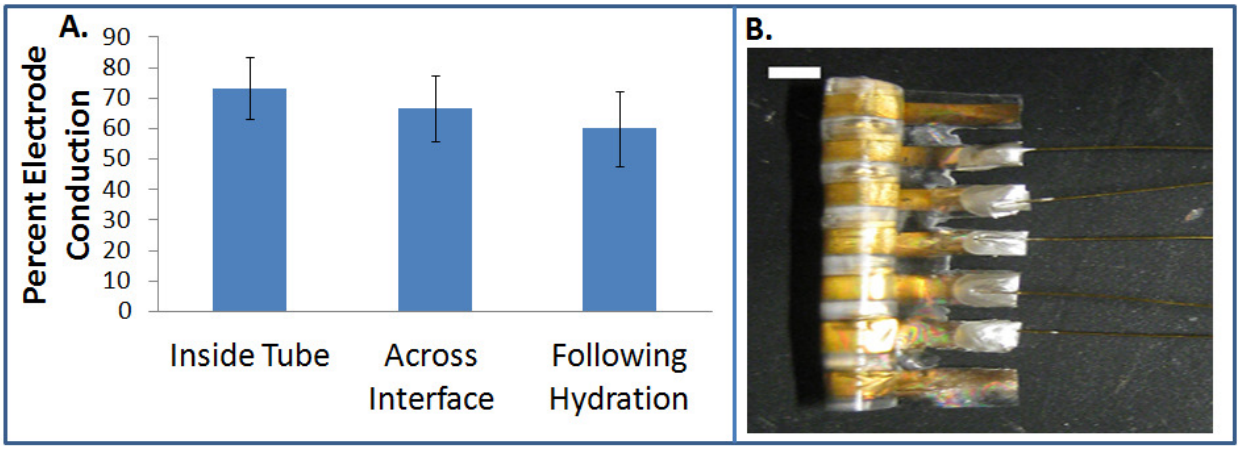

Figure 5.2 Characterization of Electronic Patterned Silk Nerve Guide Conductivity (a) Conductivity measurements inside the silk tube, across the silk tube connector pads, and following 1 week hydration in PBS (b) Image of the electronic patterned silk nerve guide and electronic Interface. For a clear view of the electrodes, inside layer is shown. Scale bar is 1 mm.

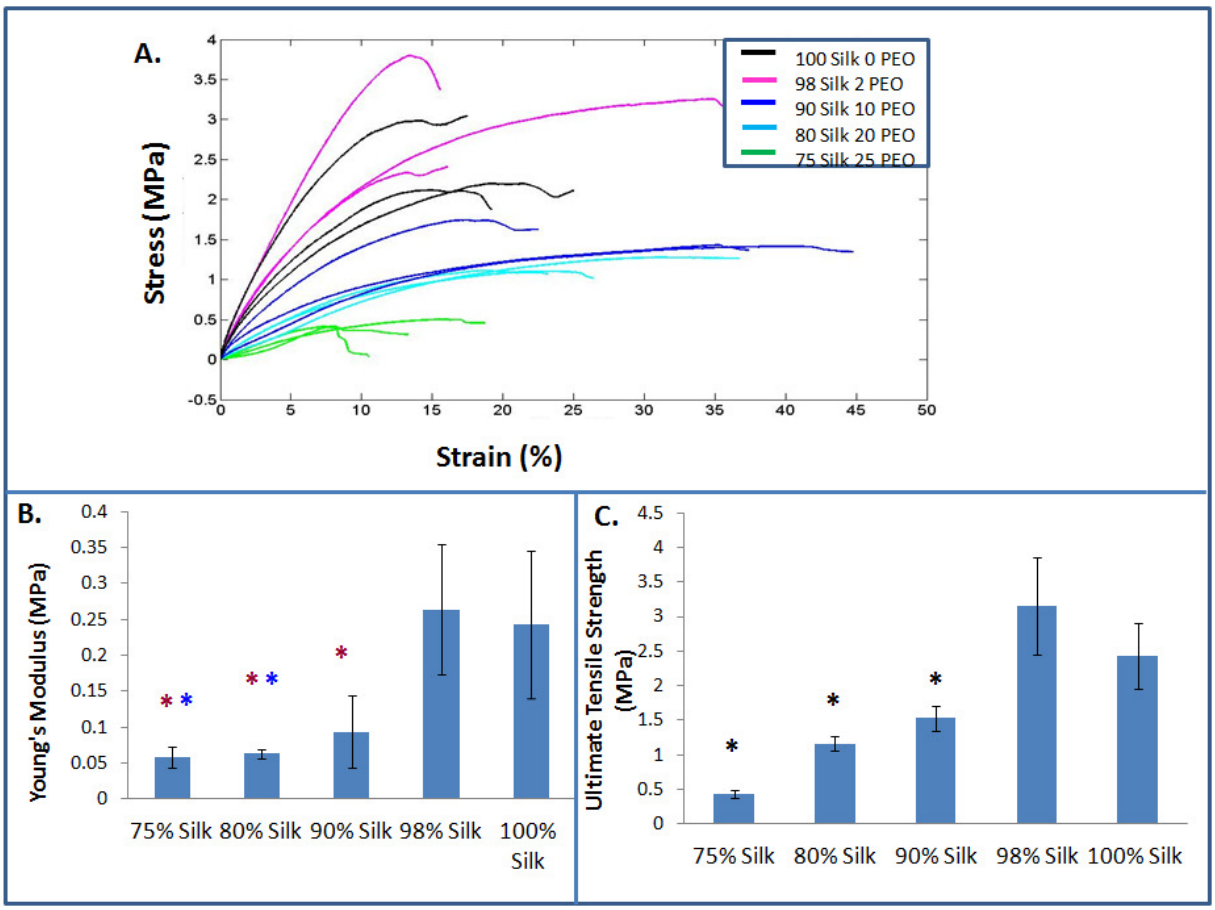

Figure 5.3 Electronic Patterned Silk Nerve Guide Mechanical Characterization (a) Stress-strain curve of electronic silk nerve guides having varying silk and PEO ratios. Stress is defined in MPa as force per area. Percent strain in the axial direction is defined as the difference between the final sample length and the initial sample length divided by the initial sample length. (b) Young's modulus of electronic patterned silk nerve guides at varying silk and PEO ratios. The red asterisk denotes statistical differences ($p < 0.05$) between the group marked and the 98/2 Silk/PEO group. The blue asterisk denotes statistical differences ($p < 0.05$) between the group marked and the 100/0 Silk/PEO group. (c) Ultimate tensile strength. The black asterisk ($p < 0.05$) marks statistical differences ($p < 0.05$) between the group marked and all other groups.

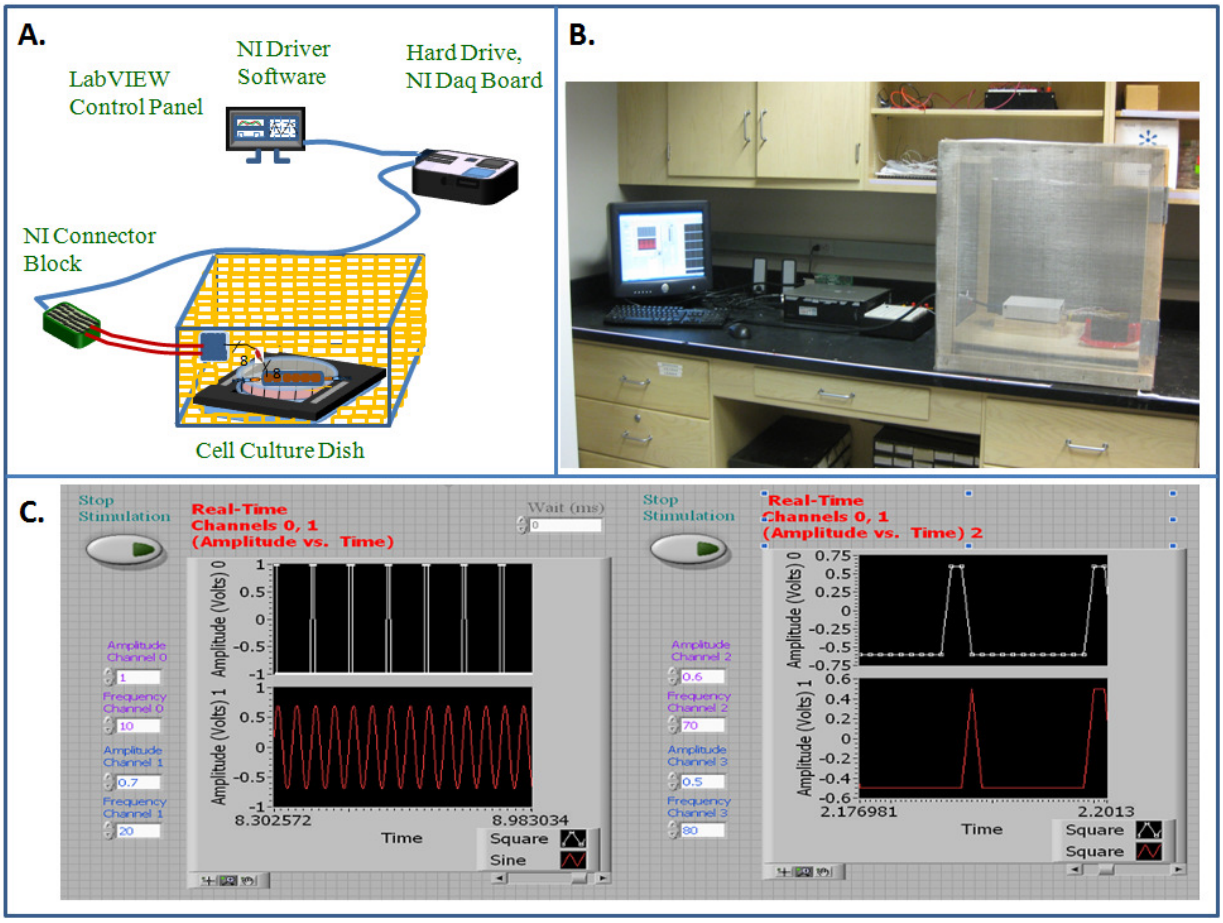

Figure 5.4 External Neural Stimulator (a) Design. The main components include are labeled in green (b) Stimulation Device. While this stimulation device is for the purpose of neuron experiments, this device may be used for stimulation of any cell type. The Faraday cage avoids electromagnetic interference from external sources, such as lights and wall outlets. (c) LabVIEW stimulation program. Amplitude and Frequency of each output channel are entered by the user.

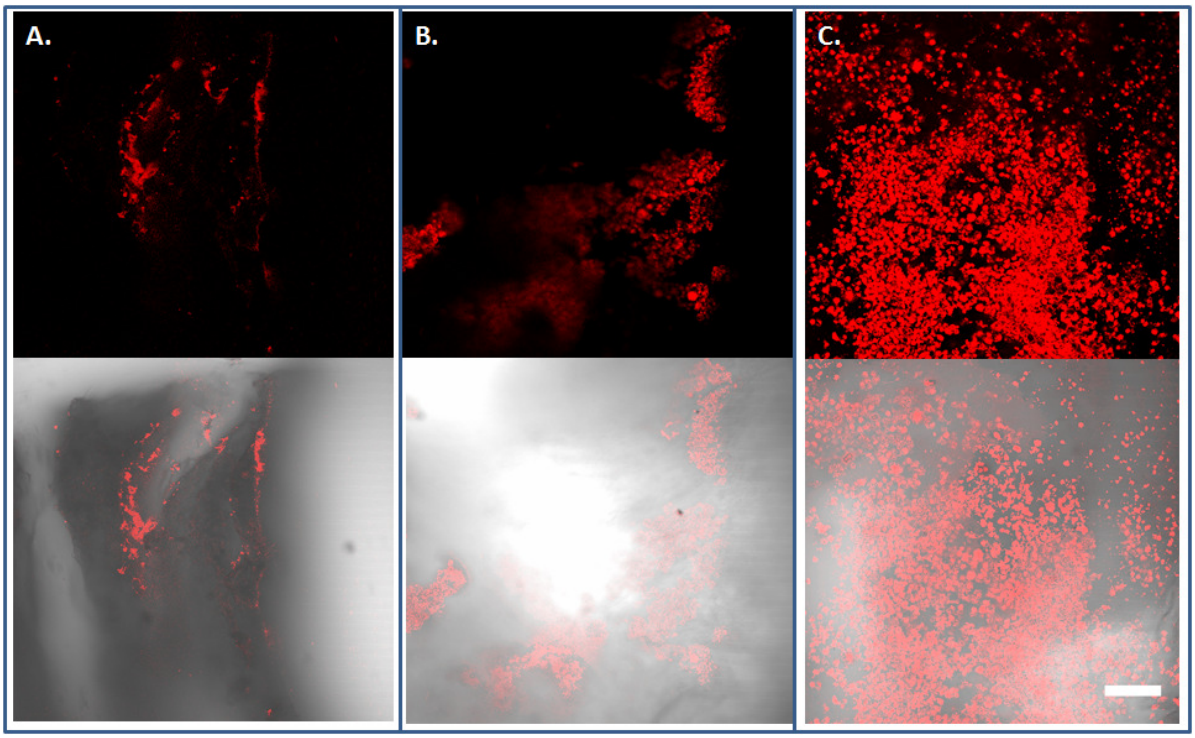

Figure 5.5 Stem cell seeding density in silk nerve guides (a) 1 million cells/cm^2 (b) 2 million cells/cm^2 (c) 4 million cells/cm^2. (top panel) DiI stained stem cells only (bottom panel) Overlay of stem cells attached on silk guide. Scale bar = 100 um.

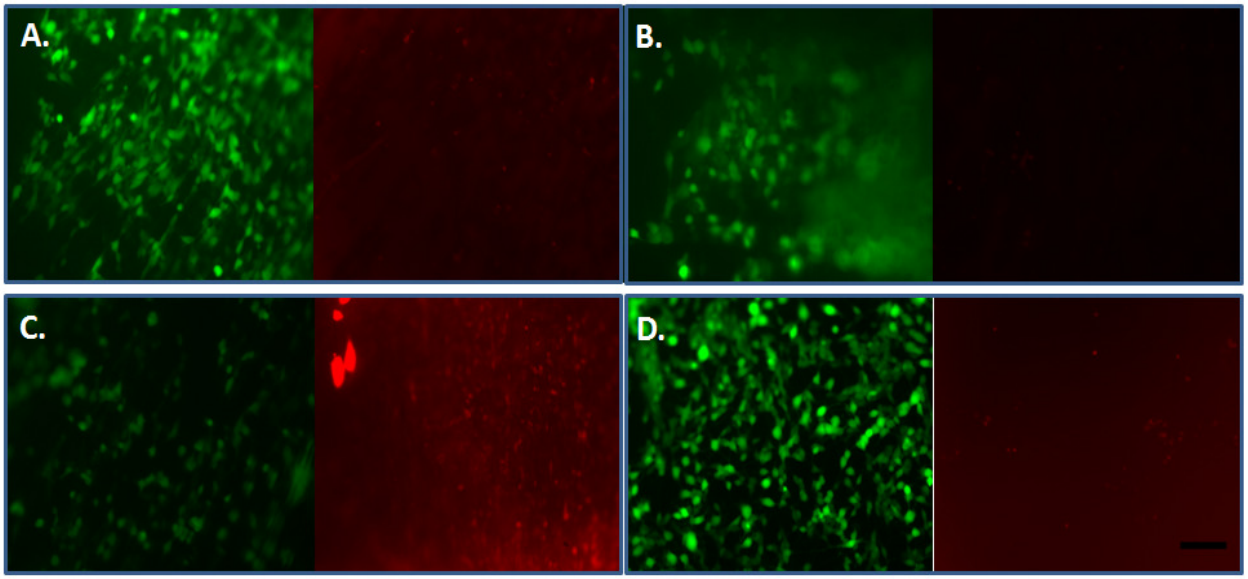

Figure 5.6 SH-SY5Y differentiating neurons in electronic nerve guides following three days after cell seeding (a) patterned guides only (b) perpendicular electrodes (c) parallel electrodes (d) gradient stimulation. (left panel) stain of live cells (right panel) stain of dead cells. Scale bar = 150 um.

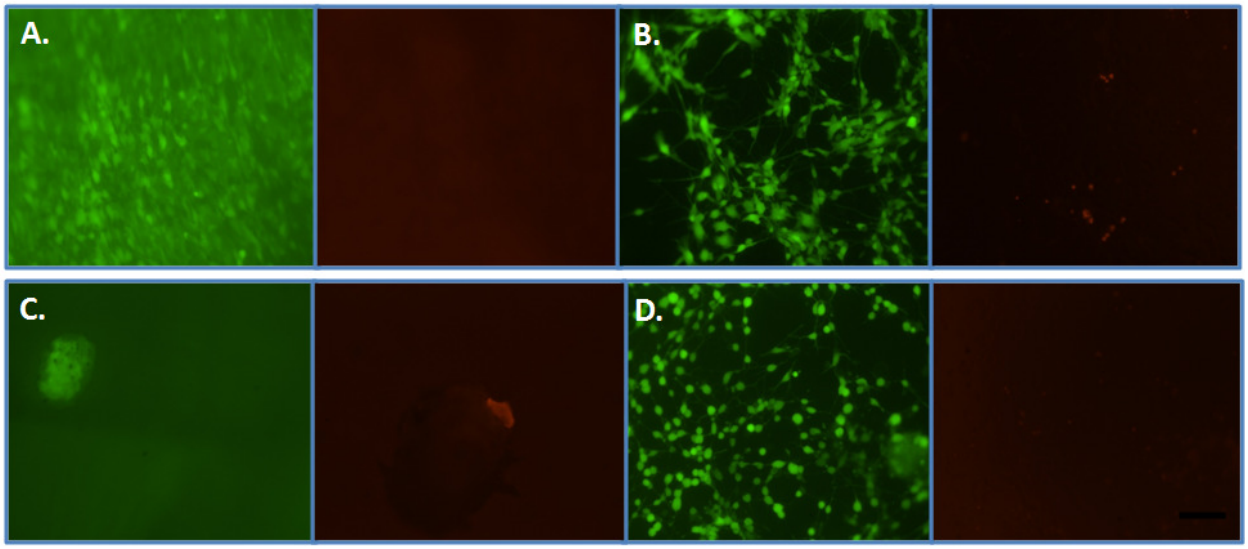

Figure 5.7 SH-SY5Y differentiating neurons in electronic nerve guides following seven days after cell seeding (a) patterned guides only (b) perpendicular electrodes (c) parallel electrodes (d) gradient stimulation. (left panel) stain of live cells (right panel) stain of dead cells. Scale bar = 150 um.

Chapter 6: MECHANISM

6.1 Introduction

Successful peripheral nerve repair is dependent upon the ability of the surrounding microenvironment to provide biochemical and biophysical cues for guiding sprouting axons from the proximal to distal stump, for encouraging axon outgrowth prior to distal stump atrophy, and providing for the remyelination of newly repaired axons (Kehoe et al., 2011). During nerve regeneration, it has been reported that several well known signaling cascades and pathways, including the mitogen-activated protein kinase (MAPK) pathway, the MAPK-kinase (MEK) pathway, the phosphatidylinositol 3-kinase (PI3-Kinase)/Akt pathway, the JNK pathway, the phospholipase Cγ (PLCγ)/ pathway, and the ERK pathway, are involved (**Figure 6.1**). During peripheral nerve regeneration, the MAPK & MEK pathways are known as central mediators in axon sprouting and neural differentiation (Waetzig et al., 2005). The MAPK pathway has been described in several articles to be crucial for neuritogenesis while contributing to neuron survival (Airaksinen et al., 2002; Kaplan et al., 2000). The PI3-kinase/Akt and ERK pathways play a role in activating Schwann cell proliferation and migration following injury.

These regenerative pathways are activated by several receptors and ion channels, including but not limited to, tyrosine kinase receptor A (Trk-A), tyrosine kinase receptor B (Trk-B), tyrosine kinase receptor C (Trk-C), p75 neurotrophin receptor (p75NTR), roundabout (Robo) 2, GDNF-family receptor-α1 (GFR-α1), the G-coupled receptors, and the tenascin-C integrin α9 + β1 (Airaksinen et al., 2002; Kaplan et al., 2000; Waetzig et al., 2005). It is also well known that NGF activates the TRK-A receptor, BDNF activates the TRK-B receptor, and NT-3 activates the TRK-C receptor. The p75NTR receptor, a low affinity binding receptor, is also activated in the presence of several neurotrophins, including NGF, BDNF, and NT-3 (Kiryushko et al., 2004). GDNF activates one of four GFRα receptors, the GFR-α1 receptor, forming a complex with transmembrane receptor, RET (Airaksinen et al., 2002; Yang et al., 2010; Zhang et al., 2009). Activation of TRK and RET receptors occurs through the phosphorylation of tyrosine residues on

the intracellular membrane domains allowing access to high affinity binding sites of several proteins, such as FRS2, downstream of tyrosine kinase 4/5 (DOK4/5), insulin receptor substrate 1/2 (IRS1/2), enigma, and Src-homologous and collagen like protein (Shc) (Airaksinen et al., 2002). These proteins activate downstream signaling pathways (Airaksinen et al., 2002) that push actin filaments (F-actin) in the growth cone outwards (**Figure 6.1**).

Schwann cells play a large role in nerve regeneration through mutliple ways. For example, it is well known that Schwann utilize biophysical means for directing axons from the proximal stump into the endoneurial tubes of the distal stump (Mackinnon et al., 1988). Biochemically, Schwann cells release growth factors, specifically NGF and GDNF, that activate receptors including Trk-A, GFR-α1, RET, and signaling cascades, for enhancing regeneration (Airaksinen et al., 2002; Yang et al., 2010; Zhang et al., 2009). Schwann cells can also release endogenous factor, Slit1 (Zhang et al., 2010). Slit1 may directly activate neurons for regeneration by activating the robo2 receptor (Zhang et al., 2010), which activates the MEK and ERK pathway. Slit1 may indirectly control nerve regeneration by controlling glial behavior (Zhang et al., 2010).

As Scwann cells emerge from the nerve stumps, they come into contact with fibroblasts at the site of injury. Ephrin-B/EphB2 signaling between fibroblasts and Schwann cells help sort these cells, allowing for Schwann cell migration into a position for aligning axons across the injury site. Interestingly, a loss of EphB2 results in impaired directional regrowth (Parrinello et al., 2010)

During regeneration, chondroitin sulfate proteoglycans (CSPGs), as well as inhibitory myelin-associated glycoproteins (MAGs) (Tomita, 2007), are upregulated by Schwann cells and macrophages. CSPGs are inhibitory regulators of axonal regeneration following nerve injury (Carulli, 2005; Muir, 1989; Zuo, 1998). CSPGs promote axon death and block access to Schwann cell basal lamina tubes and laminin molecules

(Salonen, 1987). CSPGs must be degraded by those same cells before axonal growth can continue (Braunewell, 1995; Zuo et al., 1998).

These surrounding cells, neurotrophic receptors, signaling cascades, and the pathways that they activate are summarized in **Figure 6.1.**

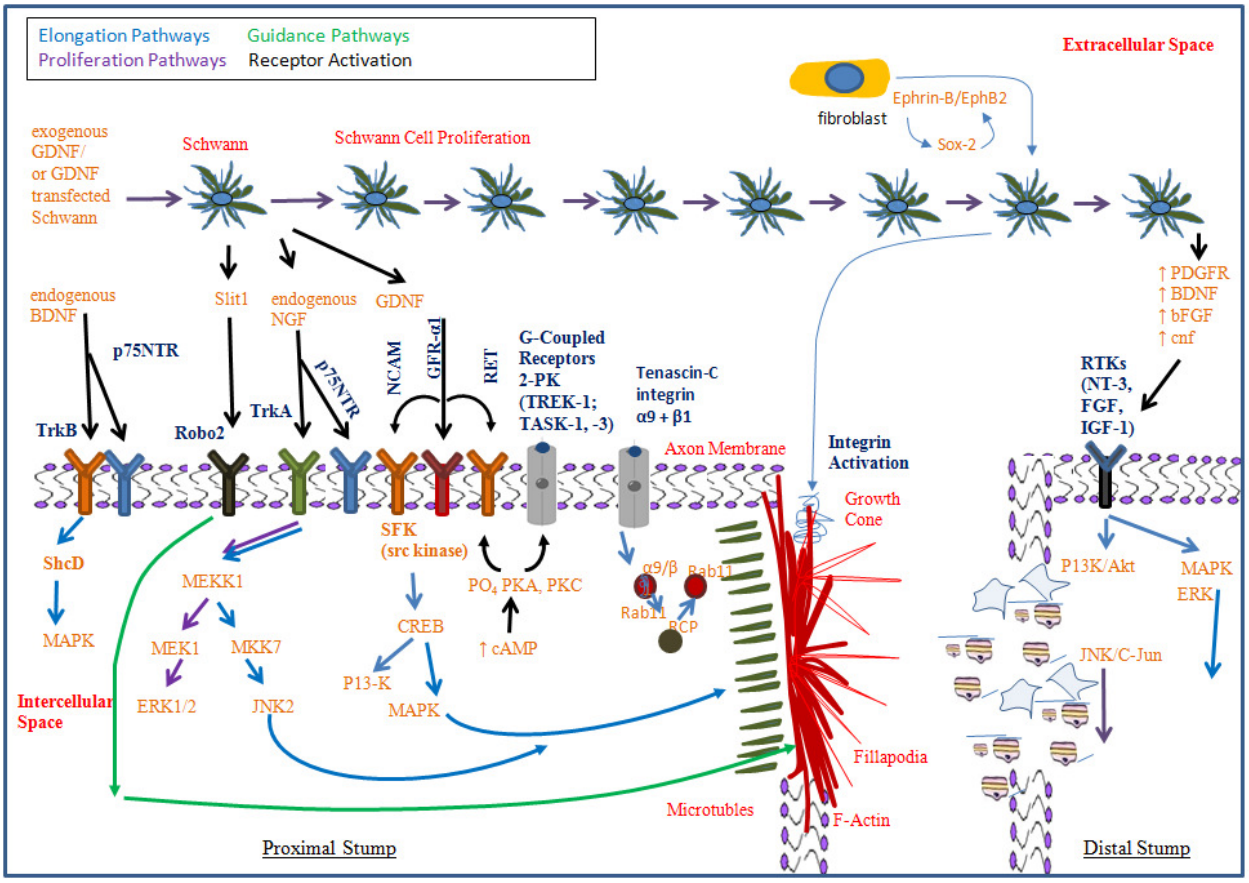

Figure 6.1: A Summary of the Primary Peripheral Nerve Regeneration Pathways. Pathways promoting axon elongation are in blue. Pathways promoting proliferation are in purple. Pathways promoting axon guidance are in green. Black arrows show receptor activation by the corresponding growth factor labeled in orange (Airaksinen et al., 2002; Eva et al., 2010; Meyer-Franke et al., 1998; Parrinello et al., 2010; Waetzig et al., 2005; Yamazaki et al., 2009; You et al., 2010; Zhang et al., 2010; Zhang et al., 2009) (Image drawn by Marie Tupaj, Unpublished, 2010).

While endogenous growth factor release has played the accepted role in activating the neurotrophic receptors that activate the above pathways, we are interested in how electrical fields interact with cells. It has been hypothesized that electrical stimulation may increase endogenous neurotrophic factors that activate these pathways and signaling cascades (Huang et al., 2010; Wan et al., 2010b). Prior literature has also suggested that electrical stimulation may affect neural cell fate in one of several ways, including altering pH, Joule heating, mechanical stress, altering membrane potential, or altering receptor expression (Greenebaum et al., 2007; Klein et al., 2003; McCaig, 1989)(**Figure 6.2**).

In the following studies, we investigated how pH, heat, and receptor expression levels change during a moderate degree of electrical stimulation. Specifically pH levels of cell culture media were monitored over the course of stimulation treatments. Joule heating models were created for understanding the heat generated and temperature change over a range of electrical stimulation parameters. Gene expression levels of two receptors, the p75NTR receptor and the N-methyl-D-aspartame receptor (NMDAR) were examined over different electrical field strengths and frequencies.

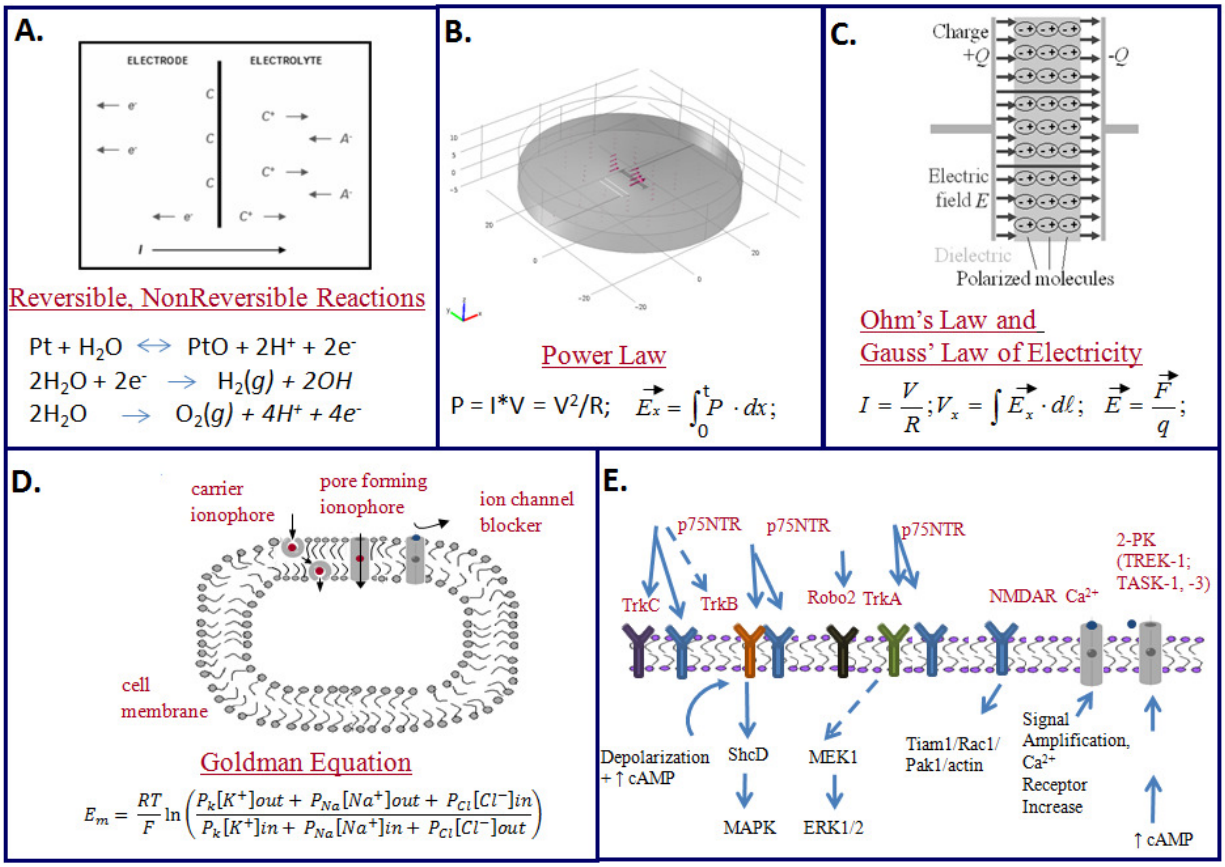

Figure 6.2: Overview of potential nerve regeneration mechanisms during electrical stimulation. Mechanisms may include (a) pH changes, (b) joule heating, (c) mechanical force, (d) altering membrane potential, or (e) altering receptor and ion channel expression. Changes in the local pH environment may be described chemically through reversible and non-reversible faradaic reactions at the electrode-electrolyte interface. Faradaic reactions produce and consume hydrogen and hydroxyl ions at the anode and cathode, respectively. Increases in cell temperature may be caused by Joule heating. Joule heating, described as increases in cell temperature due to energy supplied to the system, may be quantified through integrating the power law over time (Hronik-Tupaj et al., 2011a). As the magnitude of the electric field is in units of Newton/Coulomb, axon growth could be initiated through applied forces on the cell. Changes in extracellular ion concentration from applying an external electric field may alter membrane potential. This relationship between membrane potential from the difference between

extracellular to intercellular ion concentration can be described through the Nernst and Goldman Equations. Changes in growth factor release, receptor activation and receptor expression levels are yet another possibility (Huang et al., 2010; Klein et al., 2003) (Image by Marie Tupaj, Unpublished, 2011).

6.2 Materials & Methods

6.2.1 pH Monitoring

Electrical chambers were built according to the instructions for the design of an Alternating Current (AC) Chamber Device that is described in the materials and methods section in Chapter 2. Complete neuronal cell culture media consisting of a 50:50 composition of DMEM/F12 containing the color pH indicator phenol red (Invitrogen Corp., Grand Island, NY), 10.0% fetal bovine serum (Invitrogen Corp.), and 1.0% penicillin-streptomycin (Invitrogen Corp.) was added to the chambers. Chambers were incubated overnight at 37°C, 5% oxygen. The next morning, a 3 point calibration, using 4.0, 7.0, and 10.0 buffers, was completed on an Accumet Basic AB15 pH meter (Thermo Fisher Scientific, Waltham, MA). Following calibration, the bulb was rinsed in a buffer solution and the pH of the neural culture media was measured in three areas per dish. Specifically, the probe was placed in the top half, middle, and bottom third of the dish, between the electrodes. 0.5 V, 1 V, 5 V, 120 mV 20 Hz, 120 mV 1 kHz, 500 mV 1 kHz, 750 mV 1 kHz, or 120 mV 10 kHz waveforms were applied to each dish. pH measurements of cell culture media were taken prior to stimulation, 15 minutes into stimulation, directly after stimulation and the following day. All measurements were taken inside the incubator at 37°C and 5% oxygen. The sample size for each group was n = 3. All measurements were compared to a control group, without stimulation.

6.2.2 Joule Heating Modeling

Temperature modeling across the chamber was completed using the Joule Heating module in COMSOL Multiphysics® (Burlington, MA), version 4.2, software. COMSOL Multiphysics® approximates partial differential equations by finite element analysis methods. Briefly, the AC chambers were constructed using the COMSOL geometry feature. Chamber materials were either selected from the COMSOL Multiphysics® material library or created for the study. Materials utilized in the model included gold, and cell culture media. The material properties were defined as follows: gold ($\sigma = 4.5 * 10^7$ S/m; $\rho = 9.0$) and SH-SY5Y neuron culture media ($\sigma = 14.4$ S/m; $\rho = 78$), where where σ = materials' conductivity and ρ is the materials' relative permittivity (Eisuke Ishikawaa et al., 1997; Hyung-Kew L et al., 2005; Sun et al., 2009a). Thermal properties were defined as follows: gold ($C_p = 0.128$ J/(kg *K) ; $\rho = 19300$ Kg/m^3 ; $k = 318$ W/(m*K)) and SH-SY5Y neuron culture media, approximated to thermal properties that of saline, ($C_p = 0.94$ J/(kg *K) ; $\rho = 1024$ Kg/m^3 ; $k = 0.6$ W/(m*K)), where Cp is heat capacity at constant pressure, ρ is density, and k is thermal conductivity. Initial temperature for the device was set at 37°C. The geometry was meshed as a coarse free tetrahedral then solved for electric field direction and temperature (°C).

6.2.3 Neural Cell Membrane Receptor Gene Expression

Electrical chambers were built according to the instructions for the design of an Alternating Current (AC) Chamber Device that is described in the materials and methods section in Chapter 2. AC Chambers were sterilized with 70% ethanol and UV then SH-SY5Y stem cells were seeded into the chambers at a density of 5,000 cells/cm^2. Neural differentiation media was made and added to the chambers as also described in the material and methods section in Chapter 2. 120 mV 20 Hz, 120 mV 1 kHz, or a 500 mV 1 kHz sinusoidal waveform was applied to the chambers.

On day 3 and day 9, media was removed from the chambers. Chambers were washed with PBS then neural differentiating SH-SY5Y stem cells were trypsinized, resuspended in cell culture media, and centrifuged at 1250 rpm for 5 minutes. Following centrifugation, the supernatant was removed, cells were lysed in 1 mL of trizol (Invitrogen Corp, Grand Island, NY) then stored at -80°C. mRNA was collected using the Qiagen RNEasy Extraction kit (Qiagen, Valencia, CA). mRNA was converted to cDNA using the PTC-100 Programmable Thermocontroller (MJ Research, Inc., Waltham, MA). cDNA was amplified with the TaqMan Universal PCR Master Mix (Applied Biosystems, Foster City, CA) and the ABI Prism 7000 Sequence Detection System (Applied Biosystems). RT-PCR determined gene expression levels of a low affinity binding neurotrophic receptor, p75NTR (Applied Biosystems, Carlsbad, CA Assay ID #: Hs00609977_m1) and ion channel receptor NMDAR (Applied Biosystems, Carlsbad, CA Assay ID #: Hs00370290_m1). TaqMan® gene expression assays were purchased through Applied Biosystems (Carlsbad, CA). Relative gene expression was normalized to the housekeeping gene GAPDH (Assay ID #: Hs99999905_m1) and calculated using the formula $2^{(\text{Ct value of GAPDH} - \text{Ct value of gene of interest})}$ as previously used in our lab (Mauney et al., 2007) and recommended by the manufacturer (Perkin Elmer User Bulletin #2, Applied Biosystems, Foster City, CA). The threshold cycle (Ct) was selected in the linear range of fluorescence for all genes.

6.2.4 Statistical Analysis

pH measurements and gene expression levels were reported as the mean $\pm$ 1 standard deviation. Statistical significance for pH measurements were identified using one-way analysis of variance (ANOVA) followed by Tukey's test for multiple comparisons. Statistical significance was identified for gene expression using an unpaired two-tailed t-test. A 95% confidence interval ($p < 0.05$) was set for all tests.

In addition to reporting average pH levels prior to, during, following, and the day after stimulation, the percentage of pH change was calculated during, following stimulation, and the next day. The percent

change in pH level was calculated as compared prior to stimulation. Parameters used were organized linearly in a table format according to increasing magnitude and increasing. For easy viewing of results, percent pH change was mapped using a color coded graph.

6.3 Results

6.3.1 Stimulation Effects on Media pH

15 minutes into stimulation, statistical differences ($p < 0.05$) in pH levels were measured in the neural culture media exposed to 5V and 120 mV 20 Hz compared to the control group (**Figure 6.3B, 6.3C**). After 45 minutes of electrical stimulation and into the following day, pH differences ($p < 0.05$) were seen in the 0.5 V group compared to the controls (**Figure 6.3B**). The following day, pH differences ($p < 0.05$) were quantified at 750 mV 1 kHz compared to the control group (**Figure 6.3A**).

In the 5V group, within 15 minutes into electrical stimulation and into the following day there were observable color changes in the media, from the phenol red, between the anode and at the cathode (image not shown). This is in agreement with our measurements of significant changes in pH levels and significant differences in pH levels between nodes.

Between the 120 mV 20 Hz group and the control group there are statistical differences prior to stimulation (**Figure 6.3C**). In order to take into account differences between starting pH level in each group, the percent pH change, compared to the starting pH level prior to stimulation, was calculated. **Figure 6.4** summarizes all electrical parameters that were tried and their effects on the percent change of media pH. Overall, it can be seen from **Figure 6.4** that with increasing frequency and increasing magnitude, there is a greater change in pH.

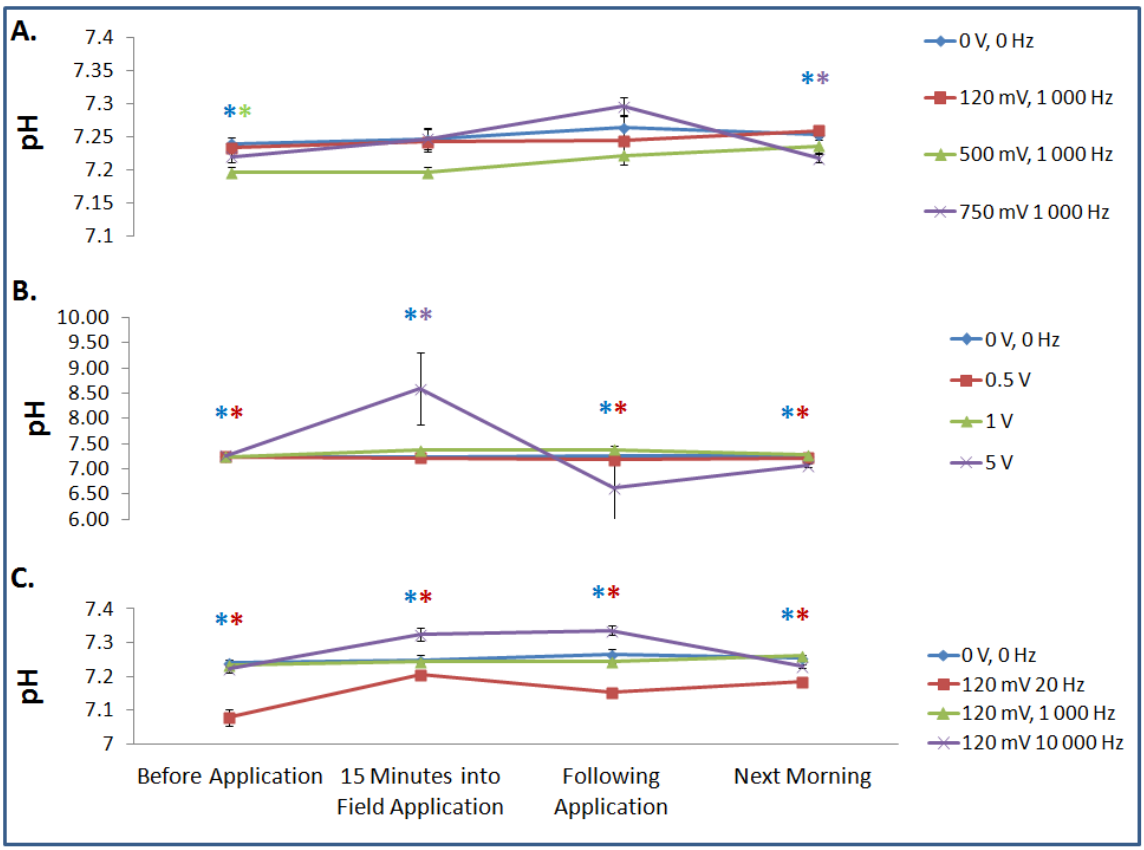

Figure 6.3: Neural Cell Culture Media pH Measurements. Media pH levels were recorded prior to field application, 15 minutes into field application, following application, and the next morning during (a) AC Electrical Stimulation, (b) DC Electrical Stimulation, and (c) over a range of frequencies.

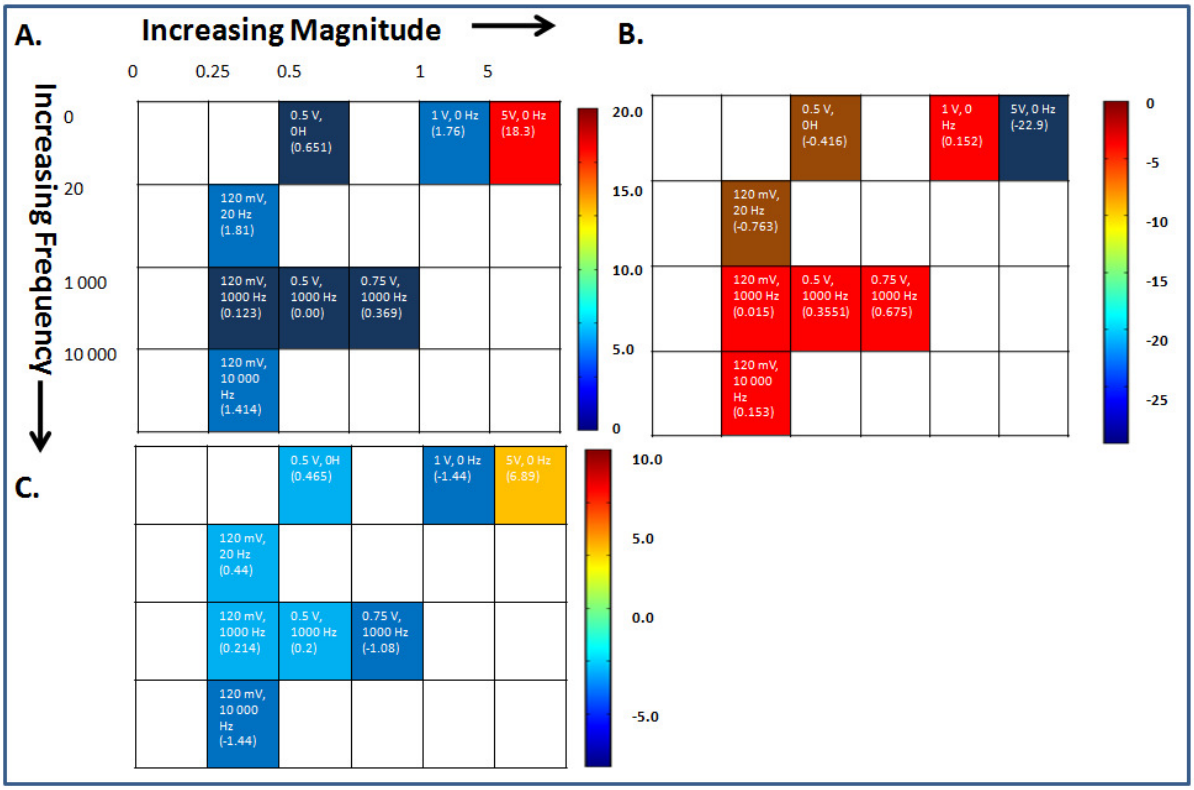

Figure 6.4: A summary of the percent of pH changes in neural cell culture media (a) during field application, (b) following field application, and (c) the next day. A positive percent change is an indication of increasing, more basic, pH levels, a negative percent change is an indication of decreasing, more acidic, pH levels. For a simple interpretation of results, the percent change in pH levels were mapped to a color coded bar. The waveform applied was written in white on the map. The actual percent change in pH levels was written on the map in parentheses below the waveform.

6.3.2 Effects from Joule Heating

The application of electric fields may increase temperature in culture medium *in vitro* or raise temperature levels in the surrounding tissue *in vivo* (Polk et al., 1996). **Figure 6.5** reveals the extent at which cell media has been heated. As current increases in the chamber, chamber temperature

increases. Cell exposed to 120 mV 1 kHz and 500 mV 1 kHz have temperature increases of 0.01° C, and 1.28° C, respectively.

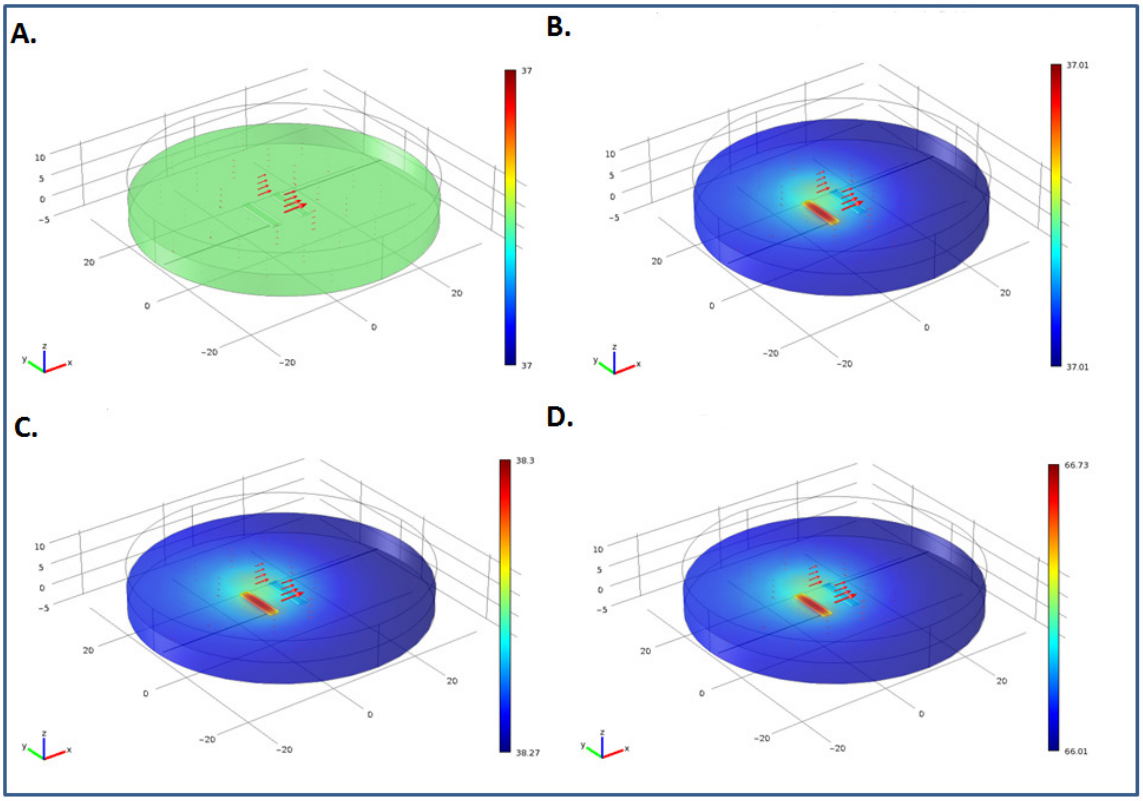

Figure 6.5: Joule Heating Models during (a) no stimulation (b) 120 mV 1,000 Hz (c) 500 mV 1,000 Hz, and (d) 5V 0 Hz. The red arrow is the direction of the electric field. Color bar is chamber temperature in degrees Celsius.

6.3.3 Transcription Factors

Changes in p75NTR and NMDAR gene expression levels were reported during nine day of electrical stimulation. Changes in NMDAR expression was down regulated over nine days compared to controls (**Figure 6.6A**). Levels of p75NTR remained unchanged over nine days compared to the unstimulated group (**Figure 6.6B**).

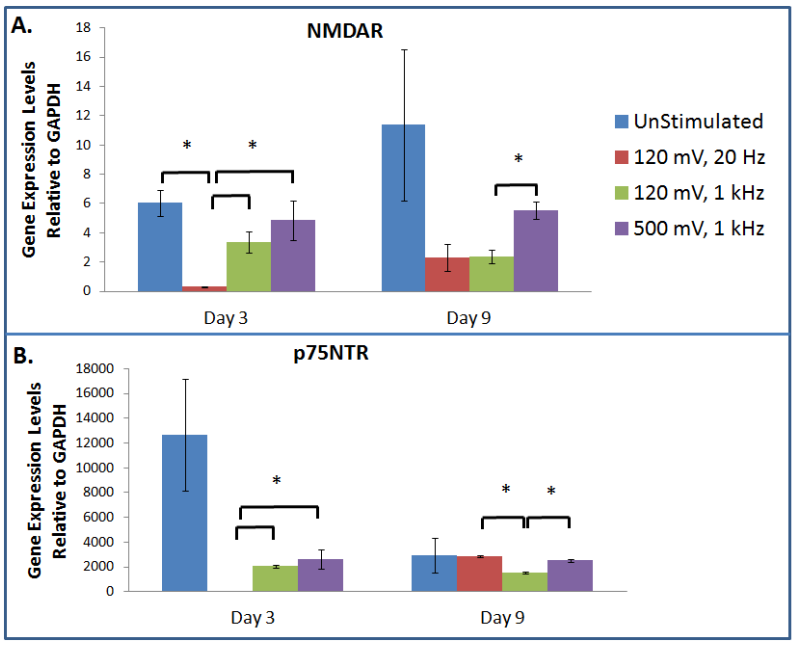

Figure 6.6: Gene Expression Results During Bioelectrical Stimulation Treatments (a) NMDAR (b) p75NTR. Statistical differences ($p < 0.05$) between groups are marked by an asterisk and bracket.

6.4 Discussion

6.4.1 pH Effects

The extent of pH change - Stimulation parameters for pH measurements were chosen based on what has been used for our studies, what has been known as the physiologically relevant ranges, and two extreme cases for reference. The two extreme cases included a control case of 0V, meaning reactions would not be present, and a higher voltage of 5V, a parameter known to induce changes in pH levels in our device. While we understand that even slight pH changes are present in all electrical stimulation studies, prior to this study it was not clear as to what extent the levels were changing. It was found that the amount of pH change was between 1% and 2% at the parameters, 120mV 20 Hz, 120 mV 1 kHz, and 500 mV 1 kHz (**Figure 6.4**). These parameters were used in all electronic studies (i.e., bioelectrical, e-film,

and e-fiber studies). It has been reported that neural media pH of 7.3 is optimal for longest neural cell culture (Potter et al., 2001).

Many of the pH levels that were recorded during and after stimulation were in the physiologically viable range (**Figure 6.3A-C**). However, it can be observed from **Figure 6.4** that with increasing frequency and increasing magnitude, there was a greater change in pH. Large standard deviation bars in the 5V group (**Figure 6.3B**) are most likely due to probe placement within the chamber. Specifically, in the 5 V group, media at the anode of our electrical device measured large decreases in pH, meaning a high concentration of hydrogen ion production, while pH levels close to the cathode had increased pH levels.

A description of reactions at the electrode-electrolyte interface between platinum electrodes and cell culture media is as follows (Chu et al., 2004; Huang et al., 2001):

$$Pt + H_20 \leftrightarrow PtO + 2H^+ + 2e^-; (1)$$

$$Pt + H_20 + e^- \leftrightarrow Pt - H + OH^-; (2)$$

$$2H_20 + 2e^- \rightarrow H_2(g)\uparrow + 2OH; (3)$$

$$2H_20 \rightarrow O_2(g)\uparrow + 4H^+ + 4e^-; (4)$$

Reaction (1) describes hydrogen ion formation at the anode while reaction (2) describes hydroxyl ion formation at the cathode. To avoid byproduct accumulation, neural prosthesthes typically use charged balanced biphasic pulses (Huang et al., 2001). Reaction (3) is hydrogen generation at the electrode-electrolyte interface (Huang et al., 2001). Reaction (4) is oxygen generation at the electrode-electrolyte interface (Huang et al., 2001).

Overall, in the literature, minimal work has been completed in understanding the effects of pH from electrical stimulation on cell viability, growth and differentiation (Huang et al., 2001). One paper

discussed that pH changes are dependent on stimulus duration (Chu et al., 2004). It was also reported larger pH changes in pulses that are monophasic compared to biphasic pulses (Chu et al., 2004).

In addition to changes in hydrogen ion concentration, Faradaic reactions also alter oxygen levels. Increases in oxygen during peripheral nerve stimulation, may increase cell proliferation (Wang et al., 2007) or aid in neurovascularization (Rutkowski et al., 2002).

Elimination of pH effects - Large changes in pH may be an indication of cytotoxic non-reversible faradaic reactions. For eliminating electrolysis byproducts from coming into contact with the cells, or for teasing out the contribution of pH changes on cells during mechanism studies, a salt bridge may be used (**Figure 6.7**). Salt bridges are electrochemical cells that work like batteries transferring electric current to ionic current through agar bridges via a set of oxidation-reduction 'redox' reactions. Salt bridges have been utilized in many electrical stimulation studies for eliminating unwanted byproducts (Tandon et al., 2009a). Protocols for salt bridge fabrication, including silver/silver chloride and copper zinc sulfate designs, have been explained in the literature (Greatbatch, 1981; Hronik-Tupaj et al., 2011a; Tandon et al., 2009b).

Other possibilities of electric field interactions with cells include a cascade of events in which changes in pH levels alter extracellular ion concentrations which alter membrane potential and receptor activation.

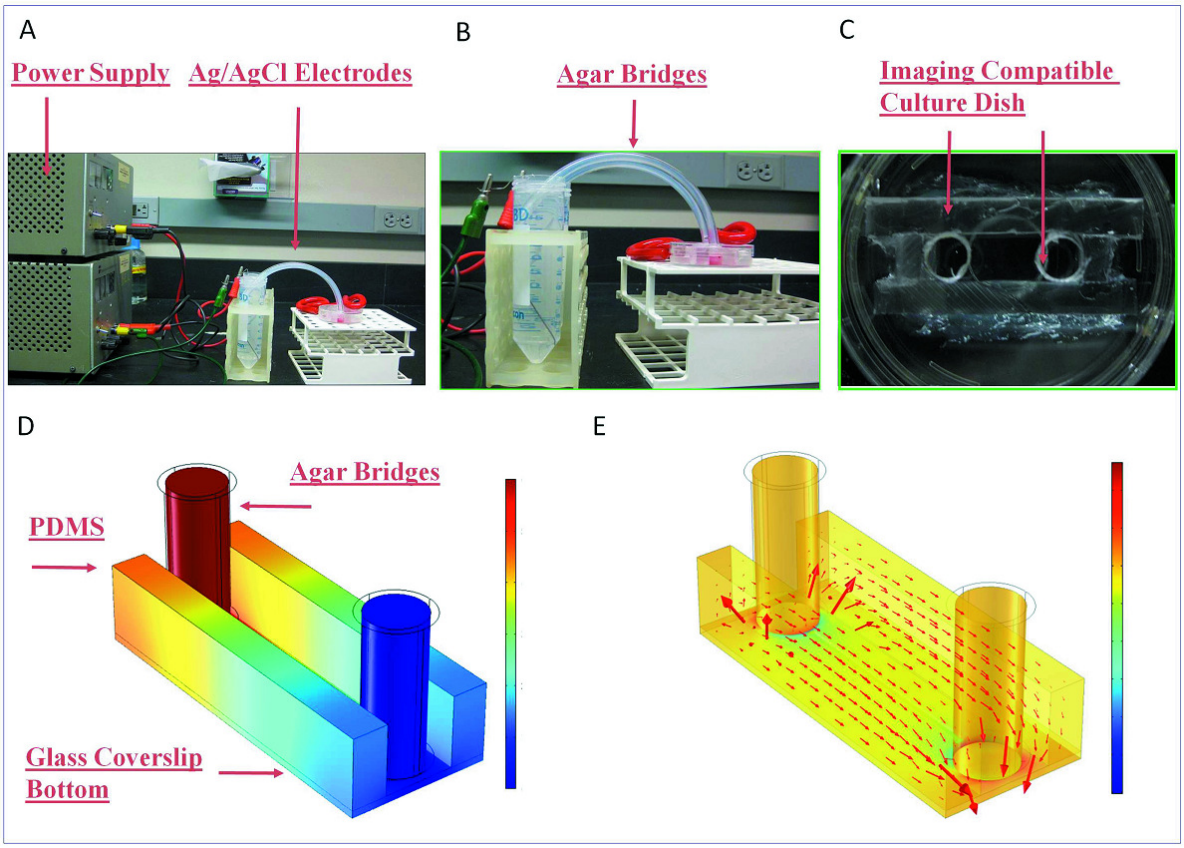

Figure 6.7: *In Vitro* Direct Current Stimulation Device (a) An example of a direct current chamber design using a salt bridge setup. Materials for this design include a power supply, silver/silver chloride electrodes, agar bridges, and an imaging compatible cell culture chamber. (b) Electric current transfers to ionic current via the silver/silver chloride electrodes and agar bridges in PBS. Silver/silver-chloride electrodes were used in this salt bridge design because they are nonpolarizable electrodes. Nonpolarizable electrodes allow for charge transfer between the electrode-electrolyte interface. This allows for a larger ionic current density in the media and a large current strength reaching the cells.This image displays the cell culture dish with agar bridges and silver chloride electrodes in 50 mL conical tubes containing phosphate buffered saline (PBS). (c) An imaging compatible chamber containing a 150 micron thick coverslip bottom. The cover slip bottom is used for imaging following electric field application. (d) The distribution of the applied voltage through the chamber. Quantitative values are not

shown as the applied voltage is user dependent. (e) The field direction and distribution throughout the DC chamber as noted by the red arrows. Field direction and strength is constant throughout the chamber as noted by arrow direction, arrow size, and color. Electric field distributions and strengths are calculated through finite element analysis software, such as COMSOL Multiphysics®. Ionic current supplied over the cells in is the mA range (Jennings et al., 2008). (Figure and caption from (Hronik-Tupaj et al., 2011a)).

6.4.2 Membrane Potential

Electric fields alter ionic currents and ion distributions in the extracellular space, thus altering membrane potential (McLeod, 1992)(**Figure 6.1D**). During electric field exposure, cell membrane potential is changed (Gross et al., 1986b). In non-excitable cells, cell membranes proximal to the anode are hyperpolarized while the cell membrane nearest to the cathode depolarizes (gross et al., 1986a; Sauer et al., 1999). In direct current fields, this polarization is constant and may be responsible for cell orientation and migration. In AC fields, this membrane depolarization and hyperpolarization is changing.

During electric field treatments, the density and distribution of voltage-gated or ligand-gated ion channels and receptors may reorganize (Jahns et al., 2007). Changes in ion channels, gap junctions, ligand binding, and membrane protein density may affect signaling cascades altering downstream processes (Jahns et al., 2007; Tandon et al., 2009b).

6.4.3 Signaling Pathways

Electric Field Receptor Activation - Possible neural receptors activated by electrical stimulation include NMDAR, the TrkA receptor, the TrkB receptor, the p75NTR receptor, the calcium channel, and the two pore domain potassium channel (Huang et al., 2010; Mathie et al., 2003; Mehta et al., 2011; Saygili et al., 2010; Wan et al., 2010a)(**Figure 6.8**). In this research, we examined the p75NTR and the NMDAR

receptors as both have been hypothesized to play a role in electric field activated regeneration pathways and both receptors are present in SH-SY5Y neurons (Costantini et al., 2006; Huang et al., 2010; Mehta et al., 2011; Singh et al., 2005). NMDAR is activated by glutamate and changes in voltage membrane potential, while the p75NTR channel is activated by neurotrophic factors, such as NGF and BDNF. p75NTR receptors and NMDAR receptors are known to activate the MAPK pathway. While we have seen changes in gene expression levels of these receptors, it cannot be said for certain if and how they play a role in regeneration. Further studies will need to incorporate protein expression assays and examine proteins further downstream.

Channel Activation *In Vivo* – *In vivo*, other cells may play the role as mediators for peripheral nerve regeneration in the presence of electric fields. For example, Schwann cells and fibroblasts may be involved in releasing factors, such as endogenous NGF and endogenous BDNF, that activate these receptors and signaling pathways (Huang et al., 2010). Finally, electrical stimulation could increase blood supply to that area (Zanakis, 1990).

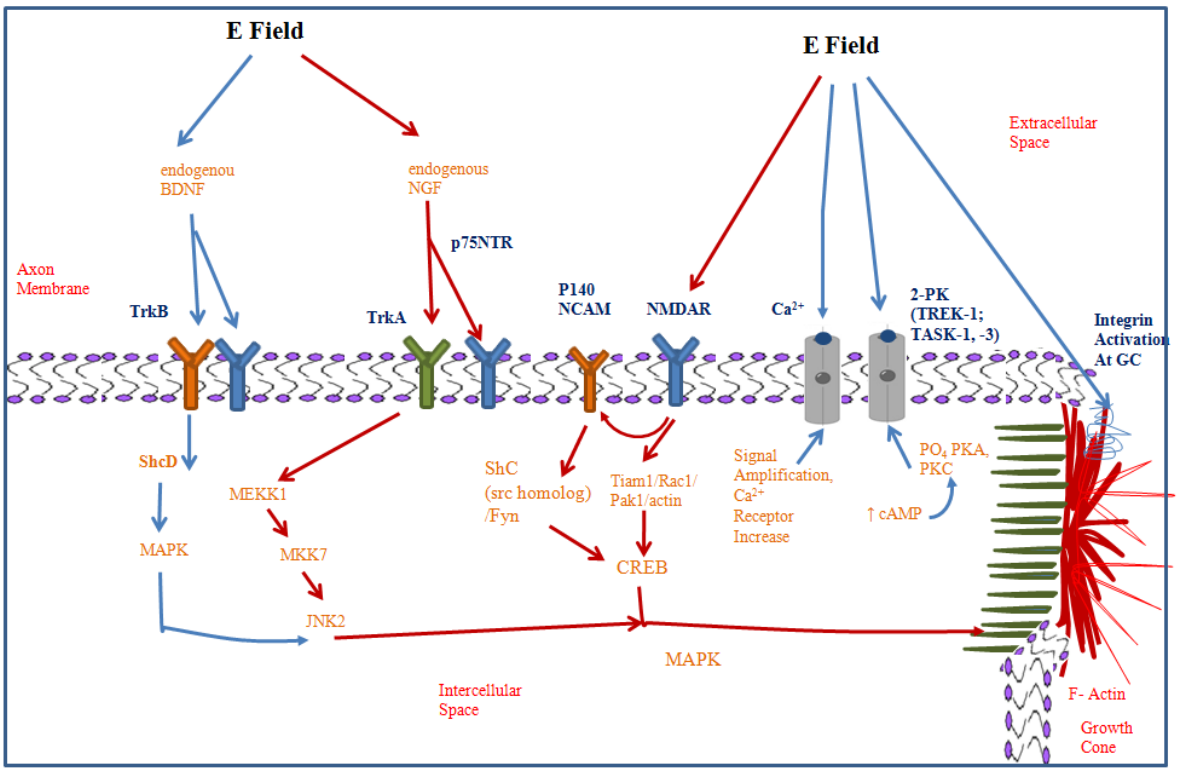

Figure 6.8: Peripheral Nerve Regeneration Pathways Activated through Electrical Stimulation. Pathways that are activated through the p75NTR and the NMDA receptors are marked in red. Additional regenerative pathways by electrical stimulation are marked in blue (Huang et al., 2010; Li et al., 2008a; Mathie et al., 2003; Mehta et al., 2011; Saygili et al., 2010; Wan et al., 2010a) (Image by Marie Tupaj, Unpublished, 2011).

6.4.4 Joule Heating

The Temperature Window for Neuron Survival - While neurons, like other cells and tissues, are commonly incubated at 37°C at 5% CO_2, neurons have a temperature window for cell survival. For example, it has been reported that neurons may survive at room temperature (20-25°C) for 4 days (Magee et al., 1991) and up to 49°C for 10 minutes. After 10 minutes at 60°C neurons were killed (Nagy et al., 1999). In our modeling studies we showed that even moderate levels of electrical stimulation injected low amounts of heat into the cell culture system (**Figure 6.5B,C**). These increases were within a

viable range for cells. While these temperature increases may be within the calibrated temperature range of the incubator, they are temperature increases above the unstimulated cells.

Heat Shock Proteins - Small cellular temperature increases may alter or upregulate transcription factors such as heat shock proteins. Heat shock proteins are small proteins, on the order of 20 - 90 kDa in size, and are involved in protein assembly, folding, repair, and degradation (Goodman et al., 2002). When exposed to higher temperatures or stress they respond through increased gene and protein expression. They are known as stress response markers.

It has been reported that these stress response markers have increased in some cells undergoing differentiation during electric field exposure (Goodman et al., 2002; Hronik-Tupaj et al., 2011b). For example, one article stated that during electric field exposure small increases in heat may upregulate stress factors such as heat shock factor 1 (HSF-1). HSF-1 then mediates increases in heat shock protein 70 (Hsp 70) and increases in MAPK/ERK1/2 phosphorylation in cells (Goodman et al., 2002). Hsp 70 may be a marker for levels of electric field exposure in humans. In another article, it was reported that electric fields may also upregulate stress factors in differentiating bone cells. In these studies, heat shock protein 27 (Hsp 27) was upregulated following response to a 20 mV/cm 60 kHz field (Hronik-Tupaj et al., 2011b).

Heat Shock Proteins in Neuron Regeneration - Phosphorylated and non-phosphorylated Hsp27 has been reported to colocalize with actin and tubulin during DRG growth (Williams et al., 2005). It is also known that heat shock protein 27 increases functional recovery following peripheral nerve injury (Ma et al., 2011). Further down the road it will be helpful to tease out the effects for heat versus electric field studies through exposing cells to the temperature ranges identified in the Joule heating models then comparing their response (i.e., differentiation, proliferation, outgrowth) with the electric field studies.

For confirming how joule heating affects the cell, tracing heat response proteins are a promising avenue.

Future *in vitro* experiments will look at expression levels of common heat shock proteins such as Hsp 27 and Hsp 70 during neuron electrical stimulation as activation from heat produced by electric fields; These studies are currently underway over the next few weeks.

Effects from Decreasing Temperature - While increases in heat may upregulate certain transcription factors, decreases in temperature may inhibit action potentials of neurons in culture through the inhibition of the sodium, potassium ATPase activity. This is important when taking extracellular recordings for assessing neuron functionality.

6.4.5 Force

It is not clear if some cells detect electric field activity at the membrane bilayer or if electromagnetic fields are able to penetrate through the membrane walls directly activating electrons in DNA cells (Goodman et al., 2002). It has also been stated that electric fields exert an electric force on the cells' membrane (panagopoulos et al., 2002). Force fields may be an explanation for physical contraction in myoblastic cell types or in changes in morphology such as in chondrocytes or fibroblasts.

6.5 Conclusions

In summary, cellular mechanisms remain to be elucidated. Identifying the underlying mechanisms correlating how cells interact with electric fields remains difficult (Aaron et al., 2004a). For example, interactions that initiate cellular responses may vary according to the applied neural tissue. Also, frequency, electric field strength, or exposure time may influence different mechanisms for altering cell

fate (Polk et al., 1996). Finally, electric fields may be initiating more than one factor, such as heat & receptor expression, and activating different signaling cascades, may yield a different cellular response.

Chapter 7: FUTURE DIRECTIONS

7.1 Introduction

In this project we demonstrated the potential of *Bombyx* Mori silk fibroin for applications in neural regeneration, we identified the potential of electrical stimulation on the rate and the extent of axon outgrowth, we identified the effect of different silk surface topographies on axon alignment, and we developed methods for incorporating these strategies into silk films and multi-layer silk tubes. There are several silk nerve guide directions and several future directions of electronic-silk systems, some of which are expanded upon in the following sections. These directions include implanting electronic patterned silk tubes *in vivo* following axotomy, designing and fabricating a tissue engineered neurovascular supply for regenerating blood vessels alongside peripheral nerves, and finally the development of a neural network *in vitro*.

7.2 Nerve Guide *In Vivo* Studies

7.2.1 Animal Models

The end goal of the peripheral nerve guide project would be a FDA approved product that performs better than the autograft for repairing gaps greater than 3 cm in humans. Prior to FDA approval and clinical use, small and large animal studies will need to be completed. Many peripheral nerve studies employ the rat sciatic nerve model as the small animal model (**Table 1.3 – 1.5**). Rats are an easier surgical model to work with, compared to the mouse model, due to their larger nerves. The sciatic nerve is typically used for *in vivo* nerve repair studies as it is the main nerve in the peripheral system. Other animal models that have been recently reported for assessing peripheral nerve repair include dogs (Ding et al., 2010) and sheep (Forden et al., 2011; Jeans et al., 2007).

As it takes approximately 2 weeks for severed axons to grow into the conduit and approximately 4 weeks to traverse a 1 cm gap in the rat sciatic nerve (De Boer et al., 2010), an ideal length of time for small animal studies that repair a 1.5 mm nerve defect would be 6 weeks. A 1.5 mm defect is used in small animal studies as it represents a 3 cm critically sized defect in humans.

Following 6 week short term animal studies, long term animal studies need to be completed. Long term studies would be valuable for following up on the extent of functional repair after regeneration. Moreover, long-term animal studies could examine the repair of longer defects, such as 4 - 5 mm and greater. Long term studies could be completed initially in small animals, such as rabbits (Azhar et al., 2004; Hill et al., 2011; McCallister et al., 2005; Sharula et al., 2010), then move to much larger animals such as non-human primates (Irintchev et al., 2011; Schmidhammer et al., 2007). For *in vivo* studies that utilize electronic nerve sieves, it is known that between 2-6 months of treatment is needed for the best regeneration results (Lago et al., 2005; Ramachandran et al., 2006; Wallman et al., 2001). It is uncertain if greater than 6 months of implantation and testing will damage surrounding healthy tissue.

7.2.2 Wireless E-Guides

When using electronic nerve guides for *in vivo* studies, integrating wireless capabilities into the guides would allow for animal mobility and safety. This would also be optimal for future clinical translation. An example of a wireless device for neural stimulation is one that has been designed for small animals and tested in zebra finches (Arfin, 2006; Arfin et al., 2009). This device consisted of an external transmitter, computer interface, a small receiver, and a small stimulator (Arfin, 2006; Arfin et al., 2009). The wireless device size is miniature, approximately 1.5 cm^2, and has low power consumption, approximately 50 µW in awake mode (Arfin, 2006; Arfin et al., 2009). The device delivers between 10 µA to 1 mA current (Arfin, 2006; Arfin et al., 2009), a range that has been reported for effective regenerative outcomes (Hronik-Tupaj et al., 2011a). Some wireless systems have already been developed for providing

untethered solutions *in vivo* and are currently manufactured by companies such as Ripple® (Salt Lake City, UT) and Plexon, Inc (Dallas, TX). As many of these systems are extremely expensive, on the order of tens of thousands, lost cost devices would need to be developed (Shirvalkar et al., 2010).

7.2.3 Electrode Designs and Functionality Testing

Nerve guides that incorporate electrodes for stimulating nerve cells also have the capability of monitoring functionality. Functionality can be monitored by detecting action potentials due to changes in either the cells' intracellular and extracellular membrane potential. Extracellular measurements of action potentials can be taken without damaging the nerve. Extracellular measurements record the difference between voltage on the extracellular side of the cell membrane and ground. Since extracellular signals are on the order of millivolts to microvolts (Henze et al., 2000), an extremely important component of neural detection systems is an amplifier. Systems that utilize bandpass filters to maximize signal to noise ratios are also helpful (Lago et al., 2005).

If functionality testing is incorporated, the current electrode design would need modification. Specifically, electrode size would need optimization. Electrode size needs to be small enough for maximizing signal to noise ratio, while still large enough to have a low enough impedance that allows for signal acquisition. For example, an electrode having 1250 um^2 surface area has impedance of 0.3 to 0.8 MΩ, while an electrode having 177 um^2 surface area has impedance between a 1.8 – 2.5 – 1.5 MΩ impedance (Kipke, 2010). For decreasing electrode impedance while increasing surface area for stimulation, detection, and tissue integration, 3D porous electrodes may be designed. With the information received from functionality testing, the user may even adjust the stimulation treatments (i.e. amplitude, current, time).

Over time, changes at the electrode-tissue interface, such as tissue composition and electrode health, may need examining. Electrode impedance spectroscopy (EIS) measurements would be a valuable tool

for electrode characterization following implantation and over the long term (Johnson et al., 2005; Lempka et al., 2009). Impedance measurements would require acquiring a potentiostat and frequency response analyzer (Lempka et al., 2009).

Since the silk nerve guide degrades over the long term *in vivo*, the fate of the current non-degradable electrode would need to be considered. Design changes may include modifying the electrode shape from a tube to a cuff for easier removal, or changes in conducting material towards something degradable. Immune response of these material and device components would also need examination.

7.3 Development of a Tissue Engineered Neurovascular System

Blood vessels interface with the peripheral nervous system as they lie longitudinally within the epineurium and send branches across the perineurium to create a capillary network in the endonerium (Campbell, 2008; Mackinnon et al., 1988). It is known that vascular cells, which lie within the blood vessels, may aid in nerve regeneration by secreting neurotrophic factors such as BDNF and artemin (ARTN), a member of GDNF family, for encouraging axon outgrowth and axon alignment along the vessel (Lopatina et al., 2011). For the repair of limb and digits, and for the repair of more severe nerve axonotomies, a vascular supply, in addition to a copious nerve supply, may be necessary (Thornton, 1970b; Whimister, 1978b).

7.3.1 Multi-Channel Conduits

Since small diameter silk blood vessels have already been designed and characterized in our lab (Lovett et al., 2007; Lovett et al., 2010), these blood vessels could easily be interfaced with our silk nerve guides as a next step towards functional nerve repair and limb and digit salvage. As one design approach, nerve guides and blood vessels may be built separately then interfaced using extracellular matrix components

or extracellular matrix like components, including collagen and gelatin. As another design approach, nerve and blood vessels may be molded as one unit using standard soft lithography techniques, as previously reported (Tansey et al., 2011; Yao et al., 2010a). More specifically, this neurovascular conduit may be created in the form of a multi-channel guide, with each channel submillimeter in diameter. The small diameter of each channel may help increase nerve guidance. In addition, the conduit designs mimic the structure of the native sciatic nerve and blood vessels.

To date, the literature reporting on the fabrication of neurovascular conduits is extremely limited. Thus, this would be an extremely new and exciting research area. Following neurovascular conduit fabrication, characterization of neurovascular conduits is needed. Nerve conduits have been commonly characterized by their porosity, degradation, and mechanical properties; Blood vessels have been characterized according to thrombotic potential, porosity, nutrient and oxygen diffusion, and mechanical properties such as burst pressure and degradation. Thus, neurovascular conduits would need to be characterized according to design needs of both nerve conduits and blood vessels. Conduit properties would need to replicate properties of the native tissue. For mechanical characteristics, the Young's modulus in the longitudinal direction for peripheral nerves is approximately 8.5 - 40 MPa (Bueno et al., 2008). Blood pressure of capillaries is around 15–40 mmHg (Williams et al., 1988). Nerve guides would need to be at least 80% porous as porosity is important for nutrient diffusion, oxygen diffusion and ultimately nerve regeneration (Belkas et al., 2004). Cellular response in regards to Schwann cell attachment, proliferation, and migration, and endothelial cell attachment, and thrombosis would need assessment. Degradation profiles would vary depending on the injury need.

7.3.2 Neurovascular Supply Functionalization

Like the nerve guide designs, neurovascular channels would also need to be functionalized. For promoting tissue regeneration and integration, vascular agents, could be incorporated into the blood

vessel channels, while neurotrophic agents could be incorporated into the guidance channels. Neurotrophic factors that have been used for peripheral nerve repair are listed in **Table 1.3** and the type of neuron fibers that they regenerate are summarized in **Table 7.1**. Blood vessel channels may be prevascularized for an antithrombotic effect. Nerve guide channels may be seeded with Schwann cells for increasing conduction velocities. Finally, additional applications of neurovascular channels include models for understanding carpel tunnel syndrome or diabetic neuropathy.

Table 7.1: Neurotrophic factors for peripheral nerve repair

Growth Factor(s)	***Regenerative Capabilities***	***References***
NGF	Sensory	(Wang et al., 2010a; Xu et al., 2011)
GDNF	Sensory; Motor	(Kokai et al., 2011; Moore et al., 2010; Wood et al., 2009)
BDNF	Motor	(Boyd et al., 2002)
HGF	Motor, sensory, parasympathetic	(Li et al., 2008b)

7.4 Development of a Neural Network *In Vitro*

A neural network, specifically those which are biological in nature, refers to a group of neurons from the central or peripheral nervous system that is interconnected to complete a specific task or function. Creating neural networks *in vitro* may be useful for studying signaling diseases of the central nervous system, such as epilepsy, and Parkinson's, or understanding the nerve material interface for applications such as improving neural attachment to prosthetic devices.

7.4.1 Chemical Guidance Cues

In the developing nervous system, chemical and geometrical cues are used for guiding the wiring of neural networks (Staii et al., 2011). For attaching and guiding nerve cells on substrates, much research

has been done on utilizing biochemical factors, such as poly lysine (-d,-l), laminin, and RGD peptide (Ananthanarayanan et al., 2010; Azemi et al., 2010; Davis et al., 2002; Gobbels et al., 2010; Green et al., 2009; Haile et al., 2008; Hiraoka et al., 2009; Ignatius et al., 1998; Kafi et al., 2010; Nojehdehian et al., 2010; Ruiz et al., 1999; Stauffer et al., 2006; Thanawala et al., 2007; Yamada et al., 2010). It is known that poly lysine may be a valuable option for nerve attachment to substrates, while laminin has proven valuable for axon outgrowth (Banker et al., 1998).

These adhesion peptides and proteins may be deposited onto biomaterial surfaces via surface adsorption, biomaterial blends, electrostatic attachment, and covalent attachment. As a new option for adhesive proteins, there is a set of proteins called neural cell adhesion molecules (NCAM). NCAMs are a transmembrane glycoprotein containing extracellular and intracelluar transmembrane domains consisting of several N-terminal Ig-like domains linked to fibronectin-like or other domains, which are expressed on neuron and glial cell surfaces (Kunz et al., 2002). Functions of NCAMs include neurite outgrowth, development, cell-cell adhesion, growth cone guidance, axonal pathfinding.

Utilizing NCAM for coupling to silk fibroin will allow for neuron attachment, while having biocompatibility, and full degradability. Since neural cell adhesion sites may be 5 – 200 nm, high resolution patterning on the nanometer scale may be useful (Staii et al., 2011). Since criteria for the development of a neural network includes the deposition of both cytophilic and cytophobic cues for controlling neuron growth on surfaces (Staii et al., 2011), both adhesion proteins and cytophobic proteins could be utilized. While studies have been completed examining short term attachment, up to 14 days, to neural surfaces, there have been few studies examining long term attachment (Ananthanarayanan et al., 2010; Azemi et al., 2010; Davis et al., 2002; Gobbels et al., 2010; Green et al., 2009; Haile et al., 2008; Hiraoka et al., 2009; Ignatius et al., 1998; Kafi et al., 2010; Nojehdehian et al., 2010; Ruiz et al., 1999; Stauffer et al., 2006; Thanawala et al., 2007; Yamada et al., 2010). The use of

peptide and proteins, such as neural cell adhesion molecules, may be the first step towards neuron attachment and guidance for creating neural networks.

7.4.2 Neural Network Assessment Tools

Confocal, multiphoton, and second harmonic generation imaging systems are useful for assessing cellular characteristics such as morphology, growth, metabolic activity, and functionality for neural tissue engineering projects. These characteristics may be acquired via exogenous or endogenous fluorescence. For example, fluorescence resonance energy transfer (FRET) voltage dyes and confocal microscopy may be used to study and quantify neuron membrane potential for understanding neuronal network functionality. Endogenous two-photon excited fluorescence (TPEF) imaging may be used to detect cellular fluorophores such as FAD and NADH in the cells' mitochondria for quantifying metabolic activity (Rice et al., 2010). Serotonin may also be detected endogenously using a three-photon system (Maiti et al., 1997). Microtubules located in neuron axons may be identified using second harmonic generation systems and used for examining axon outgrowth.

Chapter 8: References

Aaron, R., Boyan, B., Ciombor, D., Schwartz, Z., and Simon, B. (2004a). Stimulation of Growth Factor Synthesis by Electric and Electromagnetic Fields. Clin Orthop *419*, 30-37.

Aaron, R., Ciombor, D., Deborah, M., and Simon, B. (2004b). Treatment of Nonunions with Eelctric and Electromagnetic Fields. Clin Orthop *419*, 21-29.

Adams, D., and Levin, M. (2006a). Inverse drug screens: a rapid and inexpensive method for implicating molecular targets. Genesis *44*, 530-540.

Adams, D., and Levin, M. (2006b). Strategies and techniques for investigation of biophyiscal signals in patterning. In "Analysis of Growth Factor Signaling in Embryos" (M. Whitman and A.K. Sater, Eds.) Taylor and Francis Books, 177-262.

Agholme, L., Lindstrom, T., Kagedal, K., Marcusson, J., and Hallbeck, M. (2010). An In Vitro Model for Neuroscience: Differentiation of SH-SY5Y Cells into Cells with Morphological and Biochemical Characteristics of Mature Neurons. Journal of Alzheimer's Disease *20*, 1069-1082.

Ahmed, Z., Underwood, S., and Brown, R. (2003). Nerve Guide Material Made from Fibronectin: Assessment of in vitro properties. Tissue Eng *9*, 219-231.

Airaksinen, M., and Saarma, M. (2002). The GDNF Family: Signaling, Biological Functions and Therapeutic Value. Nature Reviews Neuroscience *3*, 383-394.

Akanji, O., Lee, D., and Bader, D. (2008). The effects of direct current stimulation on isolated chrondrocytes seeded in 3D agarose constructs. Biorheology *45*, 229-243.

Alberts, B., Johnson, A., Lewis, J., Raff, M., Roberts, K., and Walter, P. (2002). Molecular Biology of the Cell, 4th edn.

Allmeling, C., Jokuszies, A., Reimers, K., Kall, S., and Vogt, P. (2006). Use of Spider Silk Fibers as an Innovative Material in a Biocompatible Artificial Nerve Conduit. Journal of Cellular and Molecular Medicine *10*, 770-777.

Aloe, L. (2011). Rita Levi-Montalcini and the Discovery of NGF, the First Nerve Cell Growth Factor. Arch Ital Biol *149*, 175-181.

Alrashdam, M., Sung, M., Kim Kwon, Y., Chung, H., Kim, S., and Lee, J. (2011). Effects of Combining Electrical Stimulation with BDNF Gene Transfer on the Regeneration of Crushed Rat Sciatic Nerve. Acta Neurochir (Wien).

Altman, G., Diaz, F., and al, e. (2003). Silk-based Biomaterials. Biomaterials *24*, 401-416.

Altman, G., Diaz, F., Jakuba, C., Calabro, T., Horan, R., Chen, J., Lu, H., Richmond, J., and Kaplan, D. (2002). Silk-Based Biomaterials. Biomaterials *24*, 401-416.

Ananthanarayanan, B., Little, L., Schaffer, D., Healy, K., and Tirrell, M. (2010). Neural Stem Cell Adhesion and Proliferation on Phospholipid Bilayers Functionalized with RGD Peptides. Biomaterials *31*, 8706-8715.

Apel PJ, Garrett JP, Sierpinski P, Ma J, Atala A, Smith TL, Koman LA, and ME, V.D. (2008). Peripheral Nerve Regeneration Using a Keratin-Based Scaffold: Long-Term Functional and Histological Outcomes in a Mouse Model. J Hand Surg Am *33*, 1541-1547.

Arfin, S. (2006). A Miniature, Implantable Wireless Neural Stimulation System. In Electrical Engineering and Computer Science (Cambridge, Massachusetts Institute of Technology).

Arfin, S., Long, M., Fee, M., and Sarpeshkar, R. (2009). Wireless Neural Stimulationin Freely Behaving Small Animals. J Neurophysiol *102*, 598-605.

Arien-Zakay, H., Nagler, A., Galski, H., and Lazarovici, P. (2007). Neuronal Conditioning Medium and Nerve Growth Factor Induce Neuronal Differentiation of Collagen-Adherent Progenitors Derived From Human Umbilical Cord Blood. J Mol Neurosci *32*, 179-191.

Ariza, C., Fleury, A., Tormos, C., Petruk, V., Chawla, S., Oh, J., Sakaguchi, D., and Mallapragada, S. (2010). The Influence of Electric Fields on Hippocampal Neural Progenitor Cells. Stem Cell Rev *6*, 585-600.
Azemi, E., Gobbel, G., and Cui, X. (2010). Seeding Neural Progenitor Cells on Silicon-Based Neural Probes. J Neurosurg *113*, 673-681.
Azhar, M., and Sara, T. (2004). Comparison of Nerve Graft and Artificial Conduits for Bridging Nerve Defects. Med J Malaysia *59*, 578-584.
Balgude, A., Yu, X., Szymanski, A., and Bellamkonda, R. (2001). Agarose Gel Stiffness Determines Rate of DRG Neurite Extension in 3D Cultures. Biomaterials *22*, 1077-1084.
Banker, G., and Goslin, K. (1998). Culturing Nerve Cells, 2 edn (Cambridge, Ma, MIT Press).
Belkas, J., Shoichet, M., and Midha, R. (2004). Peripheral Nerve Regeneration Through Guidance Tubes. Neurological Research *26*.
Benfenati, V., Toffanin, S., Capelli, R., Camassa, L., Ferroni, S., Kaplan, D., Omenetto, F., Muccini, M., and Zamboni, R. (2010). A Silk Platform that Enables Electrophysiology and Targeted Drug Delivery in Brain Astroglial Cells. Biomaterials *31*, 7883-7891.
Benmerah, S., Lacour, S., and Tarte, E. (2009). Design and Fabrication of Neural Implant with Thick Microchannels Based on Flexible Polymeric Materials. Conf Proc IEEE Eng Med Biol Soc, 6400-6403.
Blackiston, D., McLaughlin, K., and Levin, M. (2009). Bioelectric Controls of Cell Proliferation Ion Channels, Membrane Voltage and the Cell Cycle. Cell Cycle *8*, 3527-3536.
Blumenthal, N., Ricci, J., Breger, L., Zychlinsky, A., Solomon, H., Chen, G., and Dorfman, R. (1997). Effects of low-intensity AC and/or DC electromagnetic fields on cell attachment and induction of apoptosis. Bioelectromagnetics *18*, 264-272.
Bonica, J., and Loeser, J. (2001). Loeser, Bonica's Management of Pain.
Borgens, R., Vanable, J.J., and Jaffe, L. (1979). Role of Subdermal Current Shunts in the Failure of Frogs to Regenerate. J Exp Zool *209*, 49-56.
Borschel, G., Dennis, R., and Kuzon, W.J. (2004). Contractile Skeletal Muscle Tissue-Engineered on an Acellular Scaffold. Plast Reconstr Surg *113*, 595-602.
Boyd, J., and Gordon, T. (2002). A Dose-Dependent Facilitation and Inhibition of Peripheral Nerve Regeneration by Brain-Derived Neurotrophic Factor. Eur J Neurosci *15*, 613-626.
Braga-Silva, J. (1999). The Use of Silicone Tubing in the Late Repair of the Median and Ulnar Nerves in the Forearm. J Hand Surg Br *24*, 703-706.
Braunewell, K., et al (1995). Up-Regulation of a Chondroitin Sulphate Epitope During Regeneration of Mouse Sciatic Nerve: Evidence that the Immunoreactive Molecules Are Related to the Chondroitin Sulphate Proteoglycans Decorin and Versican. Eur J Neurosci *7*, 792-804.
Brighton, C., Wang, W., and Clark, C. (2006). Up-regulation of matrix in bovine articular cartilage explants by electric fields. Biochem Biophys Res Commun *342*, 556-561.
Brunetti, V., Maiorano, G., Rizzello, L., Sorce, B., Sabella, S., Cingolani, R., and Pompa, P. (2010). Neurons Sense Nanoscale Roughness with Nanometer Sensitivity. Proc Acad Sci USA *107*, 6264-6269.
Bueno, F., and Shah, S. (2008). Implications of Tensile Loading for the Tissue Engineering of Nerves. Tissue Eng Part B *14*, 219-233.
Burnett, M., and Zager, E. (2004). Pathophysiology of Peripheral Nerve Injury: A Brief Review. Neurosurgery Focus *16*.
Campbell, W. (2008). Evaluation and Management of Peripheral Nerve Injury. Clinical Neurophysiology *119*, 1951-1965.
Cao, J., Sun, C., Zhao, H., Xiao, Z., Chen, B., Gao, J., Zheng, T., Wu, W., Wang, J., and Dai, J. (2011). The Use of Laminin Modified Linear Ordered Collagen Scaffolds Loaded With Laminin-Binding Ciliary Neurotrophic Factor for Sciatic Nerve Regeneration in Rats. Biomaterials *32*, 3939-3948.
Carulli, D.e.a. (2005). Chrondroitin Sulfate Proteoglycans in Neural Development and Regeneration. Curr Opin Neurobiol *15*, 116-120.

Chang, C., and Hsu, S. (2007a). Effects of Unidirectional permeability in asymmetric poly(DL-lactic acid-co-glycolic acid) conduits on peripheral nerve regeneration: an in vitro and in vivo study. J Biomed Mater Res B Appl Biomater *83*, 206-215.
Chang, C., Hsu, S., Yen, H., Chang, H., and Hsu, S. (2007b). Effects of unidirectional permeability in asymmetric poly(DL-lactic acid-co-glycolic acid) conduits on peripheral nerve regeneration: an in vitro and in vivo study. J Biomed Mater Res B Appl Biomater *83*, 206-215.
Chang CJ, Hsu SH, Lin FT, Chang H, and CS, C. (2005). Low-Intensity-Ultrasound-Accelerated Nerve Regeneration Using Cell-Seeded poly(D,L-lactic acid-co-glycolic acid) Conduits: An In Civo and In Vitro Study. J Biomed Mater Res B Appl Biomater *75*, 99-107.
Chang, P., Sulik, G., and Soong, H. (1996). Galvanotropic and Galvanotactic Responses of Corneal Endothelial Cells. J Formos Med Assoc *95*, 623-627.
Chen, Y., Chang, J., Cheng, C., Tsai, F., Yao, C., and Liu, B. (2005). An in vivo evaluation of a biodegradable genipin-cross-linked gelatin peripheral nerve guide conduit material. Biomaterials *26*, 3911-3918.
Cheng, C., LeDuc, P., and Lin, Y. (2011). Localized Bimodal Response of Neurite Extensions and Structural Proteins in Dorsal-Root Ganglion Neurons with Controled Polydimethylsiloxane Substrate Stiffness. J Biomech *44*, 856-862.
Cho, Y., Shi, R., Ivanisevic, A., and Borgens, R. (2010). Functional Silica Nanoparticles-Mediated Neuronal Membrane Sealing Following Traumatic Spinal Cord Injury. J Neurosci Res *88*, 1433-1444.
Chu, A., Morris, K., Greenberg, R., and Zhou, D. (2004). Stimulus Induced pH Changes in Retinal Implants. Conf Proc IEEE Eng Med Biol Soc *6*, 4160-4162.
Chuangsuwanich, A., Charnsanti, O., Lohsiriwat, V., Kangwanpoom, C., and Thong-In, N. (2011). The Efficacy of Silver Mesh Dressing Compared wiht Silver Sulfadiazine Cream for the Treatment of Pressure Ulcers. J Med Assoc Thai *94*, 559-565.
Clarke, J., Tuft, B., Clinger, J., Levine, R., Fiqueroa, L., Allan Guymon, C., and Hansen, M. (2011). Micropatterned Methacrylate Polymers Direct Spiral Ganglion Neurite and Schwann Cell Growth Hear Res.
Cone, C.J., and Cone, C. (1976). Induction of Mitosis in Mature Neurons in Central Nervous System by Sustained Depolarization. Science *192*, 155-158.
Cone Jr, C. (1970). Variation of the transmembrane potential level as a basic mechanism of mitosis control. oncology *24*, 438-470.
Costantini, C., Scrable, H., and Puglieli, L. (2006). An Aging Pathway Controls the TrkA to p75NTR Receptor Switch and Amyloid Beta-Peptide Generation. EMBO J *26*, 1997-2006.
Costanzo, L. (2002). Physiology, 2 edn (Elsevier Science).
Cum, S. (2000). Biology of Sensory Systems.
Darmon, M. (1982). Laminin Provides a Better Substrate Than Fibronectin for Attachment, Growth, and Differentiation of 1003 Embryonal Carcinoma Cells. In Vitro *18*, 997-1003.
Davis, D., Giannoulis, C., Johnson, R., and Desai, T. (2002). Immobilization of RGD to < 1 1 1 > Silicon Surfaces for Enhanced Cell Adhesion and Proliferation. Biomaterials *23*, 4019-4027.
De Boer, R., Knight, A., Borntraeger, A., Hebert-Blouin, M., Spinner, R., Malessy, M., Yaszemski, M., and Windebank, A. (2011). Rat Sciatic Nerve Repair with a Poly-Lactic-Co-Glycolic Acid Scaffold and Nerve Growth Factor Releasing Microspheres. Microsurgery *E pub Ahead of Print*.
De Boer, R., Knight, A., Spinner, R., Malessy, M., Yaszemski, M., and Windebank, A. (2010). In Vitro and In Vivo Release of Nerve Growth Factor From Biodegradable Poly-Lactic-Co-Glycolic-Acid Microspheres. J Biomed Mater Res A *95*, 1067-1073.
Denham, M., and Dottori, M. (2011). Neural Differentiation of Induced Pluripotent Stem Cells. Methods Mol Biol *793*, 99-110.

Dhar, S., McConnel, M., Gharibjanian, N., Young, C., Rogers, J., Nguyen, T., and Evans, G. (2007). Herpes Simplex Virus-Thymidine Kinase-Based Suicide Gene Therapy as a "Molecular Switch Off" for Nerve Growth Factor Production in Vitro. Tissue Eng *13*, 2357-2365.
Di Summa, P., Kalbermatten, D., Pralong, E., Raffoul, W., Kingham, P., and Terenghi, G. (2011). Long-Term In Vivo Regeneration of Peripheral Nerves Through Bioengineered Nerve Grafts. Neuroscience *181*, 278-291.
Di Summa, P., Kingham, P., Raffoul, W., Wiberg, M., Terenghi, G., and Kalbermatten, D. (2010). Adipose-Derived Stem Cells Enhance Peripheral Nerve Regeneration. J Plast Reconstr Aesthet Surg *63*, 1544-1152.
Dillingham, T. (2002). Limb Amputation and Limb Deficiency: Epidemiology and Recent Trends in the United States. Southern Medical Journal *95*, 877-883.
Ding, F., Wu, J., Yang, Y., Hu, W., Zhu, Q., Tang, X., Liu, J., and Gu, X. (2010). Use of Tissue-Engineered Nerve Grafts Consisting of a Chitosan/Poly(Lactic-Co-Glycolic Acid)-Based Scaffold Included with Bone Marrow Mesenchymal Cells for Bridging 50-mm Dog Sciatic Nerve Gaps. Tissue Eng Part A *16*, 3779-3790.
Ding, T., Lu, W., Zheng, Y., Li, Z., Pan, H., and Luo, Z. (2011). Rapid Repair of Rat Sciatic Nerve Injury Using a Nanosilver-Embedded Collagen Scaffold Coated with Laminin and Fibronectin. Regen Med *6*, 437-447.
Diniz, P., Shomura, K., Soejima, K., and Ito, G. (2002). Effects of pulsed electomagnetic field (PEMF) stimulation on bone tissue like formation are dependent on the maturation stages of the osteoblasts. Bioelectromagnetics *23*, 398-405.
Donnelly, E., Strappe, P., McGinley, L., Madigan, N., Geurts, E., Rooney, G., Windebank, A., Fraher, J., Dockery, P., O'Brien, T., and McMahon, S. (2010). Lentiviral Vector-Mediated Knockdown of the Neuroglycan 2 Proteoglycan or Expression of Neurotrophin-3 Promotes Neurite Outgrowth in a Cell Culture Model of the Glial Scar. J Gene Med *12*, 863-872.
Dube, J., Methot, S., Moulin, V., Goulet, D., Bourdage, M., Auger, F., and Germain, L. (2005). External Electric fields induce morphological changes on human skin cells cultured in vitro (USRI).
Eisuke Ishikawaa, Seoung-Kwon Baea, Osato Miyawakia, Kozo Nakamuraa, Yasuhiko Shiinokib, and Itob, K. (1997). Freezing Injury of Cultured Rice Cells Analyzed by Dielectric Measurement. Journal of Fermentation and Bioengineering *83*, 222-226.
Emel, E., Ergun, S., Kotan, D., Gursoy, E., Parman, Y., Zengin, A., and Nurten, A. (2011). Effects of Insulin-Like Growth Factor-1 and Platelet-Rich Plasma on Sciatic Nerve Crush Injury in a Rat Model. J Neurosurg *114*, 522-528.
Erba, P., Mantovani, C., Kalbermatten, D., Pierer, G., Terenghi, G., and Kingham, P. (2010). Regeneration Potential and Survival of Transplanted Undifferentiated Adipose Tissue-Dervied Stem Cells in Peripheral Nerve Conduits. J Plast Reconstr Aesthet Surg, Epub Ahead of Print.
Esaki, S., Kitoh, J., Katsumi, S., Goshima, F., Kimura, H., Safwat, M., Yamano, K., Watanabe, N., Nonoguchi, N., Nakamura, T., Coffin, R., Miyatake, S., Nishiyama, Y., and Murakami, S. (2011). Hepatocyte Growth Factor Incorporated into Herpes Simplex Virus Vector Accelerates Facial Nerve Regeneration After Crush Injury. Gene Ther *Epub Ahead of Print*.
Etienne, O., Schneider, A., Kluge, J., Bellemin-Laponnaz, C., Polidori, C., Leisk, G., Kaplan, D., Garlick, J., and Egles, C. (2009). Soft Tissue Augmentation Using Silk Gels: An In Vitro and In Vivo Study. J Periodontol *80*, 1852-1858.
Eva, R., Dassie, E., Caswell, P., Dick, G., French-Constant, C., Norma, J., and Fawcett, J. (2010). Rab11 and Its Effector Rab Coupling Protein Contribute to the Trafficking of B1 Integrins During Axon Growth in Adult Dorsal Root Ganglion Neurons and PC12 Cells. The Journal of Neuroscience *30*, 11654-11669.
Fassina, L., Visai, L., Benazzo, F., Bennedetti, L., Calligaro, A., De Angelis, M., Farina, A., Maliardi, V., and Margenes, G. (2006). Effects of electromagnetic stimulation on calcified matrix production by SAOS-2 cells over a polyurethane porous scaffold. Tissue Eng *12*, 1985-1999.

Fassina, L., Visai, L., Saino, E., Cusella De Angelia, C., Benazzo, F., and Magenes, G. (2007). Surface Modification of titanium fiber-mesh scaffolds through a culture of human SAOS-2 osteoblasts electromagnetically stimulated. IFMBE Proceedings *16*, 238-241.
Fatemi MJ, Foroutan KS, Ashtiani AK, Mansoori MJ, Vaghardoost R, Pedram S, Hosseinpolli A, Rajabi F, and SJ, M. (2010). Comparison of divided sciatic nerve growth within dermis, venous and nerve graft conduit in rat. J Res Med Sci *15*, 208-213.
Fedoroff, S., and Richardson, A., eds.Protocols for Neural Cell Culture, 3rd edn (Humana Press).
Finley, M., Kulkarni, N., and Huettner, J. (1996). Synapse Formation and Establishment of Neuronal Polarity by P19 Embryonic Carcinoma Cells and Embryonic Stem Cells. The Journal of Neuroscience *16*, 1056-1065.
Forden, J., Xu, Q., Khu, K., and Midha, R. (2011). A Long Peripheral Nerve Autograft Model in the Sheep Forelimb. Neurosurgery *68*, 1354-1362.
Fozdar, D., Lee, J., Schmidt, C., and Chen, S. (2010a). Hippocampal Neurons Respond Uniquely to Toppographies of Various Sizes and Shapes. Biofabrication *2*, 035005.
Fozdar, D., Lee, J., Schmidt, C., and Chen, S. (2010b). Selective Axonal Growth of Embryonic Hippocampal Neurons According to Topographic Features of Various Sizes and Shapes. Int J Nanomedicine *6*, 45-57.
Fu, K., Dai, L., Chiu, I., Chen, J., and Hsu, S. (2011). Sciatic Nerve Regeneration by Microporous Nerve Conduits Seeded With Glial Cell Lined-Derived Neurotrophic Factor or Brain-Derived Neurotrophic Factor Gene Transfected Neural Stem Cells. Artif Organs.
Fujita, S., Ohshima, M., and Iwata, H. (2009). Time-Lapse Observation of Cell Alignment on Nanogrooved Patterns. J R Soc Interface *6*, S269-S277.
George, i., Geddis, m., Lill, z., Lin, h., Gomez, t., Blank, m., Oz, m., and Goodman, r. (2008). Myocardial function improved by electromagnetic field induction of stress protein hsp70. J Cell Physiol *216*, 816-823.
Ghaznavi, A., Kokai, L., Lovett, M., Kaplan, D., and Marra, K. (2011). Silk Fibroin Conduits: A Cellular and Functional Assessment of Peripheral Nerve Repair. Ann Plast Surg *66*, 273-279.
Gil, E., Park, S., Marchant, J., Omenetto, F., and Kaplan, D. (2010). Response of Human Corneal Fibroblasts on Silk Film Surface Patterns. Macromol Biosci.
Gobbels, K., Kuenzel, T., Van Ooyen, A., Baumgartner, W., Schnakenberg, U., and Braunig, P. (2010). Neuronal Cell Growth on Iridium Oxide. Biomaterials *31*, 1055-1067.
Gomez, N., Chen, S., and Schmidt, C. (2007a). Polarization of Hippocampal Neurons with Competitive Surface Stimuli: Contact Guidance Cues are Prefered Over Chemical Ligands. J Royal Soc Interface *4*, 223-233.
Gomez, N., Lu, Y., Chen, S., and Schmidt, C. (2007b). Immobilized Nerve Growth Factor and Microtopography Have Distinct Effects on Polarizatoin Versus Axon Elongation in Hippocampal Cells in Culture. Biomaterials *28*, 271-284.
Goodman, r., and blank, m. (2002). Insights into electromagnetic interaction mechanisms. J Cell Physiol *192*, 16-22.
Gordon, T., Amirjani, N., Edwards, D., and Chan, K. (2010). Brief Post-Surgical Electrical Stimulation Accelerates Axon Regeneration and Muscle Reinnervation Without Affecting the Functional Measures in Carpal Tunnel Syndrome Patients. Exp Neurol *223*, 192-202.
Gordon, T., Sulaiman, O., and Ladak, A. (2009a). Chapter 24: Electrical Stimulation for Improving Nerve Regeneration: Where Do We Stand? Int Rev Neurobiol *87*, 433-444.
Gordon, T., Udina, E., Verge, V., and Chaves, P.d. (2009b). Brief Electrical Stimulation Accelerates Axon Regeneration in the Peripheral Nervous System and Promotes Sensory Axon Regeneration in the Central Nervous System. Motor Control *13*, 412-441.

Goto, E., Mukozawa, M., Mori, H., and Hara, M. (2010). A Rolled Sheet of Collagen Gel with Cultured Schwann Cells: Model of Nerve Conduit to Enhance Neurite Growth. Journal of Bioscience and Bioengineering *109*, 512-518.
Graves, M., Hassell, T., Beier, B., Albors, G., and Irazoqui, P. (2011). Electricallly Mediated Neuronal Guidance with Applied Alternating Current Electric Fields. Ann Biomed Eng *39*, 1759-1767.
Grawanis, A., Lavdas, A., Papalois, A., Franceschini, I., Tsoutsos, D., Dubois-Dalcq, M., Matsas, R., and Ioannovich, J. (2005). Effect of Genetically Modified Schwann Cells with Increased Motility in End-to-Side Nerve Grafting. Microsurgery *25*, 423-432.
Greatbatch, W. (1981). Metal Electrodes in Bioengineering. Crit Rev Biomed Eng *5*, 1-37.
Green, R., Lovell, N., and Poole-Warren, L. (2009). Cell Attachment Functionality of Bioactive Conducting Polymers for Neural Interfaces. Biomaterials *30*, 3637-3644.
Greenebaum, B., and Sisken, B. (2007). Does Direction of Induced Electric Field or Current Provide a Test of Mechanism Invovled in Nerve Regeneration. Bioelectromagnetics *28*, 488-492.
Griffin, J., Delgado-Rivera, R., Meiners, S., and Uhrich, K. (2011). Salicylic Acid-Derived Poly(Anhydride-Ester) Electrospun Fibers Designed for Regenerating the Peripheral Nervous System. J Biomed Mater Res A *97*, 230-242.
gross, d., loew, l., and webb, w. (1986a). optical imaging of cell membrane potential changes induced by applied electric fields. Biophysical Journal *50*, 339-248.
Gross, D., Loew, L., and Webb, W. (1986b). optical imaging of cell membrane potential changes induced by applied electric fields. Biophys J *50*, 339-248.
Gu, S., Shen, Y., Xu, W., Wu, L., Li, X., Zhou, G., Gu, Y., and Xu, J. (2010a). Application of Fetal Neural Stem Cells Transplantation in Delaying Denervated Muscle Atrophy in Rats with Peripheral Nerve Injury. Microsurgery *30*, 266-274.
Gu, S., Xu, W., Xu, L., Li, X., Ochiya, T., Wang, Y., Li, J., Gu, Y., and Xu, J. (2010b). Regenerated Host Axons Form Synapses with Neurons Derived From Neural Stem Cells Transplated into Peripheral Nerves. J Int Med Res *38*, 1721-1729.
Haastert-Talini, K., Schmitte, R., Korte, N., Klode, D., Ratzka, A., and Grothe, C. (2011). Electrical Stimulation Accelerates Axonal and Functional Peripheral Nerve Regeneration Across Long Gaps. J Neurotrauma *Epub Ahead of Print*.
Haile, Y., Berski, S., Drager, G., Nobre, A., Stummeyer, K., Gerardy-Schahn, R., and Grothe, C. (2008). The effect of Modified Polysialic Acid Based Hydrogels on the Adhesion and Viability of Primary Neurons and Glial Cells. Biomaterials *29*, 1880-1891.
Hammerick, K., Longaker, M., and Prinz, F. (200). In Vitro Effects of Direct Current Electric Fields on Adipose-Derived Stromal Cells. Biochem Biophys Res Commun *397*, 2-7.
He, L., Liao, S., Quan, D., Ma, K., Chan, C., Ramakrishna, S., and Lu, J. (2010). Synergistic Effects of Electrospun PLLA Fiber Dimension and Pattern on Neonatal Mouse Cerebellum C17.2 Cells. Acta Biomater *6*, 2960-2969.
Henze, D., Borhegyi, Z., Csicsvari, J., Mamiya, A., Harris, K., and Buzsaki, G. (2000). Intracellular Features Predicted by Extracellular Recordings in the Hippocampus In Vivo. J Neurophysiol *84*, 390-400.
Hill, P., Apel, P., Barnwell, J., Smith, T., Koman, L., Atala, A., and Van Dyke, M. (2011). Repair of Peripheral Nerve Defects in Rabbits Using Keratin Hydrogel Scaffolds. Tissue Eng Part A *17*, 1499-1505.
Hiraoka, M., Kato, K., Nakaji-Hirabayashi, T., and Iwata, H. (2009). Enhanced survival of neural cells embedded in hydrogels composed of collagen and laminin-derived cell adhesive peptide. Bioconjug Chem *20*, 976-983.
Hoffman-Kim, D., Mitchel, J., and Bellamkonda, R. (2010). Topography Cell Response, and Nerve Regeneration. Annu Rev Biomed Eng *12*, 203-231.
Holy, J., Perkins, E., and Yu, X. (2011). Adhesion, Proliferation and Differentiation of Pluripotent Stem Cells on Multi-Walled Carbon Nanotubes. IET Nanobiotrechnol *5*, 41-46.

Hong, S., and Kim, G. (2010). Electrospun Micro/Nanofibrous Conduits Composed of poly(epsilon-caprolactone) and Small Intestine Submucosa Powder for Nerve Tissue Regeneration. J Biomed Mater Res B Apply Biomat *94*, 421-428.
Hotary, K., and Robinson, K. (1994). Endogenous electrical currents and voltage gradients in Xenopus embryos and the consequences of their disruption. Developmental biology *166*, 789-800.
Hronik-Tupaj, M., and Kaplan, D. (2011a). A Review of the Responses of 2D and 3D Engineered Tissues to Electric Fields. Tissue Engineering Part B, In Press.
Hronik-Tupaj, M., Rice, W., Cronin-Golomb, M., Kaplan, D., and Georgakoudi, I. (2011b). Osteoblastic differentiation and stress response of human mesenchymal stem cells exposed to alternating current electric fields. Biomed Eng Online *10*, 9.
Huang, C., Carter, P., and Shepherd, R. (2001). Stimulus Induced pH Changes in Cochlear Implants: An In Vitro and In Vivo Study. Annals of Biomedical Engineering *29*, 791-802.
Huang, J., Ye, Z., Hu, X., Lu, L., and Luo, Z. (2010). Electrical Stimulation Induces Calcium-Dependent Release of NGF From Cultured Schwann Cells. Glia *58*, 622-631.
Hubbard Winkler, S. (2009). Care of the Combat Amputee.
Hunt, S. (2005). Neurobiology of Pain (Oxford University Press).
hunt, s., and mantyh, p. (2001). the main ascendig and descending spinal pathways. nature reviews neuroscience *2*, 83-91.
Hyung-Kew L, Sun-Il C, Seong-Jin K, Kwang-Seok Y, Euisik Y, and Kyung-Hyun K (2005). A Modular Expandable Tactile Sensor Using Flexible Polymer. IEEE International Conference on Micro Electro Mechanical Systems, 642-645.
Ignatius, M., Sawhney, N., Gupta, A., Thibadeau, B., Monteiro, O., and Brown, I. (1998). Bioactive Surface Coatings for Nanoscale Instruments: Effects on CNS Neurons. J Biomed Mater Res *40*, 264-274.
Ijiri, K., Matsunaga, S., Fukuyama, K., Maeda, S., Sakou, T., Kitano, M., and Senba, I. (1996). The effect of pulsing electromagnetic field on bone ingrowth into a porous coated implant. Anticancer Res *16*, 2853-2856.
Irintchev, A., Wu, M., Lee, H., Zhu, H., Feng, Y., Liu, Y., Bernreuther, C., Loers, G., You, S., and Schachner, M. (2011). Glycomimetic Improves Recovery After Femoral Injury in a Non-Human Primate. J Neurotrauma *28*, 1295-1306.
Ito, H., and Bassett, C. (1983). effect of weak pulsing electromagnetic fields on neural regeneration in the rat. Clin Orthop Relat Res *181*, 283-290.
Jahns, M., Lou, E., Durdle, N., Bagnall, K., Raso, J., Cinats, D., Barley, R., Cinats, J., and Jomha, N. (2007). The effect of pulsed electromagnetic fields on chondrocyte morphology. Med Biol Eng Comput *45*, 917-925.
Jeans, L., Gilchrist, T., and Healy, D. (2007). Peripheral Nerve Repair by Means of a Flexible Biodegradable Glass Fibre Wrap: A Comparison with Microsurgical Epineurial Repair. J Plast Reconstr Aesthet Surg *60*, 1302-1308.
Jennings, J., Chen, D., and Feldman, D. (2008). Transcriptional Response of Demal Fibroblasts in Direct Current Electric Fields. Bioelectromagnetics *29*, 394-405.
Jin, G., Kim, M., Shin, U., and Kim, H. (2011). Neurite Outgrowth of Dorsal Root Ganglia Neurons is Enhanced on Aligned Nanofibrous Bioploymer Scaffold with Carbon Nanotube Coating. Neurosci Lett *501*, 10-14.
Johnson, M., Otto, K., and Kipke, D. (2005). Repeated Voltage Biasing Improves Unit Recordings by Reducing Resistive Tissue Impedances. IEEE Trans Neural Syst Rehabil Eng *13*, 160-165.
Joines, W., Zhang, Y., Li, C., and Jirtle, R. (1994). The measured electrical properties of normal and malignant human tissues from 50 to 900MHz. Medical Physics *21*, 547-550.
jones-villeneuve, E., mcburnery, m., rogers, k., and kalnins, v. (1982). Retinoic acid induces embryonal carcinoma cells to differentiate into neurons and glial cell. the journal of cell biology *94*, 253-262.

Julius, D., and Basbaum, A. (2001). Molecular mechanisms of nociception. Nature *413*, 203-210.
Kafi, M., Kim, T., Yea, C., Kim, H., and Choi, J. (2010). Effects of Nanopatterned RGD Peptide Layer on Electrochemical Detection of Neural Cell Chip. Biosens Bioelectron *26*, 1359-1365.
Kakinoki, R., Nishijima, N., Ueba, Y., Oka, M., and Yamamuro, T. (1995). Relationship between axonal regeneration and vascularity in tubulation--an experimental study in rats. Neurosci Res *23*, 35-45.
Kalbermatten, D., Pettersson, J., Kingham, P., Pierer, G., Wiberg, M., and Terenghi, G. (2009). New Fibrin Conduit for Peripheral Nerve Repair. J Reconstr Microsurg *25*, 27-33.
Kandel, E., Schwartz, J., and Jessell, T. (2000). Principles of Neural Science, 4th edn (McGraw-Hill).
Kang, J., Gimble, J., and Kaplan, D. (2009). In Vitro 3D Model for Human Vascularized Adipose Tissue. Tissue Engineering Part A *15*, 2227-2236.
Kaplan, D., and Milleri, F. (2000). Neurotrophin Signal Transduction in the Nervous System. Current Opinion in Neurobiology *10*, 381-391.
Kapoor, A., Caporali, E., Kenis, P., and Stewart, M. (2010). Microtopographically Patterned Surfaces Promote the Alignment of Tenocytes and Extracellular Collagen. Acta Biomater *6*, 2580-2589.
Kawada, T., Nakayama, Y., Zheng, C., Ohya, S., Okuda, K., and Sunagawa, K. (2002). A Novel Photocurable Insulator Material for Automatic Nerve Activity Recording. Biomaterials *23*, 3169-3174.
Kehoe, S., Zhang, X., and Boyd, D. (2011). FDA Approved Guidance Conduit and Wraps for Peripheral Nerve Injury: A Review of Materials and Efficacy. Injury, Article in Press.
Kemp, S., Walsh, S., and Midha, R. (2008). Growth Factor and Stem Cell Enhanced Conduits in Peripheral Nerve Regeneration and Repair. Neurol Res *30*, 1030-1038.
Kemp, S., Webb, A., Dhaliwal, S., Syed, S., Walsh, S., and Midha, R. (2011). Dose and Duration of Nerve Growth Factor (NGF) Administration Determine the Extent of Behavorial Recovery Following Peripheral Nerve Injury in the Rat. Exp Neurol *229*, 460-467.
Kim, D., Wiler, J., Anderson, D., Kipke, D., and Martin, D. (2010a). Conducting Polymers on Hydrogel-Coated Neural Electrode Provide Sensitive Neural Recordings in Auditory Cortex. Acta Biomater *6*, 57-62.
Kim DH, Viventi J, Amsden JJ, Xiao J, Vigeland L, Kim YS, Blanco JA, Panilaitis B, Frechette ES, Contreras D, Kaplan DL, Omenetto FG, Huang Y, Hwang KC, Zakin MR*, et al.* (2010). Dissolvable Films of Silk Fibroin for Ultrathin Conformal Bio-Integrated Electronics. Nat Mater *9*, 511-517.
Kim, J., Kang, G., Nam, Y., and Choi, Y. (2010b). Surface-modified microelectrode array with flake nanostructure for neural recording and stimulation. Nanotechnology *21*.
Kim, S., Im, W., Kang, L., Lee, S., Chu, K., and Kim, B. (2008). The Application of Magnets Directs the Orientation of Neurite Outgrowth in Cultured Human Neuronal Cells. Journal of Neuroscience Methods *174*, 91-96.
Kim, U., Park, J., Kim, H., Wada, M., and Kaplan, D. (2005). Three-Dimensional Aqueous Derived Biomaterial Scaffolds From Silk Fibroin. Biomaterials *26*.
Kipke, D. (2010). Microfabricated Silicon Probes for Interfacing with the Nervous System: Examples and Design Considerations. In Implantable Neuroprosthetics: Technologies and Techniques (Ann Arbor, University of Michigan).
Kiryushko, D., Berezin, V., and Bock, E. (2004). Role of Cell Adhesion Molecules. Ann NY Acad Sci *1014*, 140-154.
Kitani, H., Ikeda, H., Atsumi, T., and Watanabe, R. (1997). Efficiency of Neural Differentiation of Mouse p19 Embryonal Carcinoma Cells is Dependent on the Seeding Density. Cell Transplantation *6*, 521-525.
Klein, J., Tendi, E., Dib-Haji, S., Fields, R., and Waxman, S. (2003). Patterned Electrical Activity Modulates Sodium Channel Expression in Sensory Neurons. J Neurosci Res *74*, 192-198.
Klesse, L., Meyers, K., Marshall, C., and Parada, L. (1999). Nerve Growth Factor Induces Survival and Differentiation Through Two Distinct Signaling Cascades in PC12 Cells. Oncogene *18*, 2055-2068.

Kokai, L., Bourbeau, D., Weber, D., McAtee, J., and Marra, K. (2011). Sustained Growth Factor Delivery Promotes Axonal Regeneration in Long Gap Peripheral Nerve Repair. Tissue Eng Part A *Epub Ahead of Print*.
Kondo, H., Hashimoto, S., Yamasaki, K., Ono, K., Okada, M., Fujisato, T., Kobayashi, H., Mochizuki, S., Ohsuga, M., Yoshiura, M., Tsutsui, H., Akazawa, K., Kawai, T., Uto, S., Tsujita, K*., et al.* (2008). Movement of Cultured Myotube with Electrical Stimulation. WMSCI 2008: 12th World Multi-Conference on Systemics, Cybernetics and Informatics *II*, 104-109.
Koob, A., and Borgens, R. (2006). Polyethylene Glycol Treatment After Traumatic Brain Injury Reduces Beta-Amyloid Precursor Protein Accumulation in Degenerating Axons. J Neurosci Res *83*, 1558-1563.
Koob, A., Colby, J., and Borgens, R. (2008). Behavioral Recovery from Traumatic Brain Injury After Membrane Reconstruction Using Polyethylene Glycol. J Biol Eng *2*.
Koppes, A., Seggio, A., and Thompson, D. (2011). Neurite Outgrowth is Significantly Increased by the Simulataneous Presentation of Schwann Cells and Moderate Exogenous Electric Fields. J Neural Eng *8*.
Kuffler, D. (1990). Long-term survival and Sprouting in Culture by Motorneurons Isolated From the Spinal Cord of Adult Frogs. J Comp Neurol *302*, 729-738.
Kullenberg, J., Rosatini, F., Vozzi, G., Bianchi, F., Ahluwalia, A., and Domenici, C. (2008). Optimization of PAM Scaffolds for Neural Tissue Engineering: Preliminary Study on an SH-SY5Y Cell Line. Tissue Eng Part A *14*, 1017-1023.
Kunz, B., Lierheimer, R., Rader, C., Spirig, M., Ziegler, U., and Sonderegger, P. (2002). Axonin-1/TAG-1 mediates cell-cell adhesion by a cis-assisted trans-interaction. The journal of biological chemistry *277*, 4551-4557.
Ladak, A., Olson, J., Tredget, E., and Gordon, T. (2011). Differentiation of Mesenchymal Stem Cells to Support Peripheral Nerve Regeneration in a Rat Model. Exp Neurol *228*, 242-252.
Lago, N., Ceballos, D., Rodriguez, F., Stieglitz, T., and Navarro, X. (2005). Long Term assessment of axonal regeneration through polyimide regenerative electrodes to interface the peripheral nerve. Biomaterials *26*, 2021-2031.
Lari, H., Hashim, B., Qian, H., Chua, J., and Haas, J. (2001). Nerve Regeneration (Providence, Brown University).
Larson, B., Abeytunge, S., and Rajadhyaksha, M. (2011). Performance of Full-Pupil Line-Scanning Reflectance Confocal Microscopy in Human Skin and Oral Mucose In Vivo. Biomed Opt Express *2*, 2055-2067.
Lawrence, B., Marchant, J., Pindrus, M., Omenetto, F., and Kaplan, D. (2009). Silk Film Biomaterials for Cornea Tissue Engineering. Biomaterials *30*, 1299-1308.
Lawrence, B., Wharram, S., Kluge, J., Leisk, G., Omenetto, F., Rosenblatt, M., and Kaplan, D. (2010). Effects of Hydration on Silk Film Material Properties. Macromol Biosci *10*, 393-403.
Leach, M., Feng, Z., Gertz, C., Tuck, S., Regan, T., Naim, Y., Vincent, A., and Corey, J. (2011). The Culture of Primary Motor and Sensory Neurons in Defined Media on Electrospun Poly-L-lactide Nanofiber Scaffolds. J Vis Exp *48*.
Lee, J., Bashur, C., Gomez, N., Goldstein, A., and Schmidt, C. (2010a). Enhanced Polarization of Embryonic Hippocampal Neurons on Micron Scale Electrospun Fibers. J Biomed Mater Res A *92*, 1398-1406.
Lee, J., Bashur, C., Milroy, C., Forciniti, L., Goldstein, A., and Schmidt, C. (2011). Nerve Growth Factor-Immobilized Electrically Conductiing Fibrous Scaffolds for Potential Use in Neural Tissue Engineering. IEEE Trans Nanobioscience *Epub Ahead of Print*.
Lee, T., Kim, I., Hwang, S., and Kim, S. (2010b). Functional Regeneration of Severed Peripheral Nerve Using an Implantable Electrical Stimulator. Conf Proc IEEE Eng Med Biol Soc, 1511-1514.
Lempka, S., Miocinovic, S., Johnson, M., Vitek, J., and McIntyre, C. (2009). In Vivo Impedance Spectroscopy of Deep Brain Stimulation Electrodes. J Neural Eng *6*.

Li, G., Livi, L., Gourd, C., Deweerd, E., and Hoffman-Kim, D. (2007a). Genomic and Morphological Changes of Neuroblastoma Cells in Response to Three-Dimensional Matrics. Tissue Eng *13*, 1035-1047.
Li, J., and Shi, R. (2007b). Fabrication of Patterned Multi-Walled Poly-L-Lactic Acid Conduits for Nerve Regeneration. J Neurosci Methods *165*, 257-264.
Li, L., El-Hayek, Y., Liu, B., Chen, Y., Gomez, E., Wu, X., Ning, K., Li, L., Chang, N., Zhang, L., Wang, Z., Hu, X., and Wan, Q. (2008a). Direct-Current Electrical Field Guides Neuronal Stem/Progenitor Cell Migration. Stem Cells *26*, 2193-2200.
Li X, Wang W, Wei G, Wang G, Zhang W, and X, M. (2010). Immunophilin FK506 loaded in chitosan guide promotes peripheral nerve regeneration. Biotechnol Lett *32*, 1333-1337.
Li, Z., Peng, J., Wang, G., Yang, Q., Yu, H., Guo, Q., Wang, A., Zhao, B., and Lu, S. (2008b). Effects of Local Release of Hepatocyte Growth Factor on Peripheral Nerve Regeneration in Acellular Nerve Grafts. Exp Neurol *214*, 47-54.
Lietz, M., Ullrich, A., Schulte-Eversun, C., Oberhoffner, S., Fricke, C., Muller, H., and Schlosshauer, B. (2006). Physical and biological performance of a novel block copolymer nerve guide. Biotechnol Bioeng *93*, 99-109.
Lin, Y., Ramadan, M., Hronik-Tupaj, M., Kaplan, D., Philips, B., Sivak, W., Rubin, J., and Marra, K. (2011). Spatially Controlled Delivery of Neurotrophic Factors in Silk Fibroin-Based Nerve Conduits for Peripheral Nerve Repair. Ann Plast Surg *67*, 147-155.
Liu, B. (2008). Fabrication and evaluation of a biodegradable proanthocyanidin-crosslinked gelatin conduit in peripheral nerve repair. J Biomed Mater REs A *87*, 1092-1102.
Liu, J., Wang, C., Wang, J., Ruan, H., and Fan, C. (2011). Peripheral Nerve Regeneration Using Composite Poly(Lactic Acid-Caprolactone)/Nerve Growth Factor Conduits Prepared by Coaxial Electrospinning. J Biomed Mater Res A *96*, 13-20.
Lopatina, T., Kalinina, N., Karagyaur, M., Stambolsky, D., Rubina, K., Revischin, A., Pavlova, G., Parfyonova, Y., and Tkachuk, V. (2011). Adipose-Derived Stem Cells Stimulate Regeneration of Peripheral Nerves: BDNF Secreted by These Cells Promotes Nerve Healing and Axon Growth De Novo. PLos One *6*, e17899.
Lopes, F., Schroder, R., da Frota Junior, M., Zanotto-Filho, A., Muller, C., Pires, A., Meurer, R., Colpo, G., Gelain, D., Kapczinski, F., Moreira, J., da Cruz Fernandes, M., and Klamt, F. (2010). Comparison between Proliferative and Neuron-Like SH-SY5Y cells as an in vitro model for Parkinson Disease Studies. Brain Research *14*, 85-94.
Lovett, M., Cannizzaro, C., Daheron, L., Messmer, B., Vunjak-Novakovic, G., and Kaplan, D. (2007). Silk Fibroin Microtubes for Blood Vessel Engineering. Biomaterials *28*, 5271-7279.
Lovett, M., Eng, G., Kluge, J., Cannizzaro, C., Vunjak-Novakovic, G., and KAplan, D. (2010). Tubular Silk Scaffolds for Small Diameter Vascular Grafts. Organogenesis *6*, 217-224.
Lozano, J., and Monarrez, L. (2003). Prologue Histology Resource. In Prologue Histology Labs, J. Lozano, and L. Monarrez, eds. (San Francisco, University of California San Francisco School of Medicine Office of Educational Technology).
Lu, Q., Wang, X., Hu, X., Cebe, P., Omenetto, F., and Kaplan, D. (2010). Stabilization and Release of Enzymes from Silk Films. Macromol Biosci *10*, 359-368.
Lundborg, G., Dahlin, L.B., Danielsen, N., Gelberman, R.H., Longo, F.M., Powell, H.C., and Varon, S. (1982). Nerve regeneration in silicone chambers: influence of gap length and of distal stump components. Exp Neurol *76*, 361-375.
Lundborg, G., Rosen, B., Dahlin, L., Holmberg, J., and Rosen, I. (2004). Tubular Repair of the Median or Ulnar Nerve in the Human Forearm: A 5-Year Follow-Up. The Journal of Hand Surgery: Journal of the British Society for Surgery of the Hand *29*, 100-107.
Lykissas, M., Batistatou, A., Charalabopoulos, K., and Beris, A. (2007). The role of neurotrophins in axonal growth, guidance, and regeneration. Curr Neurovasc Res *4*, 143-151.

Ma, C., Omura, T., Cobos, E., Latremoliere, A., Ghasemlou, N., Brenner, G., Van Veen, E., Barrett, L., Sawada, T., Gao, F., Coppola, G., Gertler, F., Costigan, M., Geschwind, D., and Woolf, C. (2011). Accelerating Axonal Growth Promotes Motor Recovery After Peripheral Nerve Injury in Mice. J Clin Invest, Epub Ahead of Print.
Ma, W., Tavakoli, T., Derby, E., Serebryakova, Y., Rao, M., and Mattson, M. (2008). Cell-Extracellular Matrix Interactions Regulate Neural Differentiation of Human Embryonic Stem Cells. BMC Dev Biol *8*.
MacKenzie, E., Castillo, R., Jones, A., Bosse, M., Kellam, J., Pollak, A., Webb, L., Swiontkowski, M., Smith, D., Sanders, R., Jones, A., Starr, A., McAndrew, M., Patterson, B., and Burgess, A. (2007). Health-Care Costs Associated with Amputation or Reconstruction of a Limb-Threatening Injury. The Journal of Bone and Joint Surgery *89*, 1685-1692.
Mackinnon, S., and Dellon, A. (1988). Wallerian Degeneration. In Surgery of the Peripheral Nerve.
Madduri, S., di Summa, P., Papaloizos, M., Kalbermatten, D., and Gander, B. (2010a). Effect of Controlled Co-Delivery of Synergistic Neurotrophic Factors on Early Nerve Regeneration in Rats. Biomaterials *31*, 8402-8409.
Madduri, S., Feldman, K., Tervoort, T., Papaloizos, M., and Gander, B. (2010b). Collagen Nerve Conduits Releasing the Neurotrophic Factors GDNF and NGF. J Control Release *143*, 168-174.
Madduri, S., Papaloizos, M., and Gander, B. (2010c). Trophically and Topographically Functionalized Silk Fibroin Nerve Conduits for Guided Peripheral Nerve Regeneration. Biomaterials *31*, 2323-2334.
Madison, R.D., Da Silva, C.F., and Dikkes, P. (1988). Entubulation repair with protein additives increases the maximum nerve gap distance successfully bridged with tubular prostheses. Brain Res *447*, 325-334.
Madison, R.D., Da Silva, C.F., Dikkes, P., Sidman, R.L., and Chio, T.-H. (1987). Peripheral nerve regeneration with entubulation repair: comparison of biodegradeable nerve guides versus polyethylene tubes and the effects of a laminin-containing gel. Exp Neurol *95*, 378-390.
Magee, J., and Schofield, G. (1991). Room Temperature Culture Extends the Useful Life of Adult Neurons for Voltage-Clamp Experiments. J Neurosci Methods *38*, 201-208.
Magnaghi, V., Conte, V., Procacci, P., Pivato, G., Cortese, P., Cavalli, E., Pajardi, G., Ranucci, E., Fenili, F., Manfredi, A., and Ferruti, P. (2011). Biological Performance of a Novel Biodegradable Polyamidoamine Hydrogel as Guide for Peripheral Nerve Regeneration. J Biomed Mater Res A *98*, 19-30.
Maiti, S., Shear, J., Williams, R., Zipfel, W., and Webb, W. (1997). Measuring Serotonin Distribution in Live Cells with Three-Photon Excitation. Science *275*, 530-532.
Mani, S., Schaefer, J., and Meiri, K. (2000). Targeted Disruption of GAP-43 in P19 Embryonal Carcinoma Cells Inhibits Neuronal Differentiation. As well as Acquisition of the Morphological Phenotype. Brain Res *853*, 384-395.
Mani, S., Shen, Y., Schaefer, J., and Meiri, K. (2001). Failure to Express GAP-43 During Neurogenesis Affects Cell Cycle Regulation and Differentiation of Neural Precursors and Stimulates Apoptosis of Neurons. Mol Cell Neurosci *17*, 54-66.
Marcoccio, I., and Vigasio, A. (2010). Muscle-In-Vein Nerve Guide for Secondary Reconstruction in Digital Nerve Lesions. J Hand Surg Am *35*, 1418-1426.
Mason, M., Tannemaat, M., Malessy, M., and Verhaagen, J. (2011). Gene Therapy for the Peripherla Nervous System: A Strategy to Repair the Injured Nerve? Current Gene Therapy *11*, 75-89.
Mathie, A., Kennard, L., and Veale, E. (2003). Neuronal Ion Channels and their Sensitivity to Extremely Low Frequency Weak Electric Field Effects. Radiation Protection Dosimetry *106*, 311-315.
Mauney, J., Nguyen, T., Gillen, K., Kirker-Head, C., Gimble, J., and Kaplan, D. (2007). Engineering adipose-like tissue in vitro and in vivo utilizing human bone marrow and adipose-derived mesenchymal stem cells with silk fibroin 3D scaffolds. Biomaterials *28*, 5280-5290.
McBurnery, M. (1993). P19 embryonal carcinoma cells. Int J Dev Biol *37*, 135-140.
McCaig, C. (1989). Studies on the Mechanism of Embryonic Frog Nerve Orientation in a Small Applied Electric Field. J Cell Sci *93*, 723-730.

McCaig, C. (1990). Nerve Branching is Induced and Oriented by a Small Applied Electric Field. J Cell Sci *95*, 605-615.
McCallister, W., McCallister, E., Trumble, S., and Trumble, T. (2005). Overcoming Peripheral Nerve Gap Defects Using an Intact Nerve Bridge in a Rabbit Model. J Reconstr Microsurg *21*, 197-206.
McCleskey, E., and Gold, M. (1999). Ion channels of nociception. Annu Rev Physiol *61*, 835-836.
McLeod, K. (1992). Microelectrode measurements of low frequency electric field effects in cells and tissues. Bioelectromagnetics *Suppl 1*, 161-178.
Mehta, A., Halder, S., Khanna, N., Tandon, O., and Sharma, K. (2011). Antagonism of Stimulation-Produced Analgesia by Naloxone and N-Methyl-D-Aspartate: Role of Opioid and N-Methyl-D-Aspartate Receptors. Human Exp Toxicol *Epub Ahead of Print*.
Meyer-Franke, A., Wilkinson, G., Kruttgen, A., Hu, M., Munro, E., Hanson Jr, M., Reichardt, L., and Barres, B. (1998). Depolarization and cAMP Elevation Rapidly Recruit TrkB to the Plasma Membrane of CNS Neurons. Neuron *21*, 681-693.
Mohanna, P., Young, R., Wiberg, M., and Terenghi, G. (2003). A Composite Poly-Hydroxybutyrate-Glial Growth Factor Conduit for Long Nerve Gap Repairs. J Anat *203*, 553-565.
Moore, A., Wood, M., Chenard, K., Hunter, D., Mackinnon, S., Sakiyama-Elbert, S., and Borschel, G. (2010). Controlled Delivery of Glial Cell Line-Derived Neurotrophic Factor Enhances Motor Nerve Regeneration. J Hand Surg Am *35*, 2008-2017.
Morokuma, J., Blackiston, D., Adams, D., Seebohm, G., Trimmer, B., and Levin, M. (2008). Modulation of potassium channel function confers a hyperproliferative invasive phenotype on embryonic stem cells. Proc Acad Sci USA *105*, 16608-16613.
Mosahebi, A., Wiberg, M., and Terenghi, G. (2003). Addition of Fibronectin to Alginate Matrix Improves Peripheral Nerve Regeneration in Tissue-Engineered Conduits. Tissue Eng *9*, 209-218.
Muir, D.e.a. (1989). Schwannoma Cell-Derived Inhibitor of the Neurite-Promoting Activity of Laminin. J Cell Biology *109*, 2353-2362.
Murakami, T., Fujimoto, Y., Yasunaga, Y., Ishida, O., Tanaka, N., Ikuta, Y., and Ochi, M. (2003). Transplanted Neuronal Progenitor Cells in a Peripheral Nerve Gap Promote Repair. Brain REs *974*, 17-24.
Nagy, I., and Rang, H. (1999). Similarities and Differences Between the Responses of Rat Sensory Neurons to Noxious Heat and Capsaicin. The Journal of Neuroscience *19*, 10647-10655.
Navarro, X., Rodriguez, F.J., Labrador, R.O., Buti, M., Ceballos, D., Gomez, N., Cuadras, J., and Perego, G. (1996). Peripheral nerve regeneration through bioresorbable and durable nerve guides. J Peripher Nerv Syst *1*, 53-64.
Nojehdehian, H., Moztarzadeh, F., Baharvand, H., Mehrjerdi, N., Nazarian, H., and Tahriri, M. (2010). Effect of Poly-L-Lysine Coating on Retinoic Acid-Loaded PLGA Microspheres in the Differentiation of Carcinoma Stem Cells into Neural Cells. Int J Artif Organs *33*, 721-730.
Oe, T., Nagashima, T., Muramoto, M., Yamazaki, T., Morikawa, N., Okitsu, O., Nishimura, S., Aoki, T., Katayama, Y., and Kita, Y. (2006). CyclinB2 and BIRC5 Genes as Surrogate Biomarkers for Neurite Outgrowth in SH-SY5Y Subclonal Cells. Neuropharmacology *50*, 1041-1047.
Oh, S., Kim, J., Song, K., Jeon, B., Yoon, J., Seo, T., Namgung, U., Lee, I., and Lee, J. (2008). Periperhal nerve regeneration within an asymmetrically porous PLGA/Pluronic F127 nerve guide conduit. Biomaterials *29*, 1601-1609.
Oh SH, Kim JH, Song KS, Jeon BH, Yoon JH, Seo TB, Namgung U, Lee IW, and JH, L. (2008). Peripheral Nerve Regeneration Within an Asymmetrically Porous PLGA/Pluronic F127 Nerve Guide Conduit. Biomaterials *29*, 1601-1609.
Oh, U. (2006). Nociceptive Membrane (Elsevier Science & Technology Books).
Omenetto, F., and DL, K. (2010). New Opportunities for an Ancient Material. Science *329*, 528-531.
Onuma, E., and Hui, S. (1985). A Calcium Requirement for Electric Field-Induced Cell Shape Changes and Preferential Orientation. Cell Calcium *6*, 281 -292.

Pahlman, S., Mamaeva, S., Meyerson, G., Mattsson, M., Bjelfman, C., Ortoft, E., and Hammerling, U. (1990). Human Neuroblastoma Cells in Culture: A Model for Neuronal Cell Differentiation and Function. 592, 25-37.
Pan, H., Cheng, F., Chen, C., Lai, S., Lee, C., Yang, D., Chang, M., and Ho, S. (2007). Post-Injury Regeneration in Rat Sciatic Nerve Facilitated by Neurotrophic Factors Secreted by Amniotic Fluid Mesenchymal Stem Cells. J Clin Neurosci *14*, 1089-1098.
Pan, H., Yang, D., Chiu, Y., Lasi, S., Wang, Y., Chang, M., and Cheng, F. (2006). Enhanced Regeneration in Injured Sciatic Nerve by Human Smniotic Mesenchymal Stem Cell. J Clin Neurosci *13*, 570-575.
panagopoulos, D., karabarbounis, a., and margaritis, l. (2002). Mechanism for action of electromagnetic fields on cells. Biochem Biophys Res Commun *298*, 95-102.
Panilaitis, B., and Altman, G. (2003). Macrophage Responses to Silk. Biomaterials *24*, 3079.
Park, B., Kang, D., Kang, E., Byun, J., Lee, J., Maeng, G., and Rho, G. (2011). Peripheral Nerve Regeneration Using Autologous Porcine Skin-Derived Mesenchymal Stem Cells. J Tissue Eng Regen Med.
Parrinello, S., Napoli, L., Ribeiro, S., Digby, P., Fedorova, M., Parkison, D., Doddrell, R., Nakayama, M., Adams, R., and Lloyd, A. (2010). EhB Signaling Directs Peripheral Nerve Regeneration Through Sox2-Dependent Schwann Cell Sorting. Cell *143*, 145-155.
Peignot, P., and Rhodes, K. (2004). Choosing a Silicone Adhesive and Treatment System. Med Device Technol *15*, 22-24.
Penna V, Munder B, Stark GB, and EM, L. (2011). An In Vivo Engineered Nerve Conduit -- Fabrication and Experimental Study in Rats. Microsurgery *31*, 395-400.
Pereira Lopes FR, Frattini F, Marques SA, Almeida FM, De Moura Campos LC, Langone F, Lora S, Borojevic R, and AM, M. (2010). Transplantation of Bone-Marrow-Derived Cells into a Nerve Guide Resulted in Transdifferentiation into Schwann Cells and Effective Regeneration of Transected Mouse Sciatic Nerve. Micron *41*, 783-790.
Pettersson, J., McGrath, A., Kalbermatten, D., Novikova, L., Wiberg, M., Kingham, P., and Novikov, L. (2011). Muscle Recovery After Repair of Short and Long Peripheral Nerve Gaps Using Fibrin Conduits. Neuroscience Letters *500*, 41-46.
Phillips JB, Bunting SC, Hall SM, and RA, B. (2005). Neural Tissue Engineering: A Self-Organizing Collagen Guidance Conduit. Tissue Eng *11*, 1611-1617.
Polk, C., and Postow, E. (1996). Handbook of Biological Effects of Electromagnetic Fields, second edn (CRC Press).
Pollock, M. (1995). Nerve Regeneration. Curr Opin Neurol *8*, 354-358.
Potter, G., Rowitch, D., and Petryniak, M. (2011). Myelin Restoration: Progress and Prospects for Human Cell Replacement Therapies. Arch Immunol Ther Exp *59*, 179-193.
Potter, S., and DeMarse, T. (2001). A New Approach to Neural Cell Culture for Long-Term Studies. Journal of Neuroscience Methods *110*.
Potucek, R., Kemp, S., Syed, N., and Midha, R. (2009). Chapter 10 Peripheral Nerve Injury, Repair, and Regeneration.
Price, R., Oe, T., Yamaji, T., and Matsuoka, N. (2006). A Simple, Flexible, Nonfluorescent System for the Automated Screening of Neurite Outgrowth. J Biomol Screen *11*, 155-164.
Pritchard, E., Szybala, C., Boison, D., and Kaplan, D. (2010). Silk Fibroin Encapsulated Powder Reservoirs for Sustained Release of Adenosine. J Control Release *144*, 159-167.
Radisic, M., Park, H., Shing, H., Consi, T., Schoen, F., Langer, R., Freed, L., and Vunjak-Novakovic, G. (2004). Functional Assembly of Engineered Myocardium by Electrical Stimulation of Cardiac Myocytes Cultured on Scaffolds. PNAS *101*, 18129-18134.
Ramachandran, A., Schuettler, M., Lago, N., Doerge, T., Koch, K., Navarro, X., Hoffmann, K., and Stieglitz, T. (2006). Design, in vitro and in vivo assessment of a multi-channel sieve electrode with integrated multiplexer. J Neural Eng *3*, 114-124.

Report, M.R. (2003). Worldwide Peripheral Neuropathy, E. Publications, ed.
Reynolds, B., Tetzlaff, W., and Weiss, S. (1992a). A Multipotent EGF-Responsive Striatal Embryonic Progenitor Cell Produces Neurons and Astrocytes. J Neurosci *12*, 4565-4574.
Reynolds, B., and Weiss, S. (1992b). Generation of Neurons and Astrocytes from Isolated Cells of the Adult Mammalian Central Nervous System. Science *255*, 1707-1710.
Rice, W., Kaplan, D., and Georgakoudi, I. (2010). Two-Photon Microscopy for Non-Invasive, Quantitative Monitoring of Stem Cell Differentiation. PLoS One *5*, e10075.
Robinson, P.H., van der Lei, B., Hoppen, H.J., Leenslag, J.W., Pennings, A.J., and Nieuwenhuis, P. (1991). Nerve regeneration through a two-ply biodegradable nerve guide in the rat and the influence of ACTH4-9 nerve growth factor. Microsurgery *12*, 412-419.
Ruiz, L., Fine, E., Voros, J., Makohliso, S., Leonard, D., Johnston, D., Textor, M., and Mathieu, H. (1999). Phosphorylcholine-containing polyurethanes for the control of protein adsorption and cell attachment via photoimmobilized laminin oligopeptides. J Biomater Sci Polym Ed *10*, 931-955.
Runge, M., Dadsetan, M., Baltrusaitis, J., Knight, A., Ruesink, T., Lazcano, E., Lu, L., Windebank, A., and Yaszemski, M. (2010). The Development of Electrically Conductive Polycaprolactone Fumarate-Polypyrrole Composite Materials for Nerve Regeneration. Biomaterials *31*, 5916-5926.
Rutkowski, G., and Heath, C. (2002). Development of a Bioartificial Nerve Graft. I. Design Based on a Reaction-Diffusion Model. Biotechnol Prog *18*, 362-372.
Salonen, V. (1987). Laminin in Traumatized Peripheral Nerve: Basement Membrane Changes During Degeneration and Regeneration. J Neurochtol *16*, 713-720.
Santiago, L., Clavijo-Alvarez, J., Brayfield, C., Rubin, J., and Marra, K. (2009). Delivery of Adipose-Derived Precursor Cells for Peripheral Nerve Repair. Cell Transplantation *18*, 145-158.
Sauer, h., rahimi, g., hescheler, j., and wartenberg, m. (1999). Effects of electrical fields on cardiomyocyte differentiation of embryonic stem cells. journal of cellular biochemistry *75*, 710-723.
Saygili, E., Schauerte, P., Kuppers, F., Heck, L., Weiss, J., Weber, C., Schwinger, R., Hoffman, R., Schroder, J., Marx, N., and Rana, O. (2010). Electrical Stimulation of Sympathetic Neurons Induces Autocrine/Paracrine Effects of NGF Mediated by TrkA. Journal of Molecular and Cellular Cardiology *49*, 79-87.
Schmidhammer, R., Redl, H., Hopf, R., Van Der Nest, D., and Millesi, H. (2007). Syntergistic Terminal Motor End-to-Side Nerve Graft Repair: Investigation in a Non-Human Primate Model. Acta Neurochir Suppl *100*, 97-101.
Scholz, T., Rogers, J., Krichevsky, A., Dhar, S., and Evans, G. (2010). Inducible Nerve Growth Factor Delivery for Peripheral Nerve Regeneration in vivo. Plast Reconstr Surg *126*, 1874-1889.
Scott, J., Afshari, M., Kotex, R., and Saul, J. (2011). The Promotion of Axon Extension In Vitro Using Polymer-Templated Fibrin Scaffolds. Biomaterials *32*, 4830-4839.
Scott, R., Marquardt, L., and Willits, R. (2010). Characterization of Poly(Ethylene Glycol) Gels with Added Collagen for Neural Tissue Engineering. J Biomed Mater Res A *93*, 817-823.
Sebastian, A., Buckle, A., and Markx, G. (2007a). Tissue engineering with electric fields: Immobilization of mammalian cells in multilayer aggregates using dielectrophoresis. Biotechnol Bioeng *98*, 694-700.
Sebastian, A., Venkatesh, A., and Markx, G. (2007b). Tissue Engineering with electric fields: Investigation of the shape of mammalian cell aggregates formed at interdigitated oppositely castellated electrodes. Electrophoresis *28*, 3821-3828.
Selimovic, S., Piraino, F., Bae, H., Rasponi, M., Redaelli, A., and Khademhosseini, A. (2011). Microfabricated Polyester Conical Microwells for Cell Culture Applications. Lab Chip *11*, 2325-2332.
Serena, E., Flaibani, M., Carnio, S., Boldrin, L., Vitiello, L., De Coppi, P., and Elvassore, N. (2008). Electrophysiologic Stimulation Improves Myogenic Potential of Muscle Precursor Cells Grown in a 3D Collagen Scaffold. Neurol Res *30*, 207-214.

Sharula, Hara, Y., Nishiura, Y., Saijilafu, Kubota, S., and Ochiai, N. (2010). Repair of the Sciatic Nerve Defect with a Direct Gradual Lengthening of Proximal and Distal Nerve Stumps in Rabbits. Plast Reconstr Surg *125*, 846-854.
Shen, Y., Mani, S., and Meiri, K. (2004). Failure to Express GAP-43 Leads to Disruption of a Multipotent Precursos and Inhibits Astrocyte Differentiation. Molecular and Cellular Neuroscience *26*, 390-405.
Sheridan, D., and Isseroff, R. (1996). Imposition of a Physiologic DC Electric Field Alters the Migratory Response of Human Keratinocytes on Extracellular Matrix Molecules. J Invest Dermatol *106*, 642 - 646.
Shi, W., Yao, J., Chen, X., Lin, W., Gu, X., and Wang, X. (2010). The Delayed Repair of Sciatic Nerve Defects with Tissue-Engineered Nerve Grafts in Rats. Artif Cells Bllod Substit Immobil Biotechnol *38*, 29-37.
Shim, S., and Ming, G. (2010). Roles of Channels and Receptors in the Growth Cone During PNS Axonal Regeneration. Experimental Neurology *223*, 38-44.
Shimizu, T., Yamato, M., Akutsu, T., Shibata, T., Isoi, Y., Kikuchi, A., Umezu, M., and Okano, T. (2002). Electrically communicating three-dimensional cardiac tissue mimic fabricated by layered cultured cardiomyocyte sheets. J Biomed Mater Res *60*, 110-117.
Shirvalkar, P., and Shapiro, M. (2010). Design and Construction of a Cost Effective Headstage for Simultaneous Neural Stimulation and Recording in the Water Maze. In J Vis Exp.
Simões MJ, Amado S, Gärtner A, Armada-Da-Silva PA, Raimondo S, Vieira M, Luís AL, Shirosaki Y, Veloso AP, Santos JD, Varejão AS, Geuna S, and AC, M. (2010). Use of chitosan scaffolds for repairing rat sciatic nerve defects. Ital J Anat Embryol *115*, 190-210.
Singh, J., and Kaur, G. (2005). Neuroprotection Mediated by Subtoxic Dose of NMDA in SH-SY5Y Neuroblastoma Cultures: Activity-Dependent Regulation of PSA-NCAM Expression. Molecular Brain Research *137*, 223-234.
Smallheiser, N., Crain, S., and Reid, L. (1984). Laminin as a Substrate for Retinal Axons in Vitro. Brain Res *314*, 136-140.
Sofia, S., McCarthy, M., Gronowicz, G., and Kaplan, D. (2001). Functionalized Silk-Based Biomaterials for Bone Formation. J Biomed Mater Res *54*, 139-148.
Staii, C., Viesselmann, C., Ballweg, J., Williams, J., Dent, E., Coppersmith, S., and Eriksson, M. (2011). Distance Dependence of Neuronal Growth on Nanopatterned Gold Surfaces. Langmuir *27*, 233-239.
Stauffer, W., and Cui, X. (2006). Polypyrrole Doped with 2 Peptide Sequences from Laminin. Biomaterials *27*, 2405-2413.
Sufan, W., Suzuki, Y., Tanihara, M., Ohnishi, K., Suzuki, K., Endo, K., and Nishimura, Y. (2001). Sciatic Nerve Regeneration Through Alginate with Tubulation or Nontubulation Repair in Cat. J Neurotrauma *18*, 329-338.
Sun, F., Zhou, K., Mi, W., and Qiu, J. (2011). Combined Use of Decellularized Allogeneic Artery Conduits with Autologous Transdifferentiated Adipose-Derived Stem Cells for Facial Nerve Regeneration in Rats. Biomaterials *32*, 8118-8128.
Sun, J., Vajandar, S., Xu, D., Kang, Y., Hu, G., Li, D., and Li, D. (2009a). Experimental Characterization of Electrical Current Leakage in poly (dimethylsiloxane) Microfluidic Devices. Microfluid Nanfluid *6*, 589-598.
Sun, L., Hsieh, D., Yu, T., Chiu, H., Lu, S., Luo, G., Kuo, T., Lee, O., and Chiou, T. (2009b). Effect of pulsed electromagnetic field on the proliferation and differentiation potential of human bone marrow mesenchymal stem cells. Bioelectromagnetics *30*, 251-260.
Sun, M., McGowan, M., Kingham, P., Terenghi, G., and Downes, S. (2010). Novel Thin-Walled Nerve Conduit with Microgrooved Surface Patterns for Enhanced Peripheral Nerve Repair. J Mater Sci Mater Med *21*, 2765-2774.
Sun, S., Liu, Y., Lipsky, S., and Cho, M. (2007). Physical Manipulation of Calcium Oscillations Facilitates Osteodifferentiation of Human Mesenchymal Stem Cells. FASEB J *21*, 1472-1480.

Sun, S., Titushkin, I., and Cho, M. (2006). Regulation of Mesenchymal Stem Cell Adhesion and Orientation in 3D Collagen Scaffold by Electrical Stimulus. Bioelectrochemistry *69*, 133-141.
Sundar, S., Kundu, J., and Kundu, S. (2010). Biopolymeric Nanoparticles. Sci Technol Adv Mater *11*.
Sundelacruz, S., Levin, M., and Kaplan, D. (2009). Role of Membrane Potential in the Regulation of Cell Proliferaiton and Differentiation. Stem Cell Rev *5*, 231-246.
Szybala, C., Pritchard, E., Lusardi, T., Li, T., Wilz, A., Kaplan, D., and Boison, D. (2009). Antiepileptic Effects of Silk-Polymer Based Adenosine Release in Kindled Rats. Exp Neurol *219*, 126-135.
Tandon, N., Cannizzaro, C., Chao, P., Maidhof, R., Marsano, A., Au, H., Radisic, M., and Vunjak-Novakovic, G. (2009a). Electrical Stimulation Systems for Cardiac Tissue Engineering. Nat Protoc *4*, 155-173.
Tandon, N., Goh, B., Marsano, A., Chao, P., Montouri-Sorrentino, C., Gimble, J., and Vunjak-Novakovic, G. (2009b). Alignment and elongation of human-derived stem cells in response to direct-current electrical stimulation. Conf Proc IEEE Eng Med Biol Soc *1*, 6517-6521.
Tansey, K., Seifert, J., Botterman, B., Delgado, M., and Romero, M. (2011). Peripheral Nerve Repair Through Multi-Luminal Biosynthetic Implants. Ann Biomed Eng *39*, 1815-1828.
Tegeder, I., Costigan, M., Griffin, R., Abele, A., Belfer, I., Schmidt, H., Ehnert, C., Nejim, J., Claudiu, M., Scholz, J., Wu, T., Allchorne, A., Diatchenko, L., Binshtok, A., Goldman, D*., et al.* (2006). GTP Cyclohydrolase and Tetrahydrobiopterin Regulate Pain Sensitivity and Persistence. Nature Medicine *12*, 1269-1277.
Thanawala, S., Palyvoda, O., Georgiev, D., Khan, S., Al-Homoudi, I., Newaz, G., and Auner, G. (2007). A Neural Cell Culture Study on Thin Film Electrode Materials. J Mater Sci Mater Med *18*, 1745-1752.
Thomas, S., Rogers, J., Krichevsky, A., Dhar, S., and Evans, G. (2010). Inducible Nerve Growth Factor Delivery for Peripheral Nerve Regeneration in vivo. Plast Reconstr Surg *126*, 1874-1889.
thornton, c. (1970a). amphibian limb regeneration and its relation to nerves. am zoologist *10*, 113-118.
Thornton, C. (1970b). Amphibian Limb Regeneration and Its Relation to Nerves. American Zoologist *10*, 113-118.
Tobita, M., Orbay, H., and Mizuno, H. (2011). Adipose-Derived Stem Cells: Current Findings and Future Directions. Discov Med *11*, 160-170.
Tomita, K., et al (2007). Myelin-Associated Glycoprotein Reduces Axonal Branching and Enhances Functional Recovery After Sciatic Nerve Transection in Rats. Glia *55*, 1498-1507.
Tsai, M., Chang, W., Chang, K., Hou, R., and Wu, T. (2007). Pulsed electromagnetic fields affect osteoblast proliferation and differentiatinon in bone tissue engineering. Bioelectromagnetics *28*, 519-528.
Tsai, M., Pan, H., Liou, D., Weng, C., Hoffer, B., and Cheng, H. (2010). Adenoviral Gene Transfer of Bone Morphogenetic Protein-7 Enhances Functional Recovery After Sciatic Nerve Injury in Rats. Gene Ther *17*, 1214-1224.
Uebersax, L., Mattotti, M., Papaloizos, M., Merkle, H., Gander, B., and Meinel, L. (2007). Silk Fibroin Matrices for the Controlled Release of Nerve Growth Factor (NGF). Biomaterials *28*, 4449-4460.
Ulrich, H., and Majumder, P. (2006). Neurotransmitter Receptor Expression and Activity During Neuronal Differentiation of Embryonal Carcinoma and Stem Cells: From Basic Research Towards Clinical Applications. Cell Prolif *39*, 281-300.
Waetzig, V., and Herdegen, T. (2005). MEKK1 Controls Neurite Regrowth After Experimental Injury by Balancing ERK1/2 and JNK2 Signaling. Mol Cell Neurosci *30*, 67-78.
Wallman, L., Zhang, Y., Laurell, T., and Danielsen, N. (2001). The geometric design of micromachined silicon sieve electrodes influences functional nerve regeneration. Biomaterials *22*, 1187-1193.
Wan, L., Xia, R., and Ding, W. (2010a). Electrical Stimulation Enhanced Remyelinatoin of Injured Sciatic Nerves by Increasing Neurotrophins. Neuroscience *169*, 1029-1038.

Wan, L., Zhang, S., Xia, R., and Ding, W. (2010b). Short-Term Low-Frequency Electrical Stimulation Enhanced Remyelination of Injured Peripheral Nerves by Inducing the Promyelination Effect of Brain-DErived Neurotrophic Factor on Schwann Cell Polarization. Journal of Neuroscience Research *88*, 2578-2587.
Wang, C., Liu, J., Fan, C., Mo, X., Ruan, H., and Li, F. (2010a). The Effect of Aligned Core-Shell Nanofibres Delivering NGF on the Promotion of Sciatic Nerve Regeneration. J Biomater Sci Polym Ed *Epub Ahead of Print*.
Wang, H., Mullins, M., Cregg, J., Hurtado, A., Oudega, M., Trombley, M., and Gilbert, R. (2009). Creation of Highly Aligned Electrospun poly-L-lactic Acid Fibers for Nerve Regeneration Applications. J Neural Eng *6*, 016001.
Wang, P., Yu, H., and Tsai, W. (2010b). Modulation of Alignment and Differentiation of Skeletal Myoblasts by Submicron Ridges/Grooves Surface Structure. Biotechnol Bioeng *106*, 285-294.
Wang, X., Yang, Y., Xie, M., Yu, X., Liu, C., and Wang, X. (2007). Proliferation of Neural Stem Cells Correlates with Wnt-3 Protein in Hypoxic-Ischemic Neonate Rats After Hyperbaric Oxygen Therapy. Neuroreport *18*, 1753-1756.
Wang, Y., Rudym, D., Walsh, A., Abrahamsen, L., Kim, H., Kim, H., Kirker-Head, C., and Kaplan, D. (2008). In Vivo Degradation of Three-Dimensional Silk Fibroin Scaffolds. Biomaterials *29*, 3415-3428.
Weber, R.A., Breidenbach, W.C., Brown, R.E., Jabaley, M.E., and Mass, D.P. (2000). A randomized prospective study of polyglycolic acid conduits for digital nerve reconstruction in humans. Plast Reconstr Surg *106*, 1036-1044.
Whimister, I. (1978a). Nerve supply as a stimulator of the growth of tissues including skin II. animal evidence. Clinical and experimental dermatology *3*, 389-410.
Whimister, I. (1978b). Nerve Supply as a Stimulator of the Growth of Tissues Including Skinn II. Animal Evidence. Clinical and Experimental Dermatology *3*, 389-410.
Whitlock, E., Tuffaha, S., Luciano, J., Yan, Y., Hunter, D., Magill, C., Moore, A., Tong, A., Mackinnon, S., and Borschel, G. (2009). Processed Allografts and Type I Collagen Conduits for Repair of Peripheral Nerve Gaps. Muscle Nerve *39*, 787-799.
Willerth, S., and Sakiyama-Elbert, S. (2007). Approaches to Neural Tissue Engineering Using Scaffolds for Drug Delivery. Advanced Drug Delivery Reviews *59*, 325-338.
Williams, K., Rahimtula, M., and Mearow, K. (2005). Hsp27 and Axonal Growth in Adult Sensory Neurons In Vitro. BMC Neurosci *6*, .
Williams, S., Wasserman, S., Rawlinson, D., Kitney, R., Smaje, L., and Tooke, J. (1988). Dynamic Measurment of Human Capillary Blood Pressure. Clin Sci *74*, 507-512.
Wilz, A., Pritchard, E., Li, T., Lan, J., Kaplan, D., and Boison, D. (208). Silk Polymer-Based Adenosine Release: Therapeutic Potential for Epilepsy. Biomaterials *29*, 3609-3616.
Witzel, C., Rohde, C., and Brushart, T. (2005). Pathway Sampling by Regenerating Peripheral Axons. The Journal of Comparitive Neurology *485*, 183-190.
Wood, M., Moore, A., Hunter, D., Tuffaha, S., Borschel, G., Mackinnon, S., and Sakiyama-Elbert, S. (2009). Affinity-Based Release of Glial-Derived Neurotrophic Factor from Fibrin Matrices Enhances Sciatic Nerve Regeneration. Acta Biomater *5*, 959-968.
Wu, G., Ju, L., Jin, T., Chen, L., Shao, L., Wang, Y., and Liu, B. (2010). Local Delivery of Recombinant Human Bone Morphogenetic Protein-2 Increases Axonal Regeneration and the Expression of Tau Protein After Facial Nerve Injury. J Int Med Res *38*, 1682-1688.
Xie, F., Li, Q., Gu, B., Liu, K., and Shen, G. (2008). In vitro and in vivo evaluation of a biodegradable chitosan-PLA composite peripheral nerve guide conduit material. Microsurgery *28*, 471-479.
Xie, J., MacEwan, M., Li, X., Sakiyama-Elbert, S., and Xia, Y. (2009). Neurite Outgrowth on Nanofiber Scaffolds with Different Orders, Structures, and Surface Properties. ACS Nano *3*, 1151-1159.

Xing, Z., Chae, W., Huh, M., Park, L., Park, S., Kwak, G., Yoon, K., and Kang, I. (2011). In Vitro Anti-Bacterial and Cytotoxic Properties of Silver-Containing Poly(L-Lactide-Co-Glycolide) Nanofibrous Scaffolds. J Nanosci Nantechnol *11*, 61-65.
Xu, H., Yan, Y., and Li, S. (2011). PDLLA/Chondroitin Sulfate/Chitosan/NGF Conduits for Peripheral Nerve Regeneration. Biomaterials *Epub Ahead of Print*.
Yamada, Y., Hozumi, K., Katagiri, F., Kikkawa, Y., and Nomizu, M. (2010). Biological Activity of Laminin Peptide-Conjugated Alginate and Chitosan Matrices. Biopolymers *94*, 711-720.
Yamazaki, T., Sabit, H., Oya, T., Ishii, Y., Hamashima, T., Tokunaga, A., Ishizawa, S., Jie, S., Kurashige, Y., Matsushima, T., Furuta, I., Noguchi, M., and Sasahara, M. (2009). Activation of MAP Kinases, Akt, and PDGF Receptors in Injured Peripheral Nerves. Journal of the Peripheral Nervous System *14*, 165-179.
Yang, Y., Chen, X., Ding, F., Zhang, P., Liu, J., and Gu, X. (2007a). Biocompatibility Evaluation of Silk Fibroin with Peripheral Nerve Tissues and Cells In Vitro. Biomaterials *28*, 1643-1652.
Yang, Y., Ding, F., Wu, J., Hu, W., Liu, W., Liu, J., and Gu, X. (2007b). Development and Evaluation of Silk Fibroin-Based Nerve Grafts Used for Peripheral Nerve Regeneration. Biomaterials *28*, 5526-5535.
Yang, Y., and Han, C. (2010). GDNF Stimulates the Proliferation of Cultured Mouse Immature Sertoli Cells Via its Receptor Subunit NCAM and ERK1/2 Signaling Pathway. BMC Cell Biology *11*.
Yang, Y., Yuan, X., Ding, F., Yao, D., Gu, Y., Liu, J., and Gu, X. (2011). Repair of Rat Sciatic Nerve Gap by a Silk Fibroin-Based Scaffold Added with Bone Marrow Mesenchymal Stem Cells. Tissue Eng Part A *17*, 2231-2244.
Yang YC, Shen CC, Cheng HC, and BS, L. (2011). Sciatic nerve repair by reinforced nerve conduits made of gelatin-tricalcium phosphate composites. J Biomed Mater Res A *96*, 288-300.
Yang YC, Shen CC, Huang TB, Chang SH, Cheng HC, and BS, L. (2010). Characteristics and Biocompatibility of a Biodegradable Genipin-Cross-Linked Gelatin/β-Tricalcium Phosphate Reinforced Nerve Guide Conduit. J Biomed Mater Res B Appl Biomater *95*, 207-217.
Yao, L., Biliar, K., Windebank, A., and Pandit, A. (2010a). Multichanneled Collagen Conduits for Peripheral Nerve Regeneration: Design, Fabrication, and Characterization. Tissue Engineering: Part C *16*, 1585-1596.
Yao, L., Damodaran, G., Nikolskaya, N., Gorman, A., Windebank, A., and Pandit, A. (2010b). The Effect of Laminin Peptide Gradient in Enzymatically Cross-Linked Collagen Scaffolds on Neurite Growth. J Biomed Mater Res A *92*, 484-492.
Yao, L., O'Brien, N., Windebank, A., and Pandit, A. (2009). Orienting Neurite Growth in Electrospun Fibrous Neural Conduits. J Biomed Mater Res B Appl Biomater *90*, 483-491.
You, Y., Gong, Y., Yin, B., Yuan, J., and Peng, X. (2010). ShcD Interacts with TrkB via its PTB and SH2 Domains and Regulates BDNF-Induced MAPK Activation. BMB Reports *43*, 485-490.
Yu, W., Zhao, W., Zhu, C., Zhang, X., Ye, D., Zhang, W., Zhou, Y., Jiang, X., and Zhang, Z. (2011). Sciatic Nerve Regeneration in Rats by a Promising Electrospun Collagen/Poly(e-caprolactone) Nerve Conduit with Tailored Degradation Rate. BMC Neurosci *12*.
Yucel, D., Kose, G., and Hasirci, V. (2010a). Polyester Based Nerve Guidance Conduit Design. Biomaterials *31*, 1596-1603.
Yucel, T., Kojic, N., Leisk, G., Lo, T., and Kaplan, D. (2010b). Non-equilibrium Silk Fibroin Adhesives. Journal of Structural Biology *170*, 406-412.
Zanakis, M. (1990). Differential Effects of Various Electrical Parameters on Peripheral and Central Nerve Regeneration. Accupunct Electrother Res *15*, 185-191.
Zavan, B., Abatangelo, G., Mazzoleni, F., Bassetto, F., Cortivo, R., and Vindigni, V. (2008). New 3D Hyaluronan-based scaffold for in vitro reconstruction of the rat sciatic nerve. Neurol Res *30*, 190-196.
Zhang, H., Zheng, L., Yi, X., Chen, Z., He, Z., Zhao, D., Zhang, X., and Ma, Z. (2010). Slit1 Promotes Regenerative Neurite Outgrowth of Adult Dorsal Root Ganglion Neurons in vitro Via Binding to the Robo Receptor. Journal of Chemical Neuroanatomy *39*, 256-261.

Zhang, L., Zhengwen, M., Smith, G., Wen, X., Pressman, Y., Wood, P., and Xu, X. (2009). GDNF-Enhanced Axonal Regeneration and Myelination Following Spinal Cord Injury is Mediated by Primary Effects on Neurons. Glia *57*, 1178-1191.
Zhao, J., Zhang, L., Zhang, Y., and Shen, Y. (2011). The Differential Regulation of Gap43 Gene in the Neuronal Differentiation of P19 Cells. J Cell Physiol.
Zhao, M., Agius-Fernandez, A., Forrester, J., and McCaig, C. (1996). Directed Migration of Corneal Epithelial Sheets in Physiological Electric Fields. Invest Opthalmol Vis Sci *37*, 2548-2558.
Zhao, M., Bai, H., and Wang, E. (2004). Electrical Stimulation Directly Induces Preangiogenic Responses in Vascular Endothelial Cells by Signaling through VEGF Receptors. J Cell Sci *117*, 397-405.
Zhao, M., McCaig, C., Agius-Fernandez, A., Forrester, J., and Araki-Sasaki, K. (1997). Human Corneal Epithelial Cells Reorient and Migrate Cathodally in a Small Applied Electric Field. Curr Eye Res *16*, 973-984.
Zhou, C., Confalonieri, F., Medina, N., Zivaonivic, Y., Eshault, C., Yang, T., Jacquet, M., Janin, J., Duguet, M., Perasso, R., and Li, Z. (2000). Fine Organization of Bombyx Mori Fibroin Heavy Chain Gene. Nucleic Acids Res *28*, 2413-2419.
Ziegler, K., Gorl, R., Effing, J., Ellermann, J., Mappes, M., Otten, S., Kapp, H., Zoellner, P., Spaeth, D., and Smola, H. (2006). Reduced Cellular Toxicity of a New Silver-Containing Antimicrobial Dressing and Clinical Performance in Non-Healing Wounds. Skin Pharmacol Physiol *19*, 140-146.
Zuo, J., et al (1998). Degradation of Chondroitin Sulfate Proteoglycan Enhances the Neurite-Promoting Potential of Spinal Cord Tissue. Exp Neurol *154*, 654-662.
Zuo, J., and Hernandez, Y. (1998). Chrondroitin Sulfate Proteoglycan with Neurite-Inhibiting Activity is Up-Regulated Following Peripheral Nerve Injury. J Neurobiol *34*, 41-54.